UNIVERSITÀ DEGLI STUDI DI PALERMO

Dottorato in Energia e Tecnologie dell'Informazione
Dipartimento di Energia, Ingegneria dell'Informazione e Modelli Matematici (DEIM)
Settore Scientifico Disciplinare ING/IND19

ON THE THERMO-MECHANICAL BEHAVIOUR OF THE IFMIF TARGET ASSEMBLY UNDER STEADY STATE AND TRANSIENT OPERATIVE SCENARIOS

IL DOTTORE
ING. P. ARENA

IL COORDINATORE
CH.MA PROF.SSA M. S. MONGIOVÌ

IL TUTOR
CH.MO PROF. P. A. DI MAIO

IL CO TUTOR
PH.D. D. BERNARDI

CICLO XXIX
ANNO CONSEGUIMENTO TITOLO 2017

Index

List of acronyms

AISI	American Iron and Steel Institute
BA	Broader Approach
BP	Back-Plate
DEIM	Department of Energy, Information Engineering and Mathematic Models
DEMO	DEMOnstration Power Plant
DPA	Displacement Per Atom
EMP	ElectroMagnetic Pump
EU	European Union
FDS	Fast Disconnecting System
FEM	Finite Element Method
HEBT	High Energy Beam Transport
HFTM	High Flux Test Module
HX	Heat eXchange
IFMIF	International Fusion Materials Irradiation Facility
IN	Inlet Nozzle
IP	Inlet Pipe
ITER	International Thermonuclear Experimental Reactor
JET	Joint European Torus
JT60	Japanese Torus-60
LEBT	Low Energy Beam Transport
LFTM	Low Flux Test Module
LG	Lithium Guide
LINAC	Linear Accelerator
LL	Lithium Loop
LT	Lateral Thickness
MEBT	Medium Energy Beam Transport
MFTM	Medium Flux Test Module
ON	Outlet Nozzle
RAFM	Reduced Activation Ferritic Martensitic
R&D	Research and Development
RFQ	Radio Frequency Quadrupole
SDC-IC	ITER Structural Design Criteria for In-vessel Components
SIA	Self-Interstitial Atom
TA	Target Assembly
TC	Target Chamber

TFTR	Tokamak Fusion Test Reactor

List of symbols

A	Area
c_p	Specific heat at constant pressure
d	Distance
E	Young's modulus
F	Peak stress
F_{ij}	Viewfactors
H, h	Thermal conductance, convective heat transfer coefficient
K_{eff}, K_t	Effective bending shape factor, Creep bending shape factor
n	Neutron
P_L, $\overline{P_L}$	Local primary membrane stress, local primary membrane stress intensity
P_m, $\overline{P_m}$	Primary membrane stress, primary membrane stress intensity
P_b, $\overline{P_b}$	Primary bending stress, primary bending stress intensity
q	Heat flux
q'''	Volumetric density of heat power
Q_L, $\overline{Q_L}$	Local secondary membrane stress, local secondary membrane stress intensity
Q_m, $\overline{Q_m}$	Secondary membrane stress, secondary membrane stress intensity
Q_b, $\overline{Q_b}$	Secondary bending stress, secondary bending stress intensity
r	Radius
r_2, r_3	Elastic follow-up factors
S_d	Allowable total stress intensity
S_e	Allowable primary plus secondary membrane stress intensity
S_m	Allowable primary membrane stress intensity
S_t	Time-dependent allowable stress intensity
S_y	Yield stress intensity
t	Time
T, θ	Temperature in °C, Temperature in °K
u	Displacement
U_t	Creep usage fraction

Greek symbols

α	Coefficient of thermal expansion
ε	Thermal emissivity
ε_{sw}	Volumetric swelling strain
δ_{ij}	Kronecker's delta
γ	Gamma ray
Φt, Φt_m	Neutron fluence, thickness-averaged neutron fluence
Φ	Surface heat flux
λ	Thermal conductance
ρ	Density
σ	Stefan-Boltzmann constant
$\bar{\sigma}$, σ_{VM}	Equivalent stress, Von Mises equivalent stress
ω	Weight function

1. Introduction

The exploitation of nuclear fusion reactions is one the most attracting methods to produce electricity in a sustainable way. In fact, the fuel needed in the two most promising reactions is deuterium and tritium, two isotopes of the hydrogen which are, in a first approximation, infinite.

For this reason the international scientific community is from long time involved in a Research and Development (R&D) program aimed at the development of a nuclear fusion power plant able to produce electricity in a continuous and reliable way. During the last decade of the 20^{th} century different international facilities have shown the scientific feasibility of the fusion reaction (JET, JT-60, TFTR) adopting a reactor based on the magnetic confinement of the plasma, the so called TOKAMAK concept.

Subsequently, the efforts of the international scientific community have been focused on two further projects, ITER and DEMO, with the aim of demonstrating the engineering and commercial feasibility, respectively, of the nuclear fusion reaction. Concerning ITER, it is under construction in the site of Cadarache (France) and it should start the first operations by the end of 2025, while as far as DEMO is concerned, it is in a pre-conceptual phase.

It is important to underline that the operational conditions in which the components of these reactors are foreseen to operate, in terms of both thermal and neutronic irradiation field, will be extremely severe. Although the behaviour of structural materials under irradiation is studied from long time in fission power plants, the much higher dose levels foreseen in fusion power plants rise the necessity of investigating their behaviour in a fusion relevant irradiation scenario.

Therefore, it has been decided to develop and build a facility able to reproduce the operative conditions typical of a fusion reactor from both thermal and neutron irradiation point of view. The International Fusion Materials Irradiation Facility (IFMIF) is the result of this joint effort between Japan and the EU in the framework of the Broader Approach (BA) agreement [1].

IFMIF is an intense accelerator-based D-Li neutron source that will provide high energy neutrons at sufficient intensity to reproduce irradiation conditions relevant to a fusion power reactor in order to test and qualify candidate materials to be used in these reactors, allowing, in particular, the development of a material irradiation database for the design, construction, licensing and safe operation of DEMO [2].

IFMIF mainly consists of three sub-systems: the accelerators, the lithium target system and the test facility. Two linear accelerators provide two 125mA deuteron beams at the energy of 40 MeV that, interacting with a flowing film of liquid lithium, generate an intense flux of high energetic (14 MeV) neutrons [2]. The samples of materials, located in the test facility, are

irradiated at different dose levels and high temperature in order to investigate their behaviour when operating in fusion relevant conditions.

The IFMIF sub-system where the deuteron beams interact with the flowing lithium film is the lithium target system and, in particular, the component named Back-Plate (BP). It appears clear that the assessment of the thermo-mechanical behaviour of the BP and all the components of the Target Assembly (TA) linked to it plays a key-role in the design of the machine.

Concerning the TA, and the BP in particular, two design options are currently under investigation [3-4]. The first option is based on the so-called integral Target Assembly, where the replacement of the BP is foreseen to be executed by a remote "cut and re-weld" operation.

The second option foresees a removable BP, so that it can be easily replaced using a remote handling device without removing the whole Target Assembly. This latter concept, proposed by ENEA, is based on the adoption of a so-called BP "bayonet" design, which consists in a replaceable Back-Plate that can be inserted to and removed from the TA fixed frame by means of a sliding-skate mechanism [5].

In these last years, the assessment of the thermo-mechanical behaviour of both the BP configurations has represented a challenging issue [6-12], highlighting the necessity of further efforts in order to set-up a geometric layout of the TA able to ensure the fulfilment of the design criteria.

It is in the framework of these activities that, during the Ph.D. course of the XXIX Ciclo in Energia e Tecnologie dell'Informazione - curriculum Fisica tecnica e Ingegneria Nucleare (*Energy and Information Technologies - curriculum Applied physics and Nuclear Engineering*), held at the University of Palermo, and in the framework of a fruitful collaboration between the Department of Energy, Information Engineering and Mathematic Models (DEIM) of the University of Palermo and the ENEA-Brasimone, the thermo-mechanical behaviour of the Target Assembly of IFMIF endowed with the replaceable BP has been widely-investigated under different loading scenarios.

The work, divided in three main phases, has followed a theoretical-numerical approach based on the Finite Element Method (FEM) and the quoted FEM code Abaqus v.6.14 has been adopted [13].

The first phase of the study has aimed at the set-up of a FEM model of the IFMIF Target system mock-up present at the ENEA-Brasimone research centre and at the simulation of the pre-heating phase of the IFMIF start-up transient scenario [14]. This phase of the start-up scenario is foreseen to raise the Target system temperature up to the operational value of 250 °C as much uniformly as possible by means of a set of electric heaters placed on its external surfaces. In order to achieve this goal, a transient thermal campaign of analysis has been carried out and a time-dependent load profile for the electric heaters has been found out. The obtained results will be used to *ex-post* validate the Target system mock-up FEM model set-

up.

In the second phase, the thermo-mechanical behaviour of the IFMIF TA under the steady state nominal scenario has been assessed. The main outcome of this analysis has been that the BP is not able to safely withstand the loads of the operational scenario it undergoes.

Therefore, in the third phase of the study an optimization strategy for the BP has been set-up and several geometric configurations have been assessed. The thermo-mechanical performances of the most promising one have been investigated under the nominal steady state scenario and in a transient analysis in which the effect of the volumetric swelling strain has been considered.

The method and boundary conditions adopted, as well as the results obtained are herewith reported and critically discussed.

2. The IFMIF project

The assessment of the thermal, physical and mechanical properties of materials candidate to be adopted as structural materials for the plasma facing components in the DEMO reactor and in future fusion power reactors is the main task IFMIF has to comply.

In order to achieve this important goal, this facility has the objective of providing a neutron flux as close as possible similar to a D-T fusion plasma neutron flux, in terms of both intensity and neutron energy distribution.

IFMIF will supply this neutron flux by means of two 125 mA deuteron beams accelerated at the energy of 40 MeV [15] and interacting with a flowing film of liquid lithium, according to:

$$^{7}\mathrm{Li}(\mathrm{d},2\mathrm{n})^{7}\mathrm{Be} \qquad (2\text{-}1)$$

$$^{6}\mathrm{Li}(\mathrm{d},\mathrm{n})^{7}\mathrm{Be} \qquad (2\text{-}2)$$

As stated before, the IFMIF plant can be divided in three main sub-systems: the accelerator facility, the lithium target facility and the test facility.

2.1. The accelerator facility

The accelerator facility foreseen in IFMIF is composed of two acceleration lines, each one consisting in a set of different components (Fig. 2-1). Each line is composed of a cyclotron, a Radio Frequency Quadrupole (RFQ), a Linear Accelerator (Linac) and three Energy Beam Transport systems, at Low (LEBT), Medium (MEBT) and High (HEBT) energy, respectively.

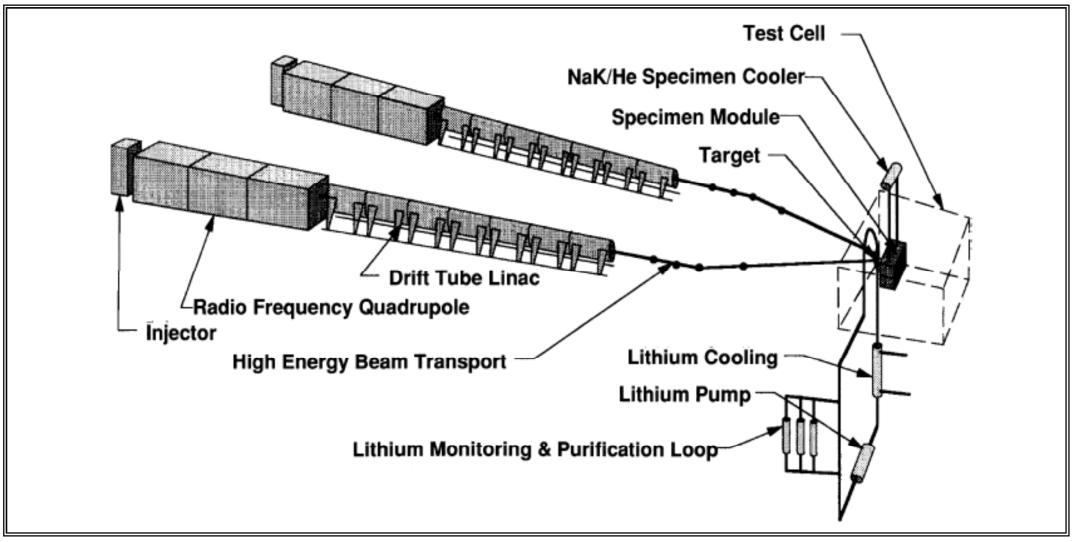

Figure 2-1. Schematic view of the IFMIF accelerator system.

A 140 mA deuteron beam at the energy of 100 keV is generated in the cyclotron and successively guided to the RFQ through the LEBT [15]. The energy of the beam is then risen up to a value of around 5 MeV, even though some energy losses in the line are foreseen and a current value of 125 mA is expected. At this point the MEBT system transfers the beam to the Linac where the beam is accelerated in 4 steps up to the nominal value of 40 MeV. Finally the HEBT transfers the deuteron beam to the target system where it is collimated and its shape is adapted to the target one. The two so obtained deuteron beams, at the power of 5 MW each, interact with the target of liquid lithium with an angle of 9°, in order to mainly produce neutrons forward-directed, where they can interact with the samples of the materials to irradiate.

2.2. The lithium target facility

The second sub-system we find in IFMIF is the lithium target facility. This section, mainly consisting in the Target Assembly (TA) and the Lithium Loop (LL), it is intended to remove the 10 MW heat power deposited by the deuterium beams, to allow a stable lithium jet with a wave amplitude less than 1 mm at a speed of 10 - 20 m/s, to control impurity levels, to guarantee a sufficient safety with respect to lithium hazard and Tritium release from the Lithium Loop and, last but not the least, to achieve the required system availability during plant lifetime [16]. A schematic view of the lithium target facility is reported in figure 2-2.

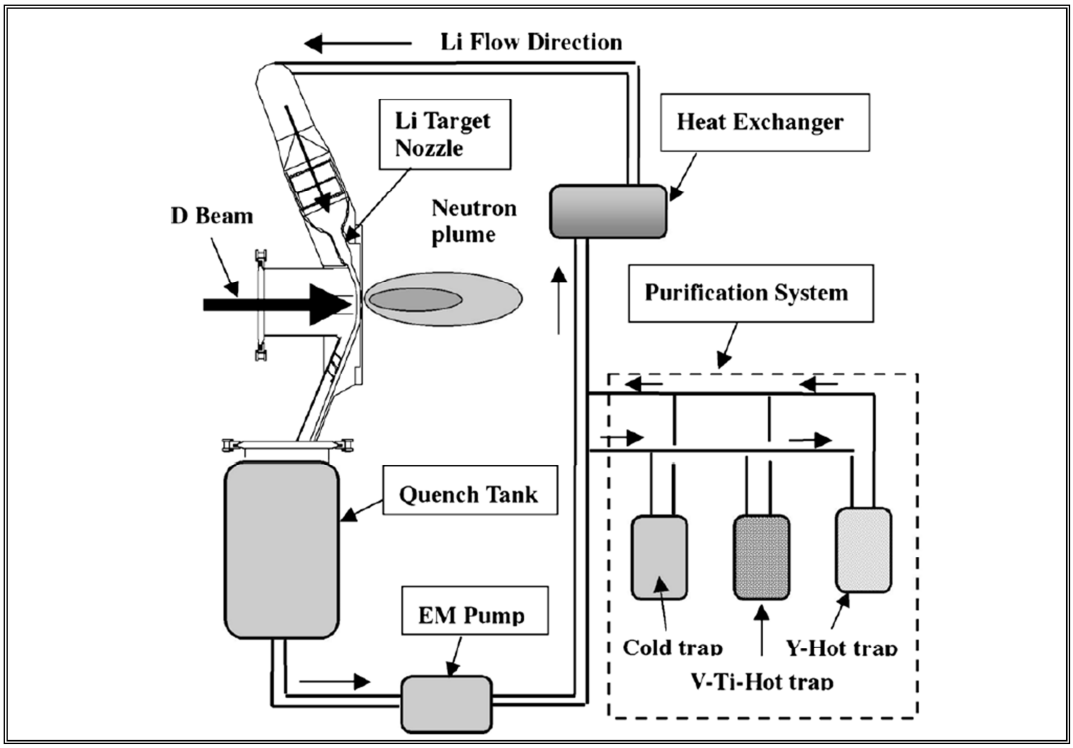

Figure 2-2. Schematic view of the lithium target facility.

The TA is devoted to provide a fast, reliable and stable flow of lithium, mainly characterized by a jet thickness of 2.5±0.1 cm, a flow velocity of 10–20 m/s and a lithium temperature ranging from 200 to 300 °C, with a reference inlet value of 250 °C [16,17]. The LL is articulated in a main loop and a purification loop and it is intended to feed lithium to the TA by ElectroMagnetic Pumps (EMPs), routing it through the Heat eXchange (HX) system and the lithium purification loop, consisting of one cold and two hot traps.

Target Assembly and Lithium Loop are connected each other by means of three Fast Disconnecting Systems (FDSs), two located in the TA lithium inlet pipe and one devoted to attach the TA lithium outlet duct to the Quench Tank.

The Target Assembly (Figs. 2-3, 2-4), made of reduce activation steel (EUROFER), is approximately 2.5 m tall and 600 kg heavy. It has to be located in the test cell as close as possible (~2 mm) to the high flux vertical test module, being supported by arms laying on a proper support framework. It mainly consists of a flow straightener, a nozzle, a Back-Plate, a target chamber, a frame, drain baffles and flanges. A more detailed description of its lay-out may be found in [2,16].

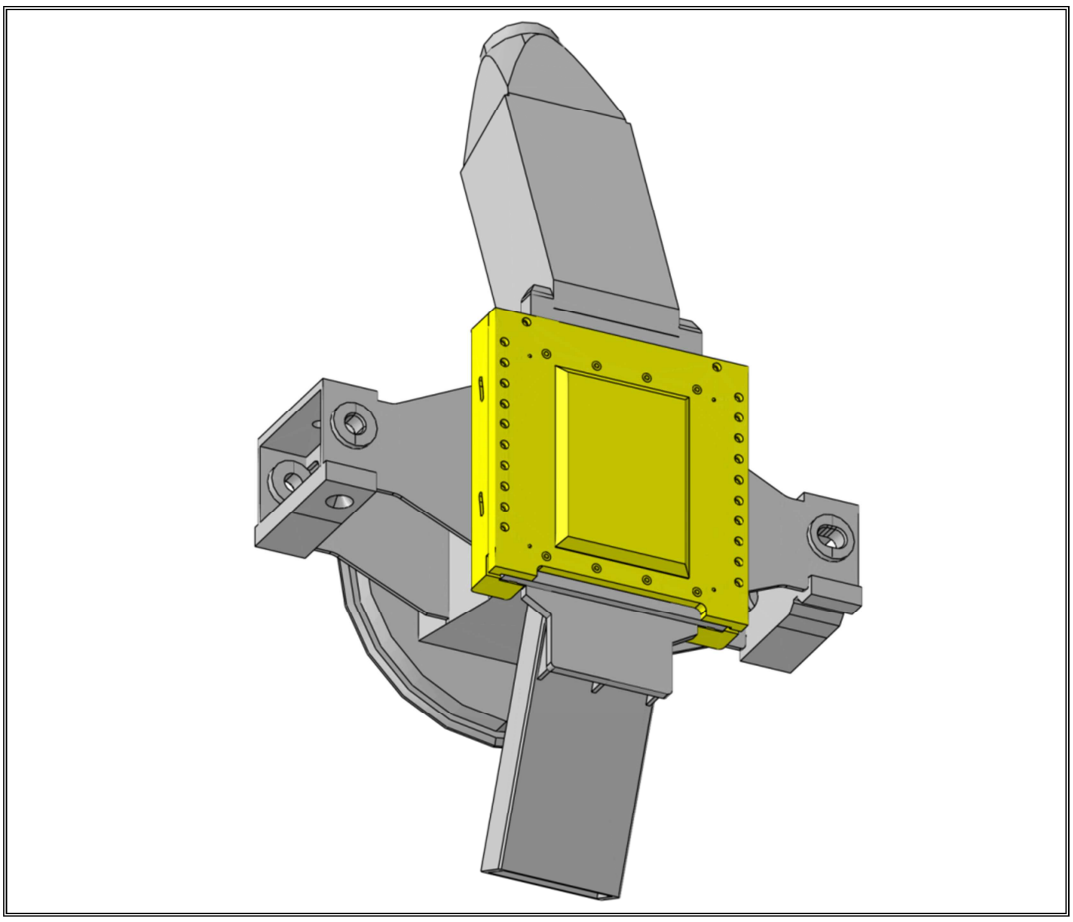

Figure 2-3. IFMIF Target Assembly.

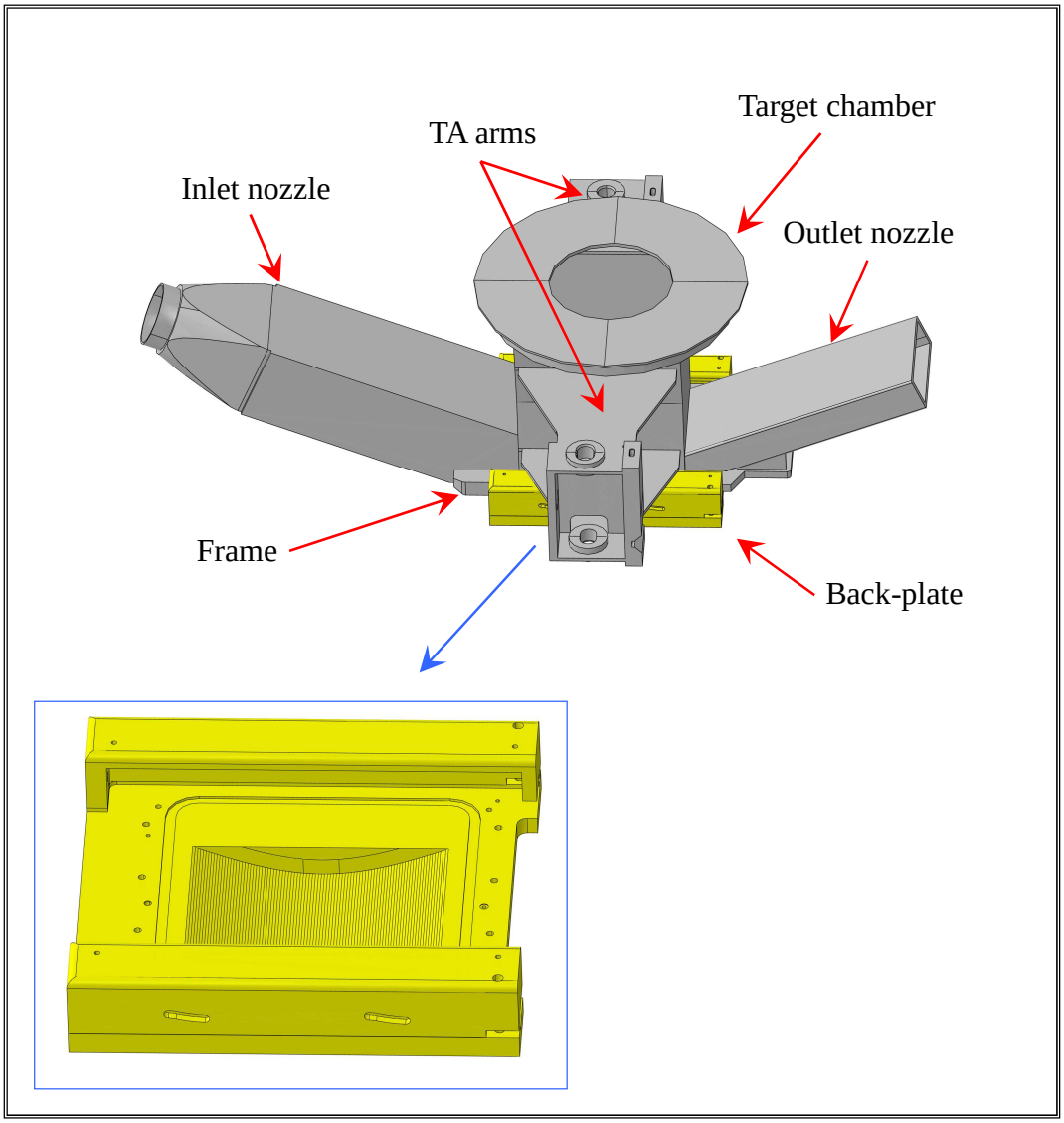

Figure 2-4. IFMIF Target Assembly exploded view.

The flow straightener, located inside the inlet nozzle, is provided to change lithium flow regime from turbulent to laminar, while the inlet nozzle is placed at the exit of the straightener to realize a stable lithium flow. In particular, since the IFMIF target nozzle is required to contract lithium flow with a contraction ratio of 10, from 1.5 m/s to 15 m/s, and no nozzle exists with a contraction ratio higher than 4 which operates at the required high speed of 15 m/s, a two-step contraction Shima type nozzle has been selected. It is characterized by contraction ratio values of 4 for the first nozzle and 2.5 for the second nozzle and it allows the transverse component of flow velocity to remain under the prescribed limit (±0.1m/s).

The Back-Plate (BP) is the most heavily loaded TA component (Fig. 2-5) and it is devoted to house the beam footprint, resulting to operate, in IFMIF, under severe conditions of

neutron irradiation damage (~50 DPA/year) [17]. Its expected lifetime under irradiation is estimated to be less than 1 year and, although the required replacement period will be defined considering irradiation effects on material properties, it should be significantly shorter than 11 months. Therefore, the reference TA design is conceived with a remotely replaceable Back-Plate.

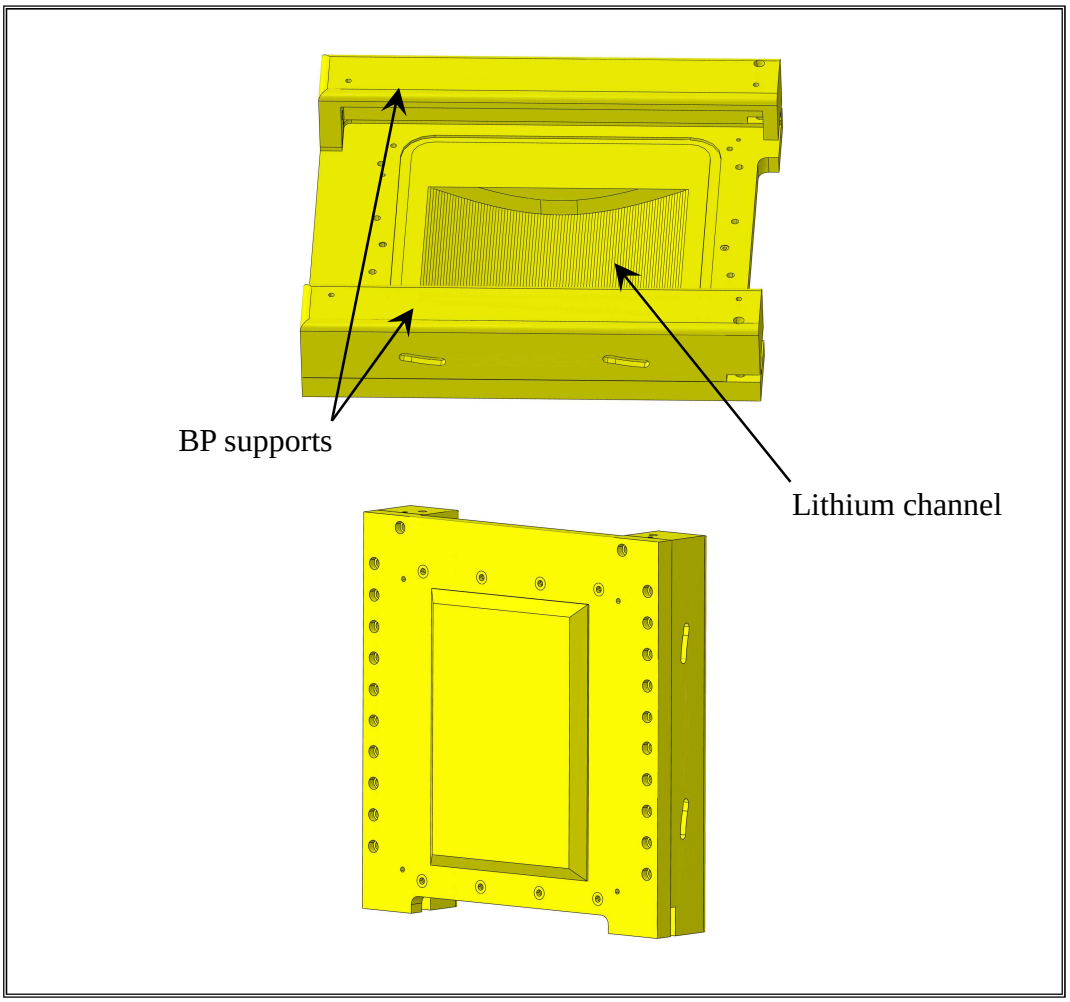

Figure 2-5. IFMIF Target Assembly Back-Plate (Front and back views).

A curved profile has been envisaged for the Back-Plate in the beam footprint region in order to allow centrifugal forces arising within lithium flow to increase its pressure and, consequently, its saturation temperature, avoiding the risk of vaporization under the 10 MW power deposition due to the interaction with deuterons.

Two design options are currently under investigation as far as IFMIF TA Back-Plate is concerned. The first option is based on the so-called integral Target Assembly which is conceived to be replaced during the planned maintenance stages of the system. The second

option foresees a removable BP, so that it can be easily replaced using a remote handling device without removing the whole Target Assembly. This latter concept, proposed by ENEA, is based on the adoption of a so-called BP “bayonet” design, which consists in a replaceable Back-Plate that can be inserted to and removed from the TA fixed frame by means of a sliding-skate mechanism [5].

The TA arms are connected to the support framework (Fig. 2-6), made of EUROFER steel too, directly fixed to the test cell ground by means of a proper bolt system. The support framework allows the sliding of one of the TA arms during the nominal operational phase in order to allow the TA deformation and maintain the alignment between the deuteron beams and the lithium footprint.

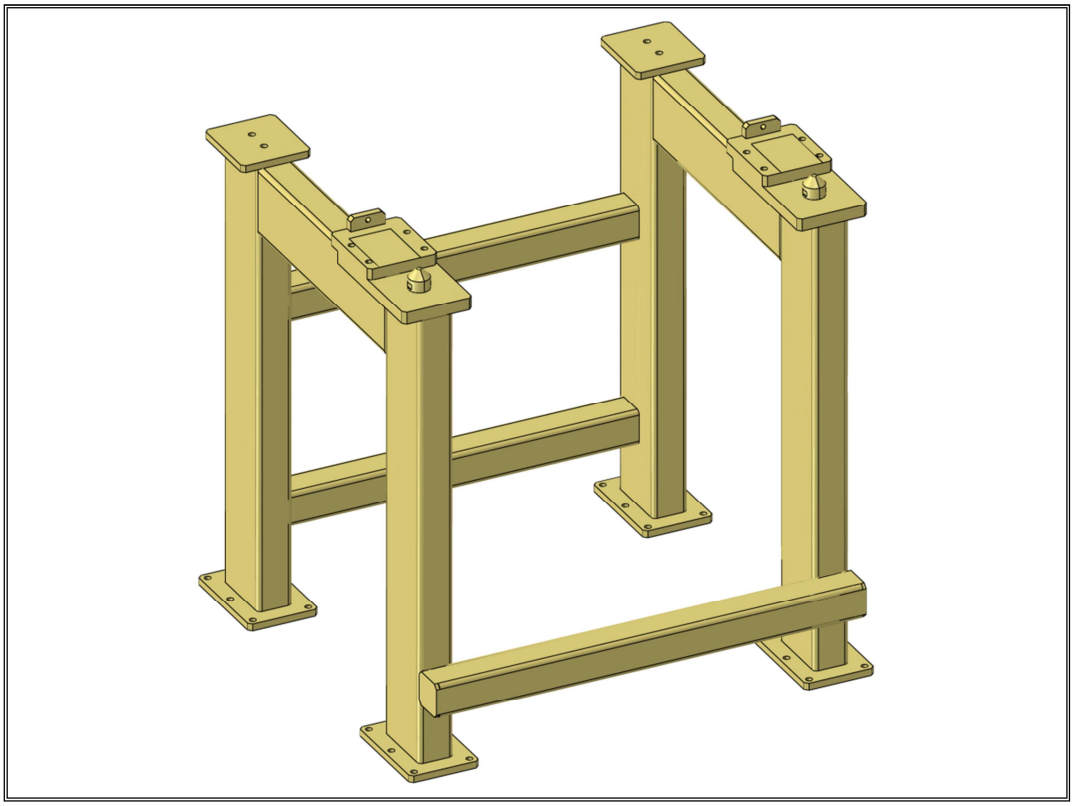

Figure 2-6. TA support framework.

The Lithium Loop is articulated in a main loop and a purification loop, being designed to operate for 20 years. Its design specifications are reported in table 2-1. Further details may be found in [16,18].

The main loop stably supplies liquid lithium of the adequate flow rate and temperature to the TA. It mainly consists of the target quench tank, the surge or overflow tank, the lithium dump tank, the organic dump tank, the main electromagnetic pump and two heat exchangers. Most of the piping and tanks are constructed of austenitic 304 stainless steel. There are, in

addition, a trace heating system (to maintain the temperature throughout the loop above the melting point of the lithium at all times the liquid lithium is present in the loop), thermal insulation, valves, electromagnetic flow meters, instrumentation and connections to vacuum and argon headers [16].

Among the main loop components, in order to investigate the thermo-mechanical performances of the IFMIF Target Assembly, attention has been paid to the lithium inlet pipe, made of EUROFER steel, devoted to supply lithium to the inlet nozzle straightener. The lithium inlet pipe is articulated in two sections, connected each other by means of two FDSs and a gimbal expansion joint (Fig. 2-7).

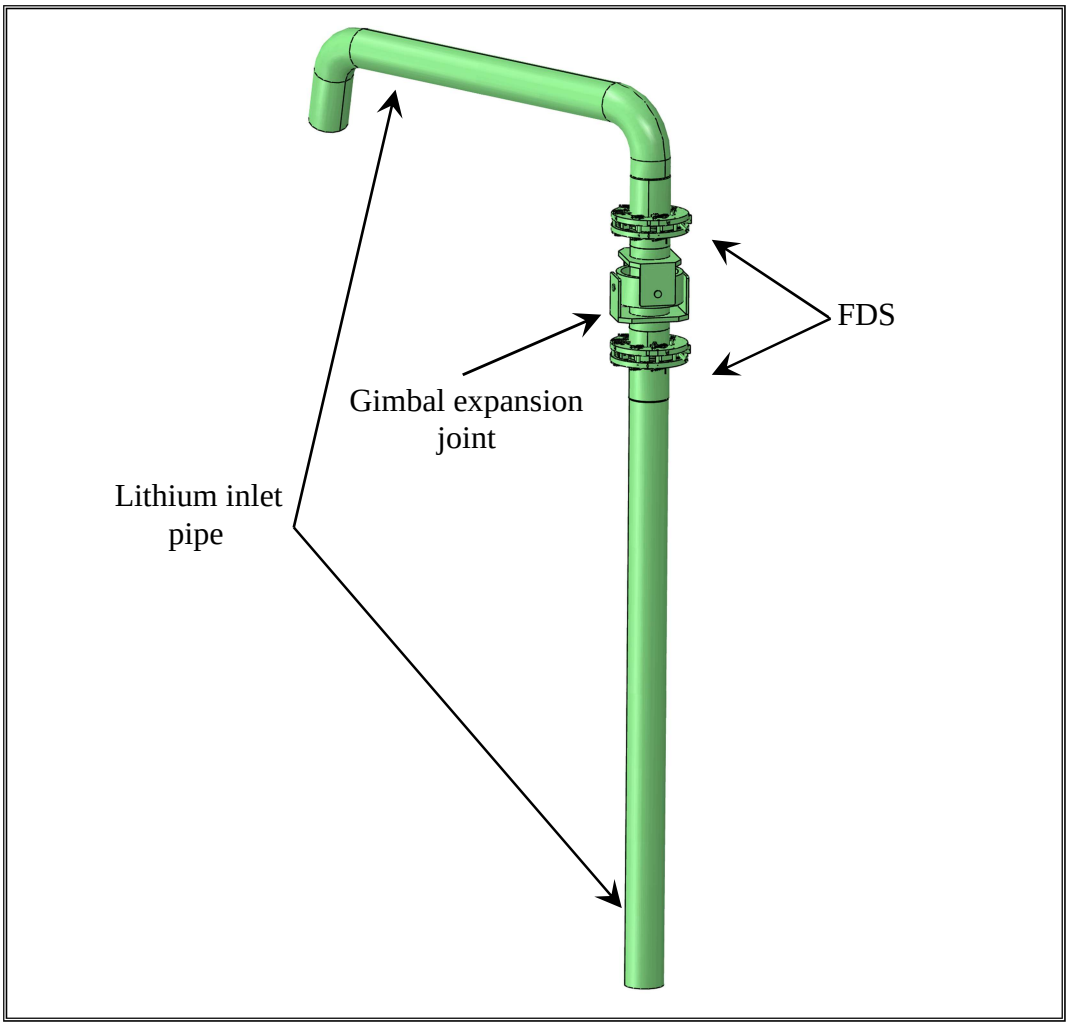

Figure 2-7. Lithium inlet pipe.

Each FDS permits to easily and quickly connect or disconnect base and removable flanges by simply acting (by remote) on only one screw. The seal is the heart and the most delicate item of the FDS project, and it is ensured by a metallic gasket operating by axial pressure

mode. Apart from the removable flange and the gasket, which are removed together with the Target Assembly, the rest of the FDS is attached to the fixed part of the Lithium Loop. The FDS is equipped with a leak detection system, used to get an alarm in case the liquid lithium would flow out of the two connected flanges. A more detailed description of FDS, leak detection system components and the detachment system functioning is reported in [19].

The gimbal expansion joint is able to compensate angular movements between the flanges of the two inlet pipe sections. It is aimed at compensating thermal expansions during IFMIF normal operation phase and misalignments during target system installation. Further details on the gimbal expansion joint foreseen for the lithium inlet pipe may be found in [19].

The purification loop consists of a cold trap and two hot traps, to remove various impurities, and of auxiliary supporting equipment. Major impurities are Protium (H), Deuterium (D), Tritium (T), ^{7}Be, activated corrosion products and other species (C, N, O) [16].

Table 2-1. Main Lithium loop specifications [19].

Lithium inventory	9 m^3
Lithium flow rate	130 l/s (maximum)
Lithium flow velocity	10 – 20 m/s (at the target section)
Lithium temperature	250 – 300 °C (nominal conditions)
	≤ 350°C (emergency)
	400 °C (design limit)
Lithium pressure	10^{-3} Pa (at vacuum interface in the target chamber)
	12 kPa (maximum value at BP interface)
	10^{-3} Pa (target quench tank under operation)

2.3. The test facility

The test facility consists in the modules devoted to housing the samples of the materials to be irradiated and all other areas and devices able to manage the specimens after the irradiation. In particular, in IFMIF there are foreseen three different irradiation modules, the High (HFTM), the Medium (MFTM) and the Low Flux Test Module (LFTM) [20]. The HFTM (Fig. 2-8) is basically a vessel with 12 irradiation rigs containing the encapsulated specimens at the desired irradiation temperature and cooled by helium gas flowing through narrow gaps of typically 1 mm width between the rig walls. The specimens are all of reduced size and they are immersed in a NaK bath [21]. An irradiation damage intensity in the range between 20-50 DPA/y is foreseen to be reached in this module.

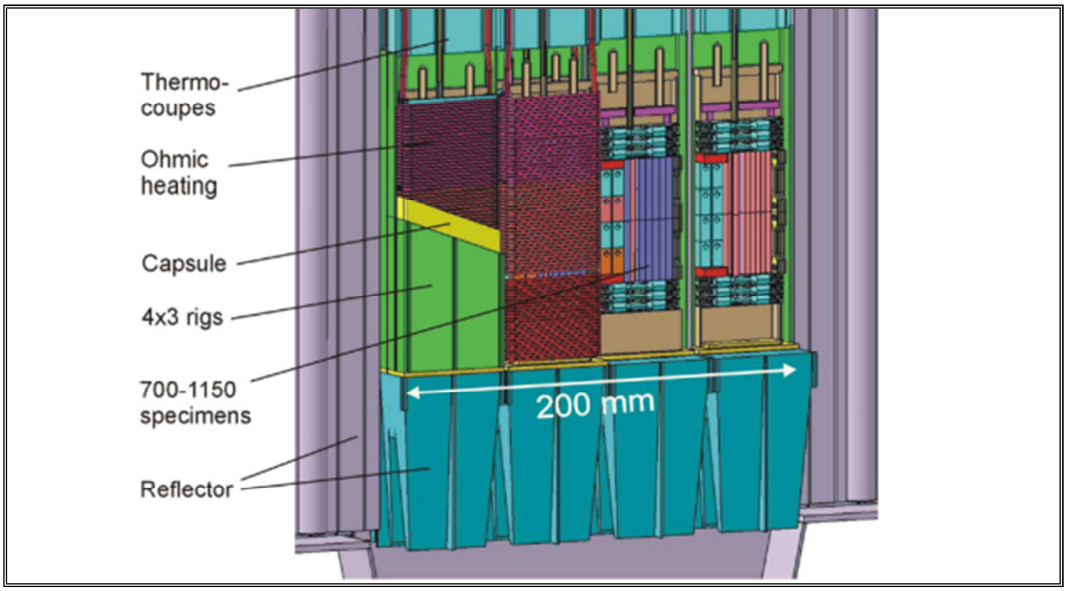

Figure 2-8. Section of the HFTM module.

The MFTM is a module where it is foreseen to perform *in situ* creep fatigue and tritium release tests, as well as test on liquid breeder materials, while the LFTM is a region where diagnostic components, ceramic and superconducting materials could be tested [21]. All these modules, together with the TA, are contained in the test cell (Fig. 2-9), a concrete building endowed with cooling channels in which helium will flow assuring the removal of the heat power deposited by neutrons and gammas interacting with the structural materials. A steel liner covers the inner walls of the test cell in order to avoid the happening of the highly energetic reactions between lithium and concrete in case of a lithium leak.

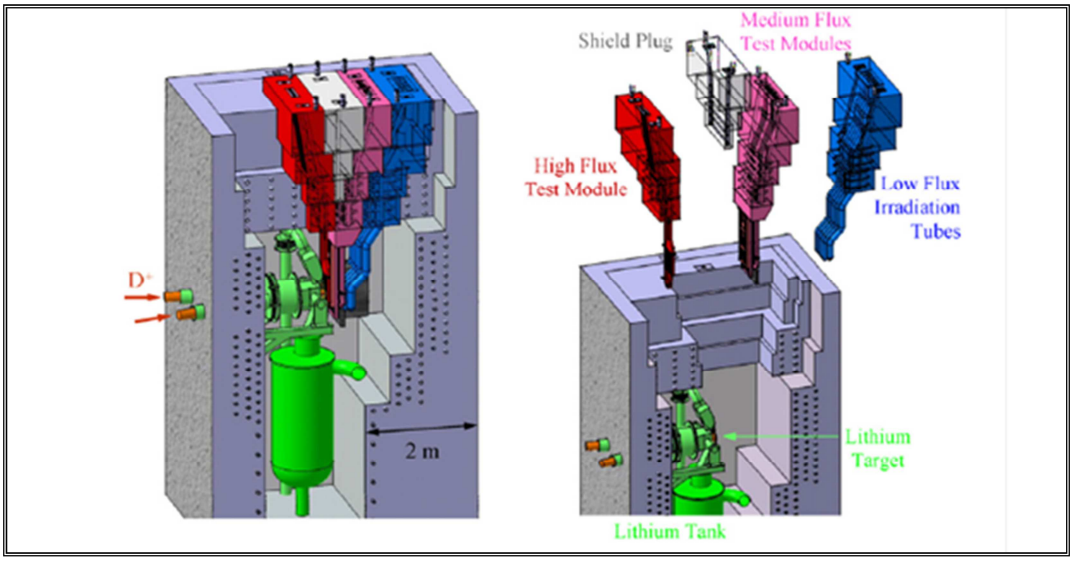

Figure 2-9. View of the test cell.

During the IFMIF/EVEDA phase of the project several mock-ups and prototypes of different section of the facility have been set-up [22]. Results obtained from these experimental activities will be carefully assessed and the most promising design solutions will be adopted to achieve the final IFMIF design, which will be developed during the next phases of the project. One of them is the mock-up of the IFMIF target system at ENEA-Brasimone, which is foreseen to experience the pre-heating phase of the IFMIF start-up transient. In particular, the experimental campaign is mainly intended to the determination of a pre-heating strategy able to gradually rise the target system temperature up to the values foreseen in the IFMIF operational phase, in order to avoid the insurgence of intense thermal stresses that could jeopardize the TA geometry and the lithium flow channel.

3. IFMIF target system mock-up thermal analysis

The determination of a strategy able to assure a gradual heating of the IFMIF TA is one of the main goals of the experimental campaign foreseen at ENEA Brasimone on the target system mock-up. In order to gradually and homogeneously rise the mock-up temperature up to the target value of 250 °C a proper time-dependent load profile has to be set-up for the electric heaters applied onto the mock-up external surfaces.

In the framework of this activity and of a fruitful collaboration existing between the ENEA and the Department of Energy, Information Engineering and Mathematic Models (DEIM) of the University of Palermo, a theoretical-numerical campaign has been launched at the DEIM in order to set-up a proper load profile for the electric heaters. The research activity has been performed adopting the Finite Element Method (FEM) and using the quoted FEM code Abaqus v.6.14 [13].

The experimental campaign foreseen at the ENEA-Brasimone research centre will be used to *ex post* validate the FEM model set-up, even though only from the thermal point of view.

3.1. The IFMIF target system mock-up

In order to qualify the design of the IFMIF target system, a mock-up of the European concept of the target system has been realized at ENEA-Brasimone [23]. It realistically reproduces the most recent design of the IFMIF target system, properly integrated with its support framework and the entire Lithium inlet pipe, including the following main components (Fig. 3-1):

- the Lithium inlet pipe;
- the gimbal expansion joint;
- the FDSs;
- the Beam Duct;
- the Inlet Nozzle;
- the Back-Plate;
- the Interface Frame;
- the Target Chamber;
- the Outlet nozzle;
- the Support Framework.

The Inlet and Outlet Nozzles, the Target Chamber and Interface Frame form the so called Target Assembly (TA). The TA is supported by the Target Chamber arms laying on the Support Framework, directly fixed to the ground by means of a proper bolt system, and it is welded to the Lithium inlet pipe. Regarding structural materials employed for the mock-up

construction, it has been realized using AISI 316 steel for the Back-Plate (BP) and AISI 304 steel for all the remaining components [23], differently from the IFMIF target system in which the European reduced activation ferritic/martensitic (RAFM) steel EUROFER has been selected as structural material for almost all the components.

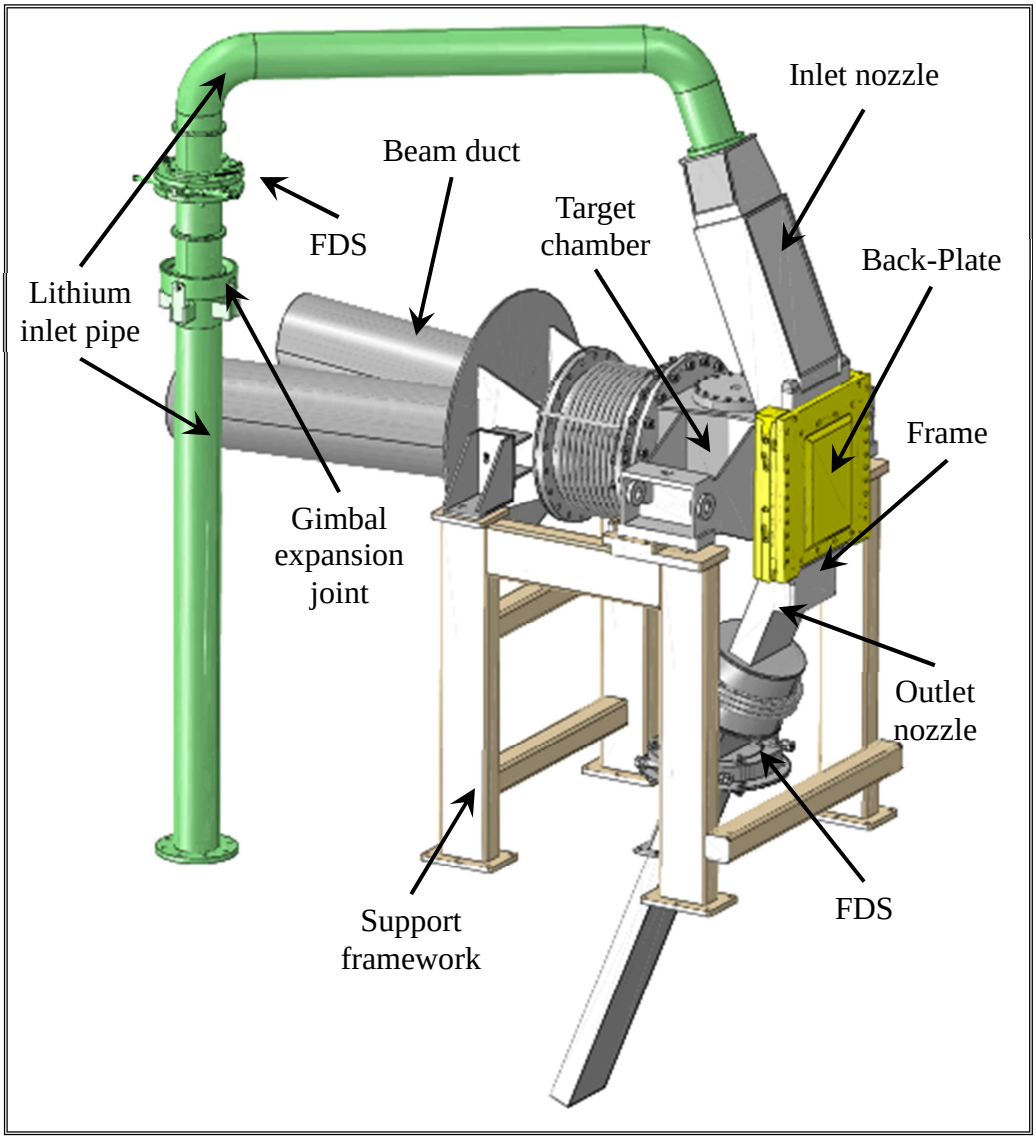

Figure 3-1. The mock-up of the IFMIF target system realized at ENEA Brasimone.

Differently from the IFMIF target system design, the mock-up realized at ENEA Brasimone is endowed with only one FDS in the Lithium inlet pipe region. Moreover, the presence of the accelerator system has been taken into account by constructing a double pipe, connected to the Target Chamber by a proper bolt system, which represents the Beam Duct foreseen in IFMIF.

It has to be underlined that the mock-up of the target system does not reproduce the whole IFMIF Lithium Loop, except for the Lithium inlet pipe. In fact, the target system mock-up does not foresee the presence of the liquid lithium, being envisaged to allow the achievement of two main goals: the validation of the remote handling devices devoted to perform the maintenance operations on the target system and the reproduction of the electric heaters action foreseen during the initial phase of the IFMIF target system start-up.

As far as the remote handling procedures are concerned [24-25], they play a fundamental role in IFMIF maintenance phase, due to the high dose rate predicted in the test cell housing the target system. In fact, nuclear activation reactions will take place between neutrons, generated within the beam footprint region, and structural materials nuclei, making the test cell internals hostile to human presence. Therefore, the periodic BP substitution and any maintenance activity foreseen for the target system must be executed using robotic devices governed by remote. Hence, experimental campaigns will be carried out on the target system mock-up in order to validate all the remote-governed devices and the pertinent operating procedures, devoted to execute the BP insertion and removal from the fixed interface frame of the Target Assembly, as well as the FDSs tightening and detachment mechanical operations [24-25].

As far as the reproduction of the IFMIF start-up is concerned, and in particular the first of the three sub-phases in which it is articulated, named pre-heating phase [14], a proper set of electric heaters is necessary to perform the pre-heating of the structure before lithium begins to flow into the target system, in order to avoid the insurgence of particularly intense thermal gradients between lithium, that enters the target system at 250 °C, and the structure at room temperature. In fact, large thermal gradients may originate particularly intense stresses within the structure, jeopardizing the seal of the gasket interposed between the BP and the frame. For this reason, particular attention should be paid to the thermal field arising within BP at the end of the pre-heating phase, since it is the most critical component of the entire target system. Therefore an excessive temperature difference between the BP lithium channel surface and the lithium flow should be avoided in order to minimize the thermal induced stress within the component.

Furthermore, during the pre-heating phase, the electric heaters action needs to be properly tuned adopting a purposely set up time-dependent load profile, in order to avoid a non-homogeneous increase of the temperature within the structure that may cause the insurgence of high thermal gradients between adjacent components. For these reasons, the experimental activity performed on the target system mock-up, aimed at reproducing the pre-heating phase, will be mainly focused onto the testing of electric heaters action and the mapping of the thermal field arising within BP.

It is obvious that the execution of the experimental activity aimed at reproducing the TA pre-heating phase has to be based on the knowledge of a purposely set up electric heaters

time-dependent load profile, able to increase the mock-up temperature within the different components as much uniformly as possible during the entire pre-heating phase of the transient operational start-up.

3.2. The FEM model

A realistic 3D model of the IFMIF target system mock-up set-up at ENEA Brasimone has been developed. The model reproduces the Target Assembly integrated with its Support Framework and the entire Lithium inlet pipe. An overview of the 3D geometric model is reported in figures 3-2 and 3-3.

It has to be noted that the two FDSs, the gimbal expansion joint of the Lithium inlet pipe and the Beam duct, foreseen in the target system mock-up design (Fig. 3-1), have not been directly included in the 3D geometric model.

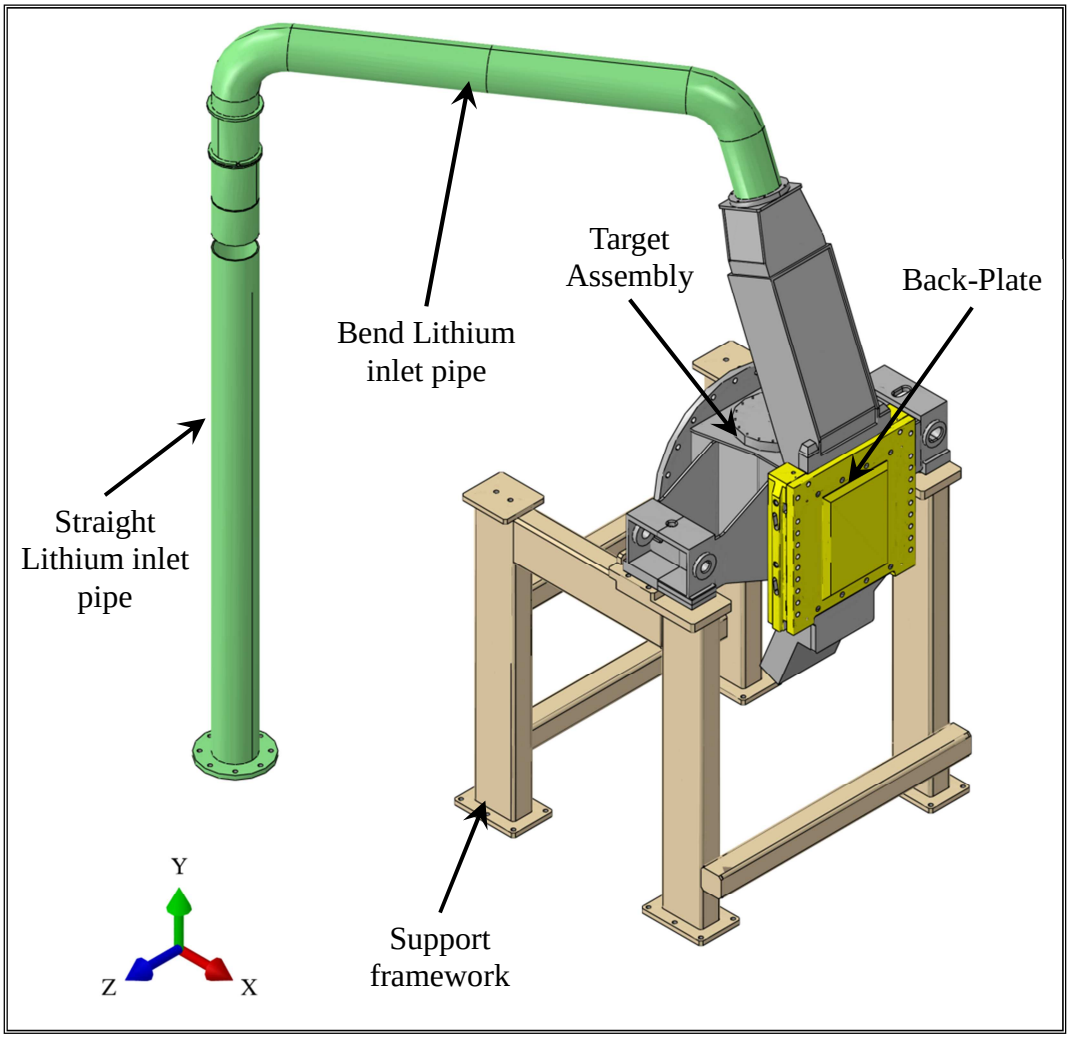

Figure 3-2. Mock-up 3D geometric model. General overview.

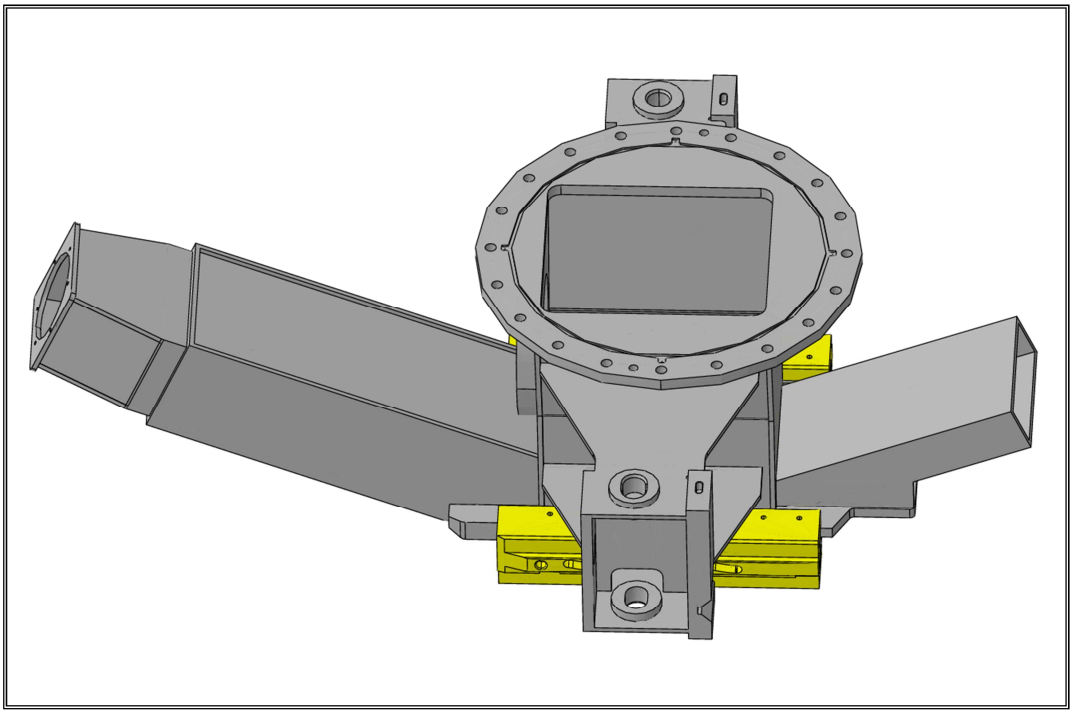

Figure 3-3. Mock-up 3D geometric model. Target Assembly and Back-Plate lateral view.

Nevertheless, their thermal effects have been simulated, as explained in the following, imposing appropriate thermal boundary conditions and contact models. This simplifying assumption leads to a substantial reduction in terms of calculation time without incurring in a significant loss of information.

A mesh independence analysis (details of the BP FEM models in Tab. 3-1) has been preliminarily performed on the BP, since it is the most critical component, in order to select an optimized spatial discretization which allows accurate results to be obtained saving calculation time. The mesh adopted for the first FEM model was not sufficiently accurate, while results obtained with the last two models were very similar. Since the requested calculation time in case of FEM model number three was ~5 times greater than FEM model number two, this last FEM model has been selected as the reference one.

Table 3-1. Characteristic values of different BP FEM models.

Approximate mesh size [m]	Model	Node number	Element number
0.020	1	55265	251657
0.010	2	86491	409208
0.005	3	192370	968198

A mesh composed of about $5 \cdot 10^5$ nodes connected in about $2 \cdot 10^6$ linear tetrahedral

elements, listed within FEM code libraries, has been finally selected for the whole model. The most representative views of the selected spatial discretization are reported in figures 3-4÷3-6. The so formed spatial discretization allows numerical simulations to be carried out in about 24 hours.

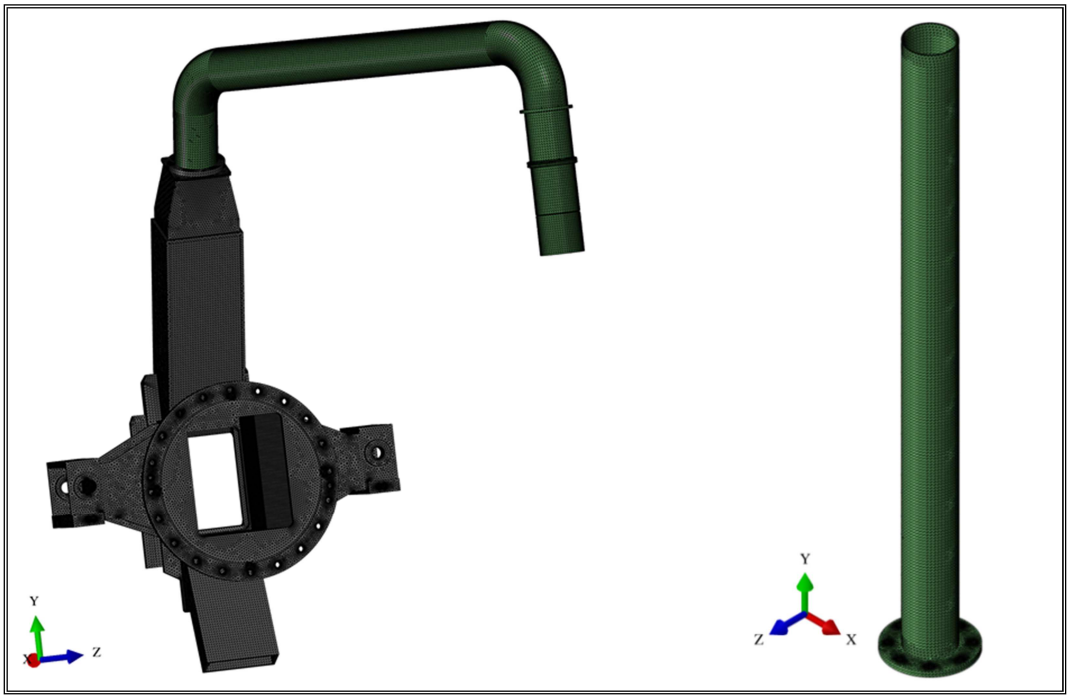

Figure 3-4. Mock-up FEM model. Target Assembly and Lithium inlet pipe exploded view.

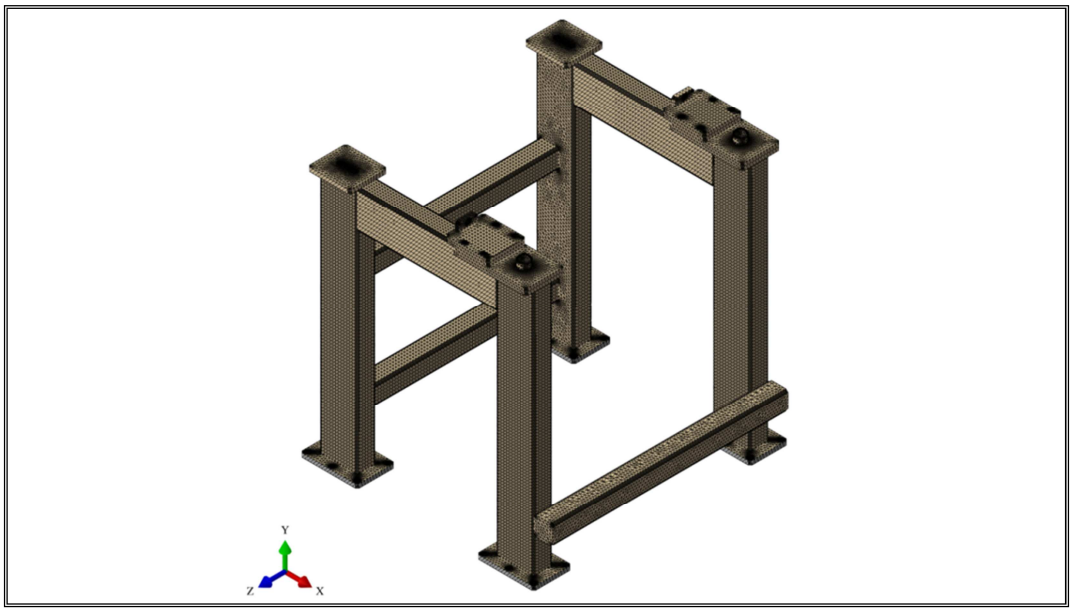

Figure 3-5. Mock-up FEM model. Particular of the Support framework.

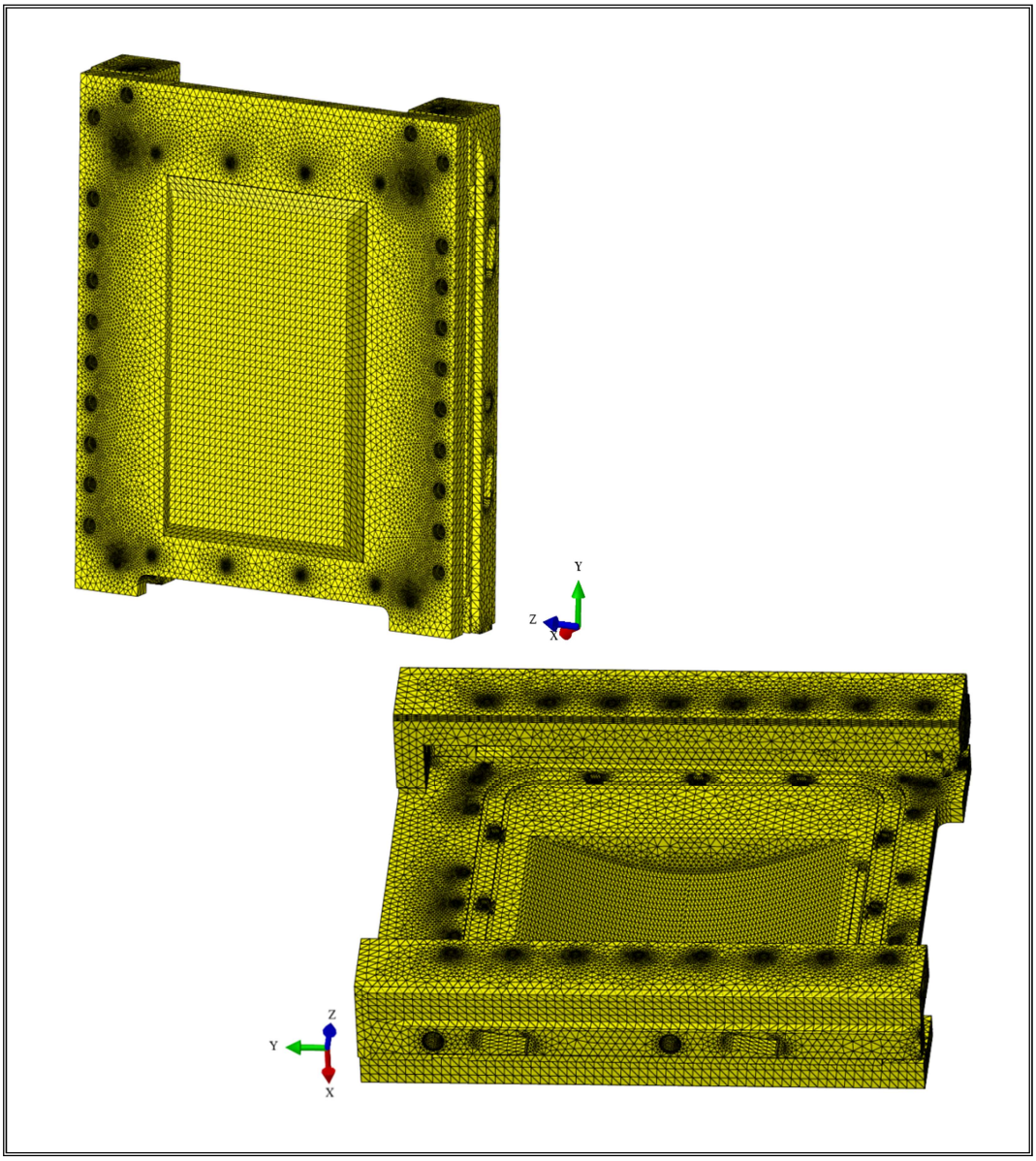

Figure 3-6. Mock-up FEM model. Particular of the Back-Plate.

3.2.1. Materials

According to the design of the IFMIF target system mock-up installed at ENEA Brasimone laboratories, AISI 304 steel has been assumed as the Target Assembly, support framework and Lithium inlet pipe structural material. As far as the Back-Plate is concerned, it has been considered to be made of AISI 316 steel.

The structural material thermo-physical properties have been assumed to depend uniquely on temperature, as indicated in [26-28]. The thermo-physical propertie values at the room temperature of 20 °C are summarized in tables 3-2 and 3-3, while temperature-dependent

behaviour of the thermo-physical properties of considered materials, normalized at the room temperature value, can be deduced from Figures 3-7 and 3-8.

Table 3-2. AISI 304 steel thermo-physical properties at 20°C [26].

AISI 304 STEEL	
λ_0	14.28 W/m K
c_{p0}	472 J/kg K
α_0	$1.53 \cdot 10^{-5}$ K^{-1}
ρ_0	7930 kg/m³

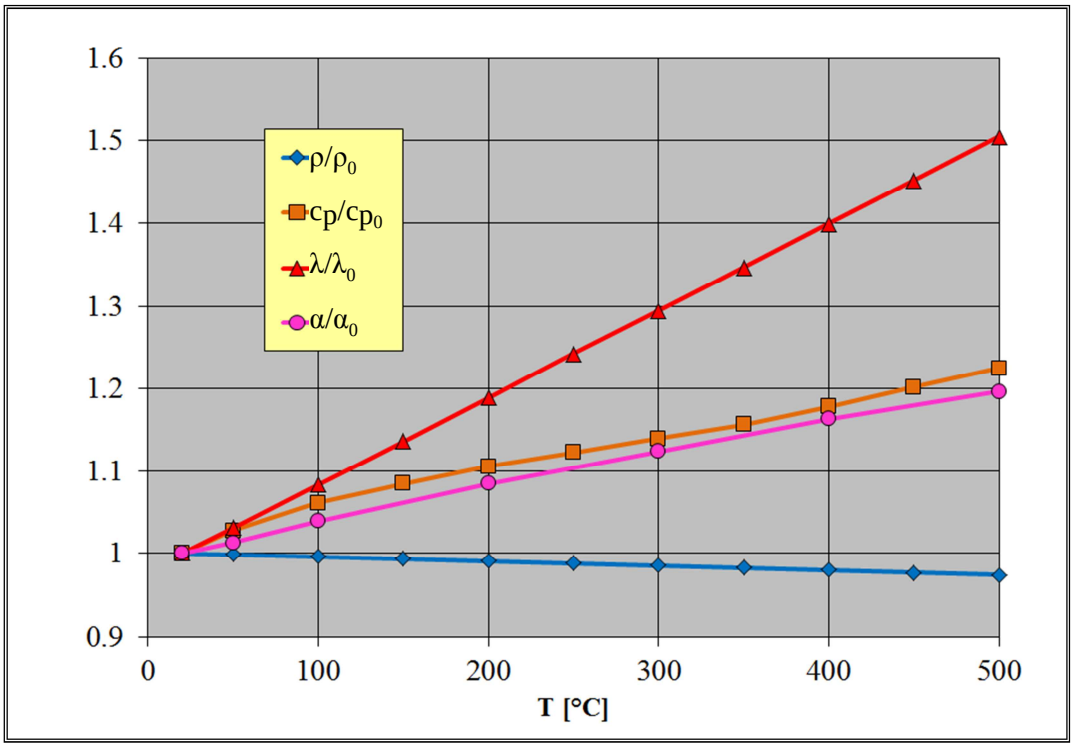

Figure 3-7. AISI 304 steel temperature-dependent thermo-physical properties.

Table 3-3. AISI 316 steel thermo-physical properties at 20°C [27-28].

AISI 316 STEEL	
λ_0	15 W/m°C
c_{p0}	452 J/kg°C
α_0	$1.54 \cdot 10^{-5}$ K^{-1}
ρ_0	7950 kg/m^3

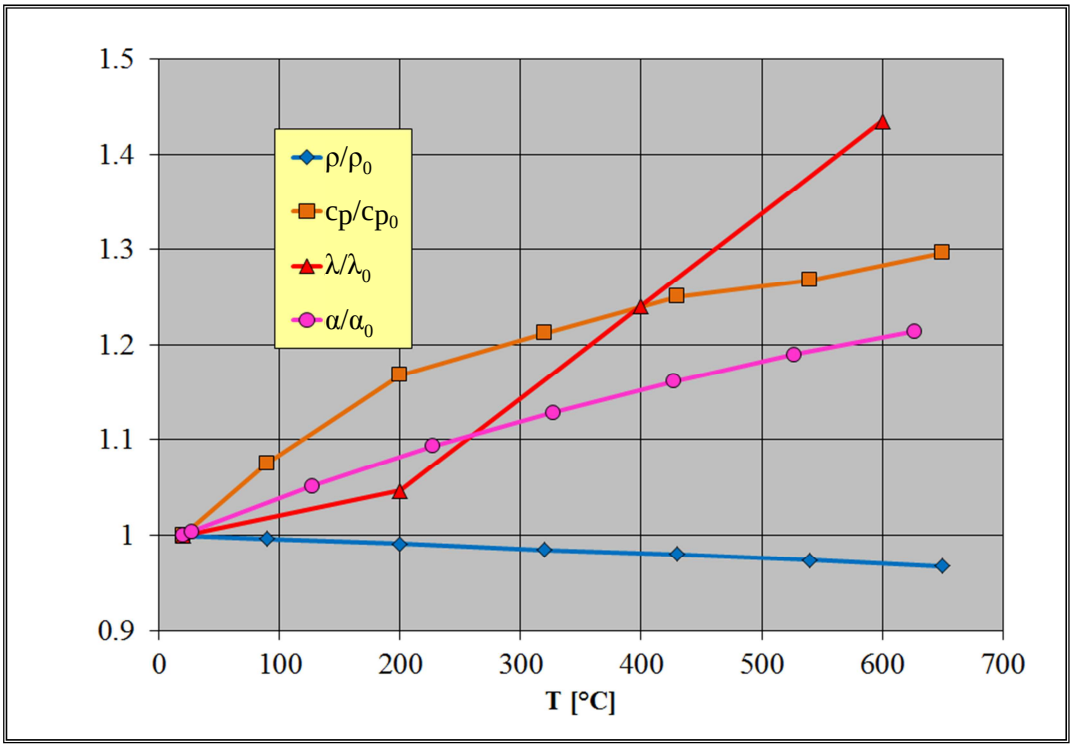

Figure 3-8. AISI 316 steel temperature-dependent thermo-physical properties.

3.2.2. Thermal interactions, loads and boundary conditions

The following thermal interactions, loads and boundary conditions have been assumed to simulate the TA, integrated with its support framework and Lithium inlet pipe, thermal behaviour under the pre-heating phase of the transient scenario:

- thermal interactions;
- heat transfer between Target Chamber and Beam duct;
- time-dependent heat fluxes;
- internal irradiation;
- external irradiation;
- TA and Support framework natural convective cooling;
- heat transfer between BP and High Flux Test Module.

Thermal interactions between frame and BP have been simulated by a thermal contact model which foresees the following functional dependence of the heat flux between two coupled nodes i and j, q_{ij}, on their temperatures, T_i and T_j:

$$q_{ij} = H\left(T_i - T_j\right) \tag{3-1}$$

where H represents the thermal conductance between the two interacting components, which has been set to 2000 W/m² °C [29]. As to the gimbal expansion joint simulation, a proper

coupling thermal model between straight and bend Lithium inlet pipe sections has been taken into account. All the other components of the model have been considered as a continuum from the thermal point of view.

Thermal interactions between Target Chamber (TC) and Beam duct have been simulated by imposing, according to [9,19], an effective thermal conductance coefficient equal to 15.8 W/m² °C on the TC flange surface (red surface in Fig. 3-9) and a non-uniform bulk temperature, T_L, analytically derived from a 1-D simplified model of the beam duct conductive-radiative heat transfer. This temperature value has been purposely set-up since the Beam duct cannot be considered in thermal equilibrium with the containment vessel atmosphere. In particular, this 1-D model has been developed to analytically find out the dependence of the Beam duct temperature spatial profile, $T(x,T_0)$, on TC flange temperature, T_0, so to obtain the functional dependence of the aforementioned bulk temperature on the corresponding TC flange temperature T_0, as $T_L(T_0)=T(L,T_0)$ (Fig. 3-10).

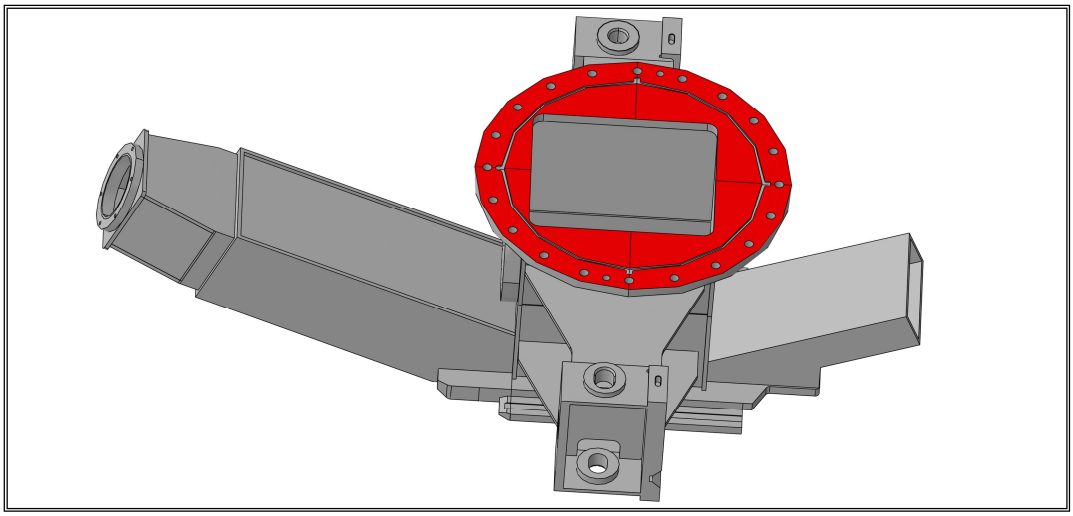

Figure 3-9. Target Chamber flange surface.

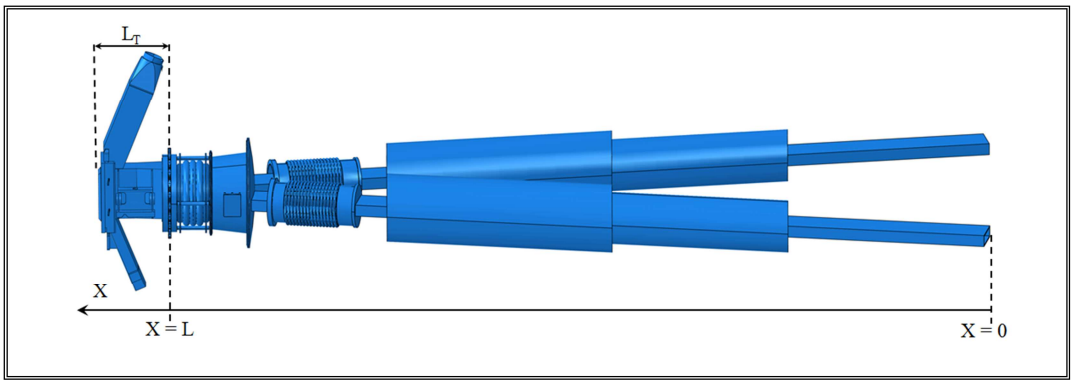

Figure 3-10. Geometric model for the $T(L,T_0)$ calculation.

The model is based on the hypothesis that beam duct radiates, with an emissivity of 0.3 [9], towards the containment vessel atmosphere assumed at 20 °C and that it is thermally coupled to the TC by means of an effective thermal conductance coefficient equal to 15.8 W/m² °C.

In order to simulate the discontinuous electric heaters action in the pre-heating phase of the start-up transient loading scenario [14], a proper set of time-dependent heat fluxes has been imposed to the mock-up external surfaces by a purposely set-up FORTRAN routine, on the basis of the electric heaters spatial arrangement foreseen for the experimental campaigns on the TA mock-up (Fig. 3-11). The values of the heat fluxes have been assumed on the basis of the technical specifications of the electric heaters devoted to perform the experimental campaigns on the TA mock-up.

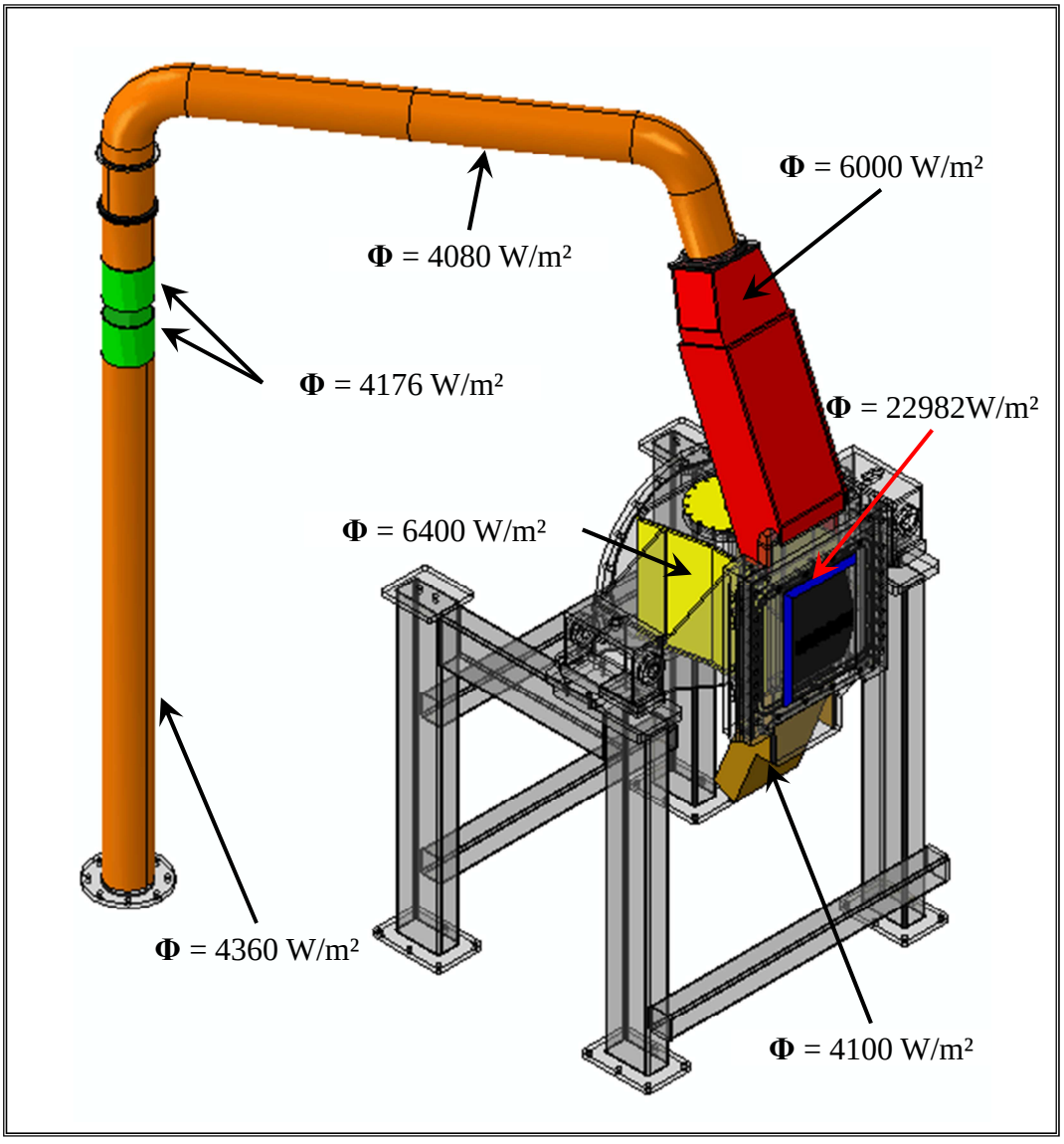

Figure 3-11. Heat fluxes from electric heaters.

Since the present study has been devoted to set-up the electric heaters load profile able to ensure a temperature increase within the structure as much uniform as possible, an iterative approach has been followed in order to determine the most appropriate electric heater load profile.

The iterative procedure has been based on modifications of the FORTRAN routine whenever a specific criterion, described in the following and based on the maximum temperature achieved within the most critical components was not met.

Radiation heat transfer occurring between internal walls of the mock-up has been modelled adopting the cavity radiation formulation widely described in [30,31]. It is based on the definition of a proper cavity articulated in mutually radiating surfaces, which result to be composed of collections of element facets.

Assuming that grey body radiation theory holds, considering only diffuse and, consequently, non-directional reflection from facets and neglecting radiation attenuation in the cavity medium, it is possible to derive, under the further hypothesis of isothermal and iso-emissive facets, the following analytical expression for the radiation heat flux, q_i, that the i-th facet receives from the rest of the facets belonging to the same cavity:

$$q_i = \frac{\sigma \varepsilon_i}{A_i} \sum_j \varepsilon_j \sum_k F_{ik} C_{kj}^{-1} \left(\theta_j^4 - \theta_i^4 \right) \tag{3-2}$$

where σ is the Stefan-Boltzmann constant, A_i is the area of i-th facet, ε_i and ε_j are the emissivities of the i-th and j-th facets, F_{ik} is the viewfactor between the i-th and k-th facets, θ_i and θ_j are the absolute temperatures of the i-th and j-th facets and C_{kj} is given by:

$$C_{kj} = \delta_{kj} - \frac{\left(1 - \varepsilon_k\right)}{A_k} F_{kj} \tag{3-3}$$

with δ_{kj} representing the Kronecker's delta.

Since the mock-up structure is internally divided in six regions by means of internal plugs, a proper set of six radiation cavities, each reproducing one of the mock-up internal regions, has been defined in the 3D FEM model. The different radiation cavities set-up do not mutually interact from the radiation heat transfer point of view, due to the presence of the afore-mentioned dividing plugs.

The surfaces forming the six radiation cavities have been highlighted in figure 3-12 using different colours.

It has to be noted that no radiation has been allowed through the cavity opening at the top of the target chamber, since it is envisaged to be closed by the pipe simulating the presence of the beam ducts, and through the outlet nozzle exit section, since it is envisaged to be closed by a plug which reproduces the presence of the quench tank flange. Emissivity value of 0.3 has been adopted for all steel walls, as indicated in [9,28].

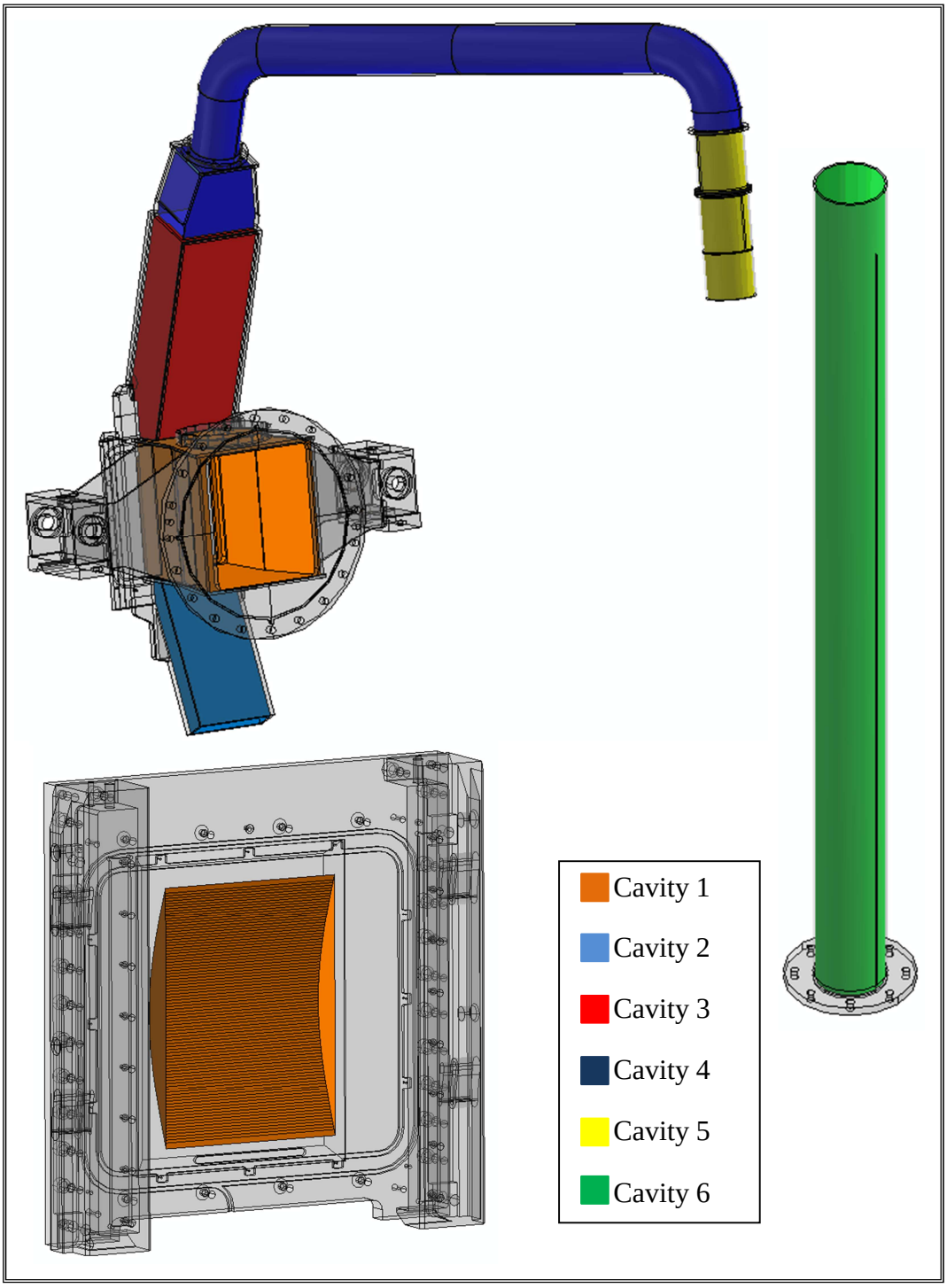

Figure 3-12. Radiation cavity surfaces.

Radiation heat transfer occurring externally between the mock-up un-insulated external surfaces and the atmosphere of the containment building has been modelled applying the following simplified condition to element facets which are supposed to be un-insulated during

the pre-heating phase of the start-up transient scenario:

$$q_{i0} = \sigma \varepsilon_i \left(\theta_i^4 - \theta_0^4 \right) \tag{3-4}$$

where q_{i0} and ε_i are, respectively, the radiation heat flux and the emissivity of the i-th element facet, set to 0.3 both for AISI 304 and AISI 316, while θ_0 is the absolute temperature of the test cell atmosphere, set to 293 K. In the present study, all the surfaces housing the electric heaters have been assumed as not radiating towards the containment building atmosphere since the external surface of electric heaters is thermally insulated. Radiating surfaces are highlighted in red in figure 3-13.

Regarding Target Assembly and Support framework natural convective cooling, the following Cauchy's boundary condition has been imposed to the nodes laying on the mock-up non-insulated surfaces (Fig. 3-13):

$$q_j = h \left(T_j - T_{atm} \right) \tag{3-5}$$

where q_j is the normal heat flux at the j-th node of the mock-up non-insulated surfaces, T_{atm} is the uniform bulk temperature of the containment building atmosphere, set to 20 °C, and h represents the convective heat transfer coefficient, which has been properly calculated and set equal to 10 W/m² °C [32].

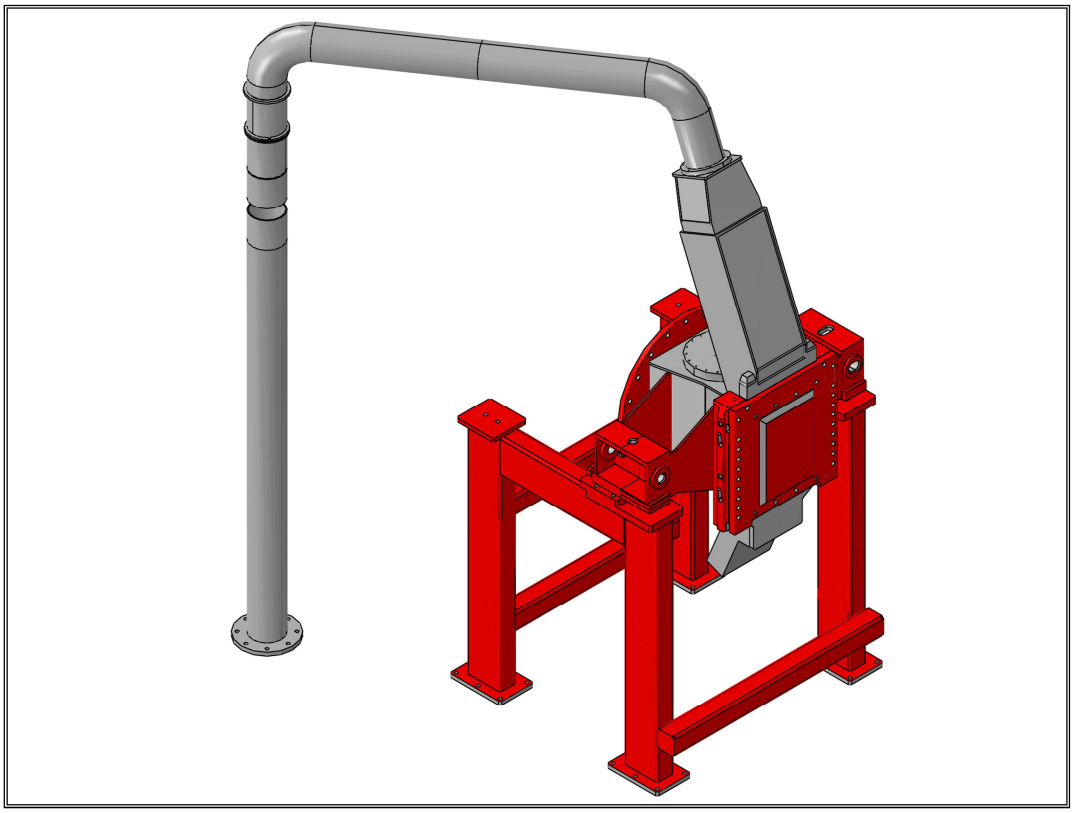

Figure 3-13. Radiating surfaces.

Thermal interactions between BP and High Flux Test Module (HFTM) have been taken into account positioning a steel plate, heated at the temperature of 50 °C, in front of the BP. The 2 mm minimum gap between the two components has been maintained as well. The heat transfer occurring between them has been simulated by imposing a Cauchy's boundary condition to the BP external surface directly facing the HFTM (Fig. 3-14), given by:

$$q_i = h\left(T_i - T_{HFTM}\right) \tag{3-6}$$

where q_i is the normal heat flux at the i-th BP node, T_{HFTM} is the uniform bulk temperature of the HFTM, set to 50°C according to [19], and h represents the thermal conductance between the two interacting components, which has been assumed to be:

$$h = \frac{\lambda}{d} \tag{3-7}$$

where λ is the thermal conductivity of containment vessel atmosphere (λ=0.026 W/m °C for air at 1 atm and 20 °C) and d represents the gap between the interacting components.

The value of h has been calculated considering that the condition of Nu = 1 can be assumed in the gap between the BP and the HFTM.

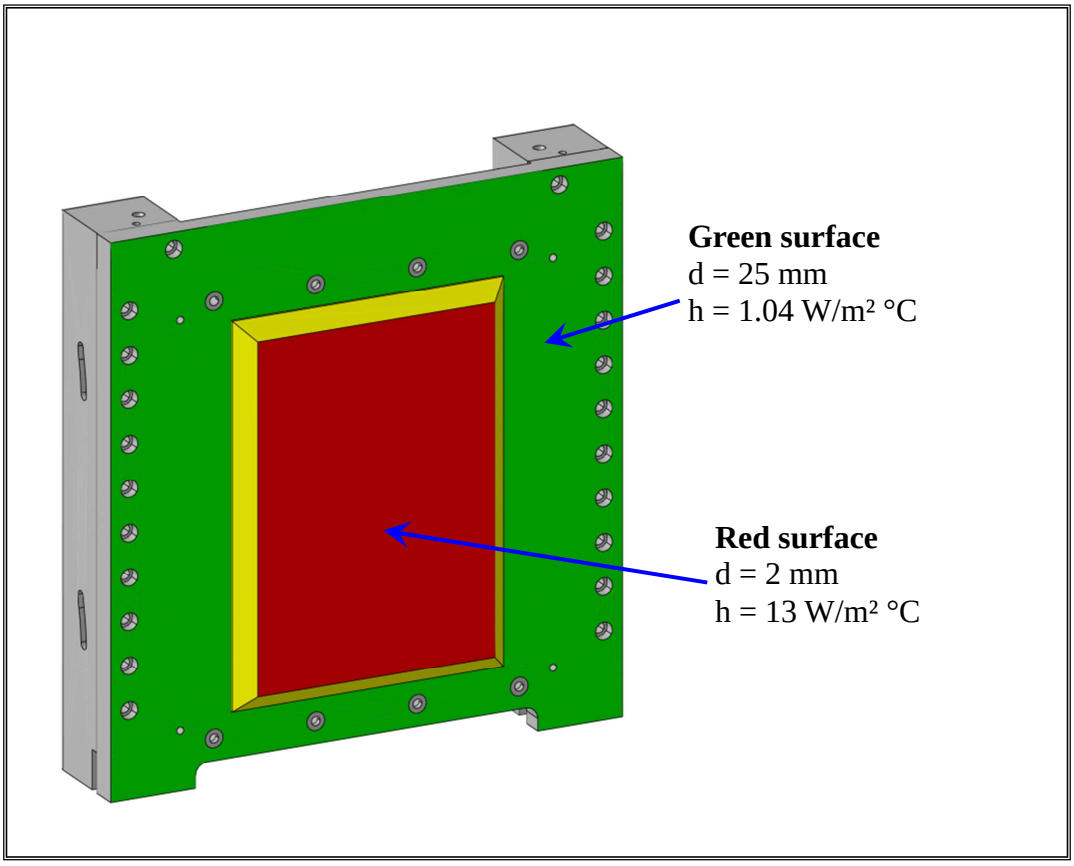

Figure 3-14. Back-plate and high flux test module thermal interaction surfaces.

3.3. Transient analysis and results

A campaign of thermal transient analyses has been carried out to investigate the target system mock-up thermal behaviour under the pre-heating phase of the IFMIF start-up loading scenario, in order to set-up a load profile for the electric heaters able to allow a structure heating as much uniform as possible.

A *try&fail* iterative procedure based on the analysis of the time evolution of the maximum temperature achieved within each component housing an electric heater has been set up in order to obtain a proper time-dependent load profile for each heater. In particular, the electric heater load profile has been modified whenever the maximum temperature increase within the above-said components was not sufficiently uniform. Moreover, once the maximum temperature of a component raised up to the reference value of 250 °C, the load profile was further modified in order to keep the maximum temperature of that component in the range between 240 °C - 260 °C, allowing the other components to be the heated up to the reference value of 250 °C. Adopting this criterion it has been possible to determine the relevant electric heater load profiles.

The obtained results have shown that, adopting this duty-cycle for the electric heaters, the steady state conditions are reached after a period of ~320 minutes. Although the heater on the BP is switched-on for the whole duration of the pre-heating phase, the maximum BP temperature is ~220 °C in the region housing the electric heater, while it remains well below 200 °C in the central region of the lithium flow channel (~125 °C).

The BP electric heater power and shape needs therefore a revision in order to ensure the achievement of higher temperatures within the BP and the lithium flow channel in particular. A strategy based on a different lay-out of the electric heaters, as well as an higher temperature value for the set point could be investigated in order to reach a temperature of at least 200 °C on the BP lithium flow channel and avoid the risk of lithium solidification.

Results in terms of maximum temperature time distributions are shown in figures 3-15 ÷ 3-18, while the thermal field arising at the end of the pre-heating phase is shown in figures 3-19 and 3-20. The electric heater load profiles have been reported in tables 3-4 ÷ 3-7.

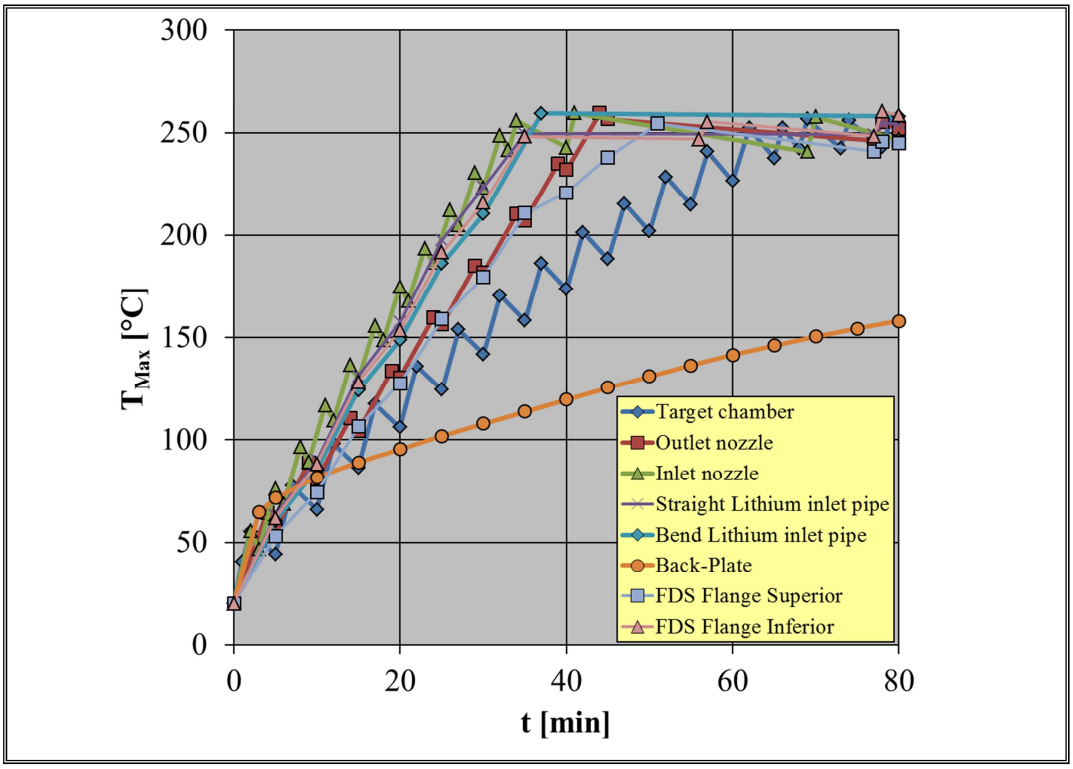

Figure 3-15. Maximum temperature vs time. 0-80 minutes.

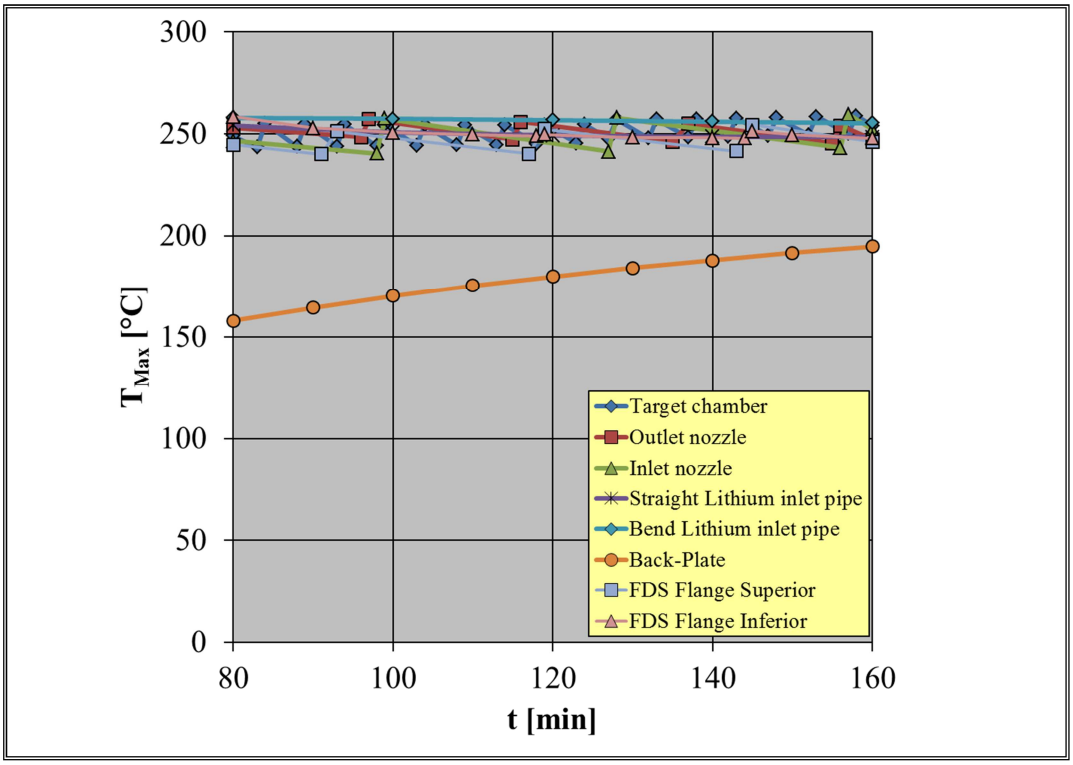

Figure 3-16. Maximum temperature vs time. 80-160 minutes.

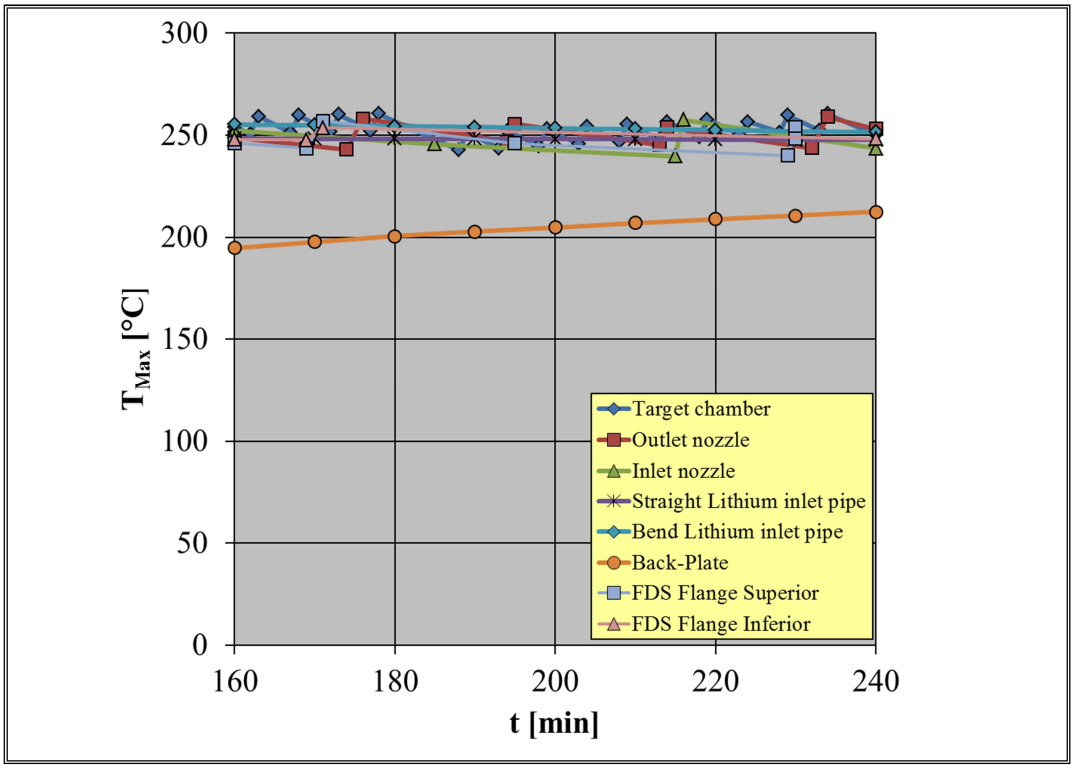

Figure 3-17. Maximum temperature vs time. 160-240 minutes.

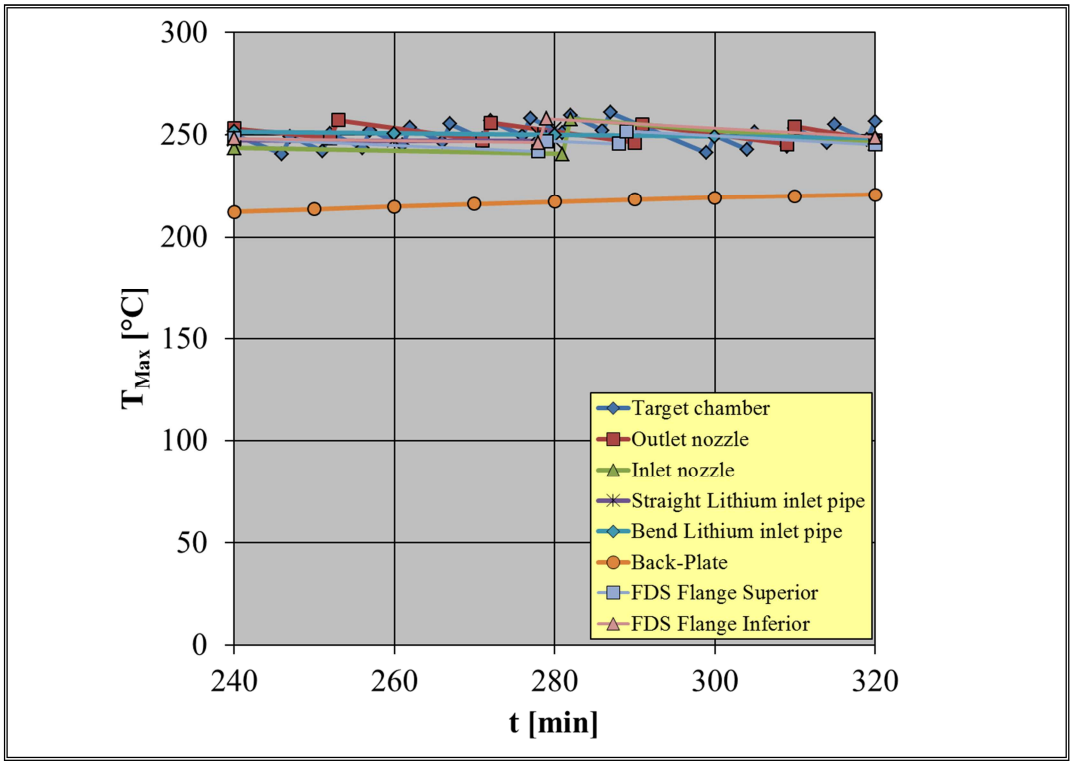

Figure 3-18. Maximum temperature vs time. 240-320 minutes.

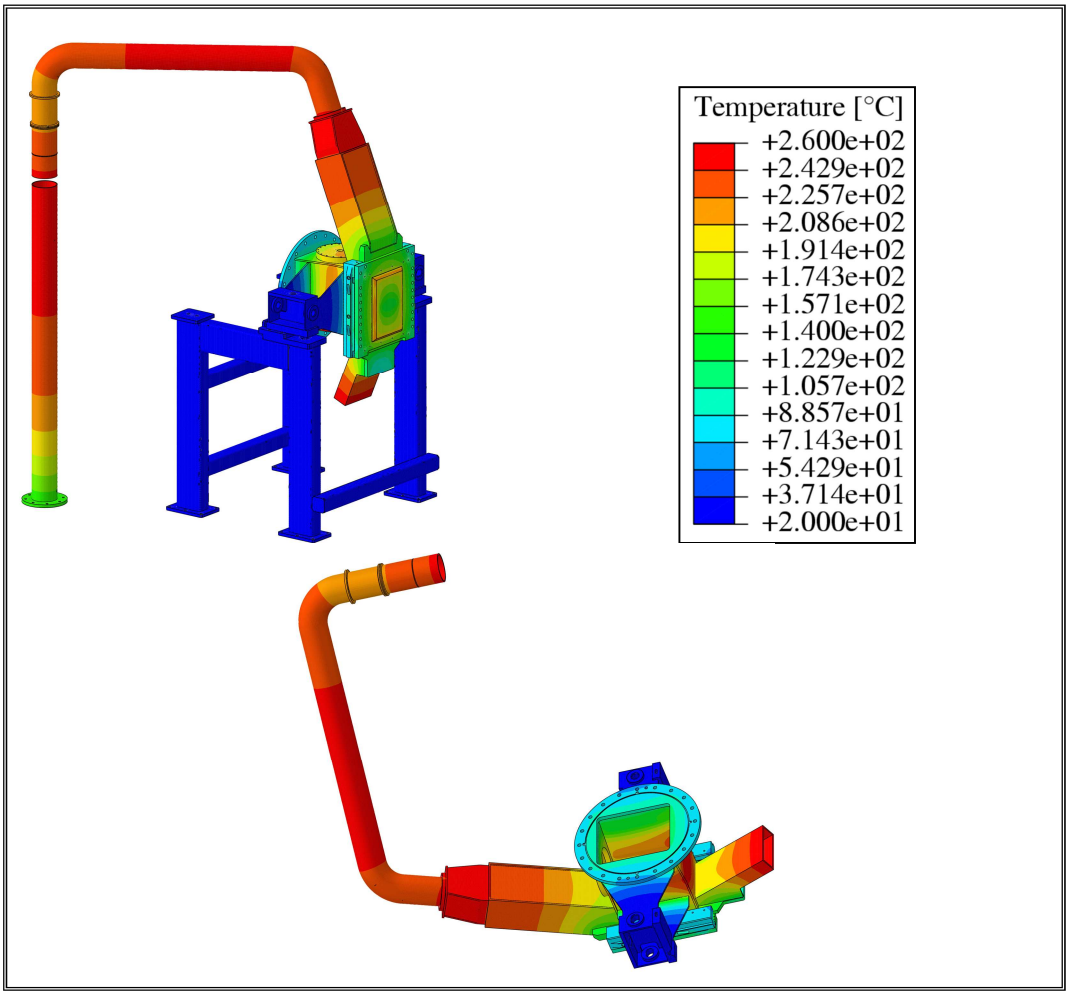

Figure 3-19. TA thermal field - t = 320 minutes.

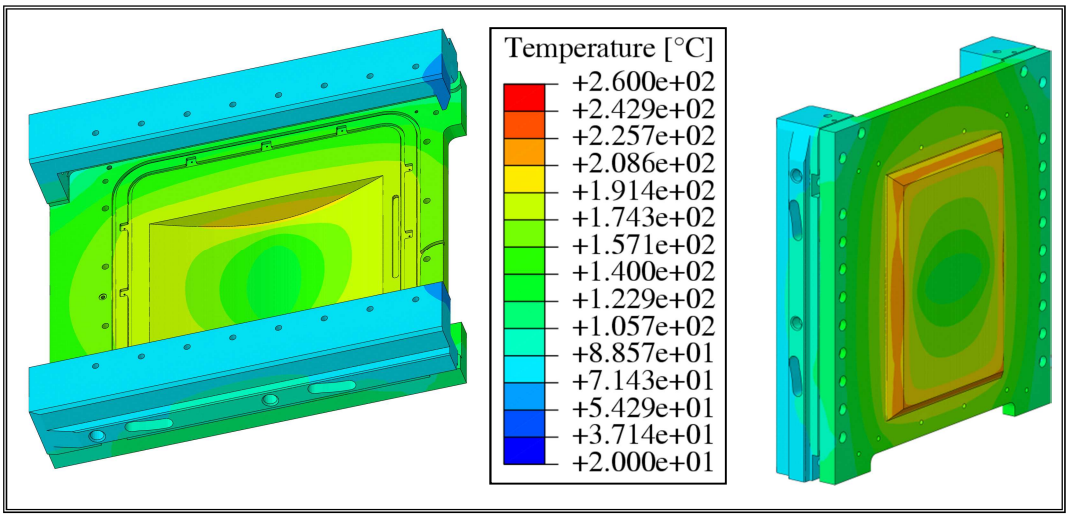

Figure 3-20. BP thermal field - t = 320 minutes.

Table 3-4. Electric heater load profile. 0-80 minutes.

Time [min]	Target chamber	Outlet nozzle	Inlet nozzle	Straight Lithium inlet pipe	Bend Lithium inlet pipe	FDS flange inferior	FDS flange superior	Back-Plate
0-1	ON	ON	ON	ON	ON	ON	ON	ON
1-2	ON	ON	ON	OFF	OFF	OFF	OFF	ON
2-3	OFF	ON	OFF	ON	ON	ON	ON	ON
3-4	OFF	ON	ON	OFF	OFF	OFF	OFF	ON
4-5	OFF	OFF	ON	ON	ON	ON	ON	ON
5-6	ON	ON	OFF	OFF	OFF	OFF	OFF	ON
6-7	ON	ON	ON	ON	ON	ON	ON	ON
7-8	OFF	ON	ON	OFF	OFF	OFF	OFF	ON
8-9	OFF	ON	OFF	ON	ON	ON	ON	ON
9-10	OFF	OFF	ON	OFF	OFF	OFF	OFF	ON
10-11	ON	ON	ON	ON	ON	ON	ON	ON
11-12	ON	ON	OFF	OFF	OFF	OFF	OFF	ON
12-13	OFF	ON	ON	ON	ON	ON	ON	ON
13-14	OFF	ON	ON	OFF	OFF	OFF	OFF	ON
14-15	OFF	OFF	OFF	ON	ON	ON	ON	ON
15-16	ON	ON	ON	OFF	OFF	OFF	OFF	ON
16-17	ON	ON	ON	ON	ON	ON	ON	ON
17-18	OFF	ON	OFF	OFF	OFF	OFF	OFF	ON
18-19	OFF	ON	ON	ON	ON	ON	ON	ON
19-20	OFF	OFF	ON	OFF	OFF	OFF	OFF	ON
20-21	ON	ON	OFF	ON	ON	ON	ON	ON
21-22	ON	ON	ON	OFF	OFF	OFF	OFF	ON
22-23	OFF	ON	ON	ON	ON	ON	ON	ON
23-24	OFF	ON	OFF	OFF	OFF	OFF	OFF	ON
24-25	OFF	OFF	ON	ON	ON	ON	ON	ON

25-26	ON	ON	ON	OFF	OFF	OFF	OFF	ON
26-27	ON	ON	OFF	ON	ON	ON	ON	ON
27-28	OFF	ON	ON	OFF	OFF	OFF	OFF	ON
28-29	OFF	ON	ON	ON	ON	ON	ON	ON
29-30	OFF	OFF	OFF	OFF	OFF	OFF	OFF	ON
30-31	ON	ON	ON	ON	ON	ON	ON	ON
31-32	ON	ON	ON	OFF	OFF	OFF	OFF	ON
32-33	OFF	ON	OFF	ON	ON	ON	ON	ON
33-34	OFF	ON	ON	OFF	OFF	OFF	OFF	ON
34-35	OFF	OFF	OFF	OFF	ON	ON	ON	ON
35-36	ON	ON	OFF	OFF	OFF	OFF	OFF	ON
36-37	ON	ON	OFF	OFF	ON	OFF	ON	ON
37-38	OFF	ON	OFF	OFF	OFF	OFF	OFF	ON
38-39	OFF	ON	OFF	OFF	OFF	OFF	ON	ON
39-40	OFF	OFF	OFF	OFF	OFF	OFF	OFF	ON
40-41	ON	ON	ON	OFF	OFF	OFF	ON	ON
41-42	ON	ON	OFF	OFF	OFF	OFF	OFF	ON
42-43	OFF	ON	OFF	OFF	OFF	OFF	ON	ON
43-44	OFF	ON	OFF	OFF	OFF	OFF	OFF	ON
44-45	OFF	OFF	OFF	OFF	OFF	OFF	ON	ON
45-46	ON	OFF	OFF	OFF	OFF	OFF	OFF	ON
46-47	ON	OFF	OFF	OFF	OFF	OFF	ON	ON
47-48	OFF	OFF	OFF	OFF	OFF	OFF	OFF	ON
48-49	OFF	OFF	OFF	OFF	OFF	OFF	ON	ON
49-50	OFF	OFF	OFF	OFF	OFF	OFF	OFF	ON
50-51	ON	OFF	OFF	OFF	OFF	OFF	ON	ON
51-52	ON	OFF	OFF	OFF	OFF	OFF	OFF	ON
52-53	OFF	OFF	OFF	OFF	OFF	OFF	OFF	ON

53-54	OFF	OFF	OFF	OFF	OFF	OFF	OFF	ON
54-55	OFF	OFF	OFF	OFF	OFF	OFF	OFF	ON
55-56	ON	OFF	OFF	OFF	OFF	OFF	OFF	ON
56-57	ON	OFF	OFF	OFF	OFF	ON	OFF	ON
57-58	OFF	OFF	OFF	OFF	OFF	OFF	OFF	ON
58-59	OFF	OFF	OFF	OFF	OFF	OFF	OFF	ON
59-60	OFF	OFF	OFF	OFF	OFF	OFF	OFF	ON
60-61	ON	OFF	OFF	OFF	OFF	OFF	OFF	ON
61-62	ON	OFF	OFF	OFF	OFF	OFF	OFF	ON
62-63	OFF	OFF	OFF	OFF	OFF	OFF	OFF	ON
63-64	OFF	OFF	OFF	OFF	OFF	OFF	OFF	ON
64-65	OFF	OFF	OFF	OFF	OFF	OFF	OFF	ON
65-66	ON	OFF	OFF	OFF	OFF	OFF	OFF	ON
66-67	OFF	OFF	OFF	OFF	OFF	OFF	OFF	ON
67-68	OFF	OFF	OFF	OFF	OFF	OFF	OFF	ON
68-69	ON	OFF	OFF	OFF	OFF	OFF	OFF	ON
69-70	OFF	OFF	ON	OFF	OFF	OFF	OFF	ON
70-71	OFF	OFF	OFF	OFF	OFF	OFF	OFF	ON
71-72	OFF	OFF	OFF	OFF	OFF	OFF	OFF	ON
72-73	OFF	OFF	OFF	OFF	OFF	OFF	OFF	ON
73-74	ON	OFF	OFF	OFF	OFF	OFF	OFF	ON
74-75	OFF	OFF	ON	OFF	OFF	OFF	OFF	ON
75-76	OFF	OFF	OFF	OFF	OFF	OFF	OFF	ON
76-77	OFF	OFF	OFF	OFF	OFF	OFF	OFF	ON
77-78	OFF	ON	OFF	OFF	OFF	ON	OFF	ON
78-79	ON	OFF	OFF	OFF	OFF	OFF	OFF	ON
79-80	OFF	OFF	OFF	OFF	OFF	OFF	OFF	ON

Table 3-5. Electric heater load profile. 80-160 minutes.

Time [min]	Target chamber	Outlet nozzle	Inlet nozzle	Straight Lithium inlet pipe	Bend Lithium inlet pipe	FDS flange inferior	FDS flange superior	Back-Plate
80-81	OFF	OFF	OFF	OFF	OFF	OFF	OFF	ON
81-82	OFF	OFF	OFF	OFF	OFF	OFF	OFF	ON
82-83	OFF	OFF	OFF	OFF	OFF	OFF	OFF	ON
83-84	ON	OFF	OFF	OFF	OFF	OFF	OFF	ON
84-85	OFF	OFF	OFF	OFF	OFF	OFF	OFF	ON
85-86	OFF	OFF	OFF	OFF	OFF	OFF	OFF	ON
86-87	OFF	OFF	OFF	OFF	OFF	OFF	OFF	ON
87-88	OFF	OFF	OFF	OFF	OFF	OFF	OFF	ON
88-89	ON	OFF	OFF	OFF	OFF	OFF	OFF	ON
89-90	OFF	OFF	OFF	OFF	OFF	OFF	OFF	ON
90-91	OFF	OFF	OFF	OFF	OFF	OFF	OFF	ON
91-92	OFF	OFF	OFF	OFF	OFF	OFF	ON	ON
92-93	OFF	OFF	OFF	OFF	OFF	OFF	ON	ON
93-94	ON	OFF	OFF	OFF	OFF	OFF	OFF	ON
94-95	OFF	OFF	OFF	OFF	OFF	OFF	OFF	ON
95-96	OFF	OFF	OFF	OFF	OFF	OFF	OFF	ON
96-97	OFF	ON	OFF	OFF	OFF	OFF	OFF	ON
97-98	OFF	OFF	OFF	OFF	OFF	OFF	OFF	ON
98-99	ON	OFF	ON	OFF	OFF	OFF	OFF	ON
99-100	OFF	OFF	OFF	OFF	OFF	OFF	OFF	ON
100-101	OFF	OFF	OFF	OFF	OFF	OFF	OFF	ON
101-102	OFF	OFF	OFF	OFF	OFF	OFF	OFF	ON
102-103	OFF	OFF	OFF	OFF	OFF	OFF	OFF	ON
103-104	ON	OFF	OFF	OFF	OFF	OFF	OFF	ON
104-105	OFF	OFF	OFF	OFF	OFF	OFF	OFF	ON

105-106	OFF	OFF	OFF	OFF	OFF	OFF	OFF	ON
106-107	OFF	OFF	OFF	OFF	OFF	OFF	OFF	ON
107-108	OFF	OFF	OFF	OFF	OFF	OFF	OFF	ON
108-109	ON	OFF	OFF	OFF	OFF	OFF	OFF	ON
109-110	OFF	OFF	OFF	OFF	OFF	OFF	OFF	ON
110-111	OFF	OFF	OFF	OFF	OFF	OFF	OFF	ON
111-112	OFF	OFF	OFF	OFF	OFF	OFF	OFF	ON
112-113	OFF	OFF	OFF	OFF	OFF	OFF	OFF	ON
113-114	ON	OFF	OFF	OFF	OFF	OFF	OFF	ON
114-115	OFF	OFF	OFF	OFF	OFF	OFF	OFF	ON
115-116	OFF	ON	OFF	OFF	OFF	OFF	OFF	ON
116-117	OFF	OFF	OFF	OFF	OFF	OFF	OFF	ON
117-118	OFF	OFF	OFF	OFF	OFF	OFF	ON	ON
118-119	ON	OFF	OFF	OFF	OFF	OFF	ON	ON
119-120	OFF	OFF	OFF	OFF	OFF	OFF	OFF	ON
120-121	OFF	OFF	OFF	OFF	OFF	OFF	OFF	ON
121-122	OFF	OFF	OFF	OFF	OFF	OFF	OFF	ON
122-123	OFF	OFF	OFF	OFF	OFF	OFF	OFF	ON
123-124	ON	OFF	OFF	OFF	OFF	OFF	OFF	ON
124-125	OFF	OFF	OFF	OFF	OFF	OFF	OFF	ON
125-126	OFF	OFF	OFF	OFF	OFF	OFF	OFF	ON
126-127	OFF	OFF	OFF	OFF	OFF	OFF	OFF	ON
127-128	ON	OFF	ON	OFF	OFF	OFF	OFF	ON
128-129	OFF	OFF	OFF	OFF	OFF	OFF	OFF	ON
129-130	OFF	OFF	OFF	OFF	OFF	OFF	OFF	ON
130-131	OFF	OFF	OFF	OFF	OFF	OFF	OFF	ON
131-132	OFF	OFF	OFF	OFF	OFF	OFF	OFF	ON
132-133	ON	OFF	OFF	OFF	OFF	OFF	OFF	ON

133-134	OFF	OFF	OFF	OFF	OFF	OFF	OFF	ON
134-135	OFF	OFF	OFF	OFF	OFF	OFF	OFF	ON
135-136	OFF	ON	OFF	OFF	OFF	OFF	OFF	ON
136-137	OFF	ON	OFF	OFF	OFF	OFF	OFF	ON
137-138	ON	OFF	OFF	OFF	OFF	OFF	OFF	ON
138-139	OFF	OFF	OFF	OFF	OFF	OFF	OFF	ON
139-140	OFF	OFF	OFF	OFF	OFF	OFF	OFF	ON
140-141	OFF	OFF	OFF	OFF	OFF	OFF	OFF	ON
141-142	OFF	OFF	OFF	OFF	OFF	OFF	OFF	ON
142-143	ON	OFF	OFF	OFF	OFF	OFF	OFF	ON
143-144	OFF	OFF	OFF	OFF	OFF	OFF	ON	ON
144-145	OFF	OFF	OFF	OFF	OFF	OFF	ON	ON
145-146	OFF	OFF	OFF	OFF	OFF	OFF	OFF	ON
146-147	OFF	OFF	OFF	OFF	OFF	OFF	OFF	ON
147-148	ON	OFF	OFF	OFF	OFF	OFF	OFF	ON
148-149	OFF	OFF	OFF	OFF	OFF	OFF	OFF	ON
149-150	OFF	OFF	OFF	OFF	OFF	OFF	OFF	ON
150-151	OFF	OFF	OFF	OFF	OFF	OFF	OFF	ON
151-152	OFF	OFF	OFF	OFF	OFF	OFF	OFF	ON
152-153	ON	OFF	OFF	OFF	OFF	OFF	OFF	ON
153-154	OFF	OFF	OFF	OFF	OFF	OFF	OFF	ON
154-155	OFF	OFF	OFF	OFF	OFF	OFF	OFF	ON
155-156	OFF	ON	OFF	OFF	OFF	OFF	OFF	ON
156-157	OFF	OFF	ON	OFF	OFF	OFF	OFF	ON
157-158	ON	OFF	OFF	OFF	OFF	OFF	OFF	ON
158-159	OFF	OFF	OFF	OFF	OFF	OFF	OFF	ON
159-160	OFF	OFF	OFF	OFF	OFF	OFF	OFF	ON

Table 3-6. Electric heater load profile. 160-240 minutes.

Time [min]	Target chamber	Outlet nozzle	Inlet nozzle	Straight Lithium inlet pipe	Bend Lithium inlet pipe	FDS flange inferior	FDS flange superior	Back-Plate
160-161	OFF	OFF	OFF	OFF	OFF	OFF	OFF	ON
161-162	OFF	OFF	OFF	OFF	OFF	OFF	OFF	ON
162-163	ON	OFF	OFF	OFF	OFF	OFF	OFF	ON
163-164	OFF	OFF	OFF	OFF	OFF	OFF	OFF	ON
164-165	OFF	OFF	OFF	OFF	OFF	OFF	OFF	ON
165-166	OFF	OFF	OFF	OFF	OFF	OFF	OFF	ON
166-167	OFF	OFF	OFF	OFF	OFF	OFF	OFF	ON
167-168	ON	OFF	OFF	OFF	OFF	OFF	OFF	ON
168-169	OFF	OFF	OFF	OFF	OFF	OFF	OFF	ON
169-170	OFF	OFF	OFF	OFF	OFF	OFF	ON	ON
170-171	OFF	OFF	OFF	OFF	OFF	OFF	ON	ON
171-172	OFF	OFF	OFF	OFF	OFF	OFF	OFF	ON
172-173	ON	OFF	OFF	OFF	OFF	OFF	OFF	ON
173-174	OFF	OFF	OFF	OFF	OFF	OFF	OFF	ON
174-175	OFF	ON	OFF	OFF	OFF	OFF	OFF	ON
175-176	OFF	ON	OFF	OFF	OFF	OFF	OFF	ON
176-177	OFF	OFF	OFF	OFF	OFF	OFF	OFF	ON
177-178	ON	OFF	OFF	OFF	OFF	OFF	OFF	ON
178-179	OFF	OFF	OFF	OFF	OFF	OFF	OFF	ON
179-180	OFF	OFF	OFF	OFF	OFF	OFF	OFF	ON
180-181	OFF	OFF	OFF	OFF	OFF	OFF	OFF	ON
181-182	OFF	OFF	OFF	OFF	OFF	OFF	OFF	ON
182-183	OFF	OFF	OFF	OFF	OFF	OFF	OFF	ON
183-184	OFF	OFF	OFF	OFF	OFF	OFF	OFF	ON
184-185	OFF	OFF	OFF	OFF	OFF	OFF	OFF	ON

185-186	OFF	OFF	OFF	OFF	OFF	OFF	OFF	ON
186-187	OFF	OFF	OFF	OFF	OFF	OFF	OFF	ON
187-188	OFF	OFF	OFF	OFF	OFF	OFF	OFF	ON
188-189	ON	OFF	OFF	OFF	OFF	OFF	OFF	ON
189-190	OFF	OFF	OFF	OFF	OFF	OFF	OFF	ON
190-191	OFF	OFF	OFF	OFF	OFF	OFF	OFF	ON
191-192	OFF	OFF	OFF	OFF	OFF	OFF	OFF	ON
192-193	OFF	OFF	OFF	OFF	OFF	OFF	OFF	ON
193-194	ON	OFF	OFF	OFF	OFF	OFF	OFF	ON
194-195	OFF	ON	OFF	OFF	OFF	OFF	OFF	ON
195-196	OFF	OFF	OFF	OFF	OFF	OFF	OFF	ON
196-197	OFF	OFF	OFF	OFF	OFF	OFF	OFF	ON
197-198	OFF	OFF	OFF	OFF	OFF	OFF	OFF	ON
198-199	ON	OFF	OFF	OFF	OFF	OFF	OFF	ON
199-200	OFF	OFF	OFF	OFF	OFF	OFF	OFF	ON
200-201	OFF	OFF	OFF	OFF	OFF	OFF	OFF	ON
201-202	OFF	OFF	OFF	OFF	OFF	OFF	OFF	ON
202-203	OFF	OFF	OFF	OFF	OFF	OFF	OFF	ON
203-204	ON	OFF	OFF	OFF	OFF	OFF	OFF	ON
204-205	OFF	OFF	OFF	OFF	OFF	OFF	OFF	ON
205-206	OFF	OFF	OFF	OFF	OFF	OFF	OFF	ON
206-207	OFF	OFF	OFF	OFF	OFF	OFF	OFF	ON
207-208	OFF	OFF	OFF	OFF	OFF	OFF	OFF	ON
208-209	ON	OFF	OFF	OFF	OFF	OFF	OFF	ON
209-210	OFF	OFF	OFF	OFF	OFF	OFF	OFF	ON
210-211	OFF	OFF	OFF	OFF	OFF	OFF	OFF	ON
211-212	OFF	OFF	OFF	OFF	OFF	OFF	OFF	ON
212-213	OFF	OFF	OFF	OFF	OFF	OFF	OFF	ON

213-214	ON	ON	OFF	OFF	OFF	OFF	OFF	ON
214-215	OFF	OFF	OFF	OFF	OFF	OFF	OFF	ON
215-216	OFF	OFF	ON	OFF	OFF	OFF	OFF	ON
216-217	OFF	OFF	OFF	OFF	OFF	OFF	OFF	ON
217-218	OFF	OFF	OFF	OFF	OFF	OFF	OFF	ON
218-219	ON	OFF	OFF	OFF	OFF	OFF	OFF	ON
219-220	OFF	OFF	OFF	OFF	OFF	OFF	OFF	ON
220-221	OFF	OFF	OFF	OFF	OFF	OFF	OFF	ON
221-222	OFF	OFF	OFF	OFF	OFF	OFF	OFF	ON
222-223	OFF	OFF	OFF	OFF	OFF	OFF	OFF	ON
223-224	ON	OFF	OFF	OFF	OFF	OFF	OFF	ON
224-225	OFF	OFF	OFF	OFF	OFF	OFF	OFF	ON
225-226	OFF	OFF	OFF	OFF	OFF	OFF	OFF	ON
226-227	OFF	OFF	OFF	OFF	OFF	OFF	OFF	ON
227-228	OFF	OFF	OFF	OFF	OFF	OFF	OFF	ON
228-229	ON	OFF	OFF	OFF	OFF	OFF	OFF	ON
229-230	OFF	OFF	OFF	OFF	OFF	OFF	ON	ON
230-231	OFF	OFF	OFF	OFF	OFF	OFF	ON	ON
231-232	OFF	OFF	OFF	OFF	OFF	OFF	OFF	ON
232-233	OFF	ON	OFF	OFF	OFF	OFF	OFF	ON
233-234	ON	ON	OFF	OFF	OFF	OFF	OFF	ON
234-235	OFF	OFF	OFF	OFF	OFF	OFF	OFF	ON
235-236	OFF	OFF	OFF	OFF	OFF	OFF	OFF	ON
236-237	OFF	OFF	OFF	OFF	OFF	OFF	OFF	ON
237-238	OFF	OFF	OFF	OFF	OFF	OFF	OFF	ON
238-239	OFF	OFF	OFF	OFF	OFF	OFF	OFF	ON
239-240	OFF	OFF	OFF	OFF	OFF	OFF	OFF	ON

Table 3-7. Electric heater load profile. 240-320 minutes.

Time [min]	Target chamber	Outlet nozzle	Inlet nozzle	Straight Lithium inlet pipe	Bend Lithium inlet pipe	FDS flange inferior	FDS flange superior	Back-Plate
240-241	OFF	OFF	OFF	OFF	OFF	OFF	OFF	ON
241-242	OFF	OFF	OFF	OFF	OFF	OFF	OFF	ON
242-243	OFF	OFF	OFF	OFF	OFF	OFF	OFF	ON
243-244	OFF	OFF	OFF	OFF	OFF	OFF	OFF	ON
244-245	OFF	OFF	OFF	OFF	OFF	OFF	OFF	ON
245-246	OFF	OFF	OFF	OFF	OFF	OFF	OFF	ON
246-247	ON	OFF	OFF	OFF	OFF	OFF	OFF	ON
247-248	OFF	OFF	OFF	OFF	OFF	OFF	OFF	ON
248-249	OFF	OFF	OFF	OFF	OFF	OFF	OFF	ON
249-250	OFF	OFF	OFF	OFF	OFF	OFF	OFF	ON
250-251	OFF	OFF	OFF	OFF	OFF	OFF	OFF	ON
251-252	ON	OFF	OFF	OFF	OFF	OFF	OFF	ON
252-253	OFF	ON	OFF	OFF	OFF	OFF	OFF	ON
253-254	OFF	OFF	OFF	OFF	OFF	OFF	OFF	ON
254-255	OFF	OFF	OFF	OFF	OFF	OFF	OFF	ON
255-256	OFF	OFF	OFF	OFF	OFF	OFF	OFF	ON
256-257	ON	OFF	OFF	OFF	OFF	OFF	OFF	ON
257-258	OFF	OFF	OFF	OFF	OFF	OFF	OFF	ON
258-259	OFF	OFF	OFF	OFF	OFF	OFF	OFF	ON
259-260	OFF	OFF	OFF	OFF	OFF	OFF	OFF	ON
260-261	OFF	OFF	OFF	OFF	OFF	OFF	OFF	ON
261-262	ON	OFF	OFF	OFF	OFF	OFF	OFF	ON
262-263	OFF	OFF	OFF	OFF	OFF	OFF	OFF	ON
263-264	OFF	OFF	OFF	OFF	OFF	OFF	OFF	ON
264-265	OFF	OFF	OFF	OFF	OFF	OFF	OFF	ON

265-266	OFF	OFF	OFF	OFF	OFF	OFF	OFF	ON
266-267	ON	OFF	OFF	OFF	OFF	OFF	OFF	ON
267-268	OFF	OFF	OFF	OFF	OFF	OFF	OFF	ON
268-269	OFF	OFF	OFF	OFF	OFF	OFF	OFF	ON
269-270	OFF	OFF	OFF	OFF	OFF	OFF	OFF	ON
270-271	OFF	OFF	OFF	OFF	OFF	OFF	OFF	ON
271-272	ON	ON	OFF	OFF	OFF	OFF	OFF	ON
272-273	OFF	OFF	OFF	OFF	OFF	OFF	OFF	ON
273-274	OFF	OFF	OFF	OFF	OFF	OFF	OFF	ON
274-275	OFF	OFF	OFF	OFF	OFF	OFF	OFF	ON
275-276	OFF	OFF	OFF	OFF	OFF	OFF	OFF	ON
276-277	ON	OFF	OFF	OFF	OFF	OFF	OFF	ON
277-278	OFF	OFF	OFF	OFF	OFF	OFF	OFF	ON
278-279	OFF	OFF	OFF	OFF	OFF	ON	OFF	ON
279-280	OFF	OFF	OFF	OFF	OFF	OFF	OFF	ON
280-281	OFF	OFF	OFF	OFF	OFF	OFF	OFF	ON
281-282	ON	OFF	ON	OFF	OFF	OFF	OFF	ON
282-283	OFF	OFF	OFF	OFF	OFF	OFF	OFF	ON
283-284	OFF	OFF	OFF	OFF	OFF	OFF	OFF	ON
284-285	OFF	OFF	OFF	OFF	OFF	OFF	OFF	ON
285-286	OFF	OFF	OFF	OFF	OFF	OFF	OFF	ON
286-287	ON	OFF	OFF	OFF	OFF	OFF	OFF	ON
287-288	OFF	OFF	OFF	OFF	OFF	OFF	OFF	ON
288-289	OFF	OFF	OFF	OFF	OFF	OFF	ON	ON
289-290	OFF	OFF	OFF	OFF	OFF	OFF	OFF	ON
290-291	OFF	ON	OFF	OFF	OFF	OFF	OFF	ON
291-292	OFF	OFF	OFF	OFF	OFF	OFF	OFF	ON
292-293	OFF	OFF	OFF	OFF	OFF	OFF	OFF	ON

293-294	OFF	OFF	OFF	OFF	OFF	OFF	OFF	ON
294-295	OFF	OFF	OFF	OFF	OFF	OFF	OFF	ON
295-296	OFF	OFF	OFF	OFF	OFF	OFF	OFF	ON
296-297	OFF	OFF	OFF	OFF	OFF	OFF	OFF	ON
297-298	OFF	OFF	OFF	OFF	OFF	OFF	OFF	ON
298-299	OFF	OFF	OFF	OFF	OFF	OFF	OFF	ON
299-300	ON	OFF	OFF	OFF	OFF	OFF	OFF	ON
300-301	OFF	OFF	OFF	OFF	OFF	OFF	OFF	ON
301-302	OFF	OFF	OFF	OFF	OFF	OFF	OFF	ON
302-303	OFF	OFF	OFF	OFF	OFF	OFF	OFF	ON
303-304	OFF	OFF	OFF	OFF	OFF	OFF	OFF	ON
304-305	ON	OFF	OFF	OFF	OFF	OFF	OFF	ON
305-306	OFF	OFF	OFF	OFF	OFF	OFF	OFF	ON
306-307	OFF	OFF	OFF	OFF	OFF	OFF	OFF	ON
307-308	OFF	OFF	OFF	OFF	OFF	OFF	OFF	ON
308-309	OFF	OFF	OFF	OFF	OFF	OFF	OFF	ON
309-310	ON	ON	OFF	OFF	OFF	OFF	OFF	ON
310-311	OFF	OFF	OFF	OFF	OFF	OFF	OFF	ON
311-312	OFF	OFF	OFF	OFF	OFF	OFF	OFF	ON
312-313	OFF	OFF	OFF	OFF	OFF	OFF	OFF	ON
313-314	OFF	OFF	OFF	OFF	OFF	OFF	OFF	ON
314-315	ON	OFF	OFF	OFF	OFF	OFF	OFF	ON
315-316	OFF	OFF	OFF	OFF	OFF	OFF	OFF	ON
316-317	OFF	OFF	OFF	OFF	OFF	OFF	OFF	ON
317-318	OFF	OFF	OFF	OFF	OFF	OFF	OFF	ON
318-319	OFF	OFF	OFF	OFF	OFF	OFF	OFF	ON
319-320	ON	OFF	OFF	OFF	OFF	OFF	OFF	ON

4. IFMIF thermo-mechanical analysis

On the basis of the thermal analysis performed on the IFMIF target system mock-up, it has been set-up a 3D FEM model of the IFMIF Target Assembly, whether endowed with the bayonet type replaceable Back-Plate, integrated with its support framework and the Lithium inlet pipe.

The research has been aimed at the assessment of the TA thermo-mechanical behaviour under the reference nominal steady state scenario, in order to verify if components might safely withstand the thermo-mechanical loads it undergoes without incurring in significant deformations, which may warp the lithium channel inducing flow instability, cause interferences with the Test Module or produce a potential misalignment between the deuteron beams and the lithium footprint.

Attention has been focussed also on the fulfilment of the SDC-IC structural safety criteria in the most critical area of the geometric domain investigated.

4.1. Nominal steady state scenario

The reference nominal steady state scenario represents the loading scenario the TA, integrated with its support framework and the Lithium inlet pipe, is envisaged to experience. In particular the nominal scenario is mainly characterized by lithium flowing within the Lithium inlet pipe and through the TA, where it enters the lithium straightener at 250 °C and at a static pressure of ~60 kPa, up to the outlet nozzle, where it reaches ~300 °C and a static pressure of 10^{-3} Pa, prior to be discharged in the quench tank [19]. During this phase, deuteron accelerators remains under full-power irradiation conditions (two 125 mA current beams), allowing heat power to be deposited by deuterons, neutrons and photons within lithium coolant, TA components, support framework and Lithium inlet pipe. The neutron swelling induced within the structural material has not been taken into account in the present research campaign, because it has been aimed at investigating exclusively the thermo-mechanical response of the structure during the nominal steady state operational phase.

4.2. The FEM model

A realistic 3D FEM model, reproducing the TA integrated with its support framework and the Lithium inlet pipe, has been developed (Fig. 4-1) and a mesh independence analysis has been performed to select an optimized spatial discretization which allows accurate results to be obtained saving calculation time, as already described in §3.2. A mesh (Figs. 4-2÷4-8) composed of ~$4.0 \cdot 10^5$ nodes connected in ~$1.55 \cdot 10^6$ linear tetrahedral elements has been selected. The so formed spatial discretization allows numerical simulations to be carried out

in about 3 hours.

The two FDSs and the gimbal expansion joint of the Lithium inlet pipe have not been directly modelled, since their mechanical effects have been simulated, as widely explained in the following, imposing, for the former, an appropriate contact model that permits to consider the flanges tightened by the FDS as perfectly tied while, for the latter, a proper kinematic model that allows the coupling of the rotational and translational displacements of the two Lithium inlet pipe sections connected by the gimbal expansion joint. Moreover, the lithium flowing on the Back-Plate and outlet nozzle internal surfaces has been modelled too.

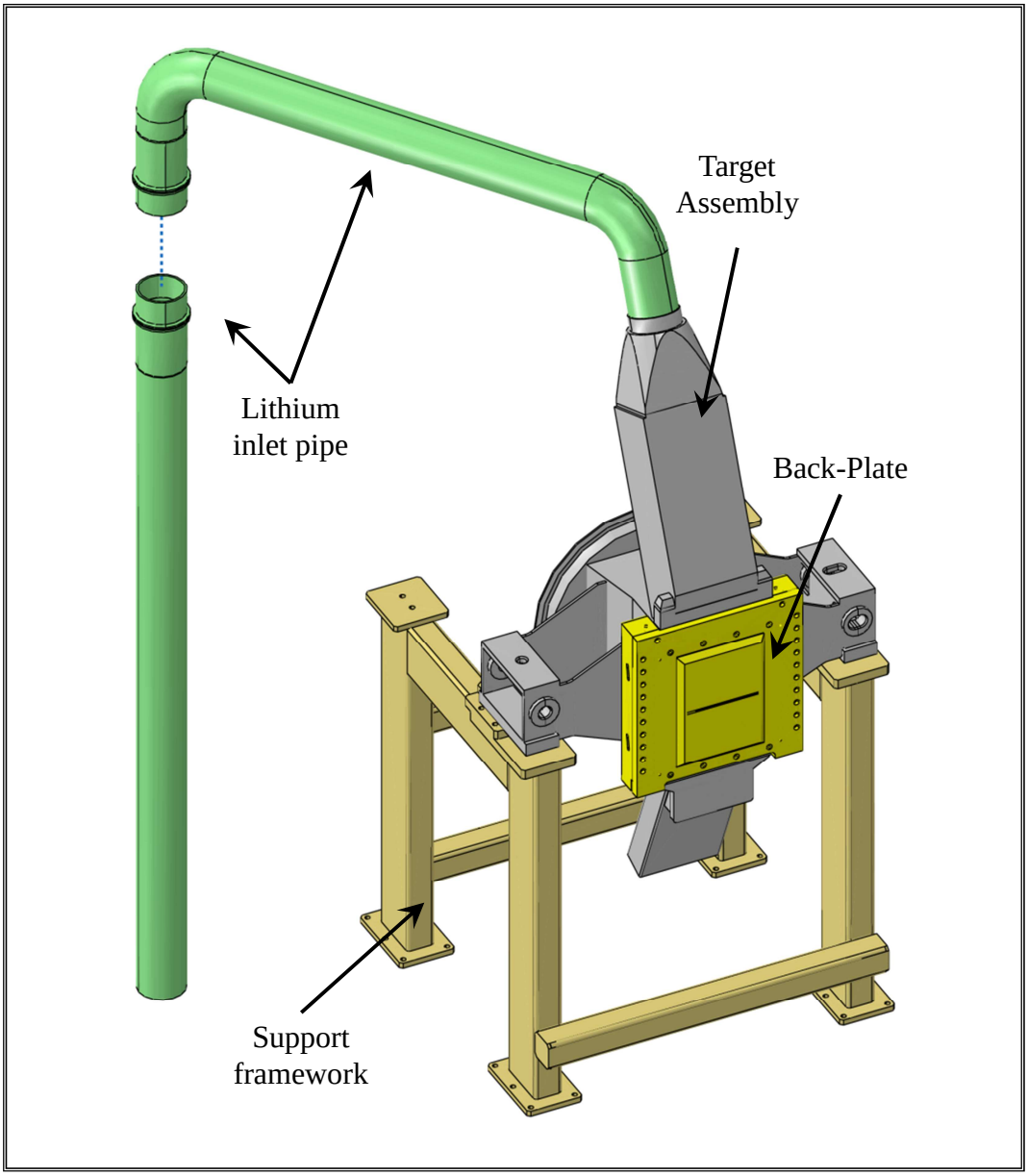

Figure 4-1. FEM model.

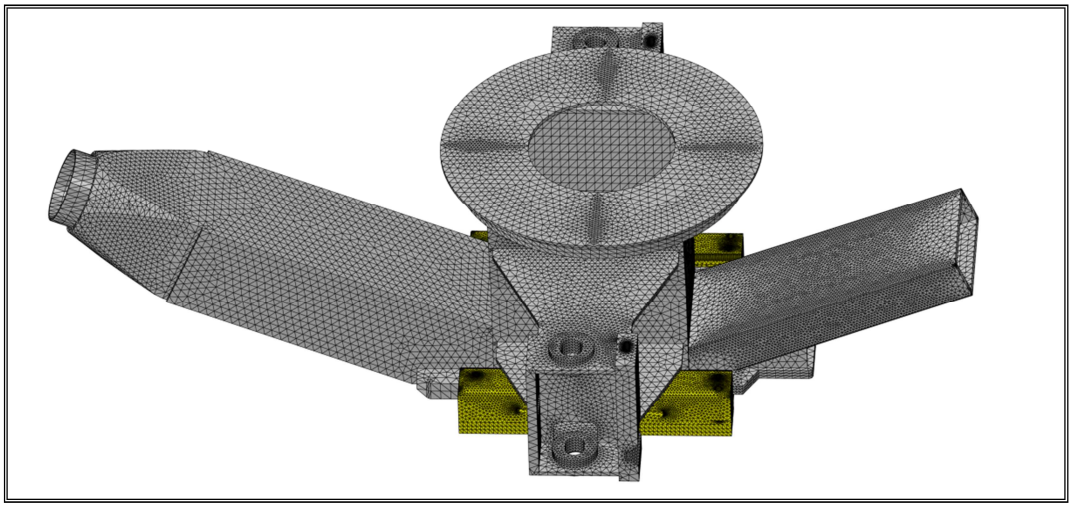

Figure 4-2. FEM model. Target Assembly lateral view.

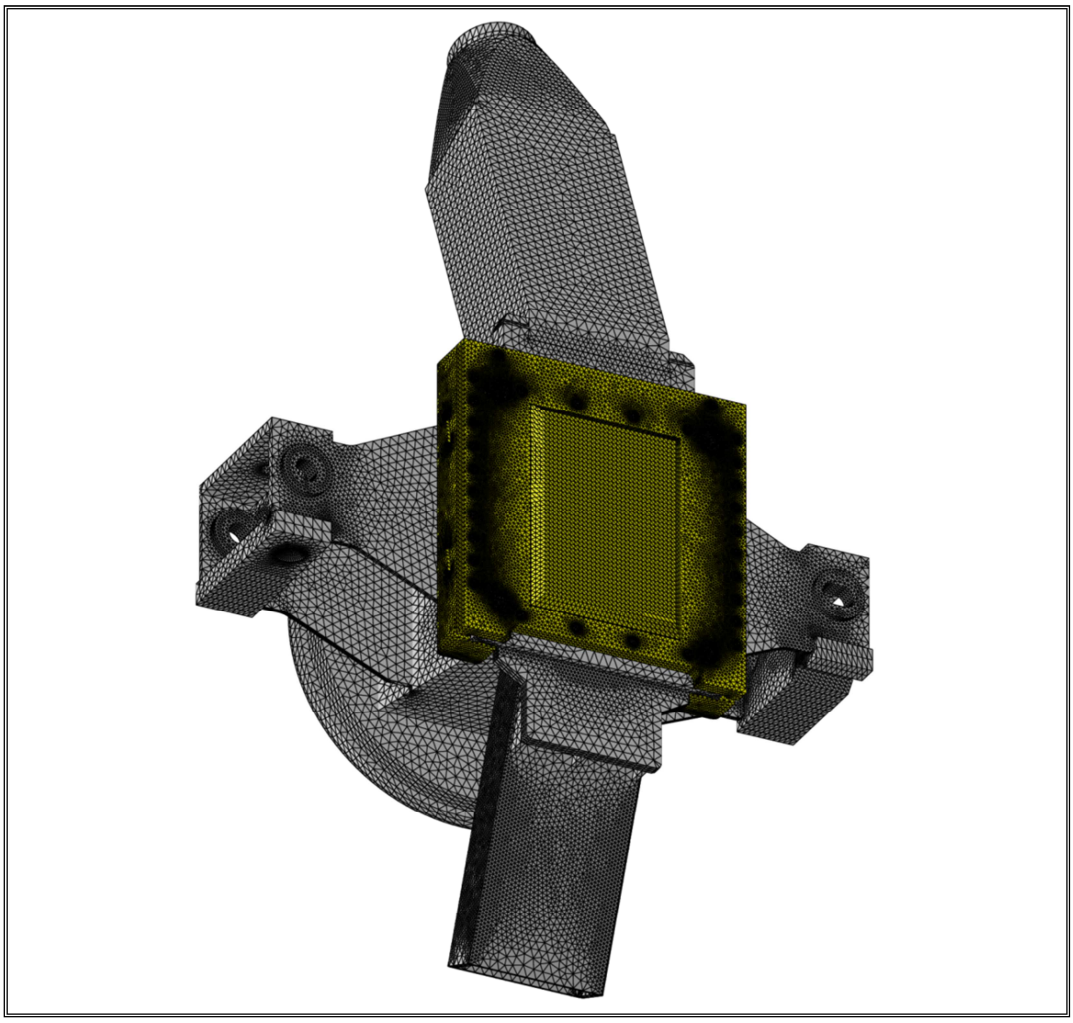

Figure 4-3. FEM model. Target Assembly front view.

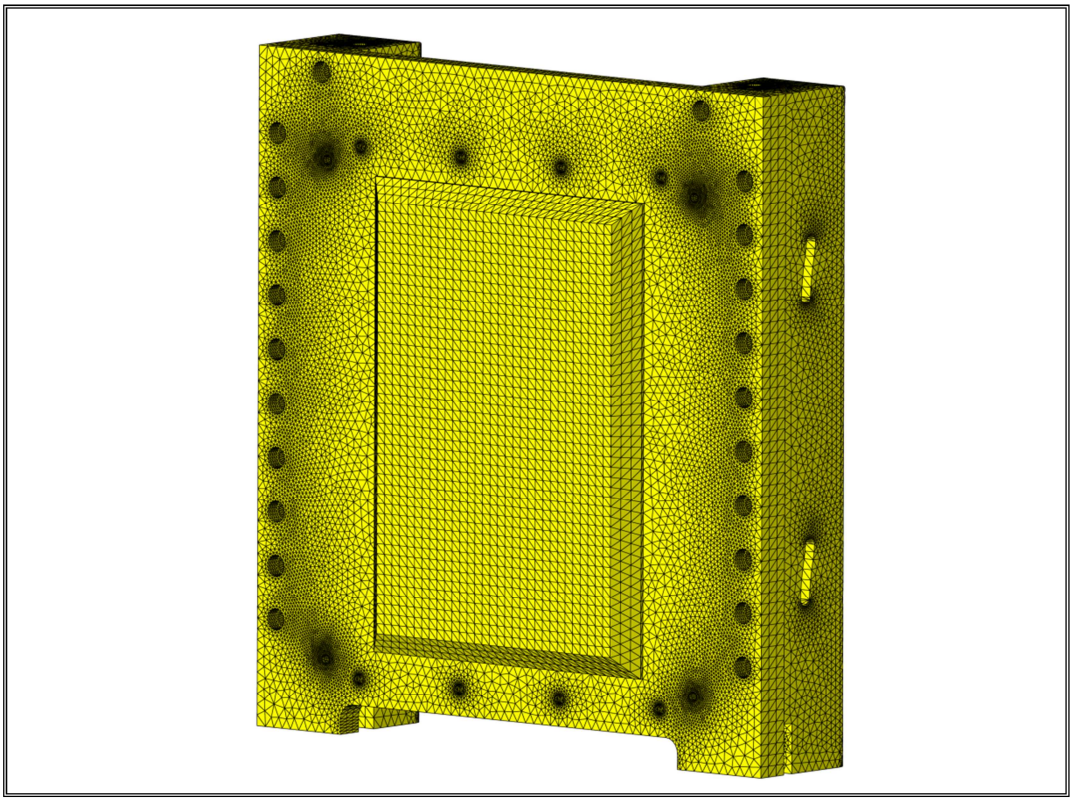

Figure 4-4. FEM model. Particular of the Back-Plate.

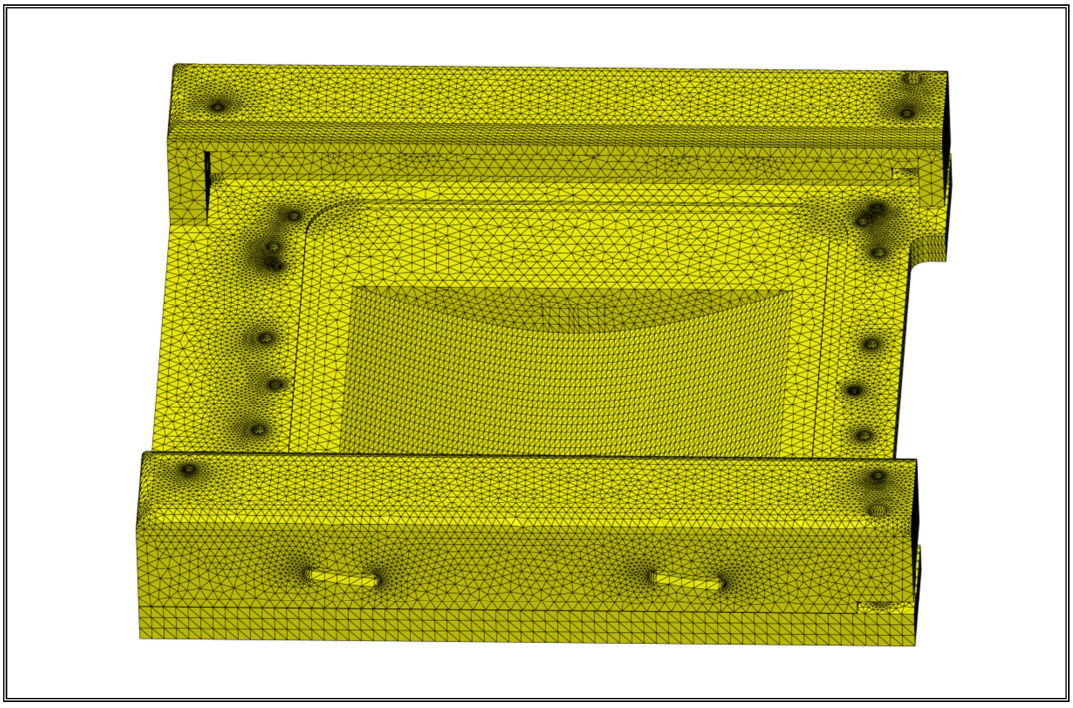

Figure 4-5. FEM model. Particular of the Back-Plate.

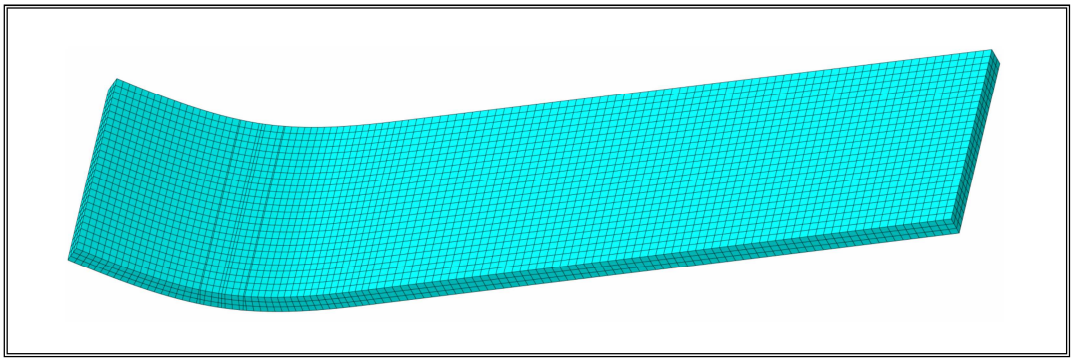

Figure 4-6. FEM model. Particular of the lithium flow domain.

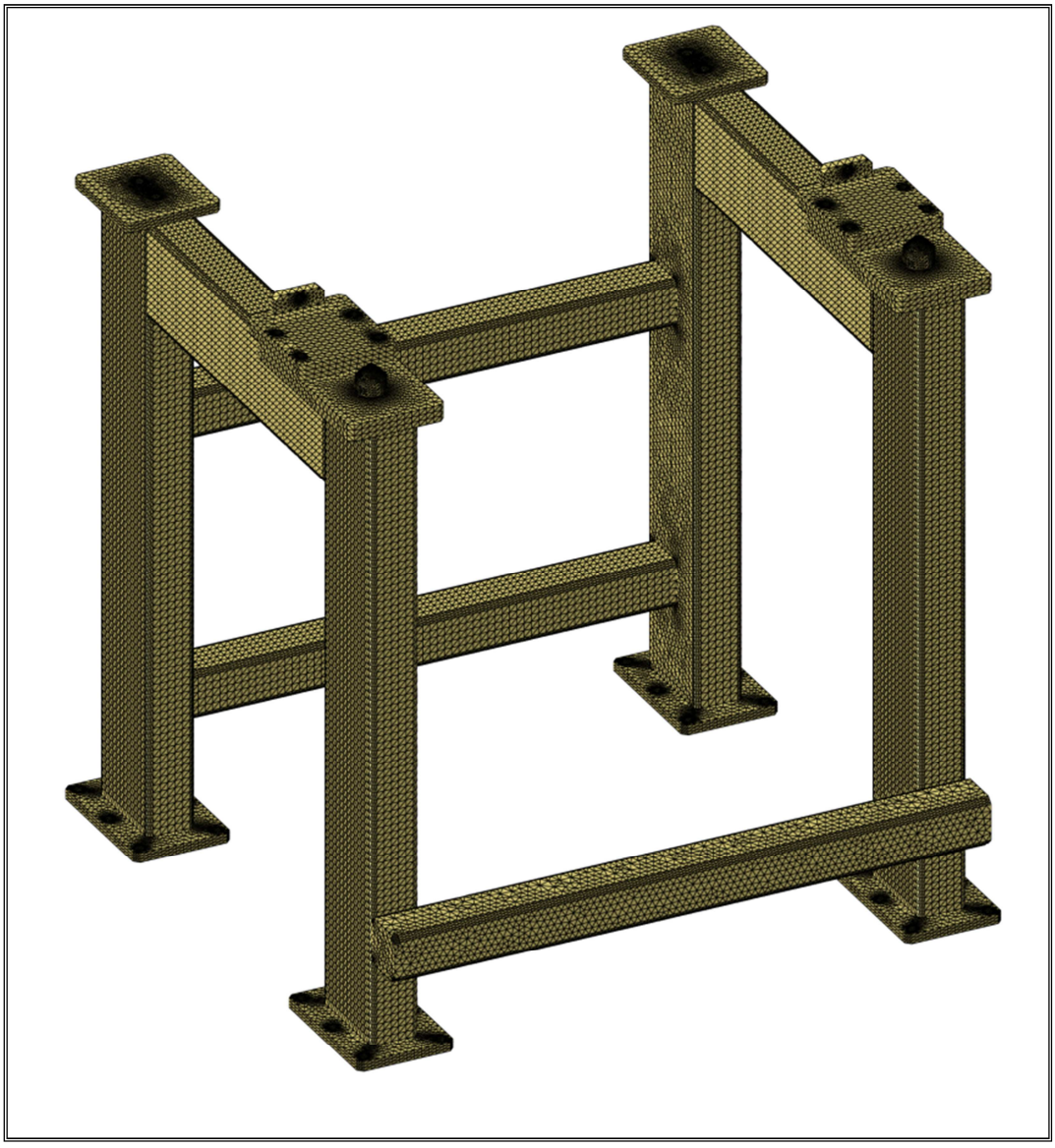

Figure 4-7. FEM model. Particular of the support framework.

Figure 4-8. FEM model. Particular of the Lithium inlet pipe.

4.2.1. Materials

According to the IFMIF Comprehensive Design Report [18] and its subsequent modifications relevant to the EU TA concept, EUROFER steel has been assumed as the TA, support framework and Lithium inlet pipe structural material. Lithium flow has been modelled too in order to properly simulate its thermal interaction with the TA. To this purpose a flow velocity at the inlet nozzle exit amounting to 15 m/s has been adopted [33]. Materials have been considered homogeneous, uniform and isotropic and their thermo-mechanical properties have been assumed to depend uniquely on temperature as indicated in [34-38]. In particular, EUROFER mechanical behaviour has been simulated adopting a linear elastic model. The temperature-dependent behaviour of considered material thermo-mechanical properties can be deduced from tables 4-1, 4-2 and from figure 4-9.

Table 4-1. EUROFER thermo-mechanical properties at 20°C [34,35].

EUROFER	
λ_0	27.66 W/m K
c_{p0}	448.0 J/kg K
α_0	$1.04 \cdot 10^{-5}$ K^{-1}
E_0	$2.06 \cdot 10^{11}$ Pa

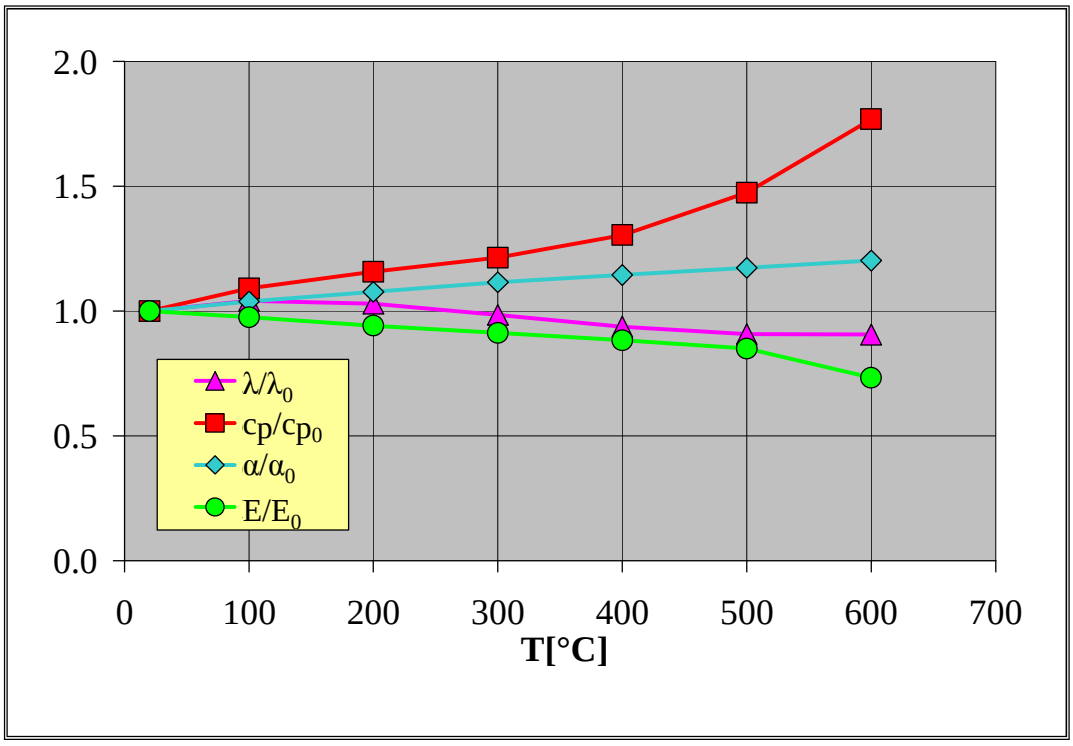

Figure 4-9. EUROFER thermo-mechanical properties vs temperature [34,35].

Table 4-2. Lithium thermo-physical properties [36,37,38].

Lithium (Temperatures in K)	
$\lambda(T)$ [W/m K]	$38.92625 + 1.230914 \cdot 10^{-2} \cdot T$
$c_p(T)$ [kJ/kg K]	$-7.538 \cdot 10^{-10} \cdot T^3 + 2.484 \cdot 10^{-6} \cdot T^2 - 2.752 \cdot 10^{-3} \cdot T + 5.174$
$\rho(T)$ [kg/m^3]	510.0

4.2.2. Thermal interactions, loads and boundary conditions

The following thermal interactions, loads and boundary conditions have been assumed to simulate the TA, integrated with its framework and Lithium inlet pipe, thermo-mechanical behaviour under nominal steady state scenario:

- thermal interactions;
- volumetric density of heat power deposited in the lithium flow footprint region;
- volumetric density of heat power deposited within TA, framework and inlet pipe;
- forced convection with lithium;
- heat transfer between BP and High Flux Test Module (HFTM) through helium gas;
- heat transfer between Target Chamber and Beam duct;
- internal irradiation;
- external irradiation;
- TA natural convection cooling;
- support framework cooling.

Concerning the thermal interactions between the different components, the same assumptions made for the thermal analysis of the mock-up of the IFMIF target system, already reported in § 3.2.2, have been taken into account.

As to thermal loads, a 40 GW/m³ volumetric density of nuclear deposited heat power (q'''_{D-Li}) has been supposed to be uniformly distributed within the beam footprint region of lithium flow domain (Fig. 4-10) to model heat power deposition due to interactions between deuterons and lithium.

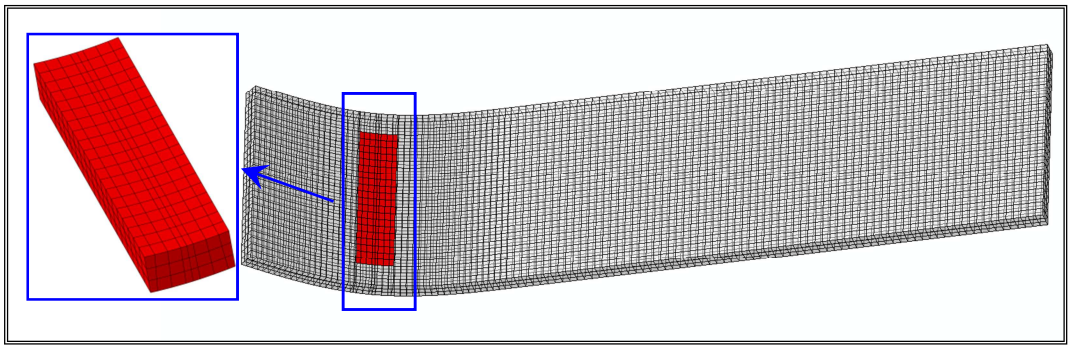

Figure 4-10. Detail of lithium flow domain beam footprint region.

Moreover, a volumetric density of nuclear deposited heat power (q‴) has been assumed within the TA, the support framework and the Lithium inlet pipe in order to properly simulate the heat power deposition process due to interactions of both neutrons arising from D-Li interactions and γ photons produced by (n,γ) reactions with the nuclei of their structural material.

In particular, regarding TA, the non-uniform spatial distribution of nuclear deposited heat power volumetric density, calculated by ENEA adopting the MCNP code [39] (Figs. 4-11 and 4-12), has been assumed and implemented in the FEM model by means of a specific user subroutine.

Furthermore, since no data for nuclear deposited heat power volumetric density within support framework and Lithium inlet pipe have been carried out by ENEA, a $1/r^2$ dependence has been supposed instead. In particular, the following formula has been adopted:

$$q'''(r) = \frac{q'''_0}{4\pi r^2} \tag{4-1}$$

where $q'''_0 = q'''_{BP,centre}/200$ and r is the distance between a generic point and the BP centre. The q‴ value at the BP centre has been divided by a factor 200 in order to obtain a certain accordance for the nuclear deposited heat power volumetric density values at the boundary between the geometric domain in which q‴ values have been carried out by ENEA and the domain for which q‴ data was not available and has been calculated using (4-1). For the estimation of the factor 200, a parametric analysis has been performed to determine the best accordance, in the boundary regions, between ENEA q‴ values and those calculated using (4-1). The so calculated nuclear deposited heat power volumetric density field within support framework and Lithium inlet pipe is reported in figures 4-13 and 4-14.

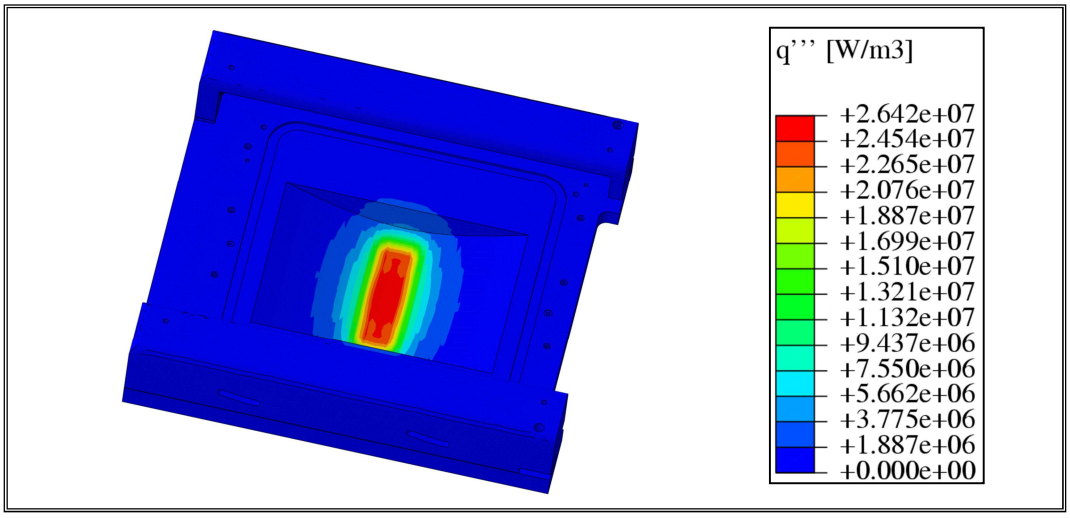

Figure 4-11. Spatial distribution of heat power volumetric density within BP.

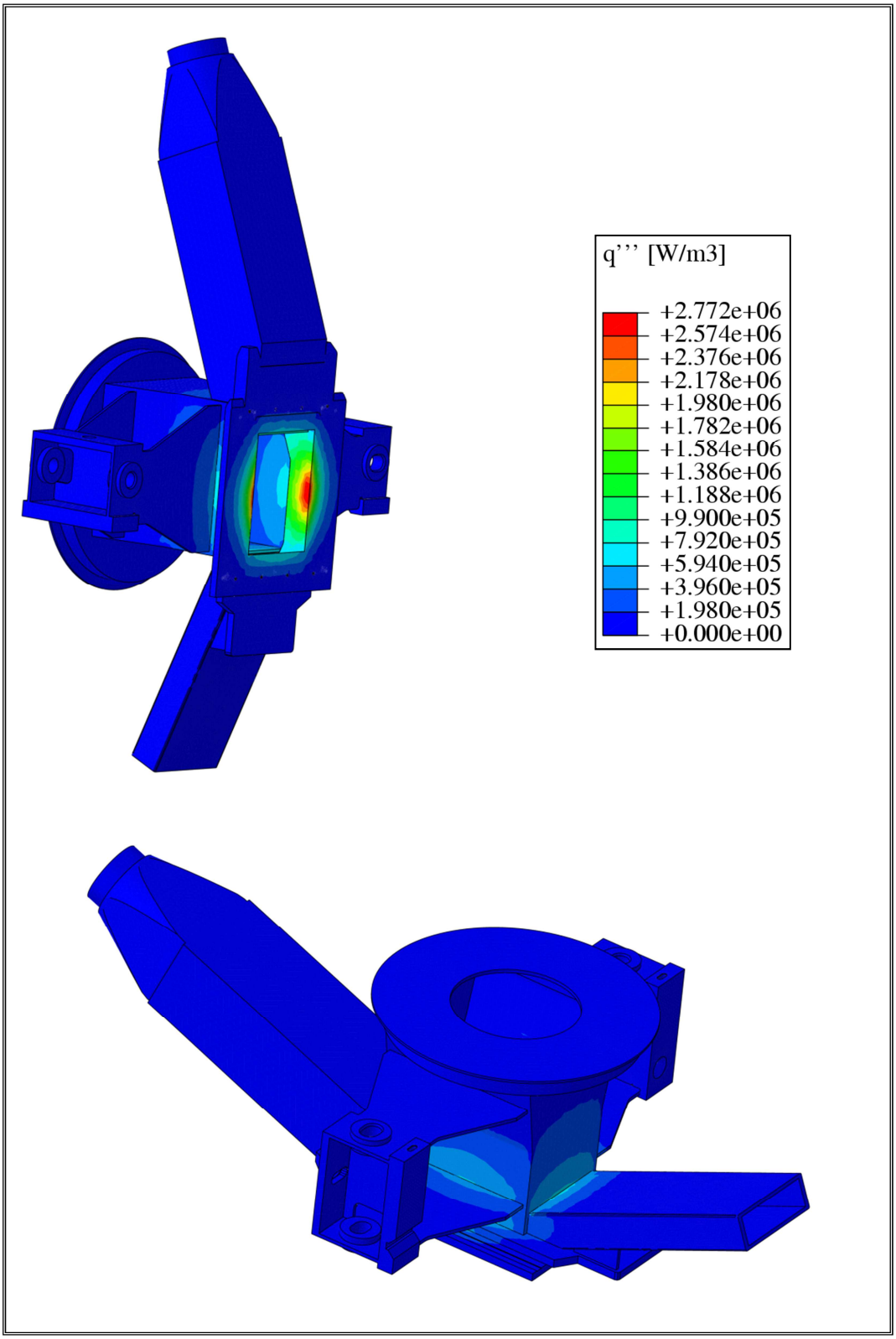

Figure 4-12. Spatial distribution of heat power volumetric density within TA.

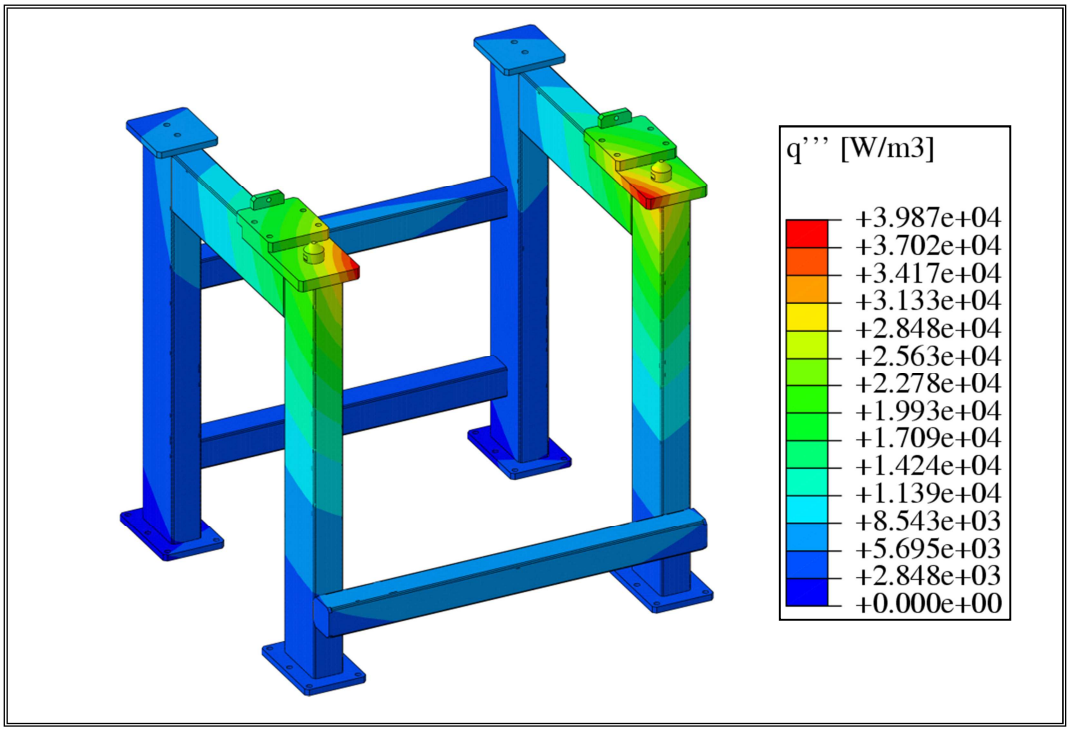

Figure 4-13. Spatial distribution of heat power volumetric density within support framework.

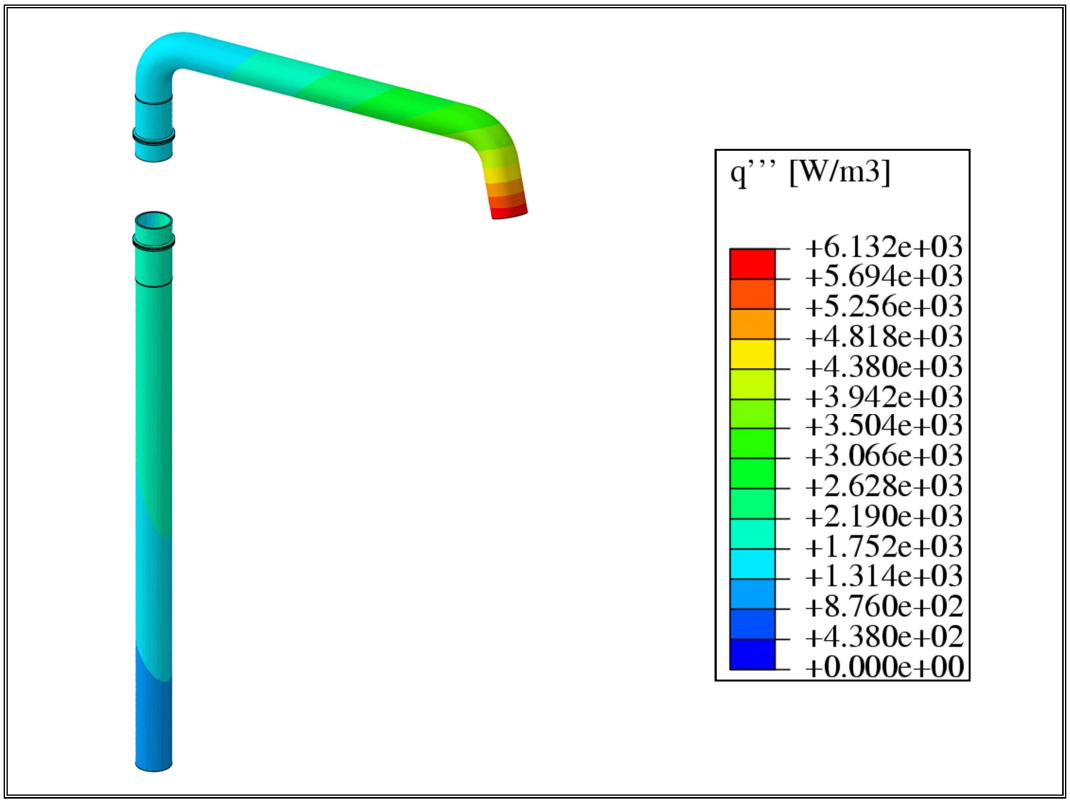

Figure 4-14. Spatial distribution of heat power volumetric density within Lithium inlet pipe.

In order to simulate the forced convective heat transfer taking place between lithium flow and the corresponding lithium wetted surfaces, two different models have been assumed for the Lithium inlet pipe and inlet nozzle internal surfaces (orange surfaces in Fig. 4-15) and for the remaining lithium wetted surfaces (blue surfaces in Fig. 4-15). As to the former surfaces, a typical convective boundary condition has been imposed to their nodes, assuming a bulk temperature equal to the lithium temperature of 250 °C and a convective heat transfer coefficient equal to 34000 W/m² °C [40]. This value has been concurred with the team involved in thermo-mechanical activities and it is the same adopted in similar calculation performed on the IFMIF TA [6-9]. On the other hand, with respect to the latter surfaces, a thermal contact model based on Eq. (3-1) has been adopted to simulate the convective heat transfer between the lithium flow domain and the pertinent TA and BP wetted surfaces, assuming according to [40] a thermal conductance amounting again to 34000 W/m² °C, even if this value has been calculated for the velocity of 20 m/s [19].

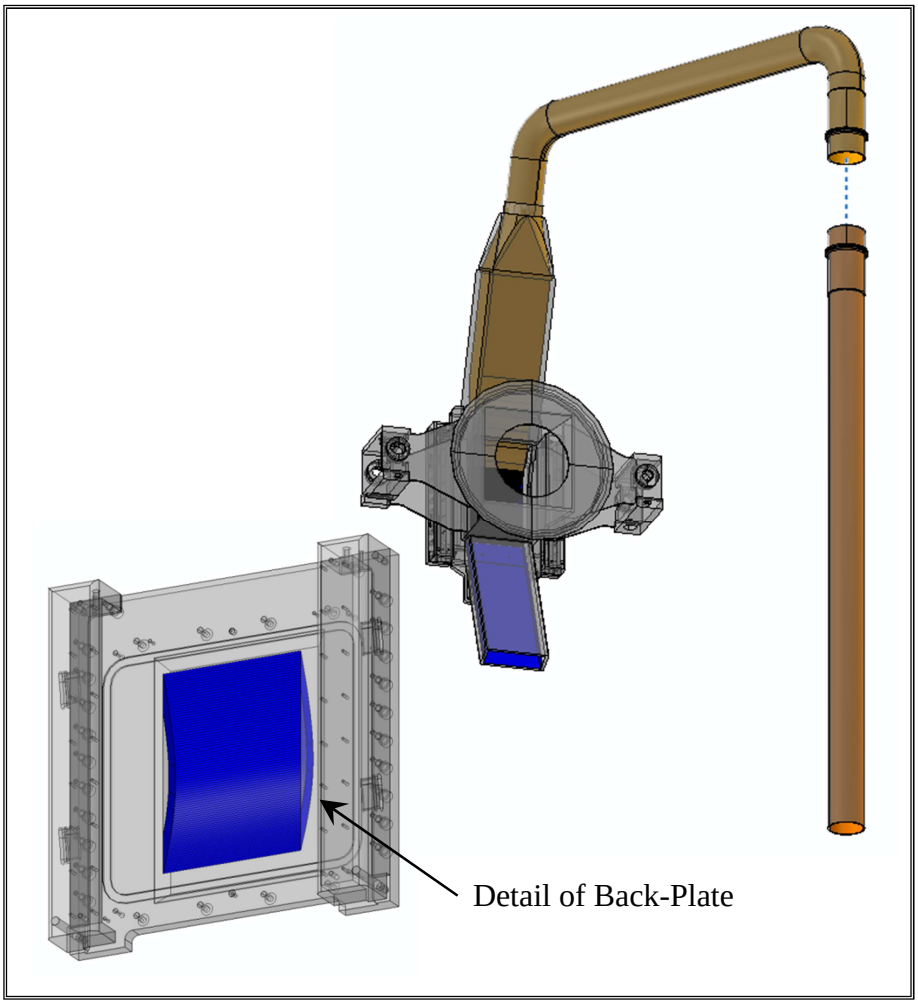

Figure 4-15. Lithium forced convection surfaces.

Thermal interactions between BP and HFTM have been taken into account since they are separated, at room temperature, by a 2 mm minimum gap. They have been simulated by imposing a Cauchy's boundary condition to the BP external surfaces directly facing the HFTM (Fig. 4-16), given by Eq (3-6).

The uniform bulk temperature of the HFTM, T_{HFTM}, has been set equal to 50 °C according to [19], while h (Eq. 3-7) has been calculated considering λ=0.1616 W/m °C for helium at 5 kPa and 50 °C [19] and different values for the gaps between the interacting components (Fig. 4-16).

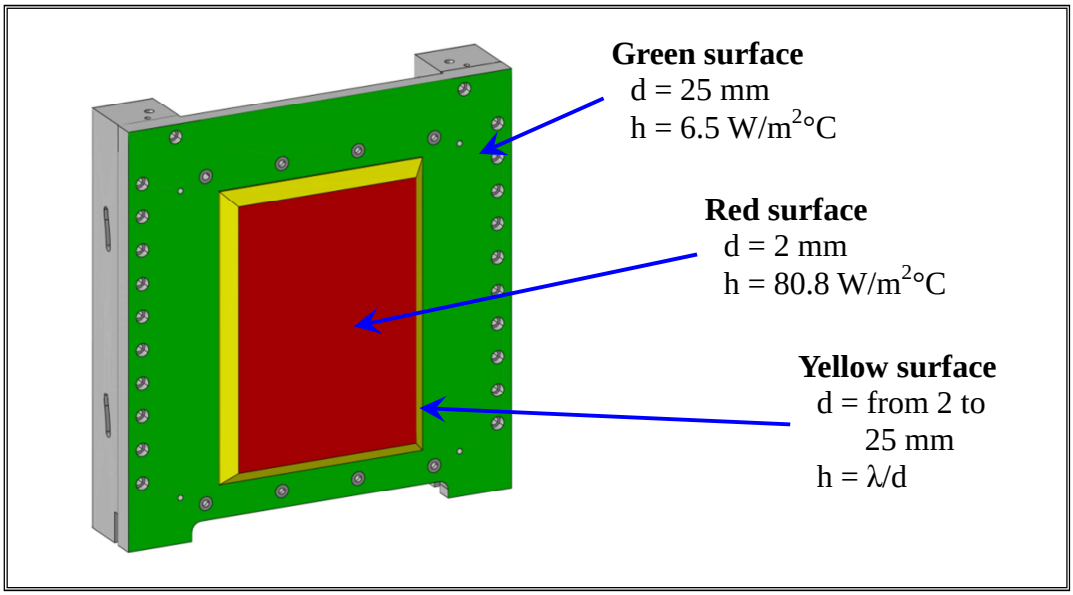

Figure 4-16. Back-Plate and high flux test module thermal interaction surfaces.

Thermal interactions between Target Chamber and Beam duct have been simulated by imposing, according to [9-19], an effective convective heat transfer coefficient equal to 15.8 W/m² °C on the TC flange surface (red surface in Fig. 4-17) and a non-uniform bulk temperature, T_L, analytically derived from a 1-D simplified model of the Beam duct conductive-radiative heat transfer, purposely set-up since, being exposed to nuclear irradiation, the Beam duct cannot be considered anymore in thermal equilibrium with the containment vessel atmosphere. In particular, this 1-D model has been developed to analytically find out the dependence of the beam duct temperature spatial profile, $T(x,T_0)$, on TC flange temperature, T_0, so to obtain the functional dependence of the aforementioned bulk temperature on the corresponding TC flange temperature T_0, as $T_L(T_0)=T(L,T_0)$ (Fig. 4-18). The model is based on the hypothesis that Beam duct radiates, with an emissivity of 0.3, towards the containment vessel atmosphere assumed at 50 °C and that it is thermally coupled to the TC by means of an effective convective heat transfer coefficient equal to 15.8 W/m^2°C.

Finally, a decreasing heat power density has been supposed to be released inside the Beam duct as a consequence of its interaction with neutrons and photons arising from the target.

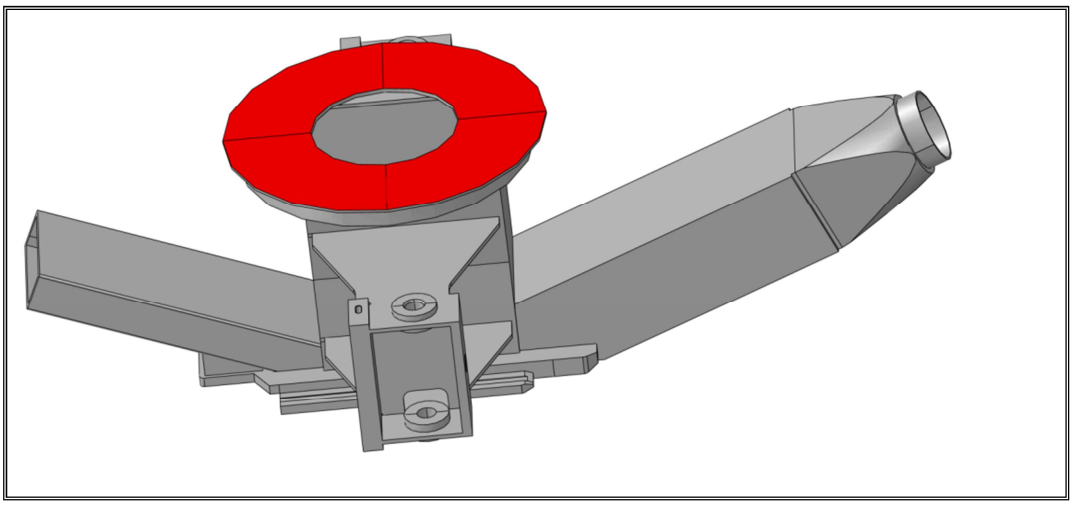

Figure 4-17. TC flange surface.

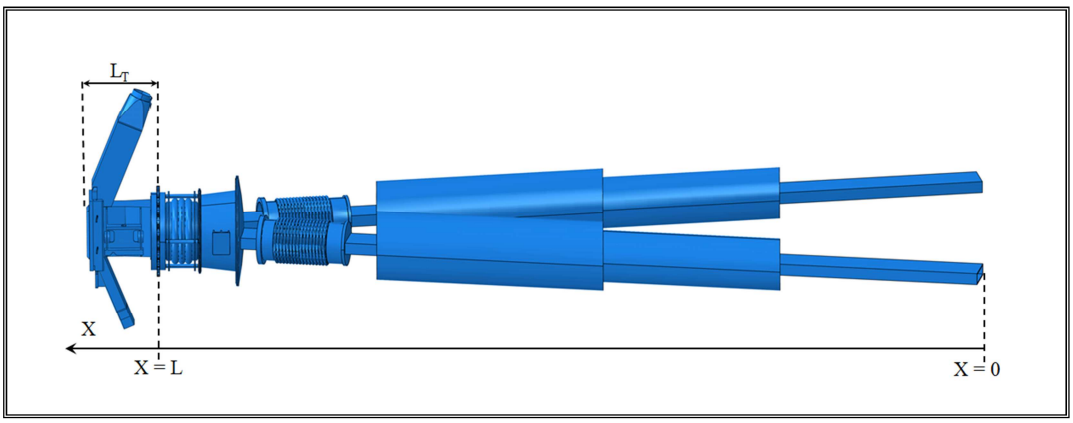

Figure 4-18. Geometric model for the $T(L,T_0)$ calculation.

Radiation heat transfer, occurring internally between lithium flow and the internal walls of target chamber and frame, has been modelled adopting the cavity radiation formulation widely described in [30, 31] and already reported in §3.2.2.

Therefore, a proper radiation cavity (red surfaces in Fig. 4-19) has been defined. This cavity includes target chamber, frame and outlet nozzle internal surfaces, as well as the lithium flow surface facing the aforementioned ones. No radiation has been allowed through the cavity opening at the top of the target chamber, since it is envisaged to be closed by beam ducts, and through the outlet nozzle exit section, since it is envisaged to be continued with the quench tank adduction duct. Emissivity values of 0.3 and 0.06 have been adopted respectively for steel walls and lithium coolant, as indicated in [9,41].

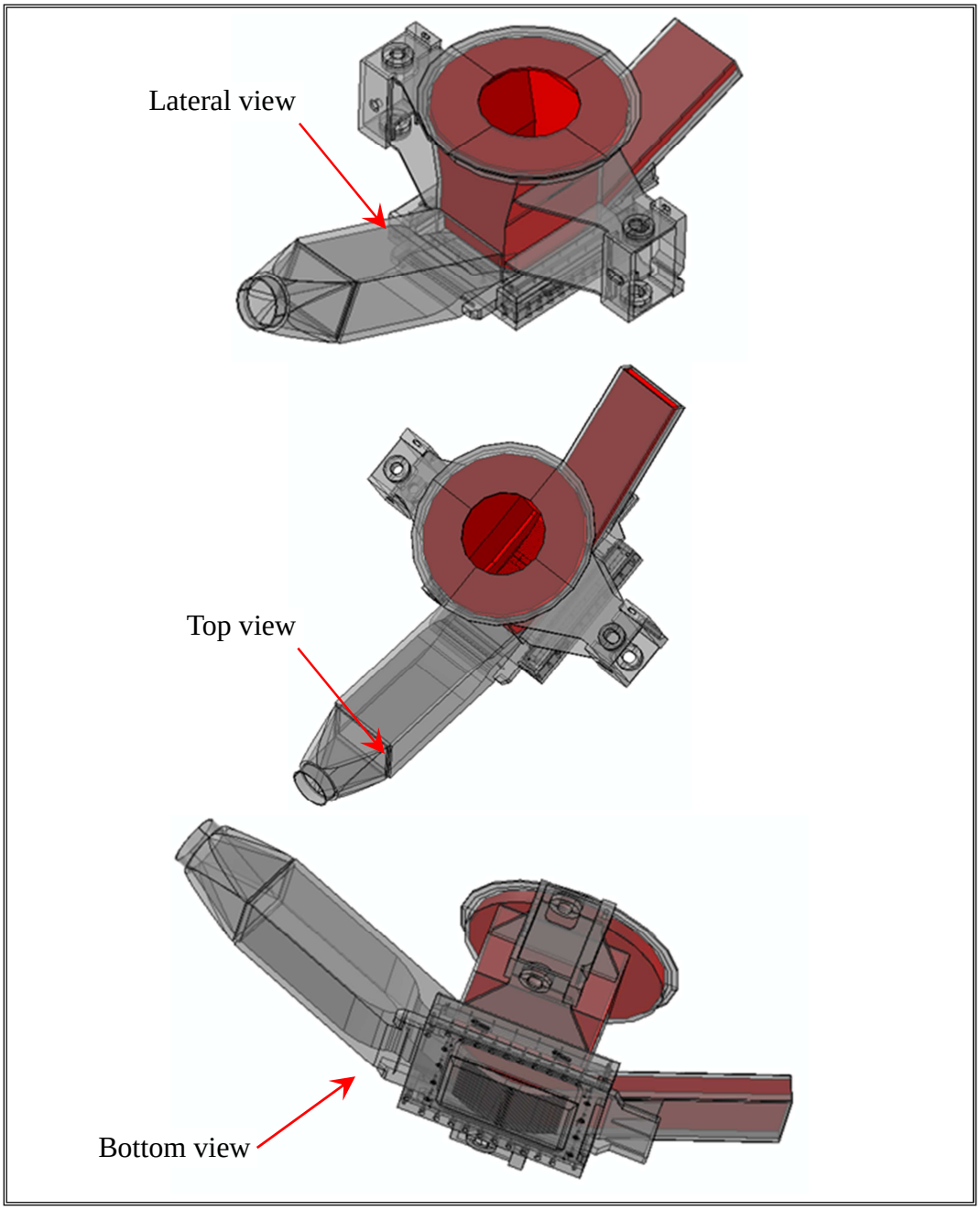

Figure 4-19. Internal radiation cavity (red surfaces – lateral, top and bottom views).

Radiation heat transfer occurring externally between the TA un-insulated external surfaces and the inner walls of its containment vessel has been modelled according to Eq. (3-4) applying the radiation condition to element facets lying on the external surfaces of BP, frame and the whole target chamber, which are supposed to be un-insulated during the nominal steady state scenario (red surfaces in Fig. 4-20).

The value of 323 K has been set for BP and frame radiation towards the HFTM, as well as

for the radiation of target chamber towards the containment vessel inner walls, while the EUROFER emissivity ε has been set equal to 0.3.

Moreover, results of the preliminary analysis have shown that, in order to ensure the thermal field arising within support framework does not overcome the EUROFER limit temperature of 550 °C, its external surfaces have to be un-insulated too. In fact, in case framework external surfaces are supposed to be completely insulated, the pure conductivity heat transfer between support framework upper flanges and target chamber arms is not adequate to remove the heat power deposited within the structure by neutrons and γ photons, therefore temperatures higher than 550 °C are predicted for the support framework. In consequence of this, support framework external radiation has been assumed and the simplified condition (3-4) has been imposed to the elements facets lying on its external surface (in red in Fig. 4-21), setting an emissivity value equal to 0.3 and a temperature of 323 K for the vacuum vessel internal atmosphere.

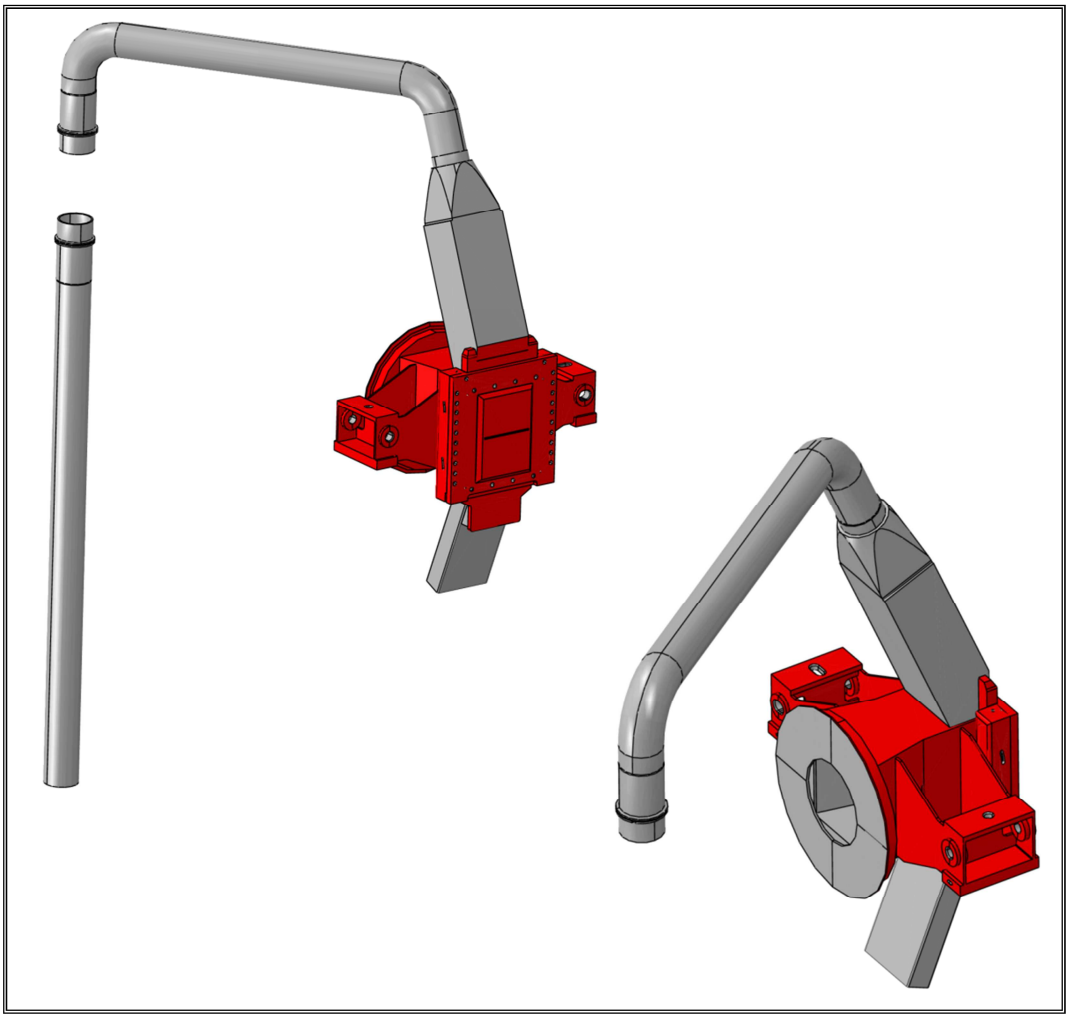

Figure 4-20. TA external radiation surfaces.

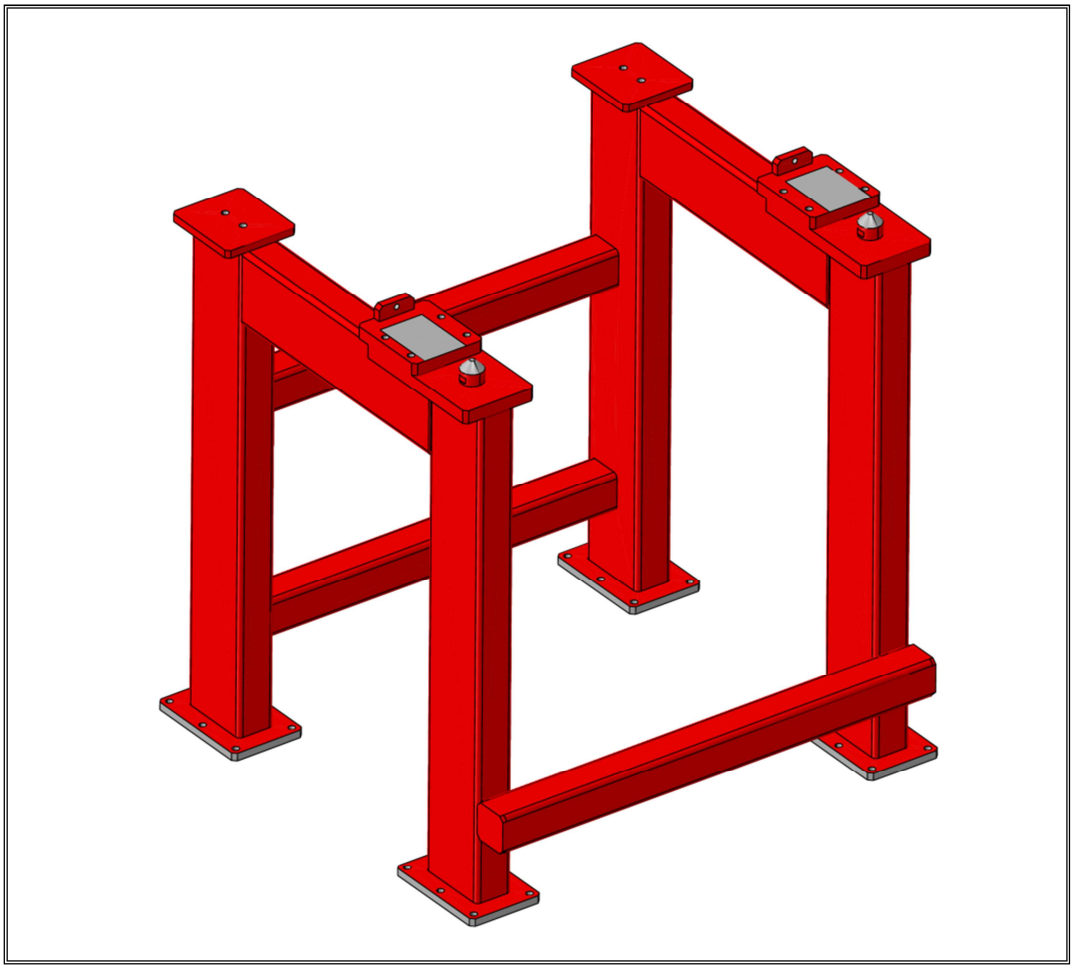

Figure 4-21. Support framework external radiation surfaces.

In order to take into account the heat transfer between helium filling the vacuum vessel atmosphere and TA external radiating surface, a convective boundary condition has been imposed to surfaces in red in Fig. 4-20 in order to simulate the natural convective heat transfer taking place between helium and the TA non-insulated surfaces. The following Cauchy's boundary condition has been imposed to the nodes laying on the TA non-insulated surface:

$$q_j = h\left(T_j - T_{He}\right) \tag{4-2}$$

where q_j is the normal heat flux at the j-th node of the TA non-insulated surface, T_{He} is the uniform bulk temperature of the vacuum vessel atmosphere, set to 50°C according to [19], and h represents the convective heat transfer coefficient, which has been properly estimated to be equal to 10 W/m² °C using the Churchill and Chu correlation [32].

As far as the support framework cooling is concerned, two different conditions have been investigated in order to assess the effects of the different framework cooling strategies on the TA thermo-mechanical performances.

In the first case taken into account, named Condition 1, the natural convection cooling between framework non-insulated surfaces (Fig. 4-21) and helium has been simulated by imposing a Cauchy's boundary condition (Eq. 4-2) in which convective heat transfer coefficient h has been set equal to 10 W/m² °C and the helium bulk temperature T_{He} has been imposed to be 50 °C.

In the second case, named Condition 2, the forced convection cooling of the support framework, using the helium filling the vacuum vessel, has been simulated. A value of 1000 W/m² °C has been supposed for the convective heat transfer coefficient, while the same value used in Condition 1 has been supposed for T_{He}.

4.2.3. Mechanical interactions, loads and boundary conditions

The following mechanical interactions, loads and boundary conditions have been assumed to simulate the TA thermo-mechanical behaviour under nominal steady state scenario:

- mechanical interactions;
- thermal deformations;
- weight force;
- internal and external pressures;
- tightening screw loads;
- skate-based clamping system loads;
- support framework constraints;
- Lithium inlet pipe constraints;
- TA system constraints;
- Lithium inlet pipe gimbal expansion joint.

Mechanical interactions between frame and Back-Plate have been simulated by a mechanical contact model, which envisages a Coulombian friction interaction, characterized by a concurred uniform friction factor of 0.74, whereas the contact surfaces between TA and the support framework have been considered as dry lubricated. In order to properly simulate the mechanical interactions between these surfaces, a mechanical contact model, adopting a Coulombian friction interaction characterized by a uniform friction factor of 0.03 [42], has been implemented. All other components, included the Lithium inlet pipe flanges connected by the two FDSs, have been considered as tied from the mechanical point of view.

As for thermal deformations, the non-uniformly distributed thermal deformation field arising within the model as a consequence of its thermal field, obtained for all the investigated framework cooling conditions, and its isotropic thermal expansion tensor have been applied to the model.

The effect of gravity has been taken into account for the whole model. In particular for TA, framework and Lithium inlet pipe a proper mechanical load has been imposed, while regarding the lithium flow its weight force is included in the pressure value applied onto all

TA surfaces wetted by lithium, as reported in the following.

According to the results of thermofluid-dynamic analysis of lithium flow reported in [19,43], a non-uniform internal pressure load has been applied to lithium wetted surfaces of Lithium inlet pipe, nozzles, frame and Back-Plate (red surfaces in Figs. 4-22÷4-24). In particular, the pressure load onto the Lithium inlet pipe wetted surface (p_{IP}) has been imposed as uniform and equal to 60 kPa, while a further uniform pressure load (p_{IN}) of 31.125 kPa, calculated as the average value between the 60 kPa at the entrance of the inlet nozzle and the 2.250 kPa at its exit, has been imposed to the inlet nozzle internal surfaces. Moreover, according to [19], the pressure load onto the Back-Plate lithium wetted surface, p_{BP}, has been assumed to depend linearly on the z coordinate, reaching its maximum (~12 kPa) at the beam footprint centre and decreasing till to 10^{-3} Pa at the Back-Plate channel exit, remaining vanishing along the outlet nozzle channel ($p_{ON} \approx 0$ Pa).

Figure 4-22. Lithium inlet pipe internal surfaces.

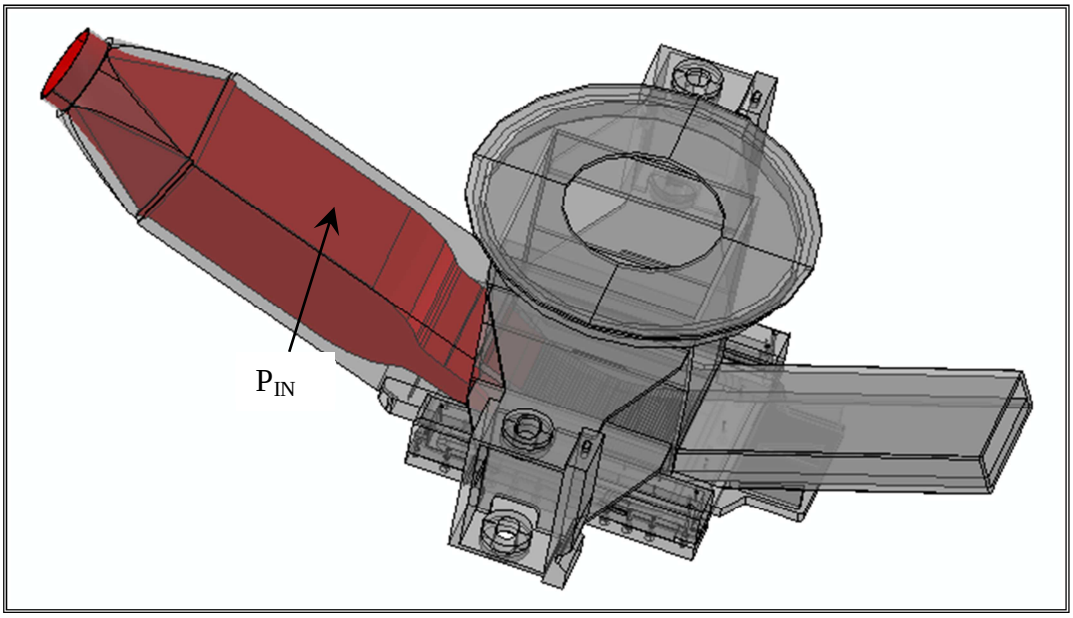

Figure 4-23. Inlet nozzle internal surfaces.

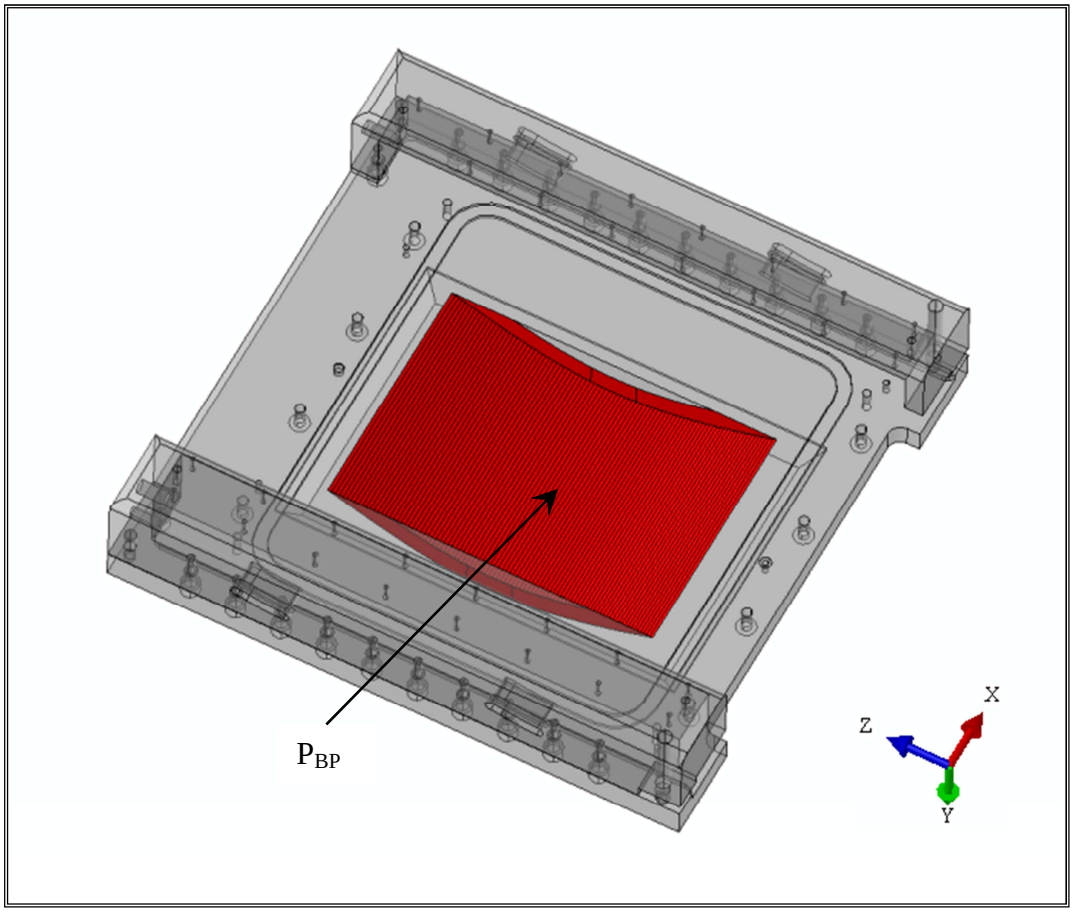

Figure 4-24. Back-Plate wetted surface.

Furthermore, a pressure of 5 kPa has been assumed for the containment vessel helium atmosphere according to [19] and it has been applied as an external pressure to the whole external surface of the model.

Mechanical loads exerted by the 8 M10 screws connecting BP to frame have been simulated by applying a pressure p_S equal to 68.963 MPa to the BP surfaces in contact with each screw washer and a BP oriented shear stress τ_S of 27.232 MPa to the lateral surface of each threaded hole of the frame (Figs. 4-25 and 4-26). These pressure loads have been calculated imposing that the tightening vertical forces exerted by screws might induce a force linear density onto the metallic gasket horizontal segments equal to a value of 180 N/mm [19], which is the force linear density value which ensures the perfect sealing of the contact between the Back-Plate and the frame during the nominal scenario.

Mechanical loads exerted by the skates onto BP and frame have been simulated by applying a pressure p_C of 2.369 MPa to the BP supports surfaces in contact with inclined cams of clamping system (Fig. 4-27) and a pressure p_R of 3.516 MPa to the frame surfaces in contact with external rollers of each skate (Fig. 4-28). These loads have been calculated imposing that the resultant forces of the clamping system might induce a force linear density onto the gasket vertical segments equal to the design sealing value of 180 N/mm.

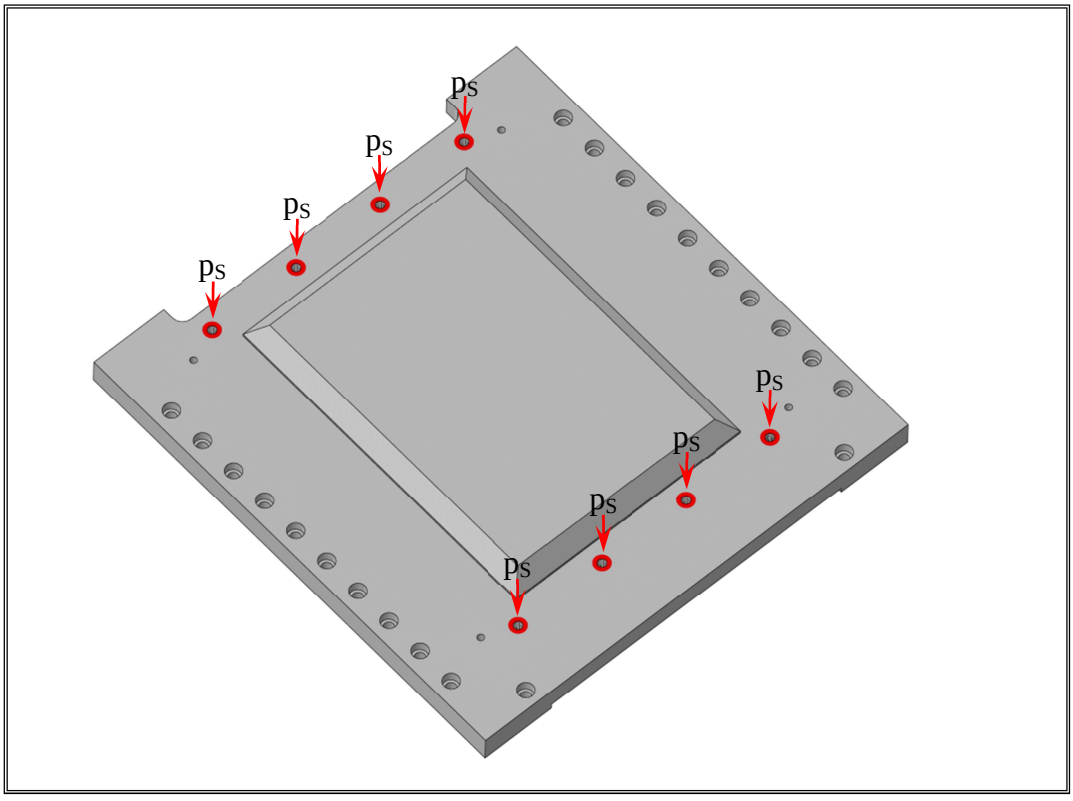

Figure 4-25. Pressure p_S along BP surface in contact with screw washers.

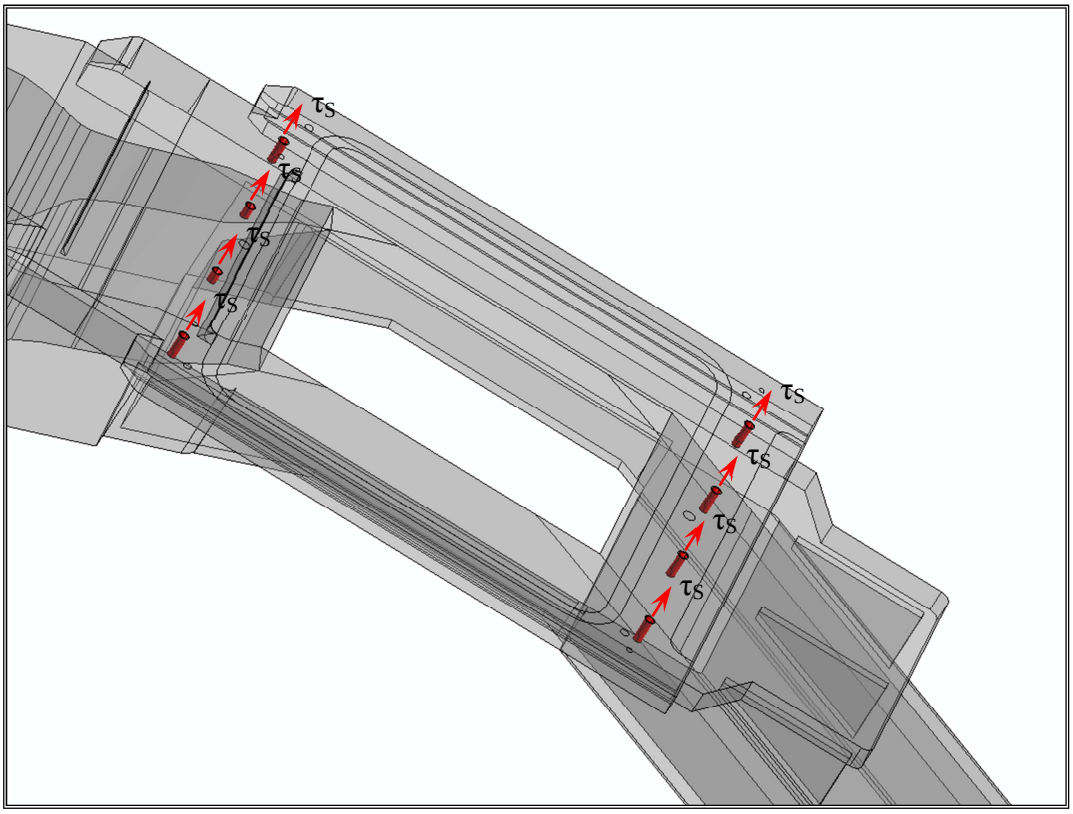

Figure 4-26. Shear stress τ_S along lateral surfaces of frame threaded holes.

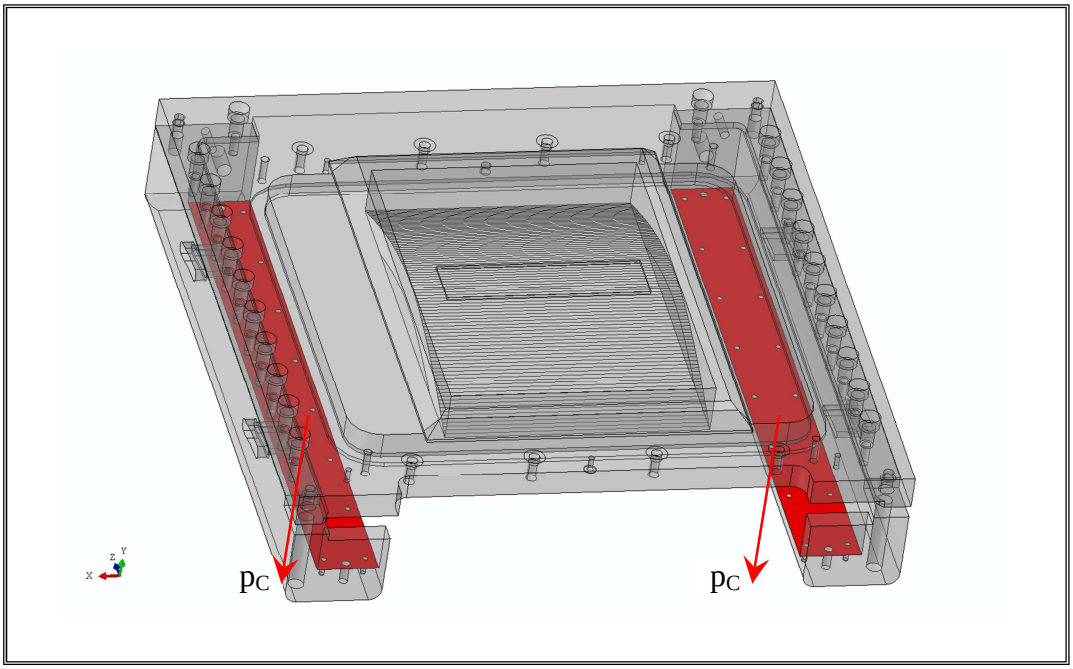

Figure 4-27. Pressure p_C along BP supports surfaces in contact with inclined cams.

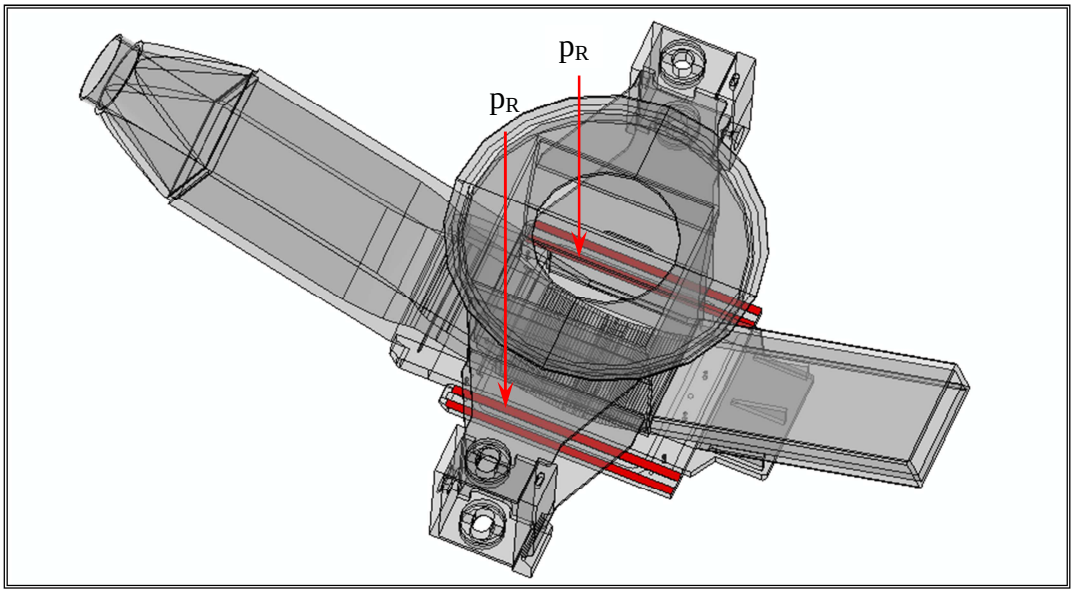

Figure 4-28. Pressure p_R along frame surfaces in contact with skate external rollers.

As far as support framework and Lithium inlet pipe mechanical constraints are concerned, all displacements (u_x, u_y, u_z) of nodes lying on surfaces highlighted in red in Figs. 4-29 and 4-30, respectively, have been prevented in order to simulate the effect of the connection of the two components to the containment vessel floor.

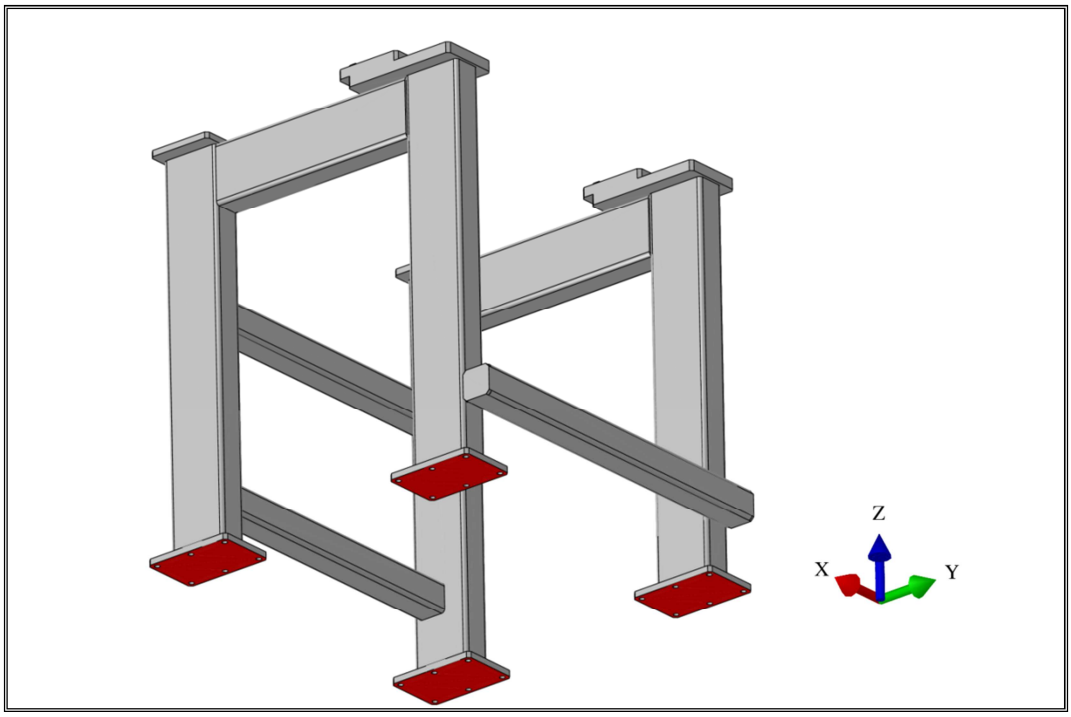

Figure 4-29. Support framework constraints.

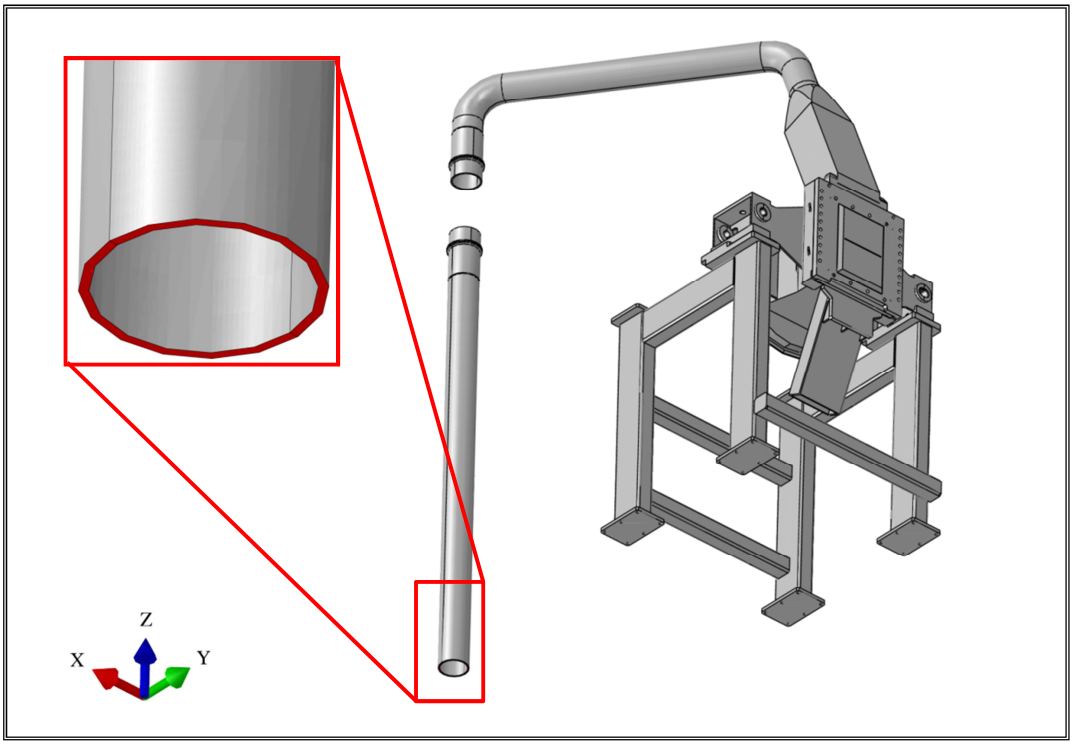

Figure 4-30. Lithium inlet pipe constraints.

Regarding TA system constraints, in order to properly take into account the mechanical effect of the bellows devoted to connect the TC to the beam duct, displacements along X and Z directions of the nodes highlighted in yellow and blue (Fig. 4-31), respectively, have been prevented. Moreover, displacements along Z direction have been prevented to nodes highlighted in red in Fig. 4-32, in order to simulate the effect of the grains devoted to avoid gap openings between TA and support framework.

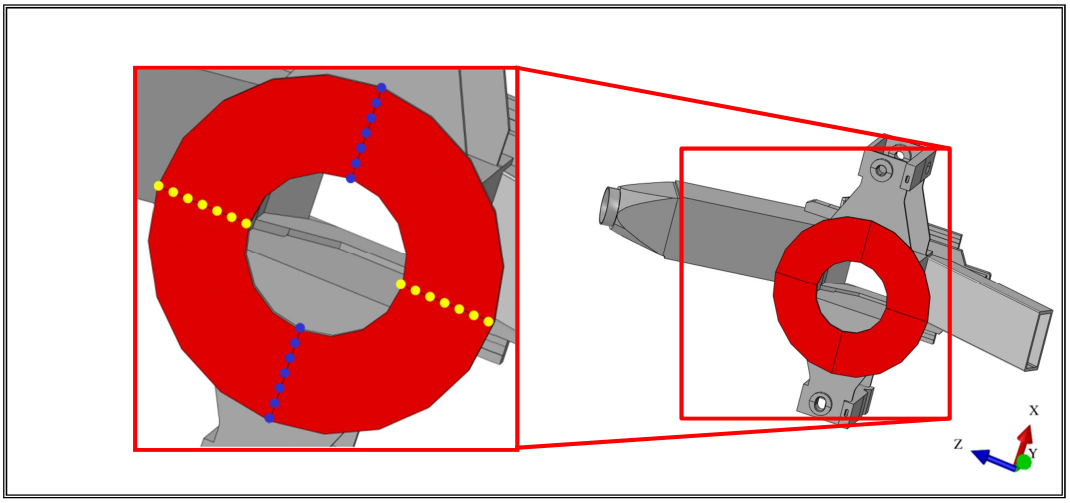

Figure 4-31. TC flange constraints.

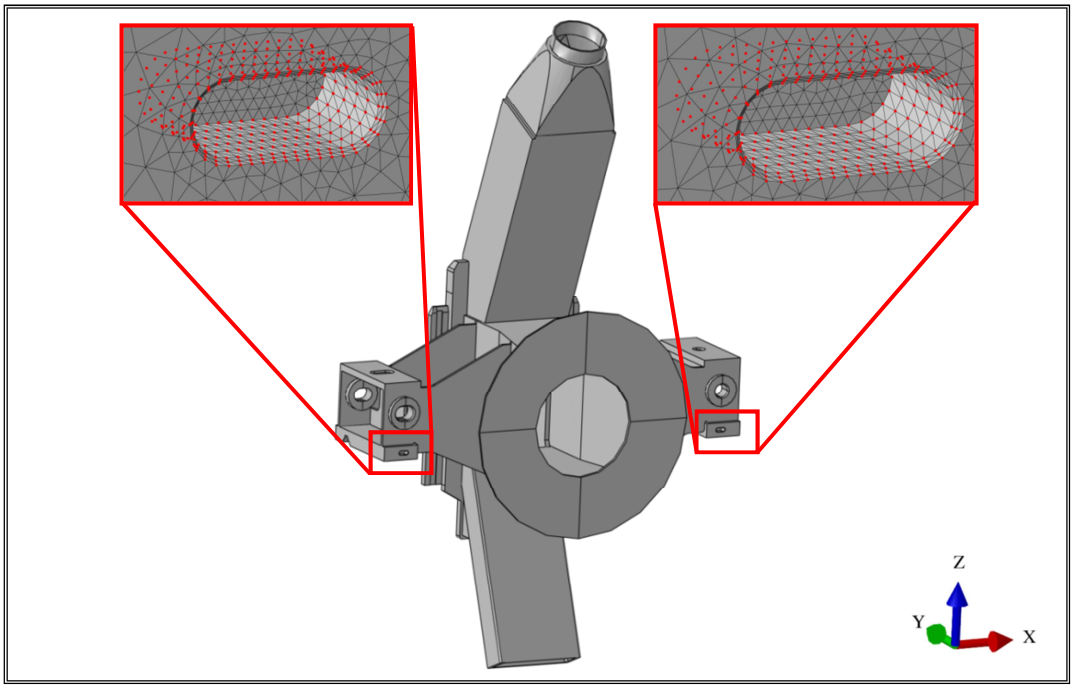

Figure 4-32. TA system constraints along Z direction.

Finally, the gimbal expansion joint, designed to connect the two sections of the Lithium inlet pipe, has been simulated. In particular, a proper kinematic coupling model has been adopted for the two flanges highlighted in red in Fig. 4-33. This kinematic model, characterized by an angular elastic spring equal to 4.2 N·m/°, allows the coupling of translational and rotational displacements of the two flanges connected.

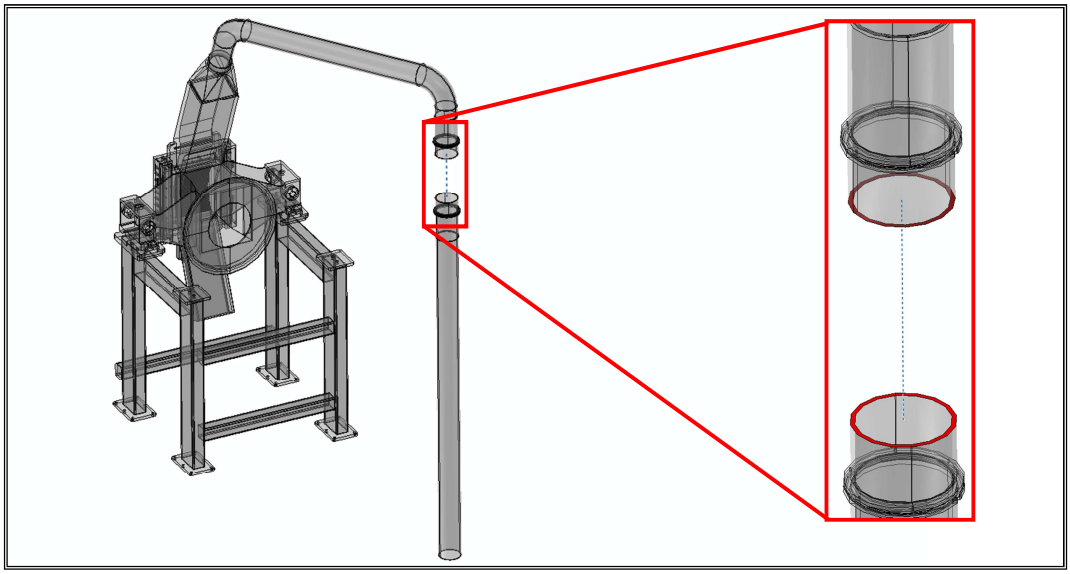

Figure 4-33. The Lithium inlet pipe flanges connected by the gimbal expansion joint.

4.3. Steady state analysis and results

An un-coupled thermo-mechanical steady state analysis has been carried out to investigate the TA, integrated with its support framework and the Lithium inlet pipe, thermo-mechanical behaviour under the reference nominal scenario in order to assess the potential aptitude of this system to safely withstand the loads it undergoes without incurring in significant deformations and yielding-induced structural crisis of the structure, with a particular attention on its replaceable Back-Plate.

Two steady state thermal analyses, one for each thermal condition taken into account, have been carried out to obtain the corresponding thermal field distribution. Every thermal analysis has been followed by two independent steady state mechanical analyses intended to separately assess the distributions of total and secondary stresses and to derive that of primary stresses as the difference.

In order to study the structure thermal behaviour, attention has been mainly focussed on the assessment of the spatial distribution of its thermal field. On the other hand, in order to investigate its mechanical behaviour, attention has been paid to the assessment of the spatial distribution of the Von Mises equivalent stress field. Moreover, in order to verify that no significant deformations occur which might warp BP channel inducing lithium flow instability and cause an overlapping between BP external surface and HFTM, a particular attention has been paid also to the analysis of the BP deformation field and to the displacements of its surface directly faced to the HFTM. Finally, the potential insurgence of a misalignment between deuteron beams and BP footprint, due to excessive BP displacements on the plane normal to the beam direction, has been investigated too.

Since the design of TA has to be based on a consistent set of rules taking into account, at the same time, regulation requirements for nuclear components, the peculiarities of EUROFER mechanical behaviour and the specific operating conditions foreseen for IFMIF environment, a stress linearization procedure has been carried out, with the specific aim of evaluating general or local primary membrane stress tensor (P_m or P_L), primary bending stress tensor (P_b), general or local secondary membrane stress tensor (Q_m or Q_L), secondary bending stress tensor (Q_b) and peak stress (F) in some particularly significant paths of TA.

Stress values calculated have been adopted to verify if the TA thermo-mechanical stress state complies with requirements prescribed by SDC-IC rules [44], that are both the most conservative and comprehensive of all possible damage modes. In particular, in SDC-IC as in conventional codes, primary stresses are limited in order to guarantee the components against M (monotonic) type damages, while secondary stresses are limited to preserve them against C (cyclic) type damages, namely the progressive deformation and the time independent fatigue [45].

As in similar safety codes, also SDC-IC foresees different operating levels with proper sets

of rules and stress limits according with loads and boundary conditions that the component is envisaged to withstand. Loads and boundary conditions typical of the IFMIF nominal steady state scenario are classified as Level A, therefore rules relevant to this operating level have been taken into account.

As to this set of rules, in case thermal-activated phenomena (thermal creep e.g.) might be neglected, the following low temperature rules are imposed by SDC-IC code in order to protect components against M type damages [44]:

$$\overline{P_m} \le S_m(T_m, \Phi t_m) \tag{4-3}$$

$$\overline{P_L + P_b} \le K_{eff} S_m(T_m, \Phi t_m) \tag{4-4}$$

$$\overline{P_L} \le \min\left[1.5 S_m(T_m, \Phi t_m), S_{y,min}(T_m, \Phi t_m)\right] \quad \text{(in local non-overlapping areas)} \tag{4-5}$$

$$\overline{P_L} \le 1.1 S_m(T_m, \Phi t_m) \quad \text{(in local overlapping areas)} \tag{4-6}$$

where $\overline{P_m}$ is the general primary membrane stress intensity, $\overline{P_L}$ is the local primary membrane stress intensity, $\overline{P_L + P_b}$ is the stress intensity of the sum of the aforementioned tensors P_L and P_b, K_{eff} is an effective bending shape factor depending on the resisting section, S_m is the allowable stress limit depending on thickness averaged temperature T_m and neutron fluence Φt_m and $S_{y,min}$ is the minimum tensile yield strength depending on thickness averaged temperature T_m and neutron fluence Φt_m too.

On the other hand, in case thermal-activated phenomena are not negligible, SDC-IC code imposes the following high temperature rules to be verified too [44]:

$$U_t\left(\overline{P_m}\right) \le 1 \tag{4-7}$$

$$U_t\left(\overline{P_L + \frac{P_b}{K_t}}\right) \le 1 \tag{4-8}$$

where K_t is the so-called creep bending shape factor and U_t is the creep usage fraction defined as:

$$U_t\left(\overline{\sigma_j}\right) = \sum_j \left(\frac{t_j}{t_{S,j}}\right) \tag{4-9}$$

that may be calculated adopting the following procedure based on the division of the component operating time t into N intervals chosen in such a way that the operating temperatures and stresses are approximately constant throughout the interval. In particular, for each interval j of duration t_j, the highest operating temperature T_j as well as the highest stress intensity $\overline{\sigma_j}$ reached are calculated. The maximum allowable time t_{Sj} at any stress $\overline{\sigma_j}$ and

temperature T_j are obtained from the proper $S_t(T,t)$ curve, that gives the allowable stress limit depending on temperature T and on component operational time t [45]. In particular, $S_t(T,t)$ curve values have been drawn from [46].

As a first approximation, assuming that loads over the overall operating period are constant, it may be shown [45] that Eqs. (4-7) and (4-8) reduces to:

$$\overline{P_m} \le S_t(T,t) \tag{4-10}$$

$$\overline{P_L + \frac{P_b}{K_t}} \le S_t(T,t) \tag{4-11}$$

As it can be deduced from previous considerations, SDC-IC and conventional codes do not take into account secondary stresses when M type damages are verified since usually material ductility allows to accommodate thermal stresses.

Anyway, since materials typically lose their ductility and become brittle when subjected to neutronic irradiation, some further rules have been included in SDC-IC code to properly take into account this phenomenon [45]. In particular, SDC-IC defines two different modes of potential failure due to the limited ductility of the materials: immediate plastic flow localisation and immediate local fracture due to exhaustion of ductility [47]. The relevant rules envisaged from SDC-IC codes are [44]:

$$\overline{P_L + Q_L} \le S_e(T_m, \Phi t_m) \quad \text{immediate plastic flow localisation} \tag{4-12}$$

$$\overline{P_L + P_b + Q + F} \le S_d(T, \Phi t, r_2) \quad \text{immediate local fracture due to exhaustion of ductility} \tag{4-13}$$

$$\overline{P_L + P_b + Q} \le S_d(T, \Phi t, r_3) \quad \text{immediate local fracture due to exhaustion of ductility} \tag{4-14}$$

where S_e is the allowable stress intensity dependent on thickness averaged temperature T_m and neutron fluence Φt_m and S_d is the allowable stress dependent on r-factors, temperature T and neutron fluence Φt of the point under consideration where localized stress arises. Analytical definitions of r-factor, S_e and S_d functions are reported in [44-47]. It has to be underlined that, given that irradiated EUROFER retains considerable ductility after necking, the potential failure mode due to immediate local fracture is not an issue, while that induced by immediate plastic flow localisation may be a matter of serious concern [46].

In order to verify if the TA thermo-mechanical stress state complies with requirements prescribed by SDC-IC rules with reference to level A criteria, proper linearization paths (Fig. 4-34) have been identified at the most heavily stressed areas of the BP, taking into account also areas where, in spite of not particularly high Von Mises equivalent stresses, high temperatures have been predicted that may result in the calculation of lower values of maximum allowable stress intensities.

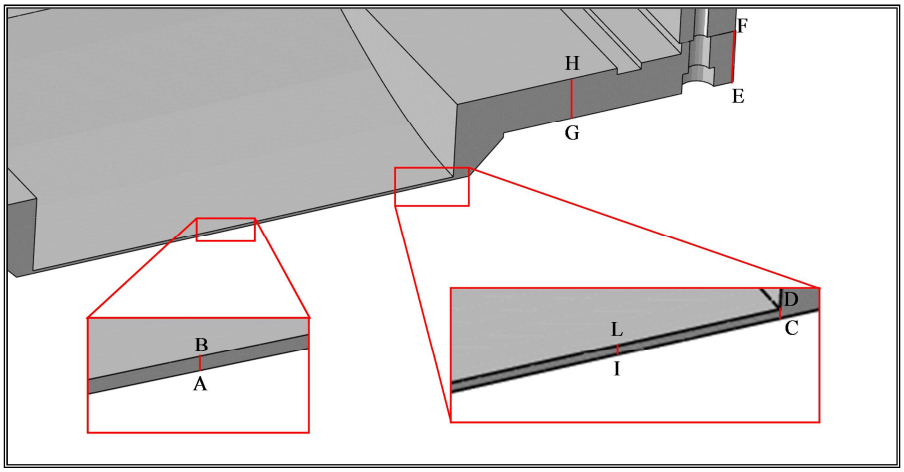

Figure 4-34. Stress linearization paths.

The obtained results in terms of thermal field, Von Mises equivalent stress (σ_{VM}) field, displacement field and SDC-IC safety rule verifications are reported in the following for all the investigated thermo-mechanical conditions (Figs. 4-35÷4-54 and Tables 4-3÷4-6). In particular, from the thermal point of view, results show that neither the limit temperature for thermal activated phenomena of 450°C [44] nor the maximum EUROFER allowable temperature of 550 °C is overcome in both the thermo-mechanical conditions taken into account. As a consequence of this, SDC-IC high temperature rules (4-10, 4-11) have not been considered and only low temperature SDC-IC safety criteria verifications (4-3, 4-4, 4-12) have been performed.

A maximum temperature slightly lower than 430 °C is predicted in a localized region of the target chamber at the edge with the frame and the Back-Plate, in both the assessed thermal scenarios. In particular, Condition 1 results have shown also that the maximum temperature of 80.4 °C reached within the support framework suggests that no further cooling strategies are necessary for it, except for the natural convection cooling already taken into account in this loading condition.

As far as the mechanical results are concerned, it can be observed that the highest values of the Von Mises equivalent stress are reached in a very small area, probably due to numerical singularities within the FEM model. In fact the whole structure experiences Von Mises equivalent stress values lower than 550 MPa in both the investigated thermo-mechanical conditions. As for the displacement field, the deformed (in red) vs. un-deformed (in grey) configuration of the whole model and a detail of the BP are reported, adopting an isotropic amplification factor equal to 50 for the deformed configuration in order to amplify the structure displacements respect to the initial configuration.

Particular attention has been paid to the potential misalignment between the deuteron beams and the BP footprint, the slipping that may occur between the TC arms and the support

framework and finally to the BP external surface displacements, in order to check that no overlapping with the HFTM surface takes place.

Mechanical results have also indicated that in Condition 1 the minimum value of the misalignment (u_x and u_z) between the deuteron beam and the BP footprint and the lowest maximum displacement of the BP external surface toward the HFTM ($u_{y,Max}$) are predicted. As a consequence of this and in addition to abovementioned thermal results, Condition 1 has been selected as the reference one. In particular, the maximum BP displacement along the beam direction amounts to 1.081 mm towards the HFTM. Therefore, BP and HFTM contact can be excluded, being 2 mm their nominal gap at room temperature.

Finally, SDC-IC safety rules for Level A criteria resulted to be generally fulfilled with comfortable margins except for those relevant to the potential loss of ductility in particular heavily stressed paths lying approximately on the BP middle section along the beam direction, suggesting the potential need of a BP design revision.

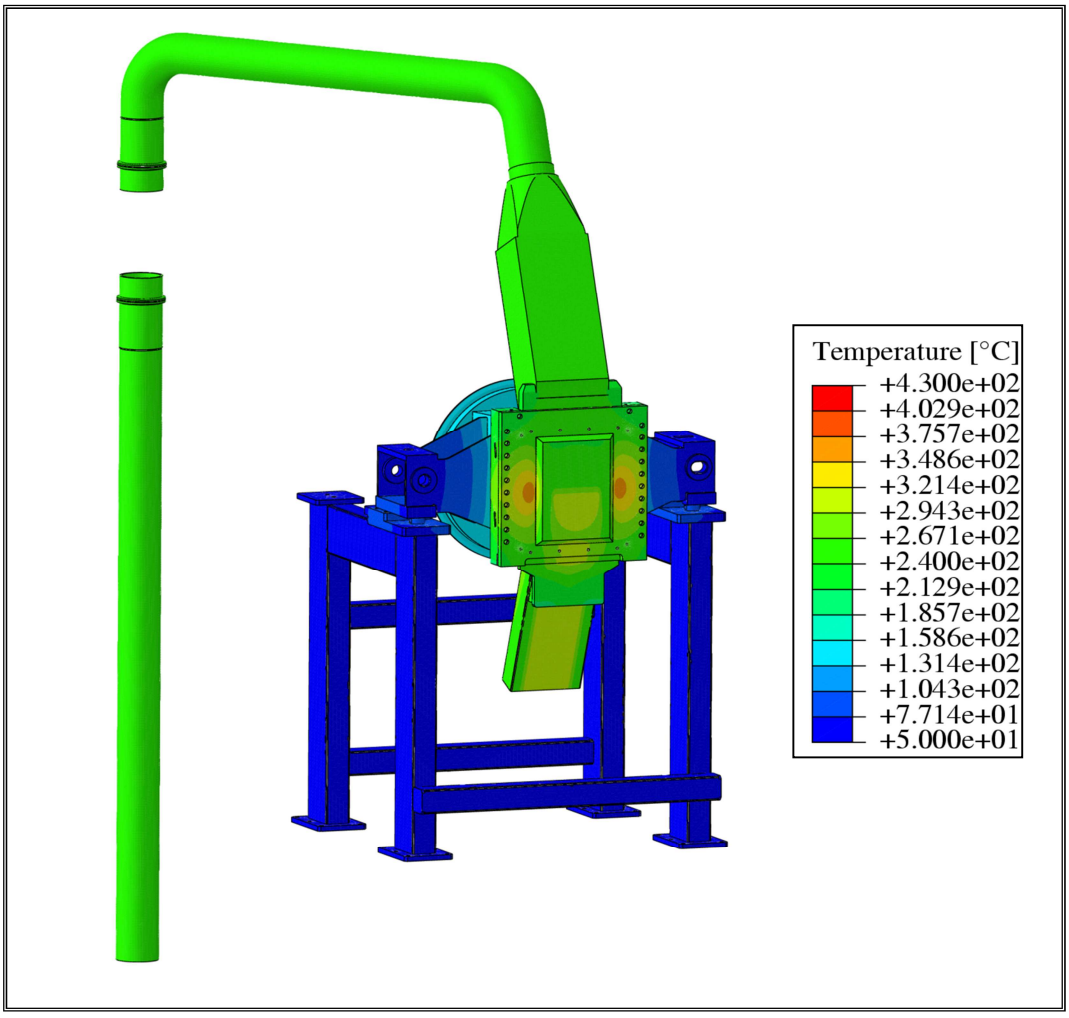

Figure 4-35. Condition 1 – Thermal field.

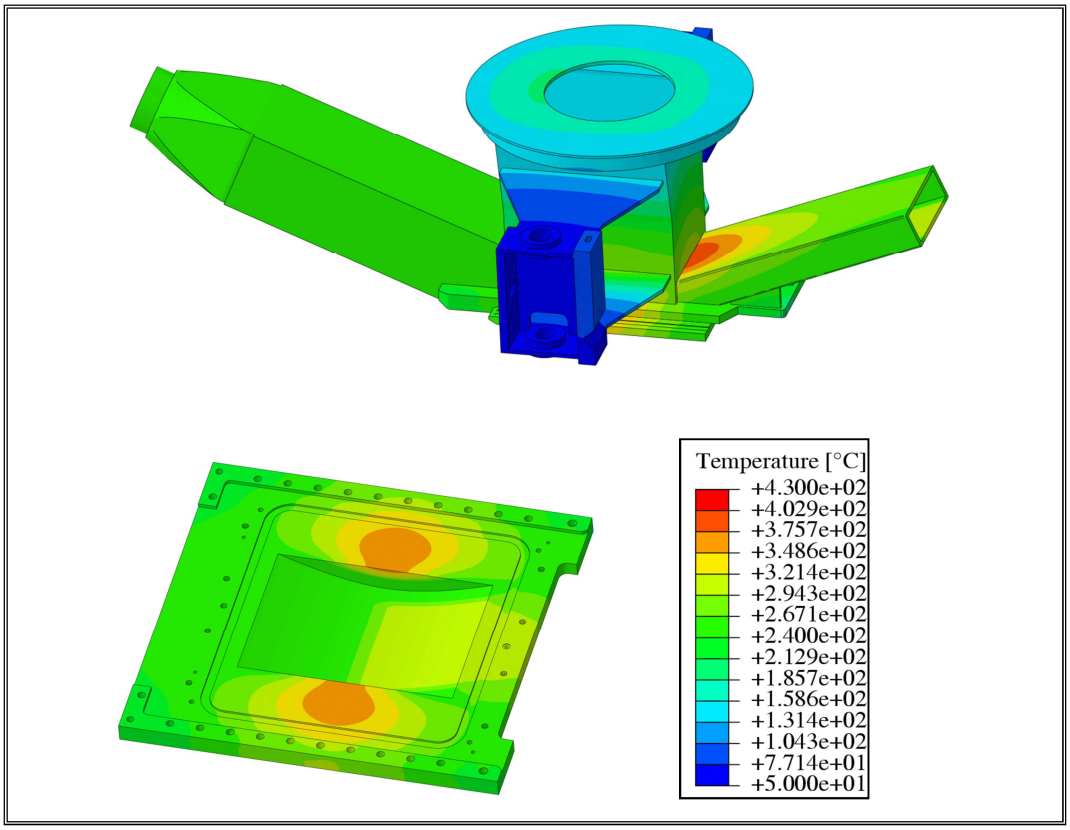

Figure 4-36. Condition 1 – TA and BP thermal field.

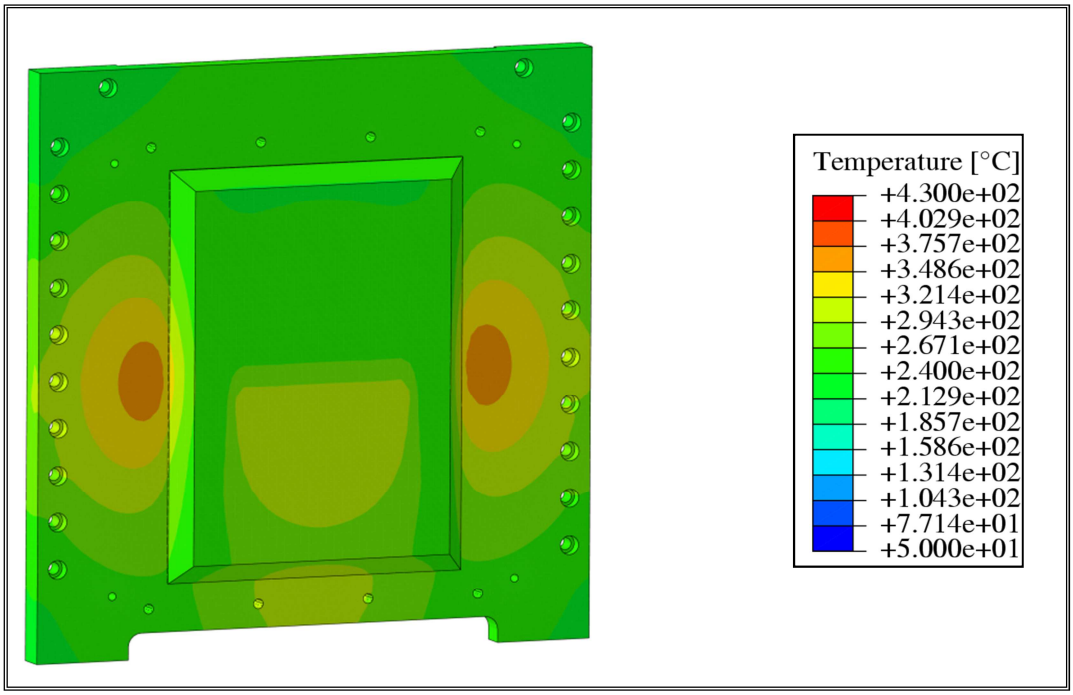

Figure 4-37. Condition 1 – BP thermal field.

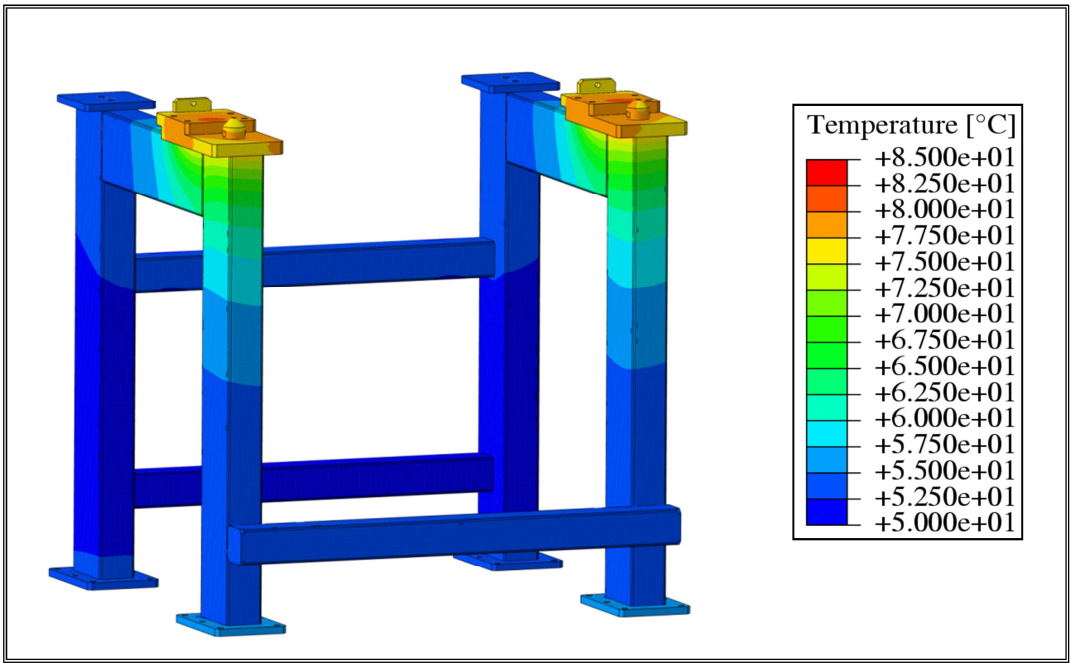

Figure 4-38. Condition 1 – Support framework thermal field.

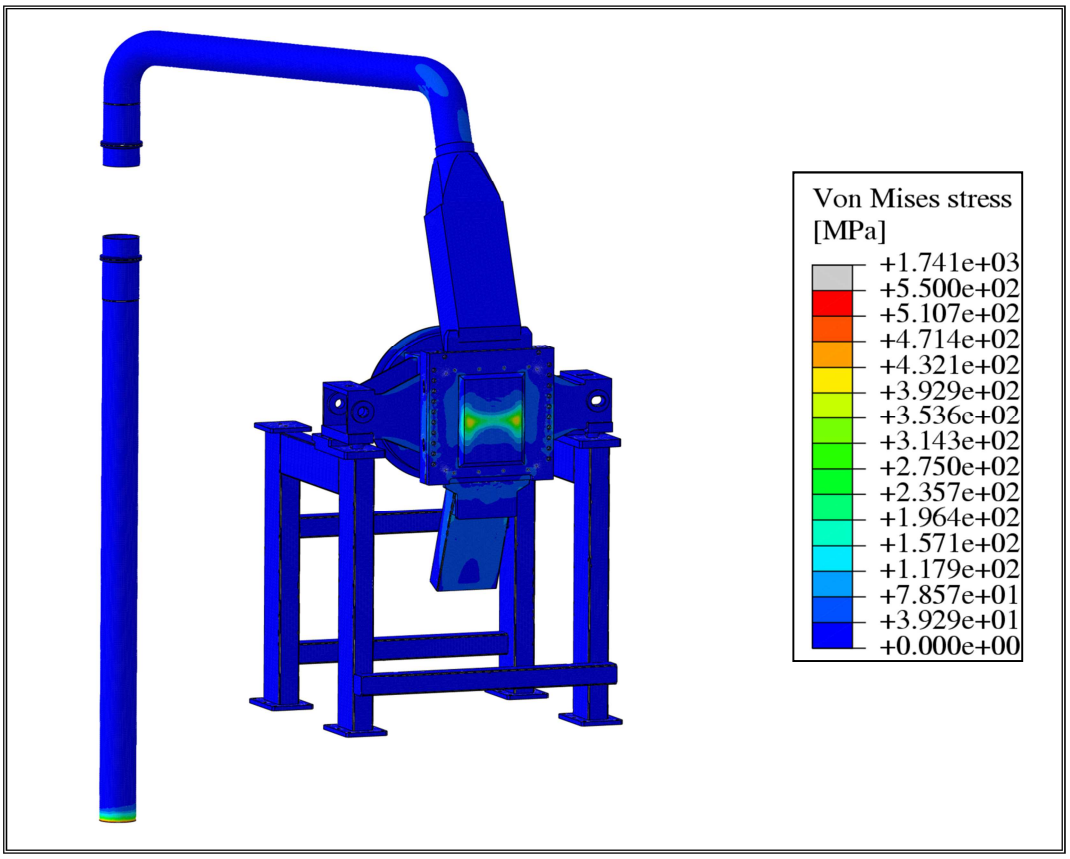

Figure 4-39. Condition 1 – Von Mises stress field.

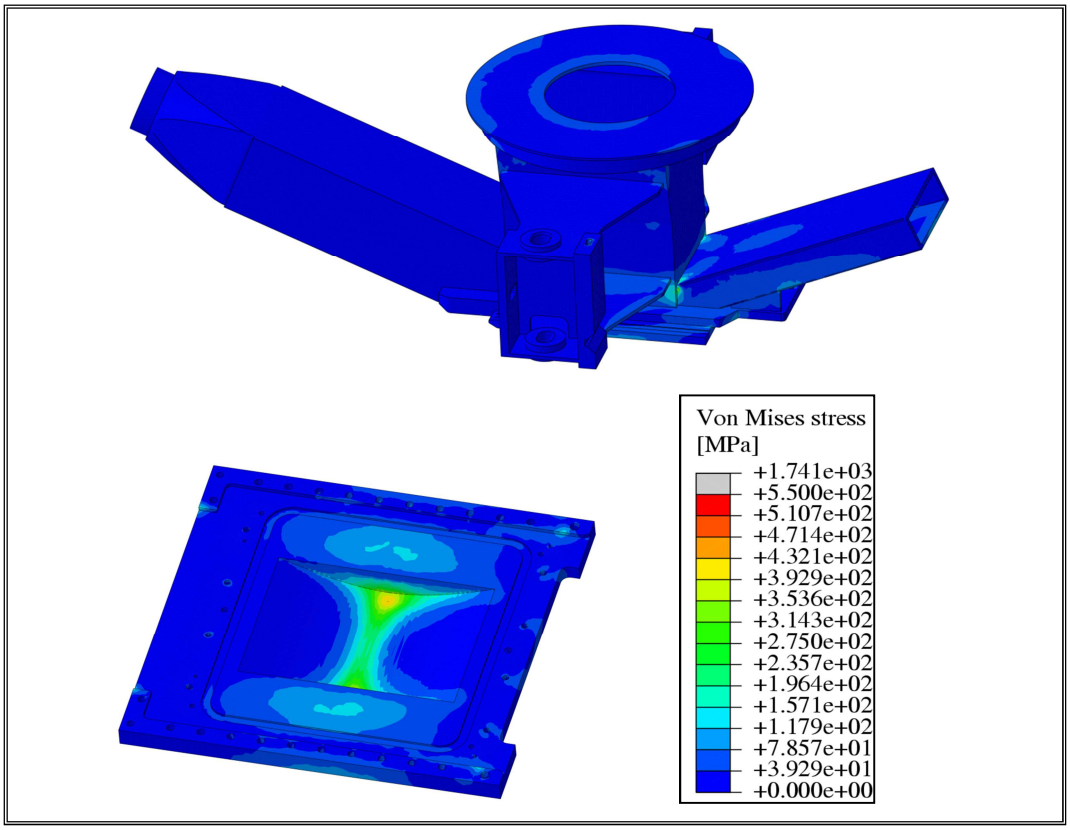

Figure 4-40. Condition 1 – TA and BP Von Mises stress field.

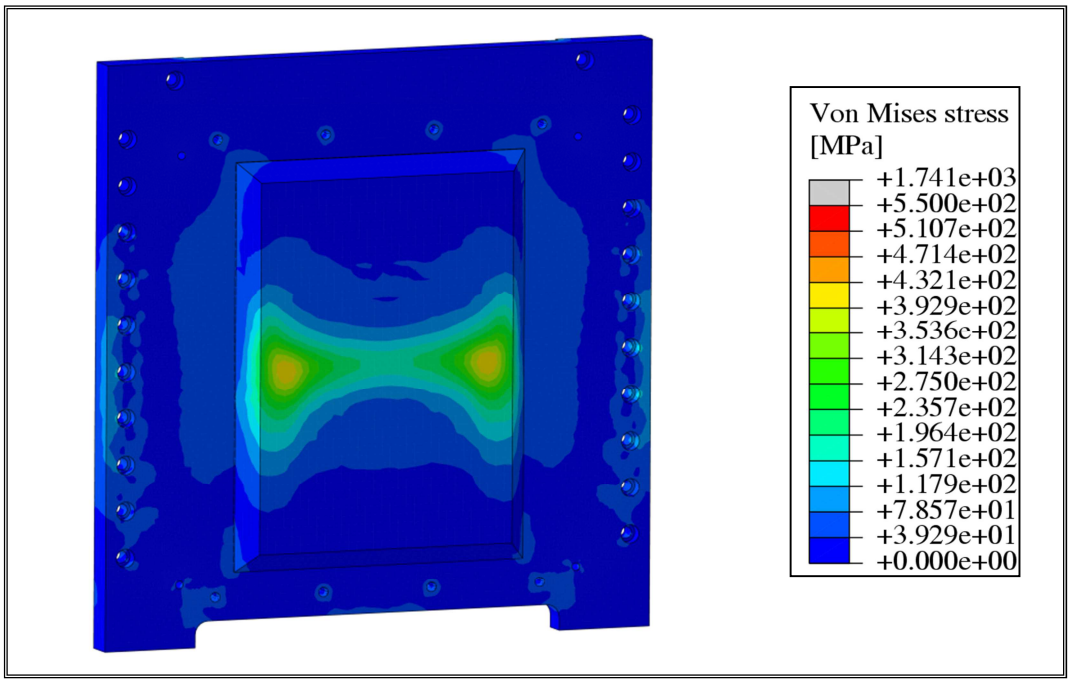

Figure 4-41. Condition 1 – BP Von Mises stress field.

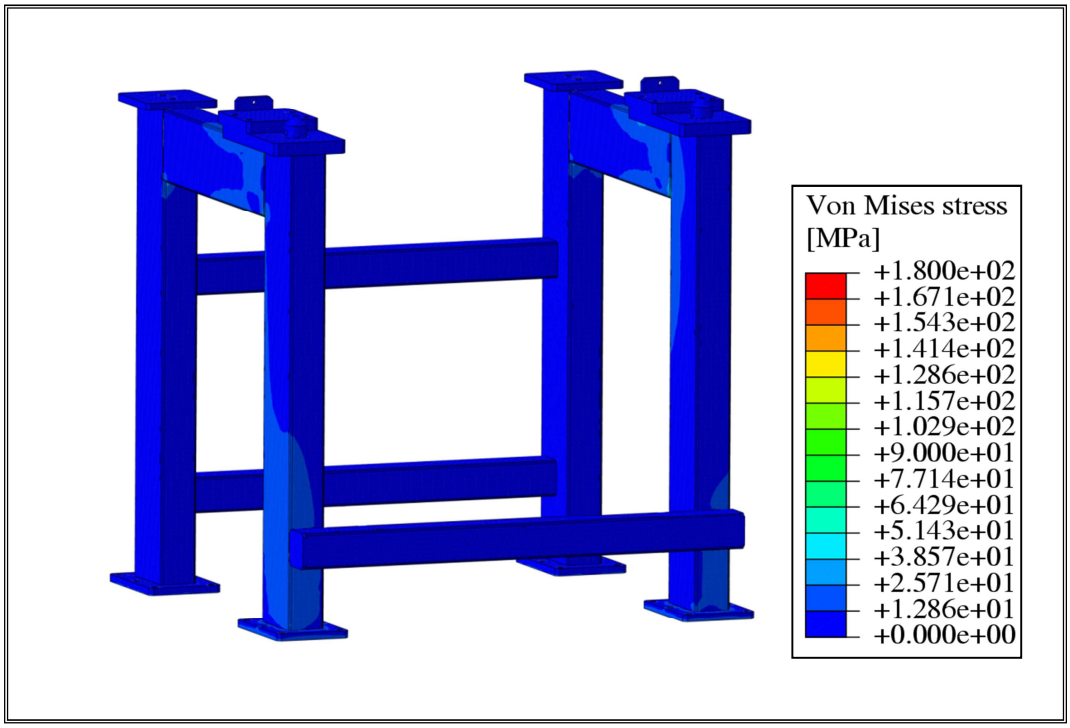

Figure 4-42. Condition 1 – Support framework Von Mises stress field.

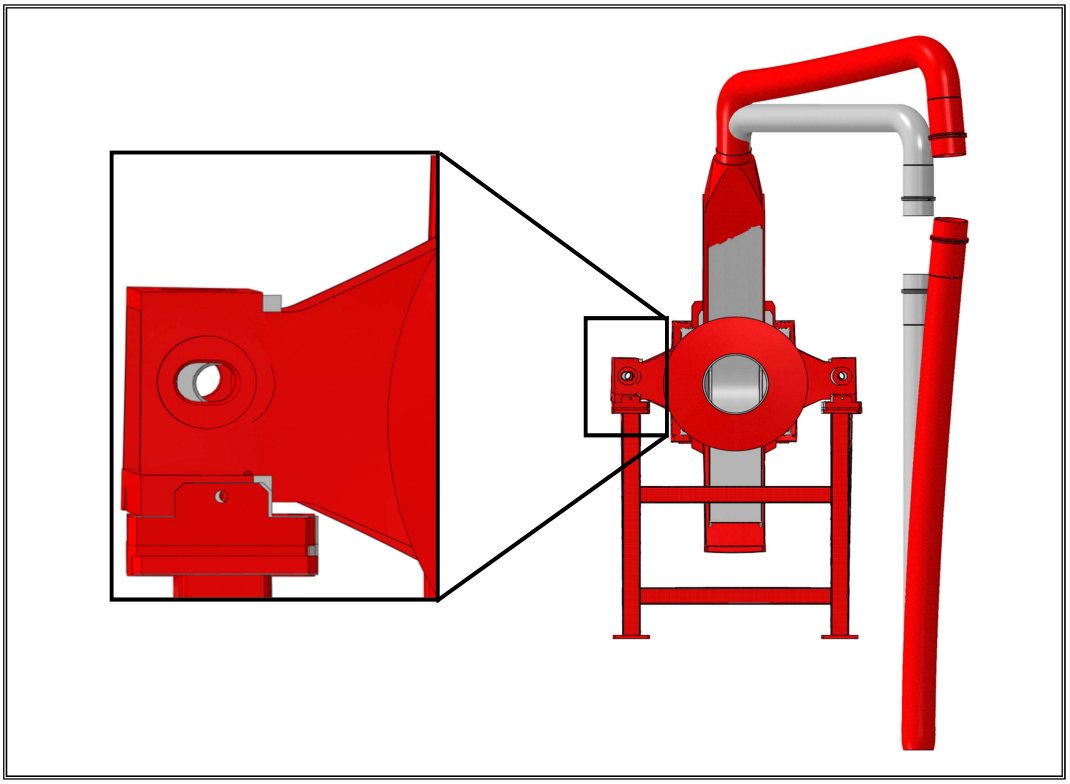

Figure 4-43. Condition 1 – Deformed vs. un-deformed configuration.

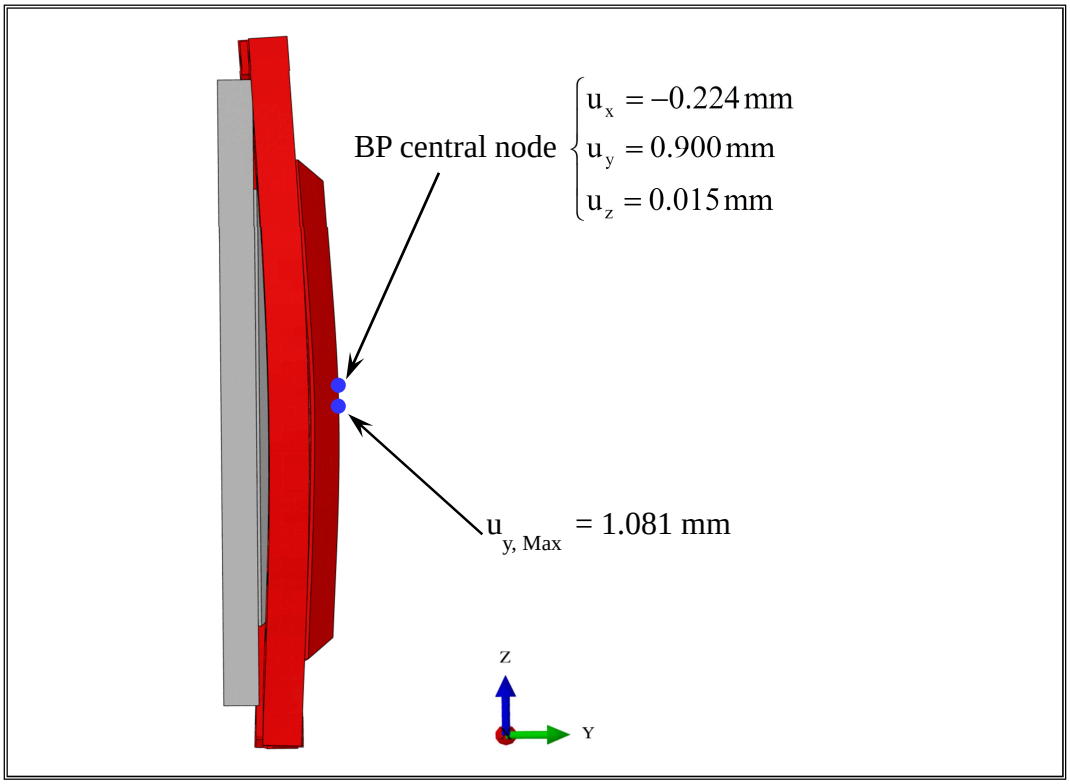

Figure 4-44. Condition 1 – BP deformed vs. un-deformed configuration.

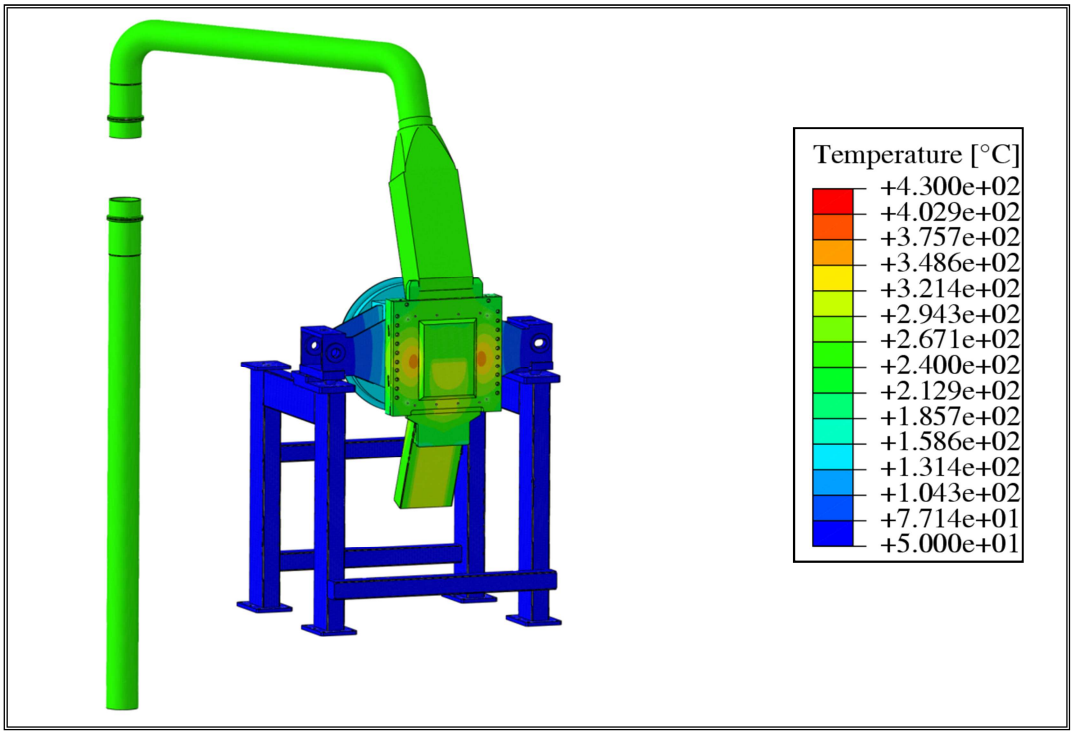

Figure 4-45. Condition 2 – Thermal field.

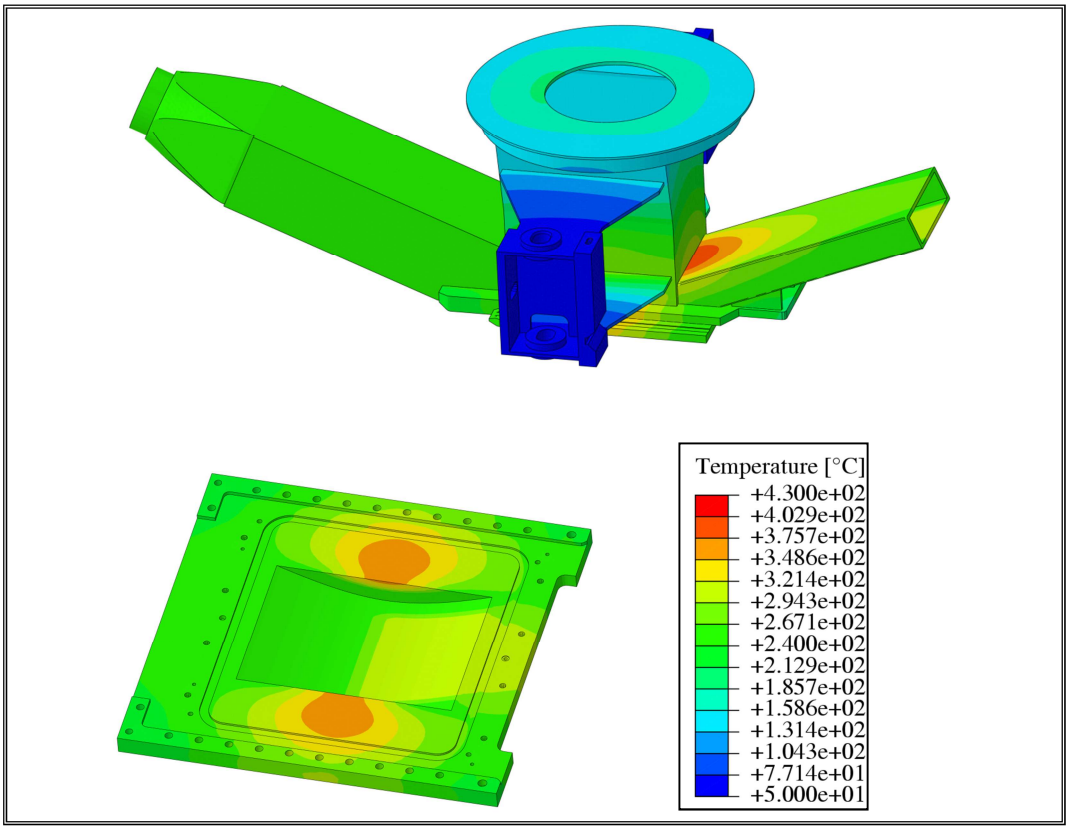

Figure 4-46. Condition 2 – TA and BP thermal field.

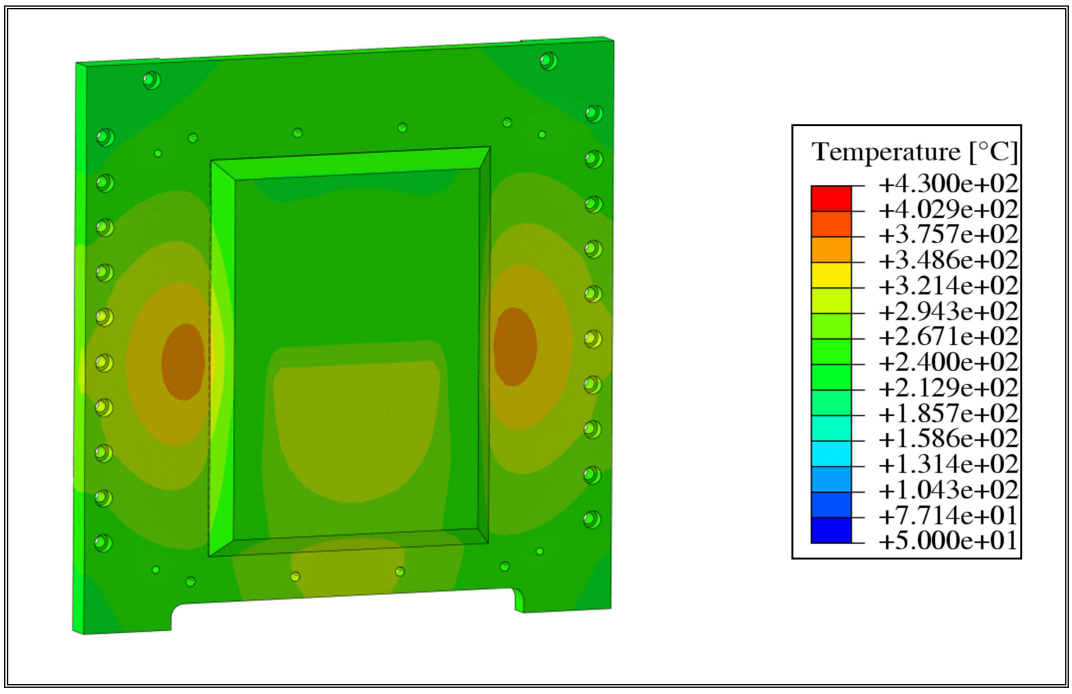

Figure 4-47. Condition 2 – BP thermal field.

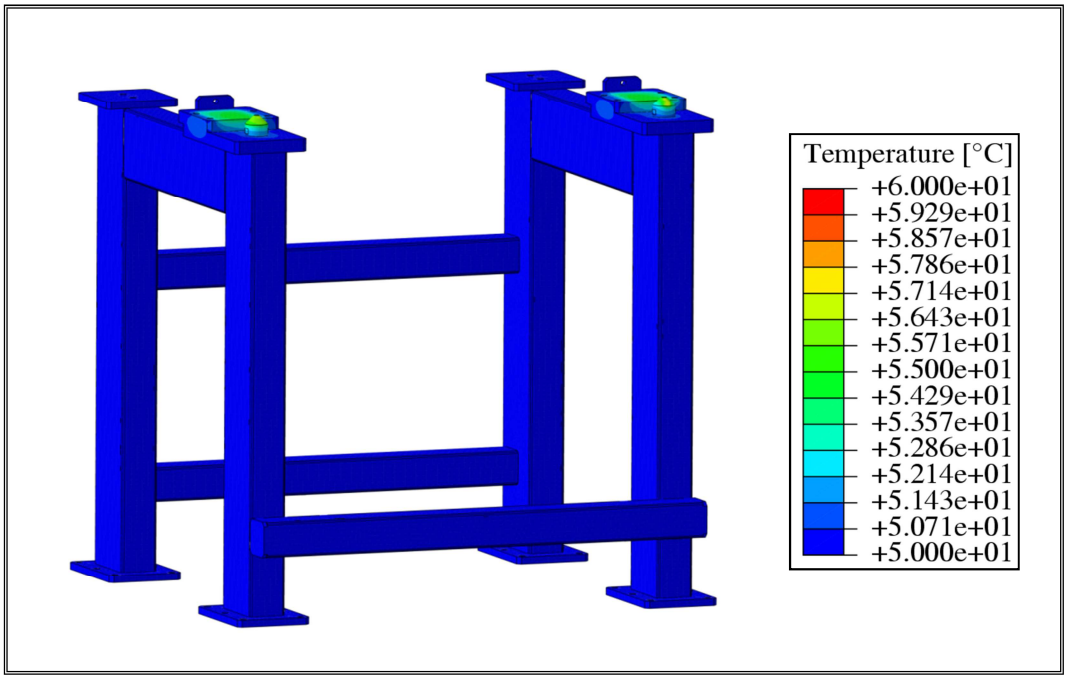

Figure 4-48. Condition 2 – Support framework thermal field.

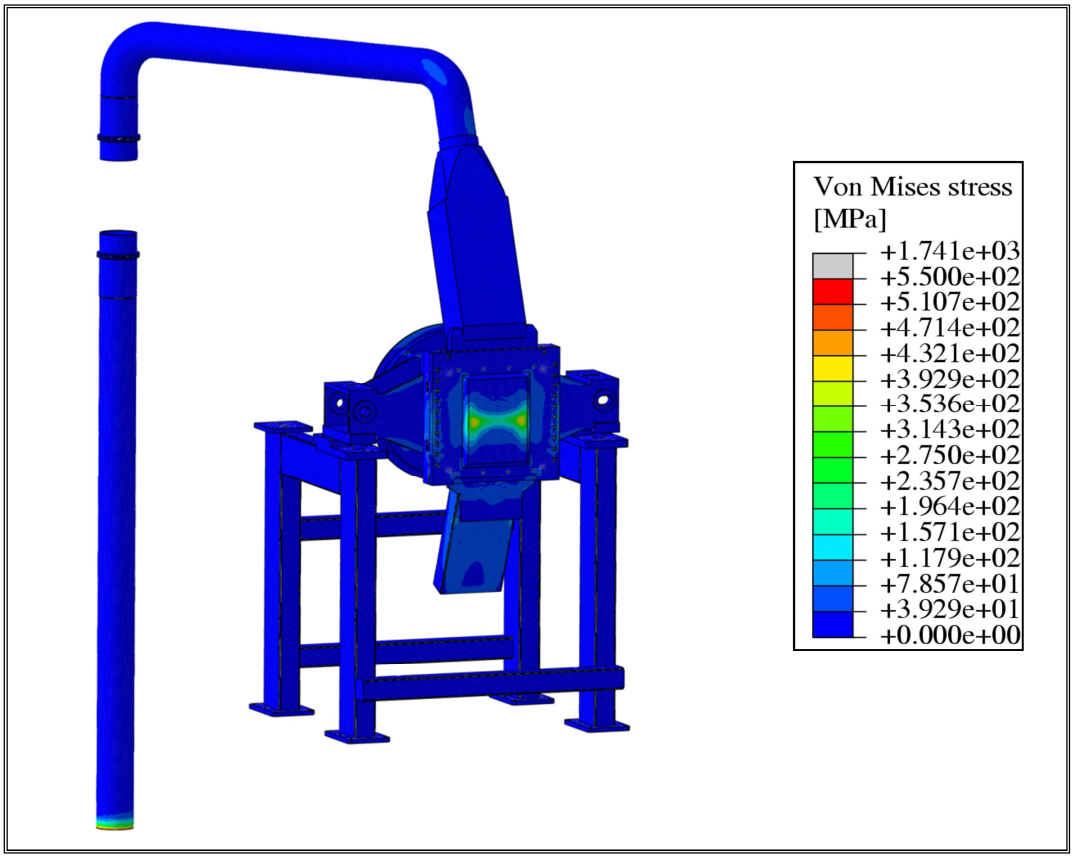

Figure 4-49. Condition 2 – Von Mises stress field.

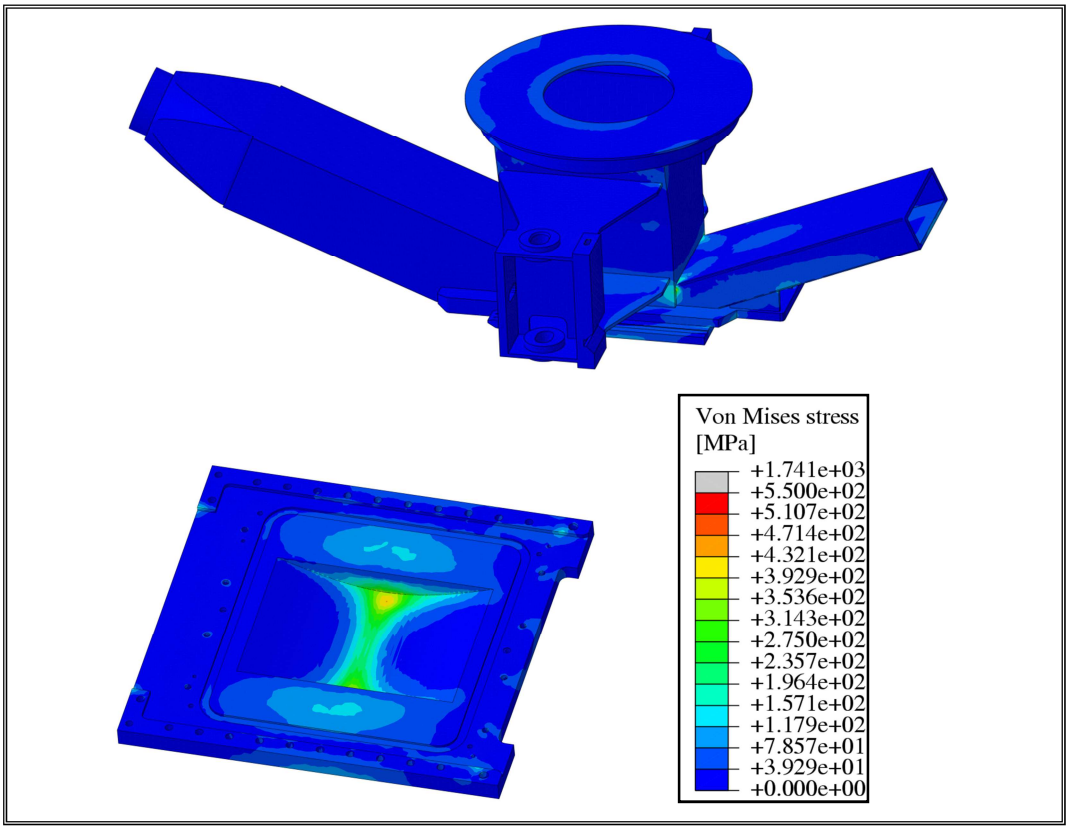

Figure 4-50. Condition 2 – TA and BP Von Mises stress field.

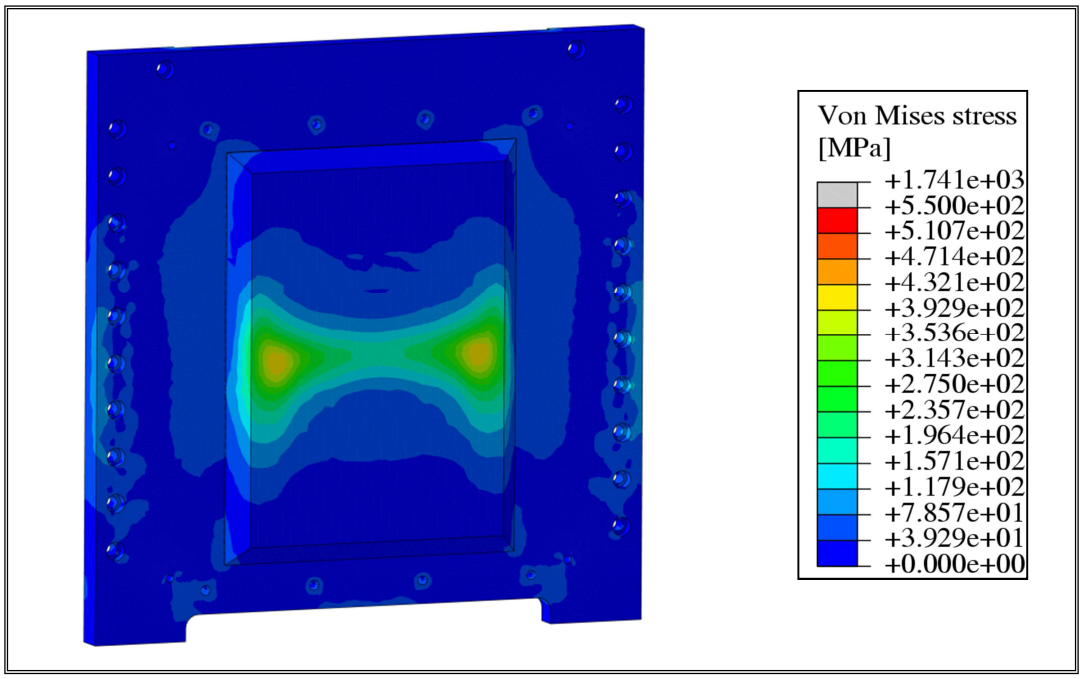

Figure 4-51. Condition 2 – BP Von Mises stress field.

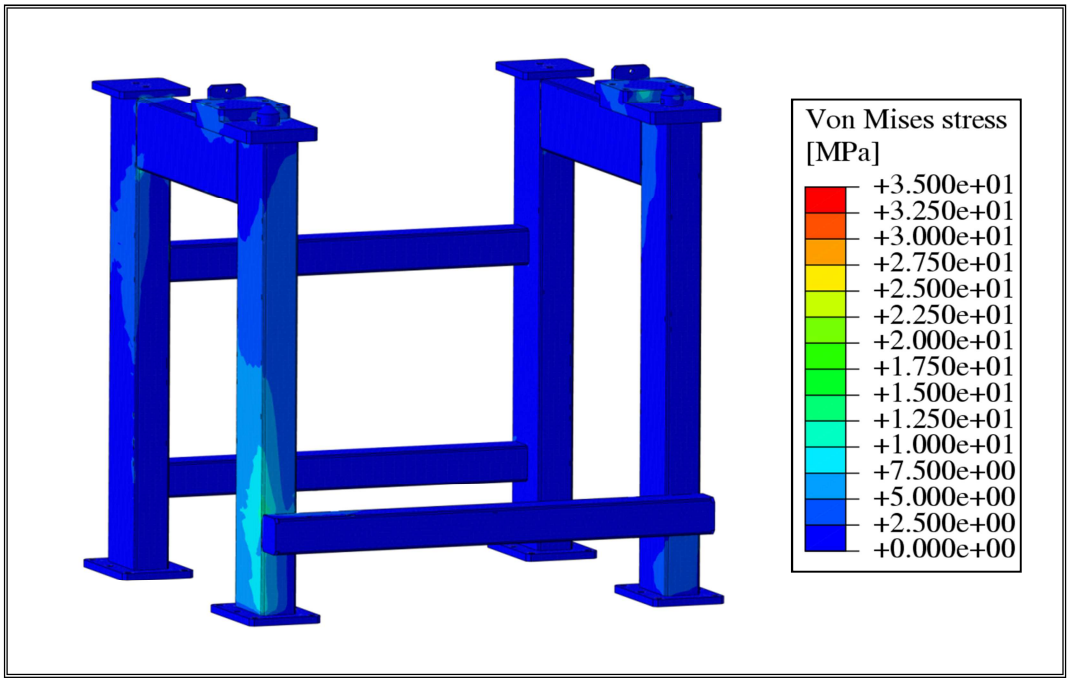

Figure 4-52. Condition 2 – Support framework Von Mises stress field.

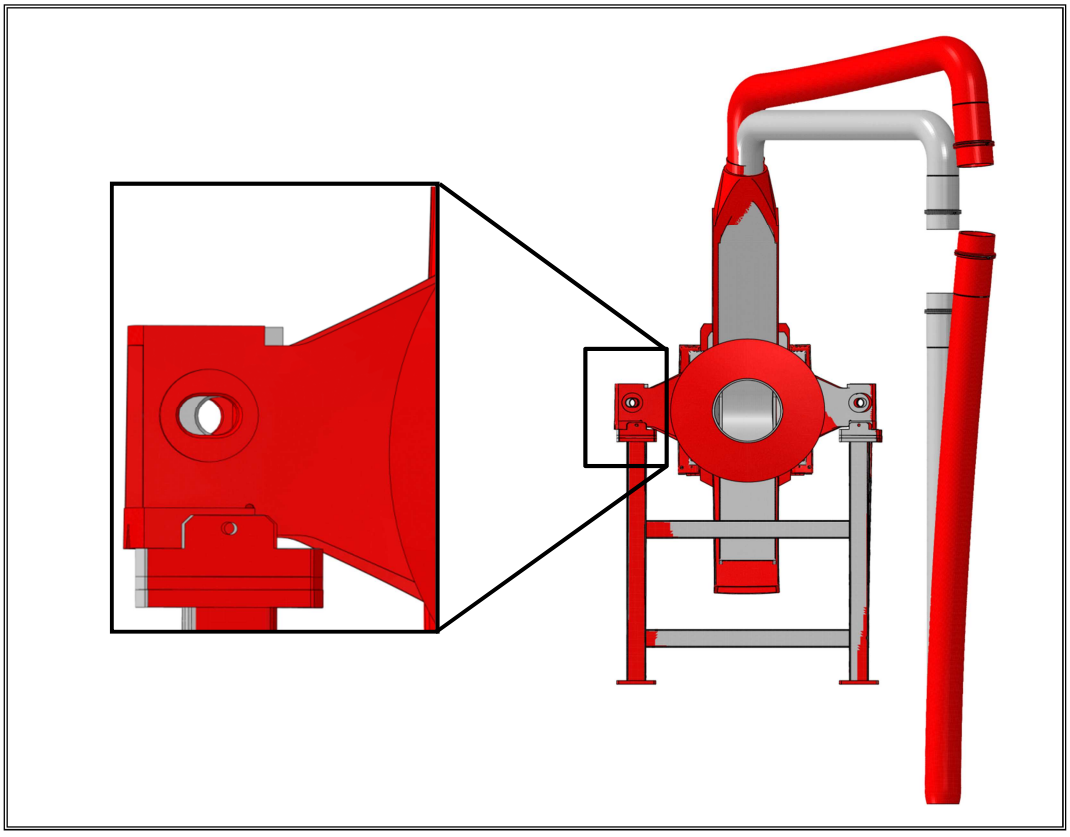

Figure 4-53. Condition 2 – Deformed vs. un-deformed configuration.

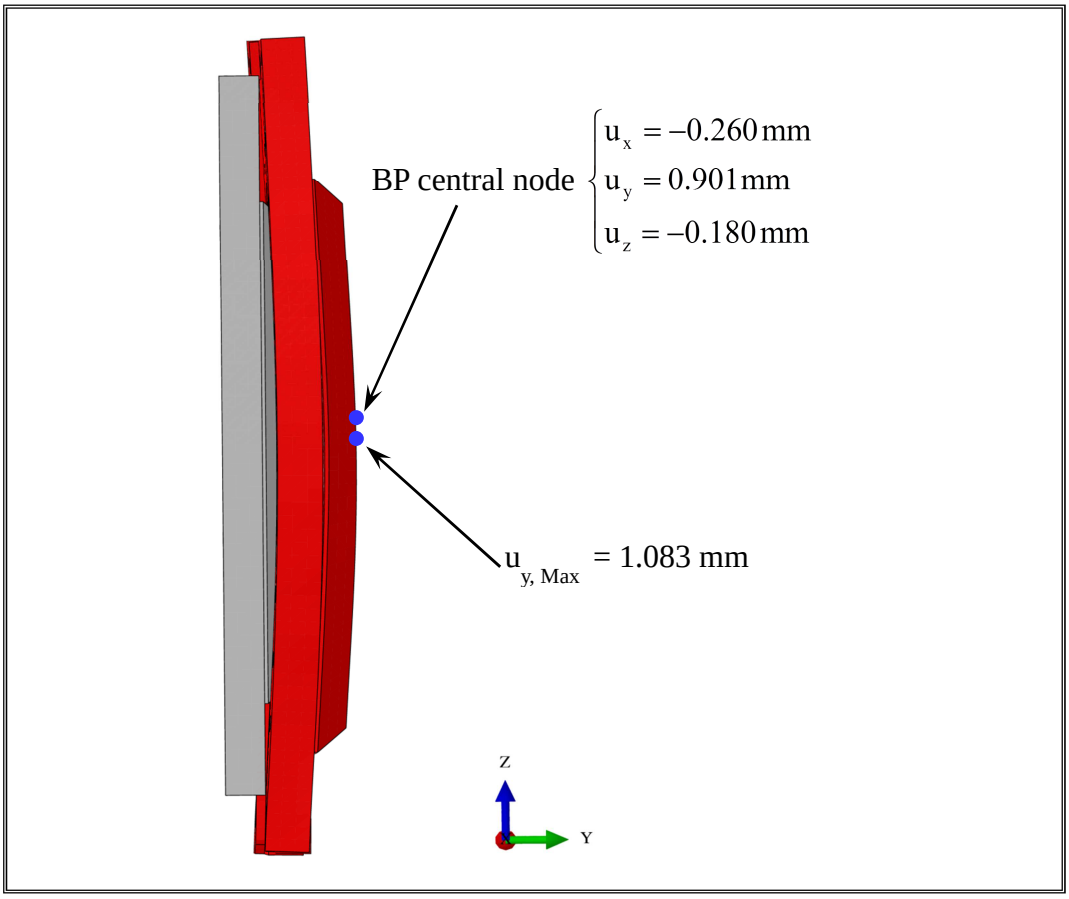

Figure 4-54. Condition 2 – Deformed vs. un-deformed configuration.

Table 4-3. Maximum and minimum component temperatures.

Maximum temperatures [°C]				
Condition	BP	TA	Inlet pipe	Framework
1	369.4	428.7	250.0	80.4
2	369.4	428.7	250.0	57.3
Minimum temperatures [°C]				
Condition	BP	TA	Inlet pipe	Framework
1	205.8	69.0	250.0	51.6
2	205.8	51.6	250.0	50.0

Table 4-4. External central BP node displacements.

Condition	u_x [mm]	u_y [mm]	u_z [mm]
1	-0.224	0.900	0.015
2	-0.260	0.901	-0.180

Table 4-5. Maximum BP displacement along the beam direction ($u_{y,Max}$).

Condition	$u_{y,Max}$ [mm]
1	1.081
2	1.083

Table 4-6. SDC-IC low temperature safety rules.

	Path AB	Path CD	Path EF	Path GH	Path IL
$T_{Max\text{-}Path}$ [°C]	286	252	296	367	250
P_m/S_m	0.0040	0.0015	0.0002	0.0006	0.0018
$(P_m+P_b)/(K_{eff}*S_m)$	0.0027	0.0012	0.0003	0.0007	0.0013
$(P_m+Q_m)/S_e$	0.6993	1.0632	0.3038	0.4930	1.4017

5. IFMIF Back-Plate optimization

The performed thermo-mechanical analyses on the IFMIF Target Assembly, integrated with its framework and Lithium inlet pipe, have put in evidence that a Back-Plate design review is needed.

A research campaign aimed at the BP geometric optimization has been therefore launched, in order to identify a BP geometric configuration able to safely withstand the loading conditions represented by the thermo-mechanical loads typical of the IFMIF nominal scenario, maximizing the BP lifetime during the neutronic irradiation period.

The research campaign has been articulated in two main sections. In the first one, a parametric approach has been followed in order to assess the potential influence of some critical geometric parameters on the thermo-mechanical performances of the BP, focusing the attention on the stress field arising within BP. In the second section, a thermo-mechanical analysis of the IFMIF TA endowed with the potential BP optimized configuration, selected at the end of the previous section, has been performed. In this analysis, the volumetric density of nuclear heat power (q‴) and DPA spatial distributions, purposely calculated by ENEA by means of a specific campaign of neutronic analyses, has been adopted, taking into account the potential IFMIF TA optimized geometric layout.

The whole optimization campaign has been divided into five phases. The first four phases have regarded the assessment of the influence that some geometric parameters have on the thermo-mechanical behaviour of the BP. The last phase has instead dealt with the thermo-mechanical behaviour of a potentially optimized TA layout, taking into account the effects of the volumetric swelling strain. Loads and boundary conditions adopted in the parametric campaign are those already described in § 4.2.2 and § 4.2.3.

5.1. Phase 1

Phase 1 of the BP design review procedure has regarded the IFMIF TA model described in § 4.2 and adopted for the thermo-mechanical analyses. On the basis of the obtained results from steady-state thermo-mechanical calculations, a BP design review procedure is needed in order to ensure the fulfilment of the design criteria prescribed by codes.

Since thermo-mechanical analyses have highlighted an intense stress intensity in the region of the lithium channel where there is a remarkable change in the BP thickness, it has been decided to investigate the influence that two geometric parameters have on the BP behaviour.

In Phase 1 of the BP design review procedure, the two geometric parameters have been identified in the thicknesses of the lithium channel (*W*) and of the BP (*D*). As far as the BP lithium channel thickness increase is concerned, the original thickness, equal to 1.8 mm and indicated with *S* in figure 5-1, has been increased to assess the influence of the added

thickness (*W*) on the overall BP thermo-mechanical performances under steady state thermo-mechanical loading conditions envisaged for it. On the basis of preliminary calculations, values of 1.2 mm and 2.0 mm, respectively, have been considered for *W*.

Concerning the BP thickness reduction, the decreasing of the original BP thickness *D* from the reference value of 32.8 mm to 17 mm has been taken into account, removing the volume originally enclosed within the red profile shown in figure 5-2.

Values of the geometric parameters taken into account and characterizing the two different configurations set-up are reported in table 5-1.

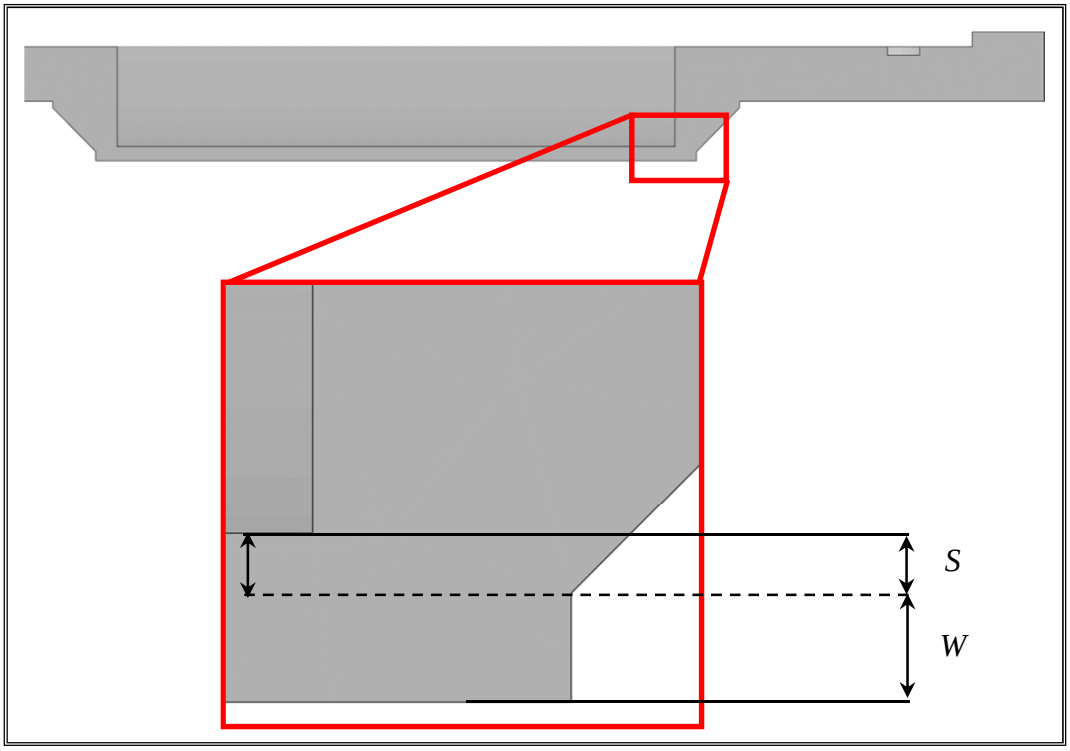

Figure 5-1. BP lithium channel thickness *S* and added thickness *W*.

Table 5-1. Summary of the BP geometric configurations taken into account in Phase 1.

Configuration	***W* [mm]**	***D* [mm]**
1	2.0	17.0
2	1.2	17.0

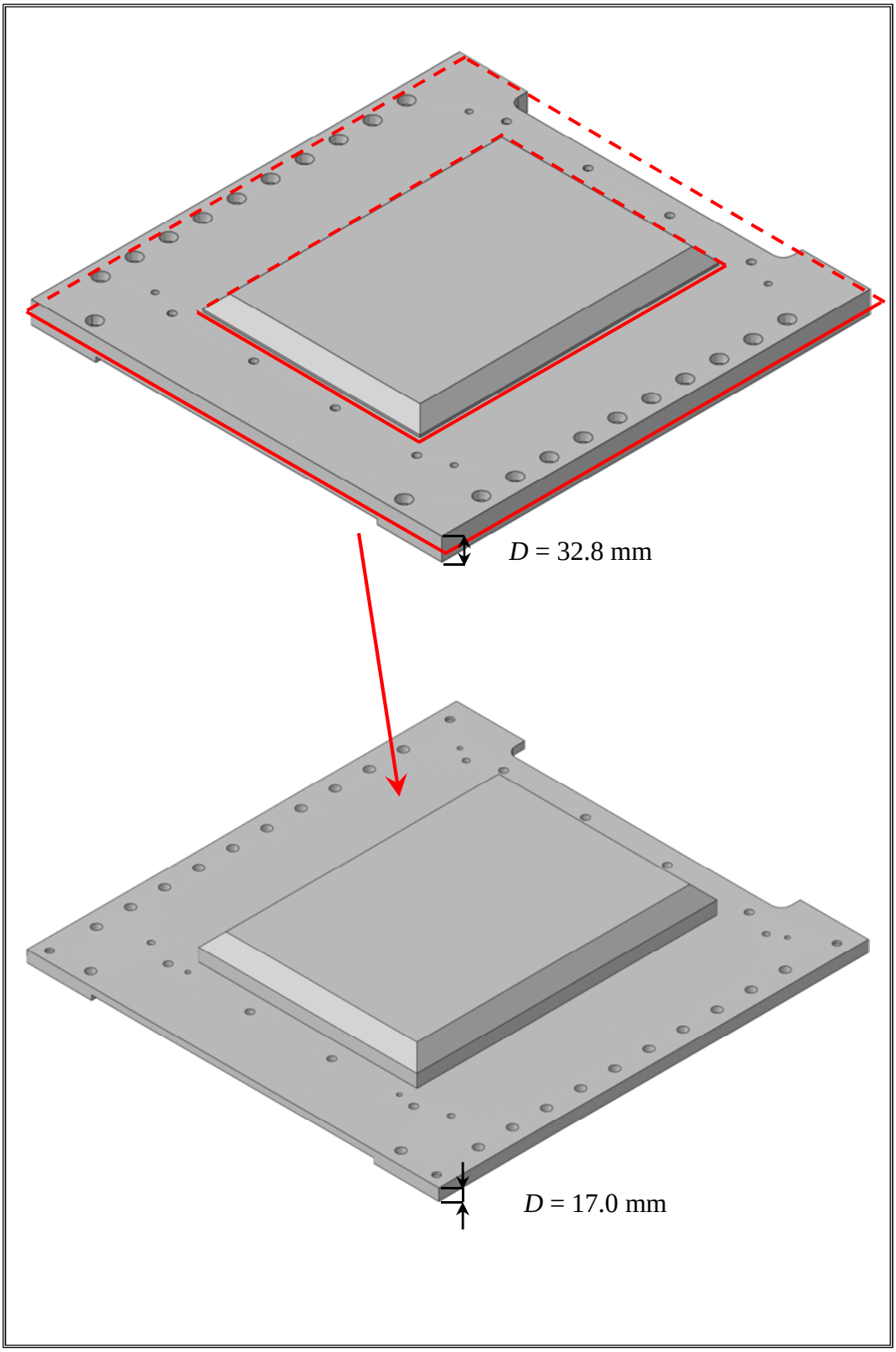

Figure 5-2. BP thickness reduction strategy.

A proper 3D FEM model has been developed for each of this two potential TA revised configurations. Concerning Configuration 1, a mesh composed of 377339 nodes connected in 1414764 linear tetrahedral and hexahedral elements has been considered, while as to Configuration 2 mesh, 383012 nodes connected in 1442623 elements have been selected with the aim to perform steady state thermo-mechanical analyses ensuring the best compromise between results accuracy and computational time saving. In particular, the TA, Lithium inlet pipe and framework FEM models are the same already shown in chapter 4, whereas a detail of the Configuration 1 BP FEM model is reported in figure 5-3.

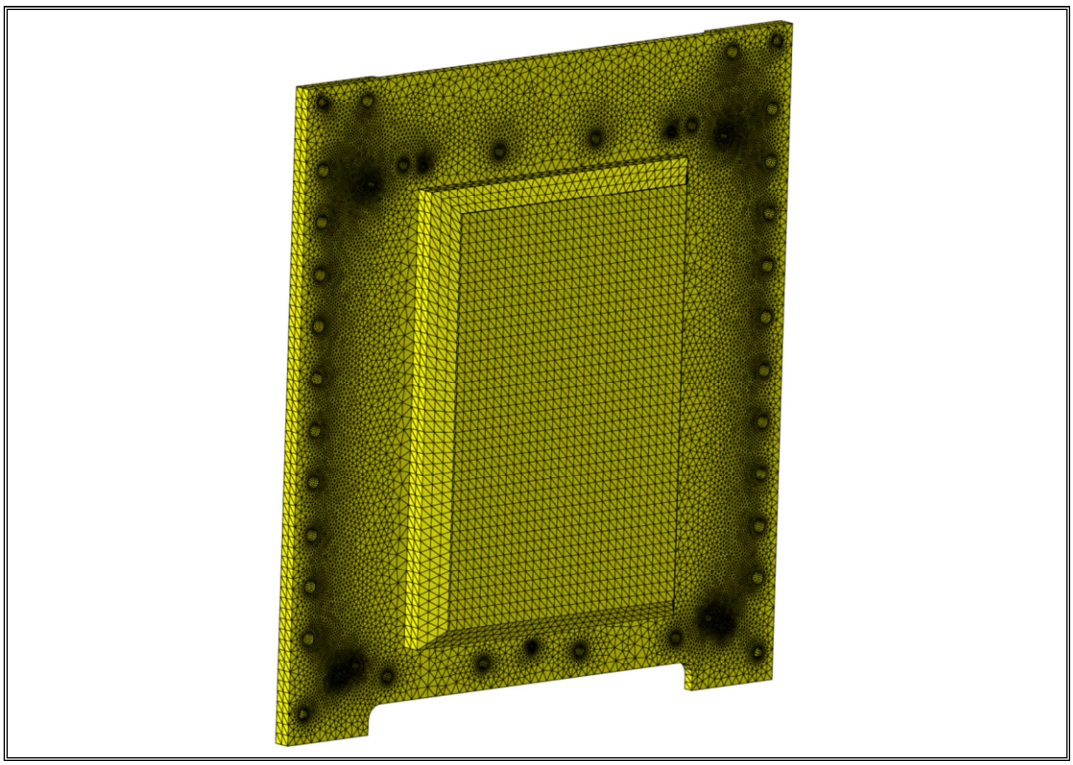

Figure 5-3. Phase 1. Configuration 1 FEM model of the BP.

Concerning materials, all the TA components, the Lithium inlet pipe and the support framework have been supposed to be made of the RAFM EUROFER steel, whose thermo-mechanical properties have been discussed in § 4.2.1. Furthermore, the lithium flow has been directly modelled using thermo-physical properties already reported in § 4.2.1.

5.1.1. Steady state analysis

Un-coupled thermo-mechanical analyses have been performed adopting the two abovementioned 3D revised TA FEM models, properly endowed with the potential BP optimized configurations. Results in terms of thermal and Von Mises stress (σ_{VM}) field are

reported in figures 5-4÷5-11. A stress linearization procedure has been subsequently performed along paths already shown in figure 4-34, in order the check the fulfilment of the SDC-IC design rules (Tables 5-2 and 5-3).

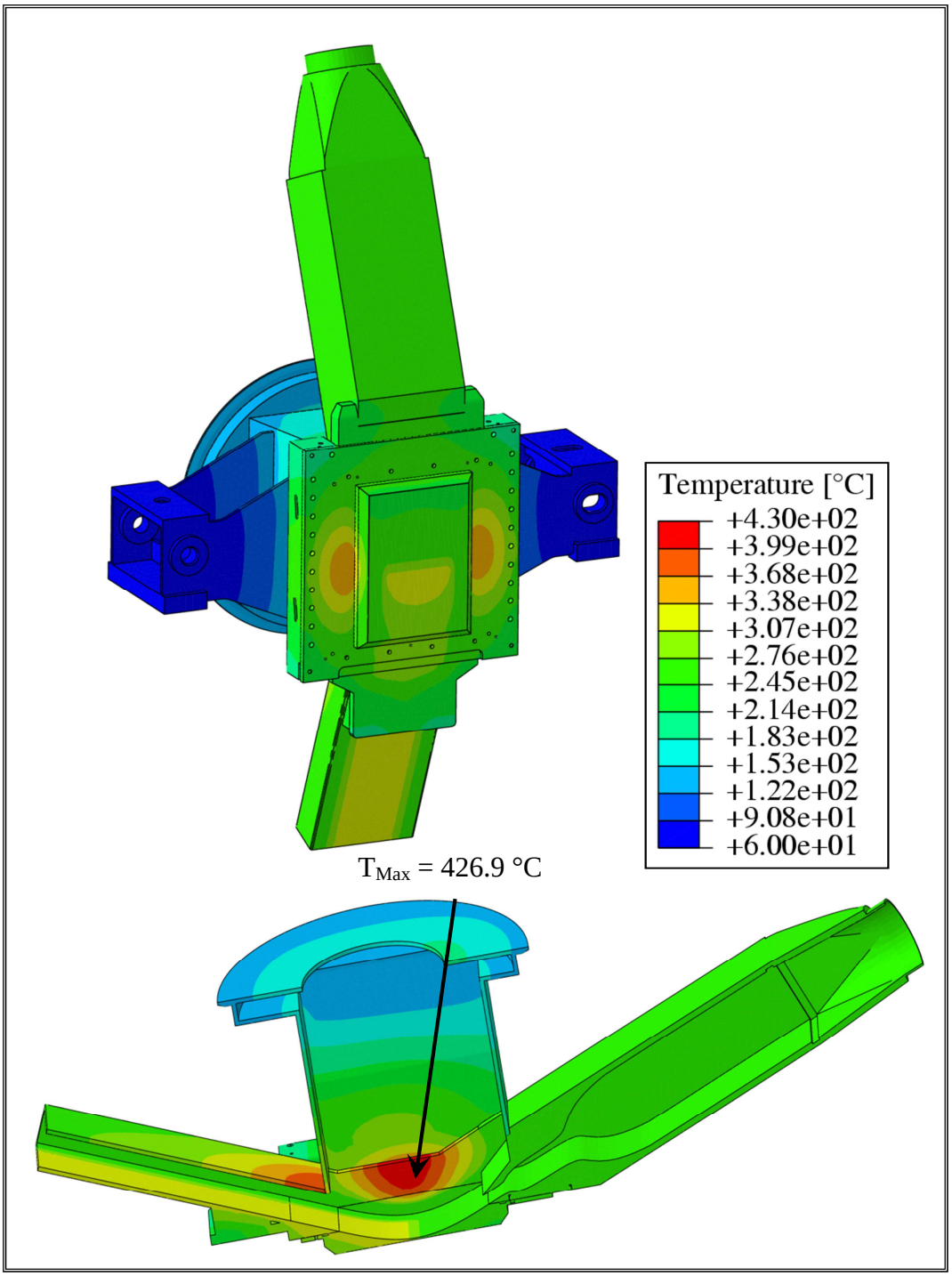

Figure 5-4. Phase 1.Configuration 1. TA thermal field.

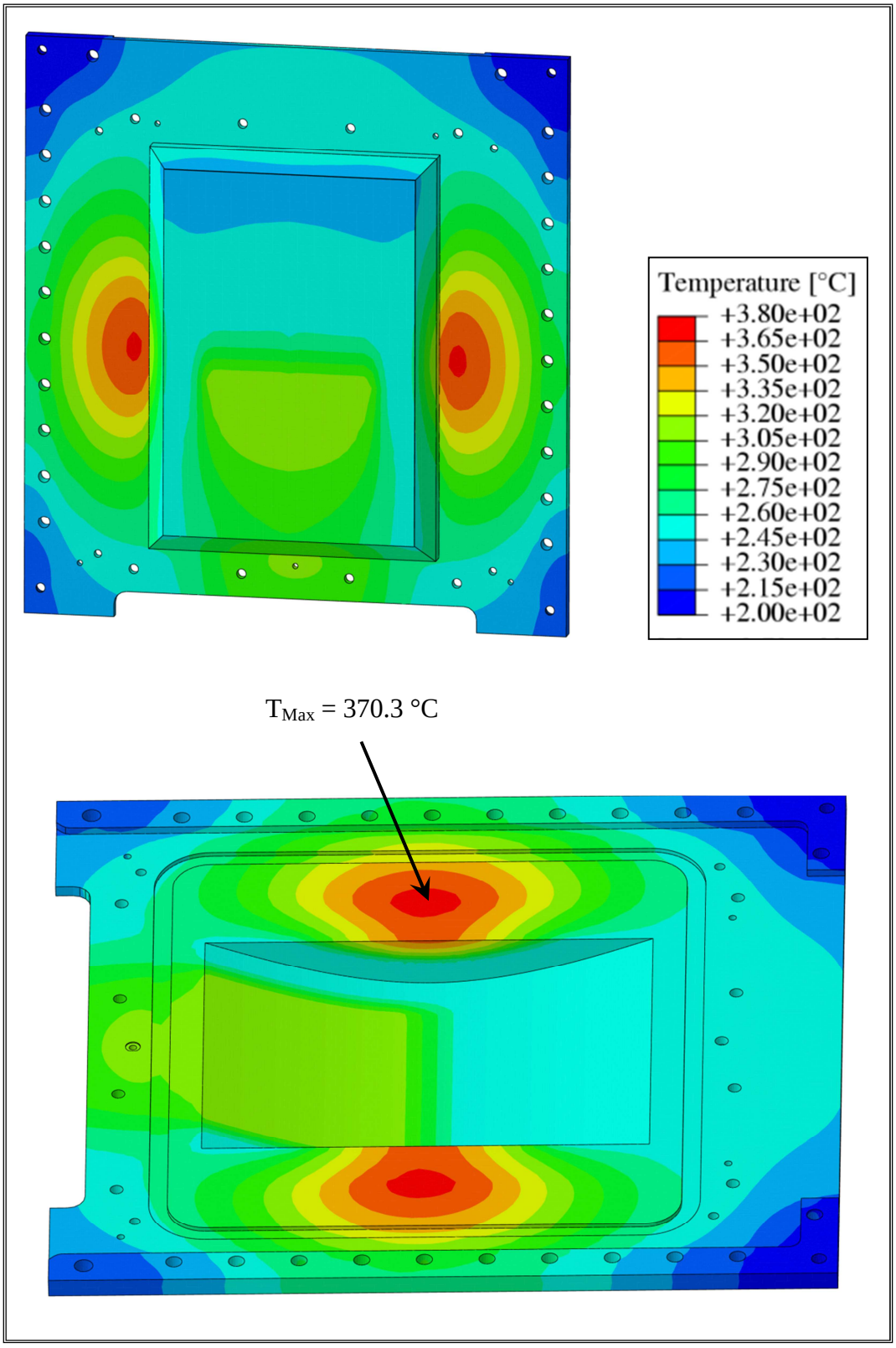

Figure 5-5. Phase 1.Configuration 1. BP thermal field.

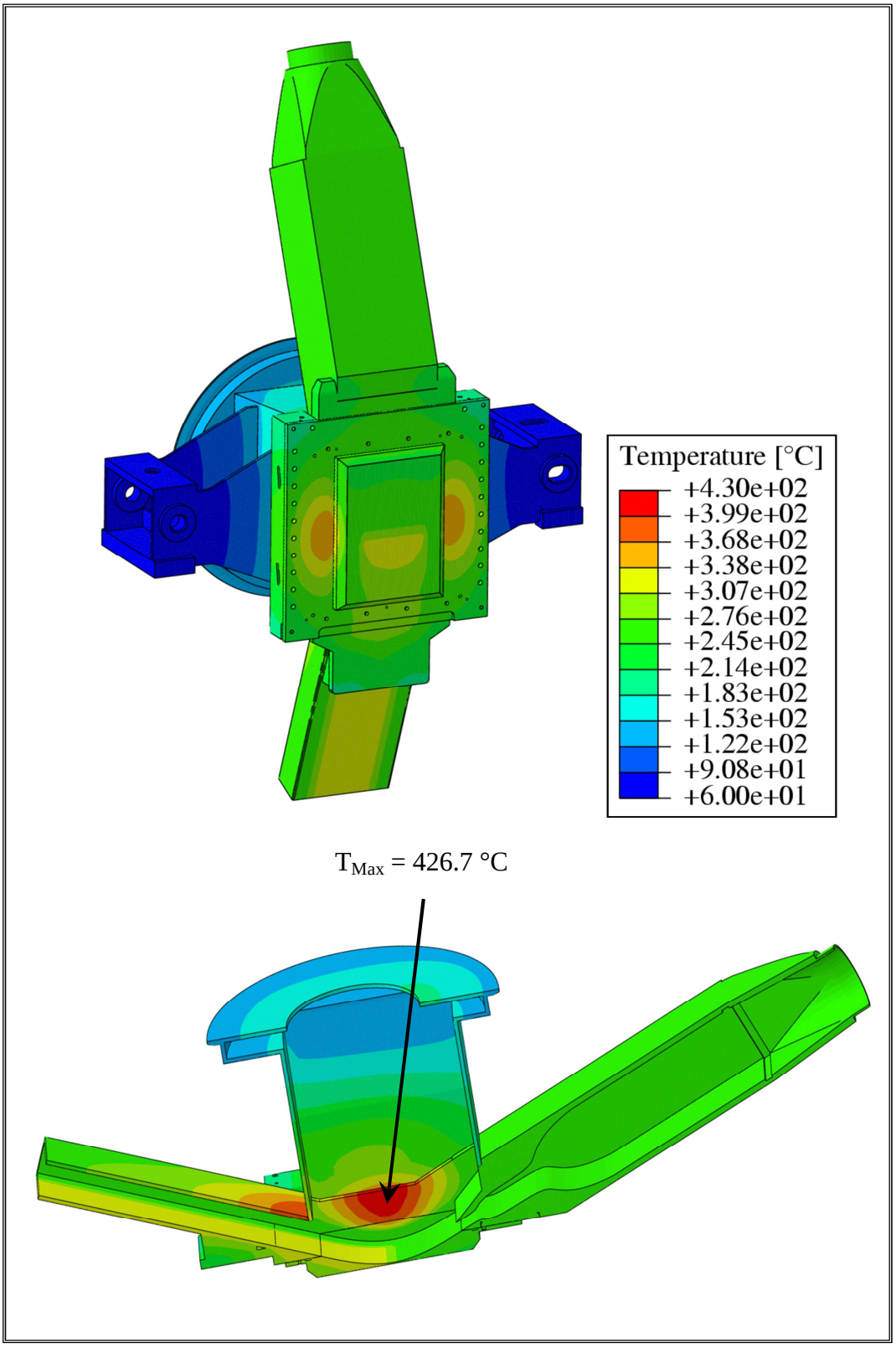

Figure 5-6. Phase 1.Configuration 2. TA thermal field.

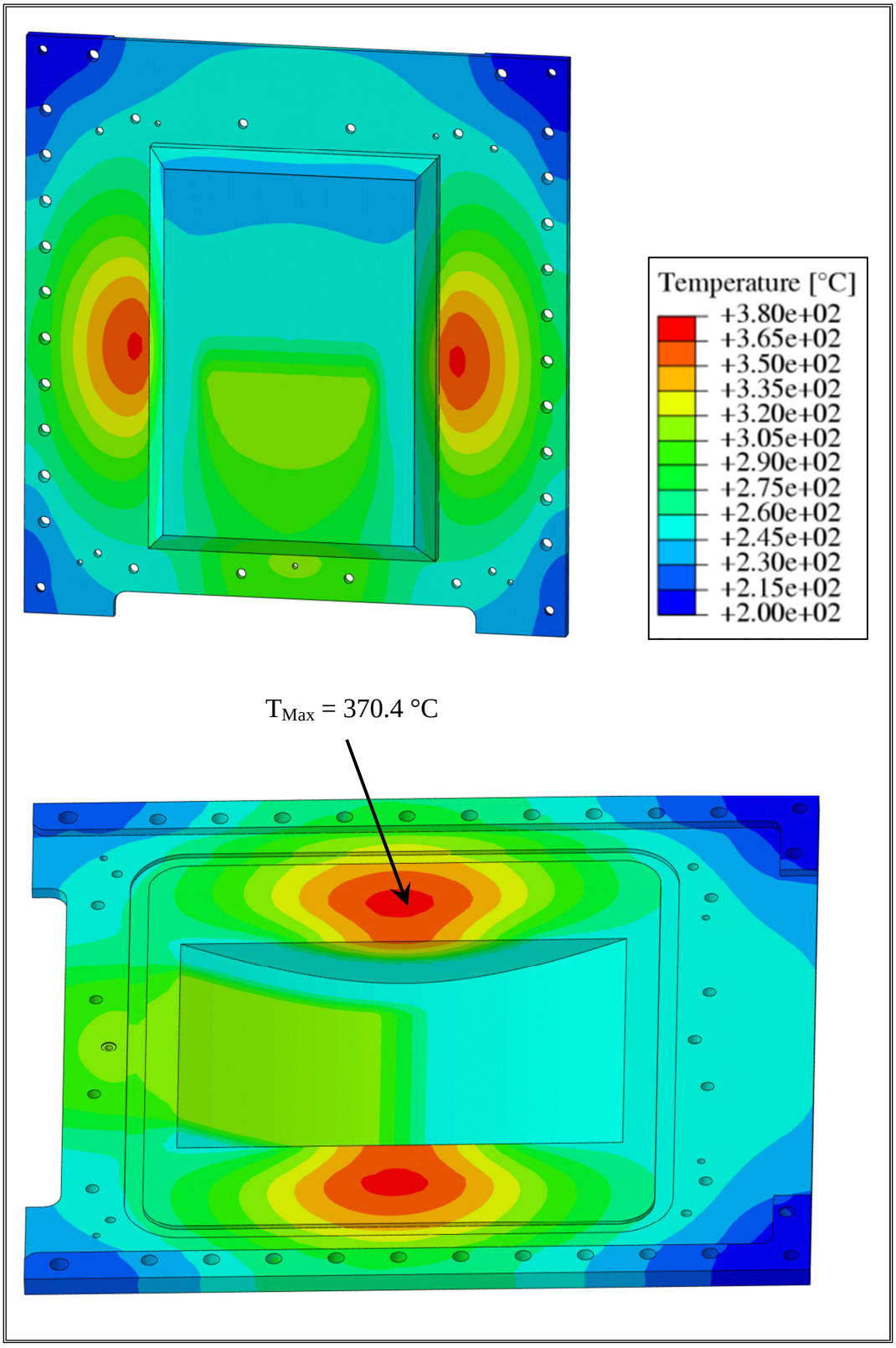

Figure 5-7. Phase 1.Configuration 2. BP thermal field.

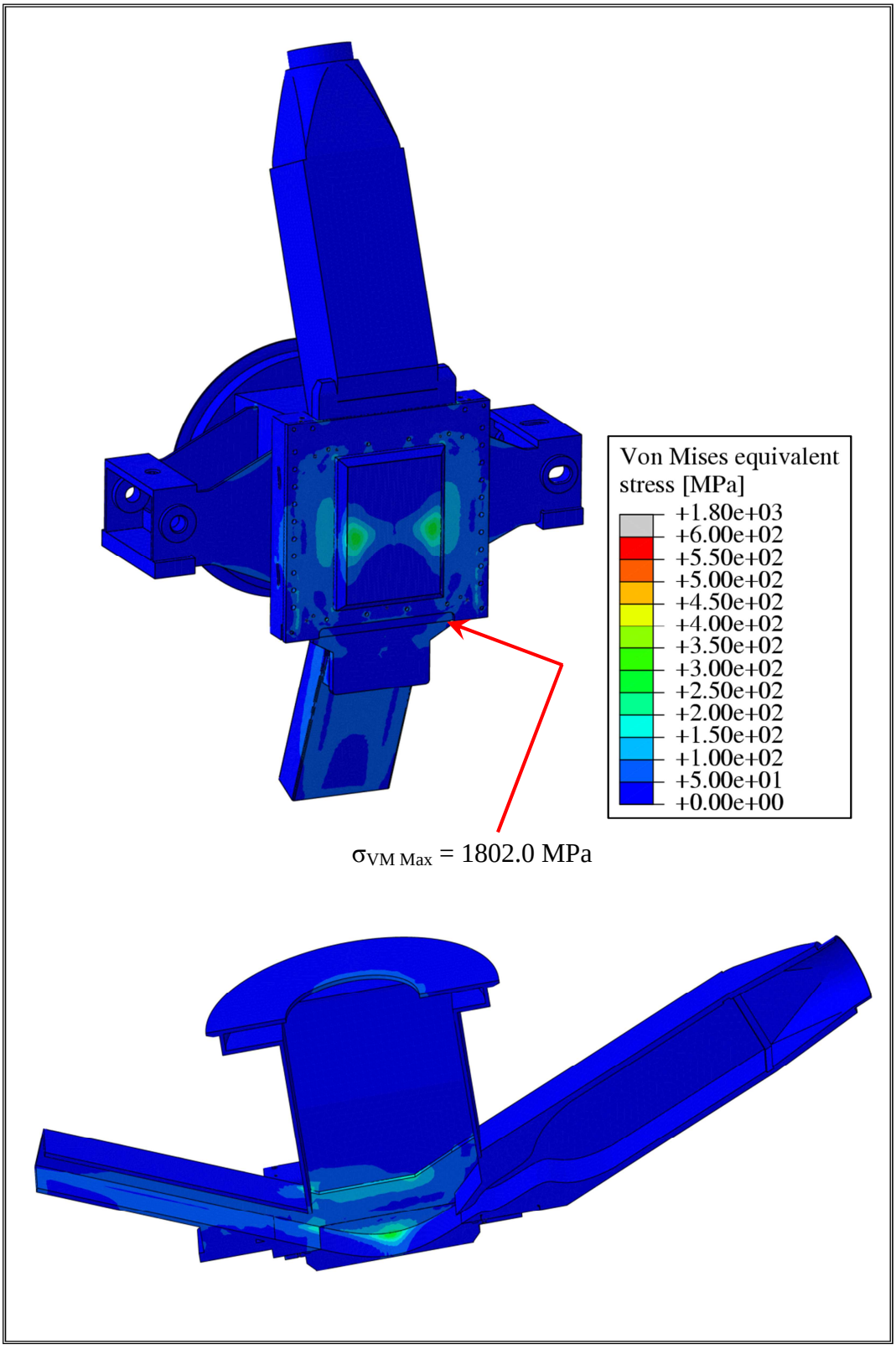

Figure 5-8. Phase 1.Configuration 1.TA Von Mises equivalent stress field.

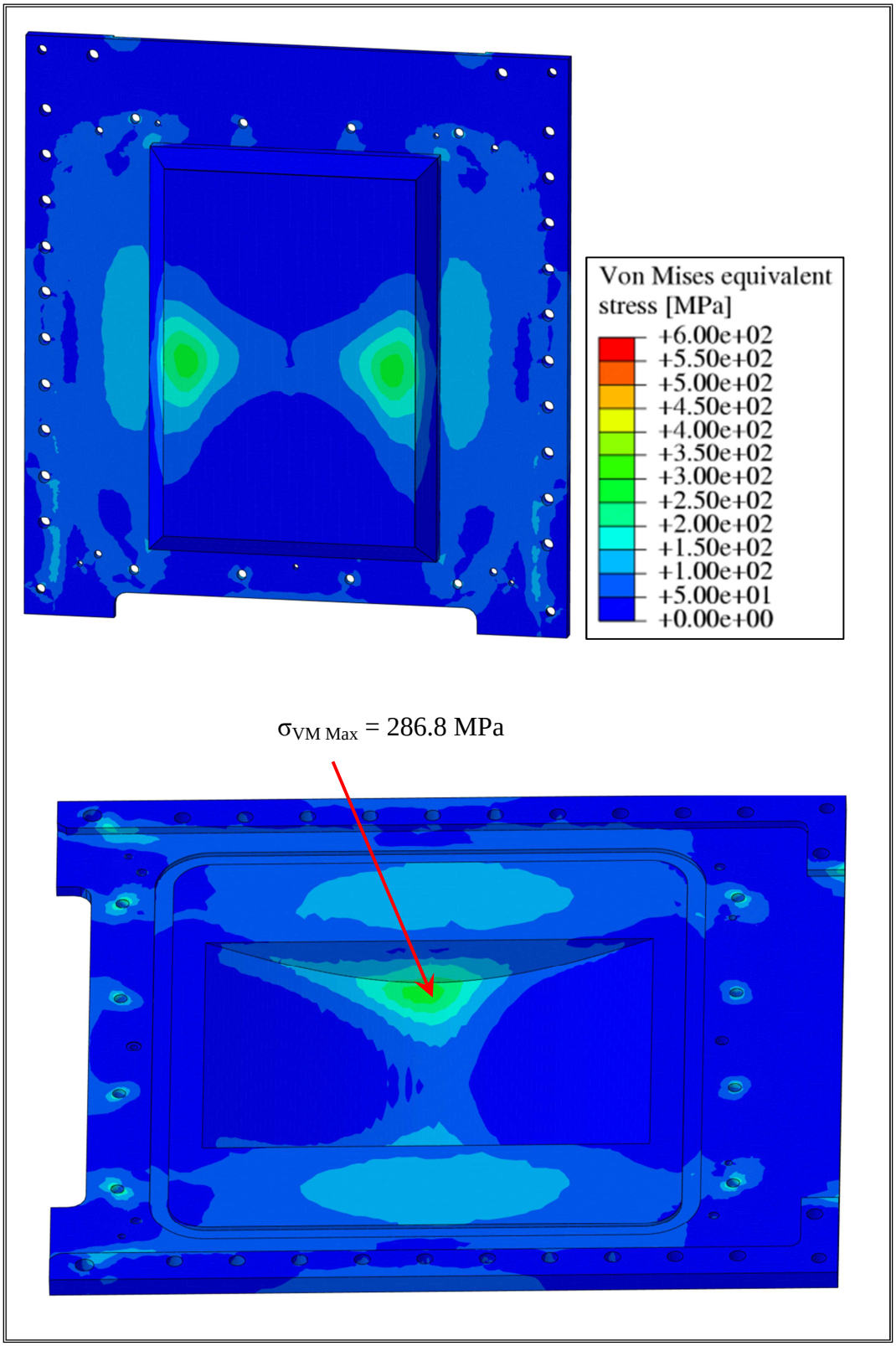

Figure 5-9. Phase 1.Configuration 1.BP Von Mises equivalent stress field.

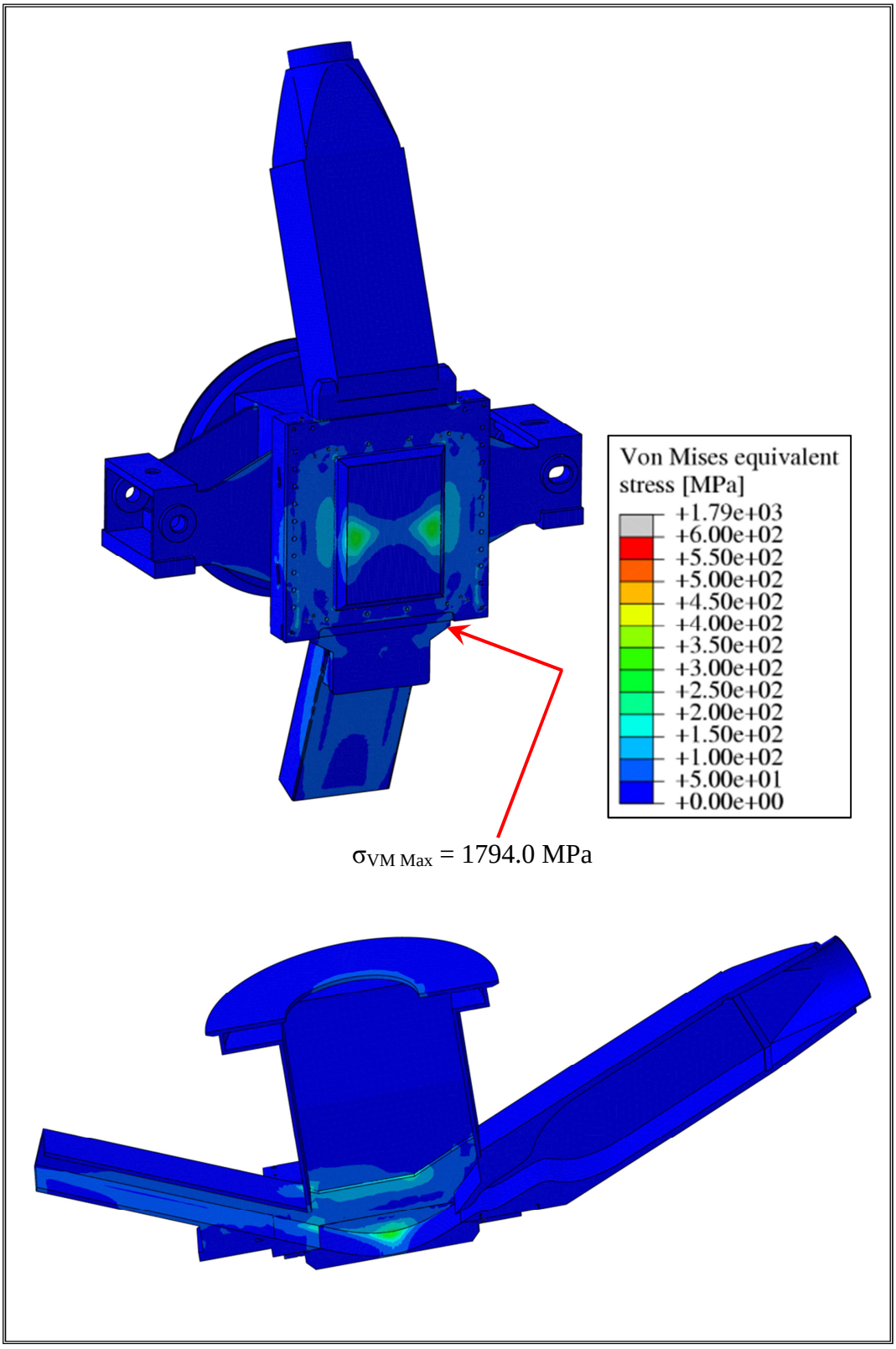

Figure 5-10. Phase 1.Configuration 2. TA Von Mises equivalent stress field.

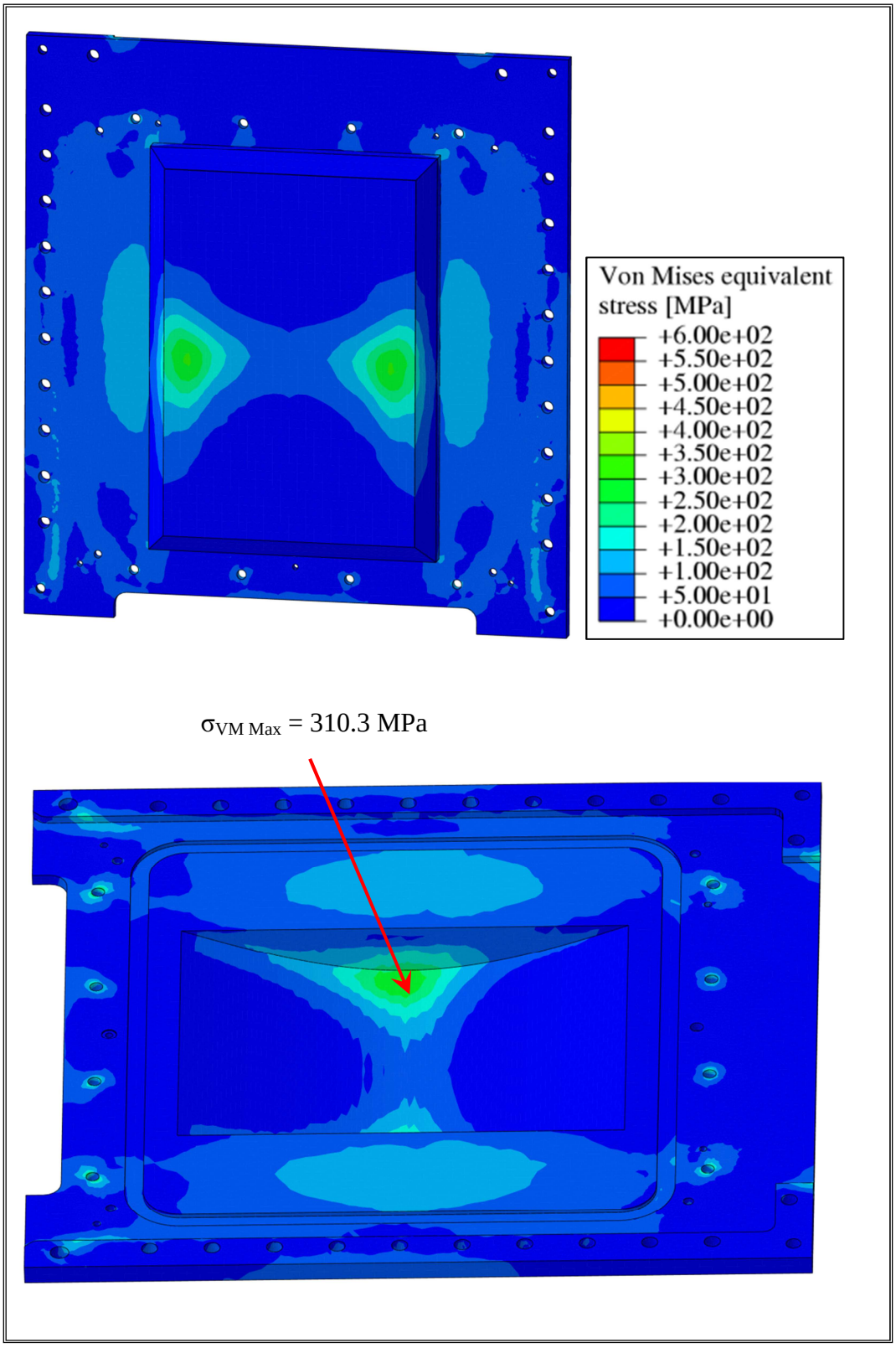

Figure 5-11. Phase 1.Configuration 2. BP Von Mises equivalent stress field.

Table 5-2. Phase 1. Configuration 1. SDC-IC safety rules verification.

	Path AB	Path CD	Path EF	Path GH	Path IL
$T_{Max\text{-}Path}$ [°C]	285.5	252.1	274.7	369.1	253.4
P_m/S_m	0.0015	0.0011	0.0004	0.0008	0.0016
$(P_m+P_b)/(K_{eff}*S_m)$	0.0014	0.0009	0.0003	0.0008	0.0011
$(P_m+Q_m)/S_e$	0.2028	0.7763	0.2503	0.7294	0.9042

Table 5-3. Phase 1. Configuration 2. SDC-IC safety rules verification.

	Path AB	Path CD	Path EF	Path GH	Path IL
$T_{Max\text{-}Path}$ [°C]	283.5	251.7	274.6	369.1	252.5
P_m/S_m	0.0015	0.0013	0.0003	0.0013	0.0017
$(P_m+P_b)/(K_{eff}*S_m)$	0.0015	0.0011	0.0002	0.0011	0.0012
$(P_m+Q_m)/S_e$	0.2841	0.8441	0.2480	0.7234	0.9850

The obtained results have shown that, from the thermal point of view, the maximum temperature is reached within lithium flow guides and it is equal to about 370 °C. This value is probably due to the huge amount of volumetric density of heat power deposited inside the lithium flow guides that leads to the insurgence of BP hotspots, in particular within regions in contact with the TA frame. As it can be observed, the maximum predicted BP temperature is lower than 450 °C and therefore the fulfilment of the SDC-IC safety rules pertinent to the thermal-activated phenomena has not been checked.

From the mechanical point of view, except for extremely localized hotspots due to geometric singularities, Von Mises equivalent stress values achieved within BP and TA are well below 600 MPa in both the investigated configurations. In particular, maximum Von Mises stress values lower than 320 MPa are predicted within BP geometric domain in both configurations.

Finally, regarding SDC-IC level A safety rules verifications, the TA model endowed with two potentially optimized BP configurations allows more encouraging results to be obtained. In fact, as to Configuration 1 results, they show a significant reduction of the $(P_m + Q_m) / S_e$ ratio along all paths considered with respect to results carried out from thermo-mechanical analyses performed on the IFMIF TA endowed with the “original” BP layout reported in §4.3. Since the added thickness of 2.0 mm might appear excessive, in order to avoid a consistent neutron flux attenuation a further BP layout has been considered in Configuration 2 where, as expected, the reduction of lithium channel additive thickness from 2.0 mm to 1.2 mm originates a general increasing of the $(P_m + Q_m) / S_e$ ratio along all paths considered, even though the pertinent safety criterion still remains verified. Although SDC-IC criteria are completely fulfilled, the mechanical behaviour of this configuration does not seem to be

encouraging in view of the need to take into account the swelling effect. In fact, even though the safety criterion involving $(P_m + Q_m) / S_e$ ratio is met, a value very close to 1.0 is predicted.

The obtained results from Phase 1 show the necessity to carry out a further campaign of parametric analyses, to investigate more deeply in detail the influence of *D* and *W* parameters on the BP thermo-mechanical behaviour. This parametric study has been carried out in Phase 2.

5.2. Phase 2

On the basis of the conclusions drawn from results of Phase 1 steady state thermo-mechanical analyses, a campaign of parametric analyses has been launched within the framework of the Phase 2 of the BP design review procedure, in order to optimize its thermo-mechanical performances under steady state nominal conditions already adopted in Phase 1.

Considering results of the previous phase of the BP design review process, proper ranges of values of the two geometric parameters taken into account have been selected in order to assess the potential combined effects of the increase of the BP lithium channel thickness and of the reduction of the BP thickness.

Since Phase 1 analyses have demonstrated that an additive thickness of 1.2 mm should ensure the SDC-IC level A design criteria fulfilment without significantly affecting IFMIF neutronic performances, values of the *W* parameter ranging between 1.0 and 1.7 mm have been considered.

Concerning the *D* parameter, since the reduction up to 17.0 mm seems to be a promising BP design review strategy, as assessed in Phase 1 analyses, values of *D* ranging between 12.8 mm and 17.8 mm have been considered, corresponding to a *D* reduction from 20 mm to 15 mm, respectively, being the original value equal to 32.8 mm.

Within these ranges of values, 8 different values of the *W* parameter have been taken into account while, regarding to the *D* parameter, 6 different values have been considered in Phase 2 of the BP design review procedure. Values of the *W* and *D* parameters taken into account for the Phase 2 parametric campaign of steady state analyses have been reported in table 5-4. Combining them, 48 BP different geometric configurations have been identified and they have been implemented within the IFMIF TA integrated with the support framework and the Lithium inlet pipe already adopted in Phase 1 of the BP design review procedure.

Consequently, 48 different 3D FEM models, in which the original BP of the IFMIF TA integrated with the support framework and the Lithium inlet pipe has been properly replaced with a different potential optimized BP geometric configuration, have been developed.

Un-coupled steady state thermo-mechanical analyses have been performed, assuming the steady state loading conditions relevant to the IFMIF nominal scenario, already described in § 4.2.2 and in § 4.2.3.

For each of the 48 assessed configuration, a stress linearization procedure has been carried

out and attention has been paid to verify whether SDC-IC safety criteria (Level A) are fulfilled along the paths already adopted for the previous phase of the BP design review procedure.

Table 5-4. Summary of the parameter values taken into account in Phase 2.

W [mm]	*D* [mm]
1.0	12.8
1.1	13.8
1.2	14.8
1.3	15.8
1.4	16.8
1.5	17.8
1.6	-
1.7	-

5.2.1. Steady state parametric analysis

Results have shown that, among the 48 configurations investigated, two BP configurations can be selected (Figure 5-12) as the reference ones since their thermo-mechanical performances under steady state loading conditions are the most promising.

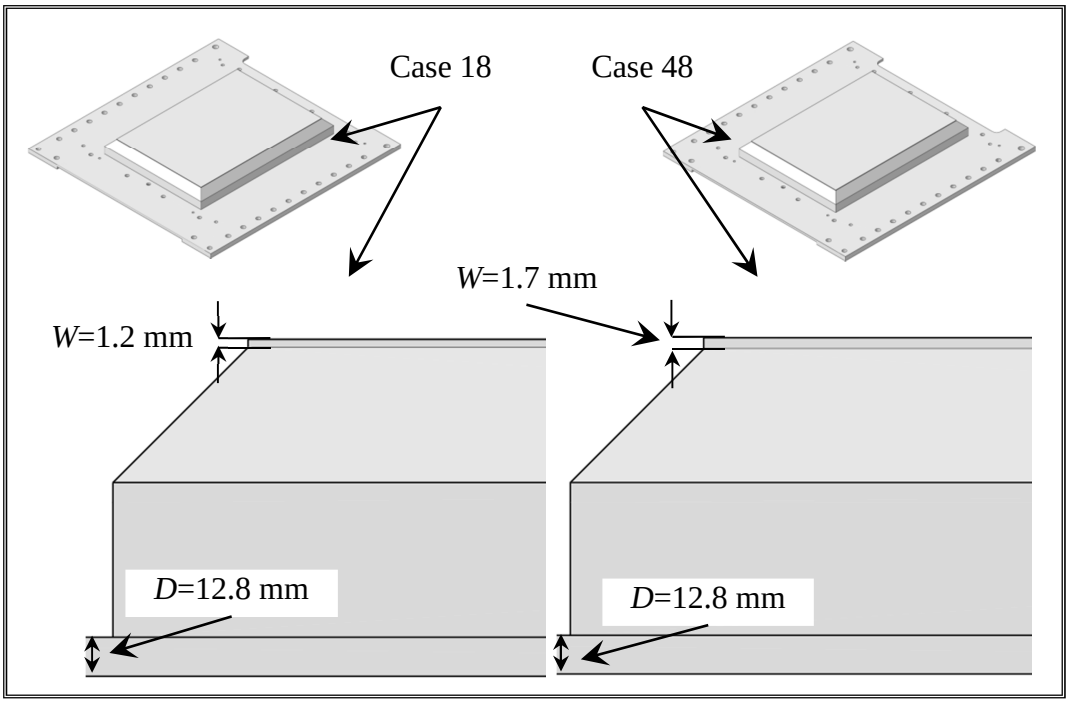

Figure 5-12. Phase 2. Case 18 and Case 48.

The first configuration, named Case 18, is characterized by a BP total thickness (*D*) of 12.8 mm and an additive thickness (*W*) of the lithium channel equal to 1.2 mm, which leads to a total lithium channel thickness of 3.0 mm, while the second one, named Case 48, foresees a *D* value of 12.8 mm and a *W* value of 1.7 mm which corresponds to an overall lithium channel 3.5 mm thick. It has to be highlighted that, as to Case 18 FEM model, a mesh of 360699 nodes and 1375714 linear elements has been set-up, while regarding Case 48, 360794 nodes connected in 1376247 linear elements have been considered.

The obtained steady state results for these two geometric configurations have been herewith reported in terms of thermal field (Figs 5-13÷5-16), Von Mises equivalent stress field (Figs 5-17÷5-20) and SDC-IC safety rule verifications (Tables 5-5 and 5-6). Concerning thermal results, it can be observed that the maximum temperature predicted within TA is achieved in both cases within the lithium guides located inside the target chamber. This leads to the insurgence of a thermal hotspot within the BP region directly in contact with the lithium guides. This is probably due to the huge amount of q‴ deposited inside the lithium guides which is transferred, by thermal conduction, to the BP.

As far as mechanical results are concerned, except for a very localized region in which high values of the Von Mises equivalent stress are calculated due to a geometric singularity, the stress fields arising within the two models are characterized by values lower than 500 MPa. Finally, regarding the SDC-IC Level A criteria fulfilment, the performances of the two abovementioned configurations are the most encouraging among those assessed, since they largely satisfy all the prescribed foreseen rules when subjected to the envisaged steady state set of thermo-mechanical loads and boundary conditions.

Table 5-5. Phase 2. Case 18. SDC-IC safety rules verification.

	Path AB	Path CD	Path EF	Path GH	Path IL
$T_{Max\text{-}Path}$ [°C]	283.5	251.8	265.2	371.9	252.5
P_m/S_m	0.0017	0.0010	0.0008	0.0009	0.0014
$(P_m+P_b)/(K_{eff}*S_m)$	0.0017	0.0010	0.0006	0.0006	0.0009
$(P_m+Q_m)/S_e$	0.1622	0.7286	0.1974	0.8027	0.8926

Table 5-6. Phase 2. Case 48. SDC-IC safety rules verification.

	Path AB	Path CD	Path EF	Path GH	Path IL
$T_{Max\text{-}Path}$ [°C]	284.7	252.1	265.1	371.9	253.0
P_m/S_m	0.0014	0.0010	0.0008	0.0007	0.0013
$(P_m+P_b)/(K_{eff}*S_m)$	0.0015	0.0008	0.0006	0.0006	0.0008
$(P_m+Q_m)/S_e$	0.1292	0.7033	0.1924	0.8028	0.8423

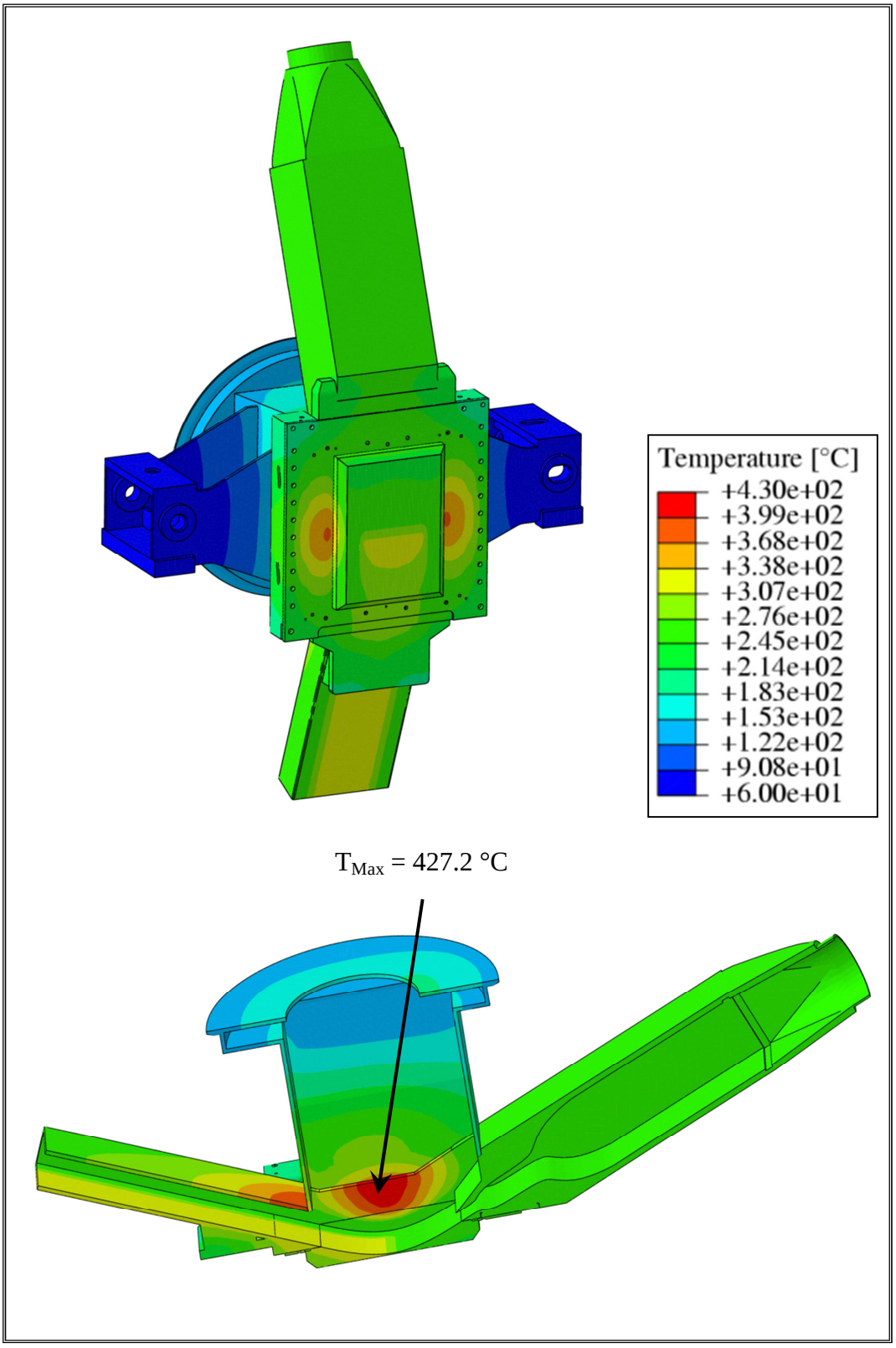

Figure 5-13. Phase 2. Case 18. TA thermal field.

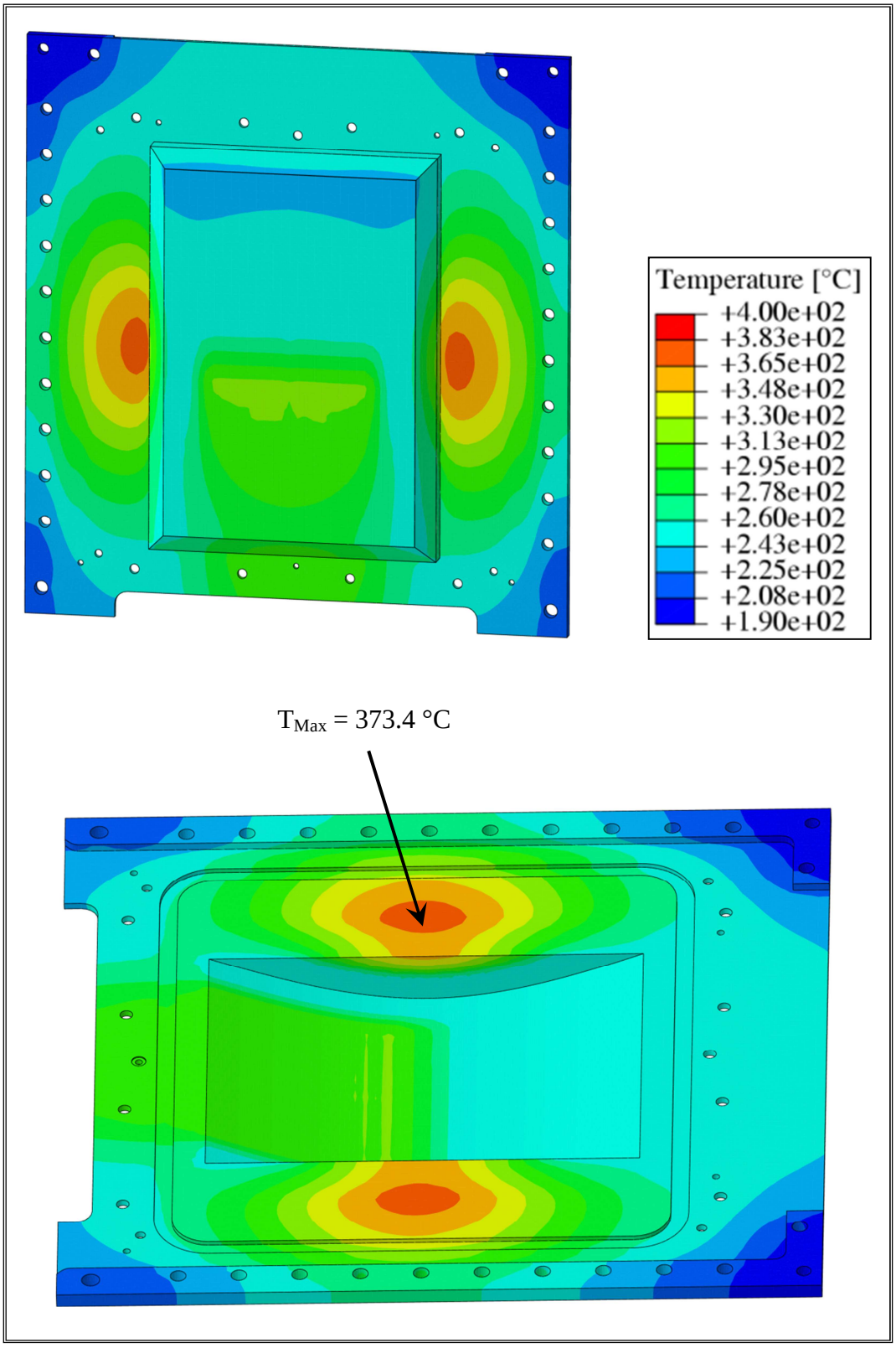

Figure 5-14. Phase 2. Case 18. BP thermal field.

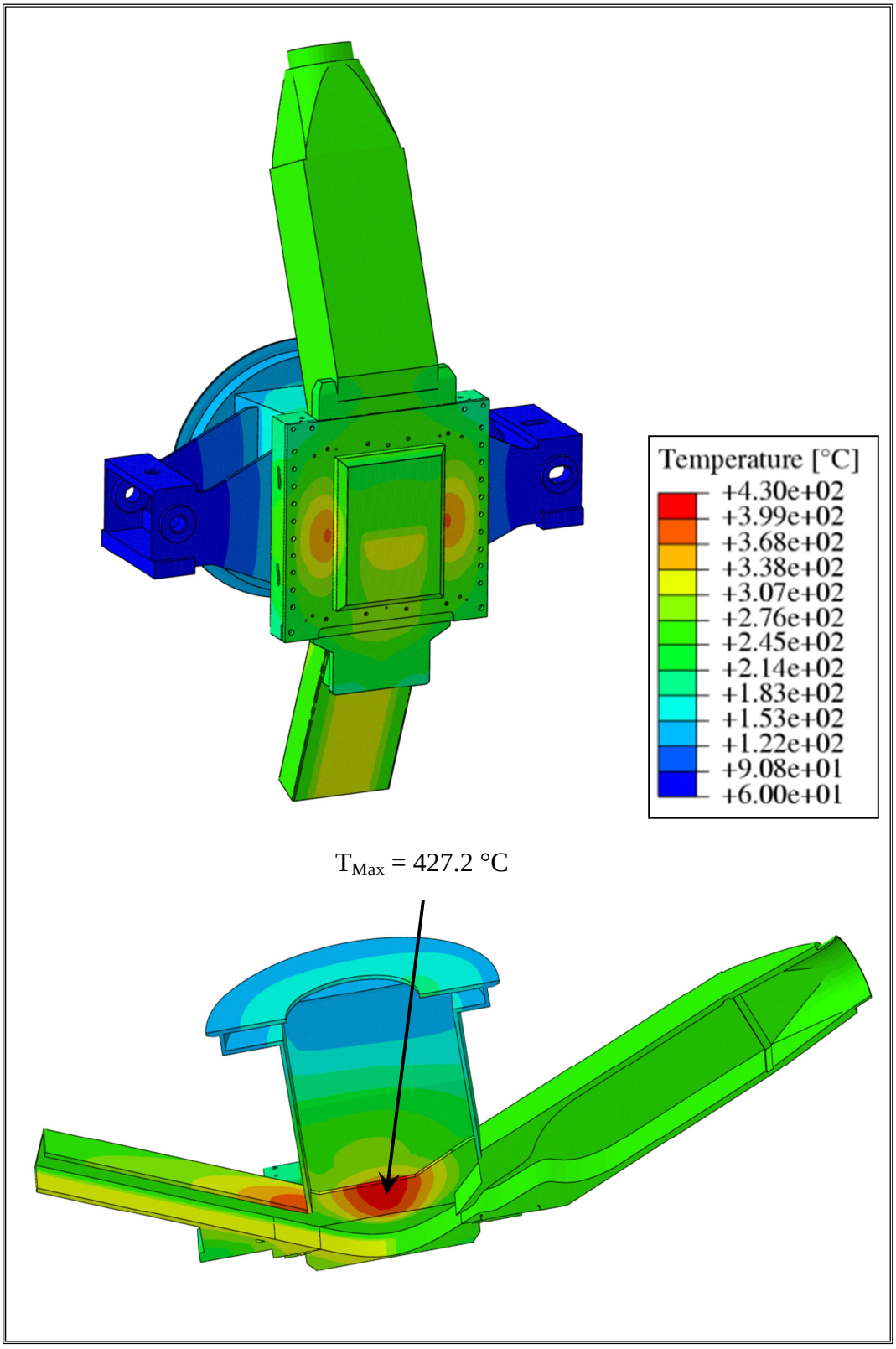

Figure 5-15. Phase 2. Case 48. TA thermal field.

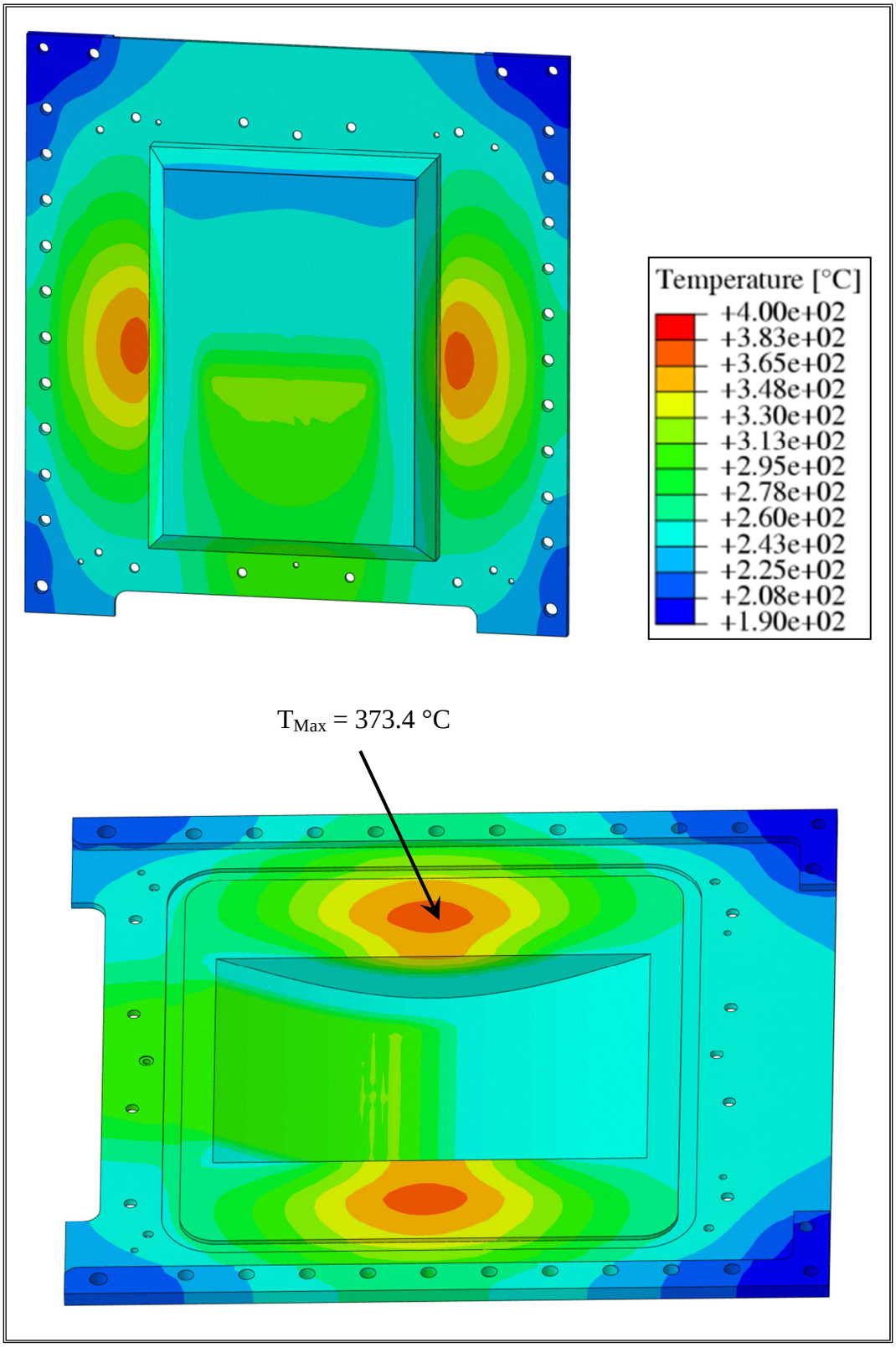

Figure 5-16. Phase 2. Case 48. BP thermal field.

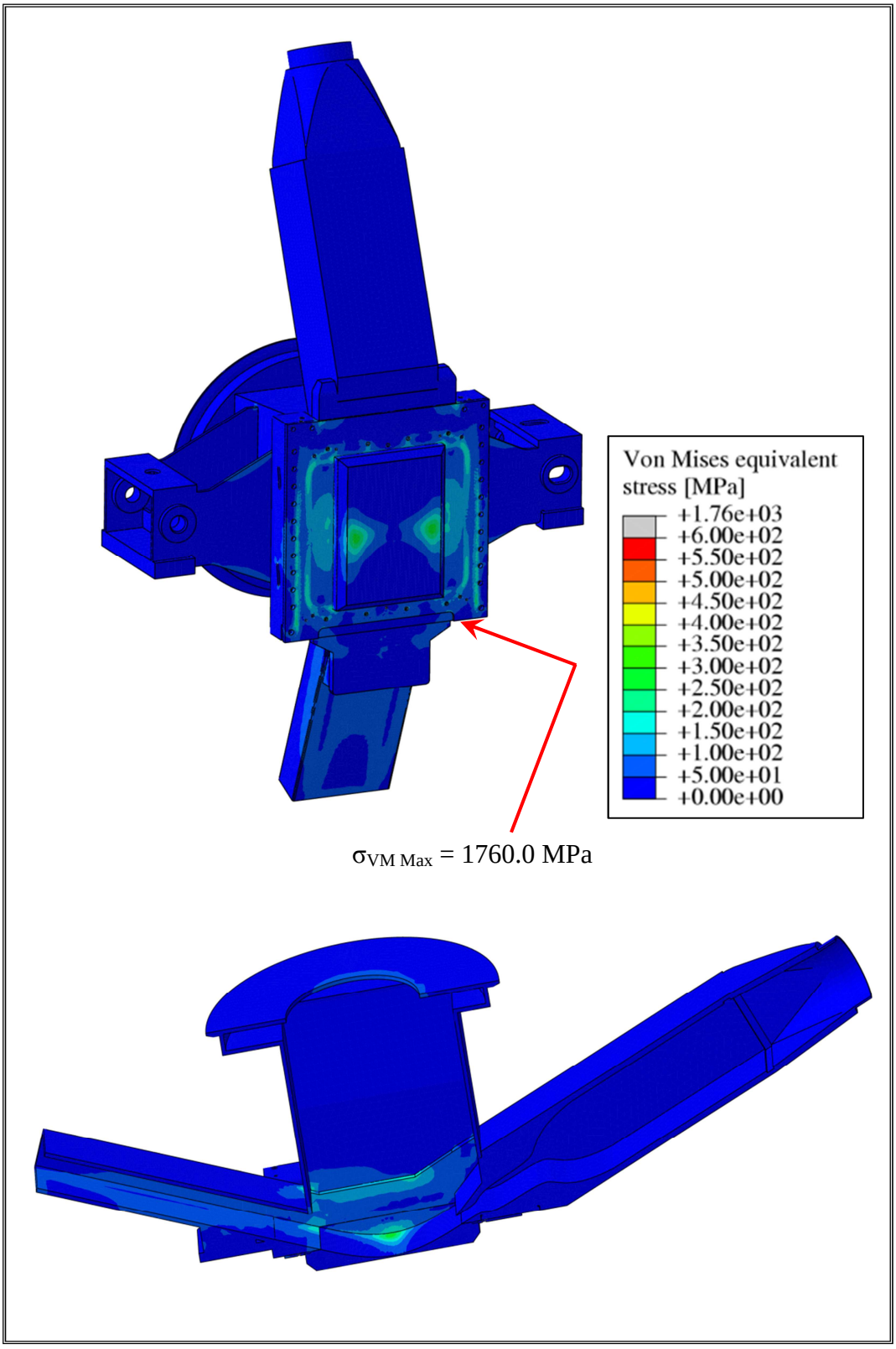

Figure 5-17. Phase 2. Case 18. TA Von Mises stress field.

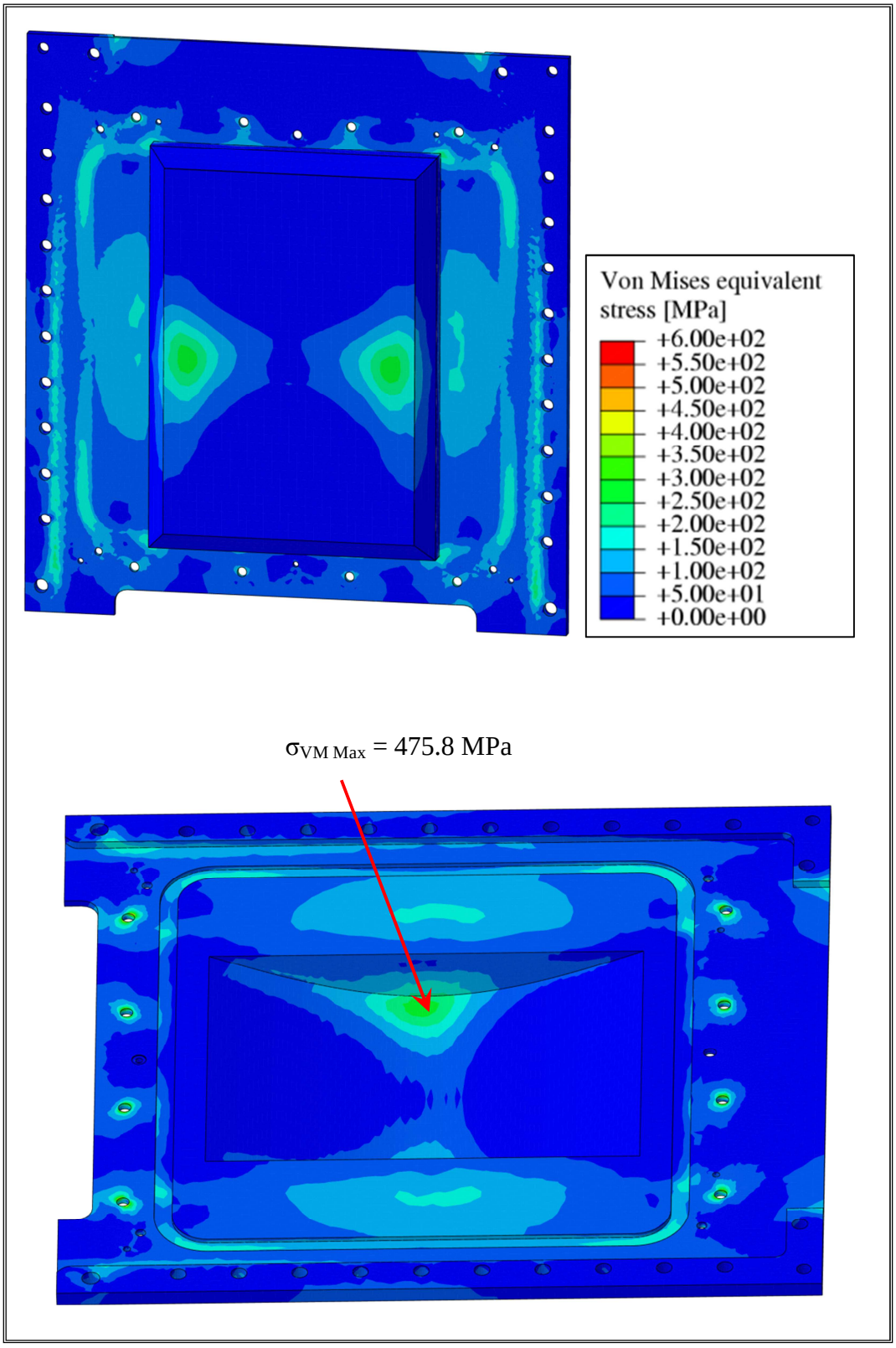

Figure 5-18. Phase 2. Case 18. BP Von Mises stress field.

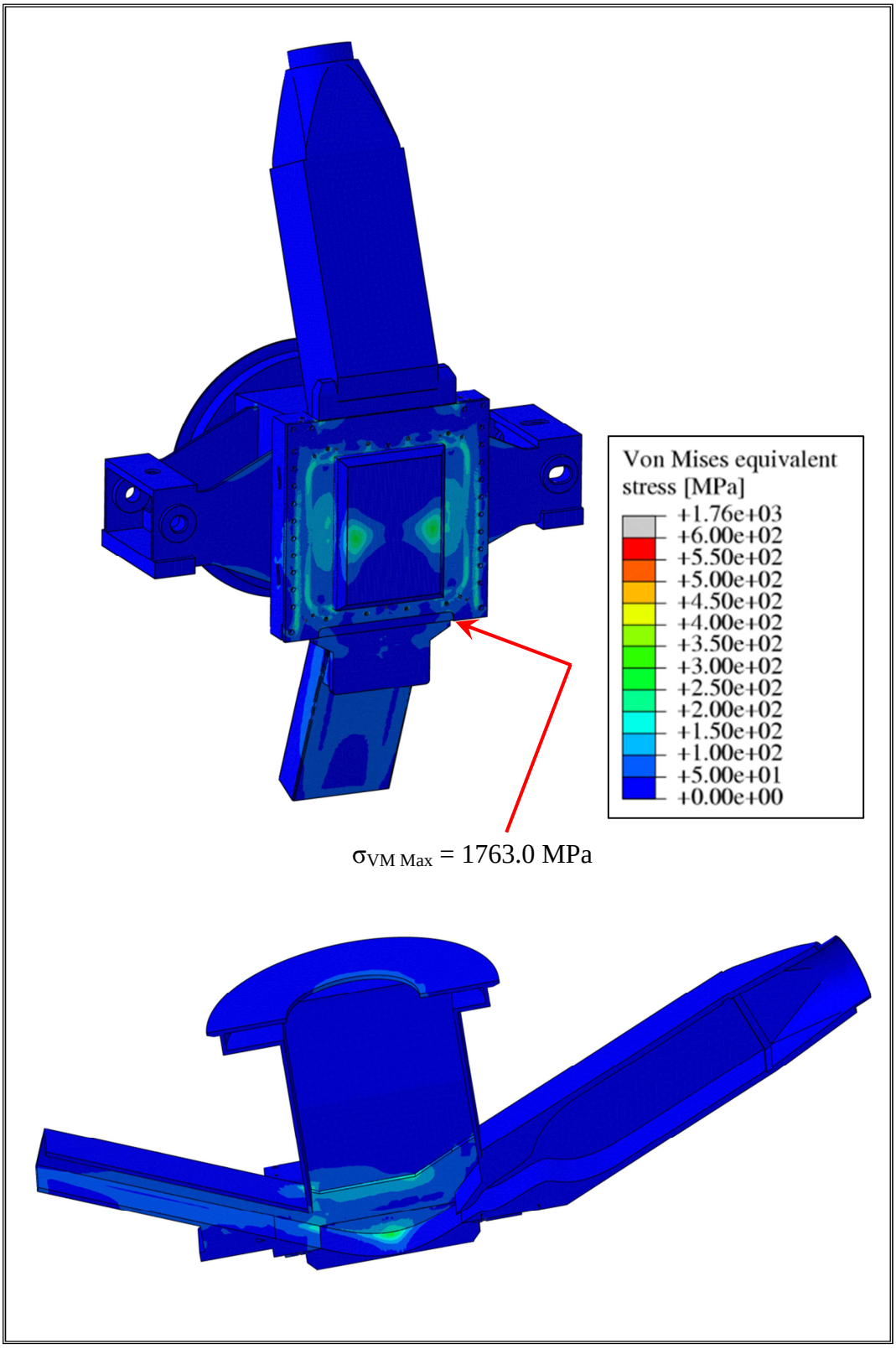

Figure 5-19. Phase 2. Case 48. TA Von Mises stress field.

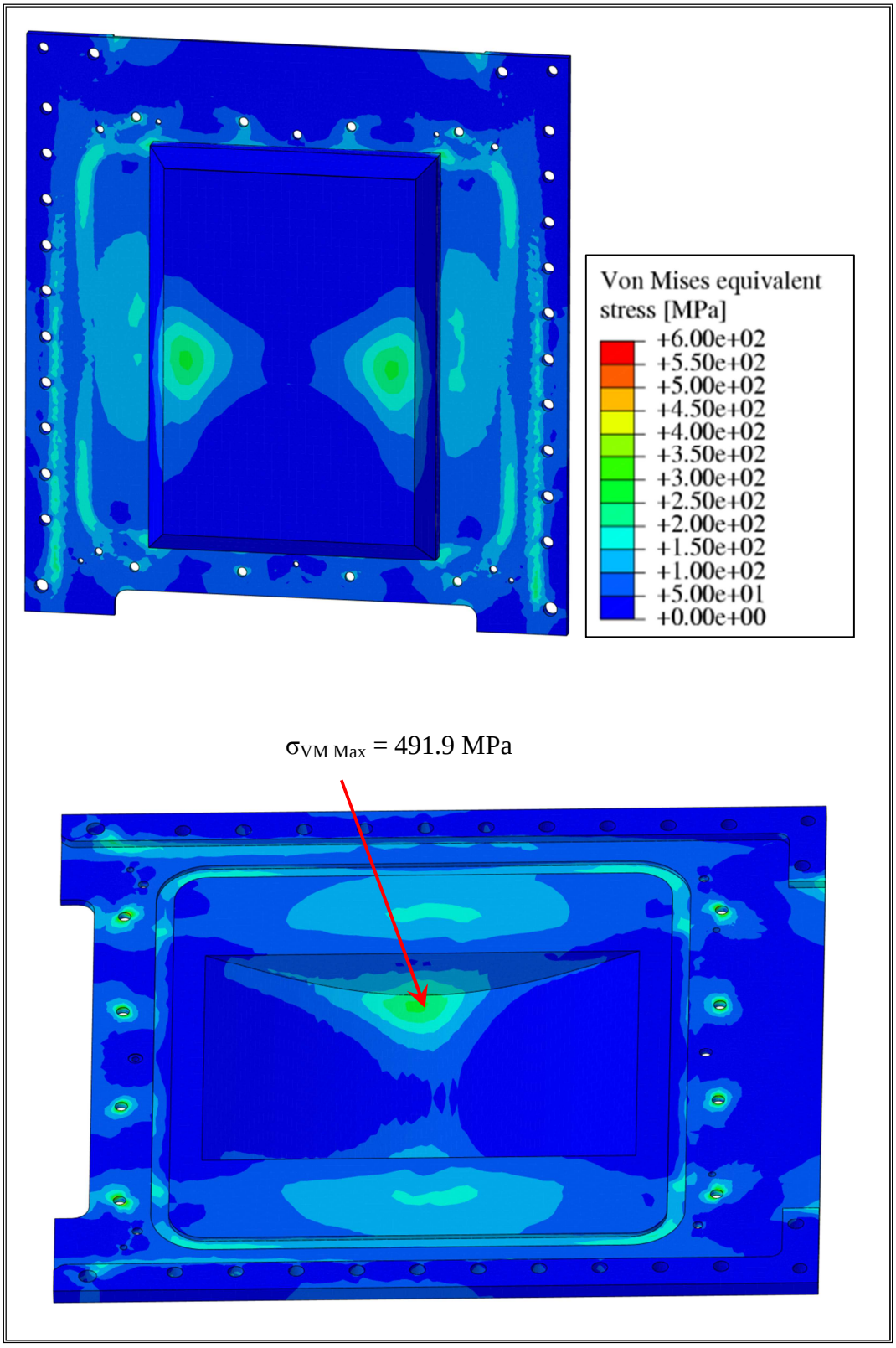

Figure 5-20. Phase 2. Case 48. BP Von Mises stress field.

Once selected the two potential optimized BP reference configurations under steady state loading conditions, transient analyses under the normal operation loading scenario, taking into account the mechanical effect of the volumetric swelling strain, have been performed, in order to estimate the BP lifetime under neutronic irradiation in both the two cases. In particular, the one year operational period under neutronic irradiation envisaged for the IFMIF TA has been simulated, in order to check if the BP is able to safely withstand the thermo-mechanical loads it undergoes for the whole duration of its nominal operational phase of one year.

5.2.2. The transient normal operation scenario

The thermal loads, interactions and boundary conditions adopted to simulate the TA thermo-mechanical behaviour in the transient normal operation loading scenario are exactly the same taken into account in the normal operation scenario already described § 4.2.2.

From the mechanical point of view, the interactions, loads and boundary conditions considered in § 4.2.3 have been integrated with the volumetric swelling strain field arising within TA as effect of a set of complex microscopic processes that typically take place when neutrons interact with structural material nuclei. In particular, the volumetric swelling strain field has been carried out imposing a linear dependence of swelling strain on DPA and, moreover, assuming that after one year of neutronic irradiation the swelling strain value achieved at the beam footprint region centre amounts to 0.75 %. Therefore, in order to set-up the volumetric swelling strain field, the DPA spatial distribution calculated by ENEA in 2013 for BP and TA geometric domains has been adopted while, as to support framework and Lithium inlet pipe, since no DPA data were available, a $1/r^2$ dependence has been supposed, like done for the volumetric density of deposited heat power reported in § 4.2.2.

Since the nominal operational phase lasts for one year, the spatial distribution of volumetric swelling strain reached at its end is reported in figures 5-21 and 5-22, with reference to Case 18 FEM model which is characterized by a BP total thickness (*D*) of 12.8 mm and an additive thickness (*W*) of the lithium channel equal to 1.2 mm.

Transient analyses reproducing one year of normal operation have been therefore performed, assuming a constant volumetric swelling strain of 0.75% per year.

The verification of the SDC-IC level A safety criteria has been carried out along the same paths taken into account in the previous phase of the optimization procedure.

The obtained results have shown that the safety criterion aimed at the checking of the immediate plastic flow localisation, which takes into account secondary stresses, is the most critical one, whereas all the other SDC-IC level A criteria remain fulfilled during the whole normal operational period simulated. The time evolution of the $(P_m + Q_m) / S_e$ ratio along the considered paths is shown in figures 5-23 and 5-24 for Case 18 and Case 48, respectively.

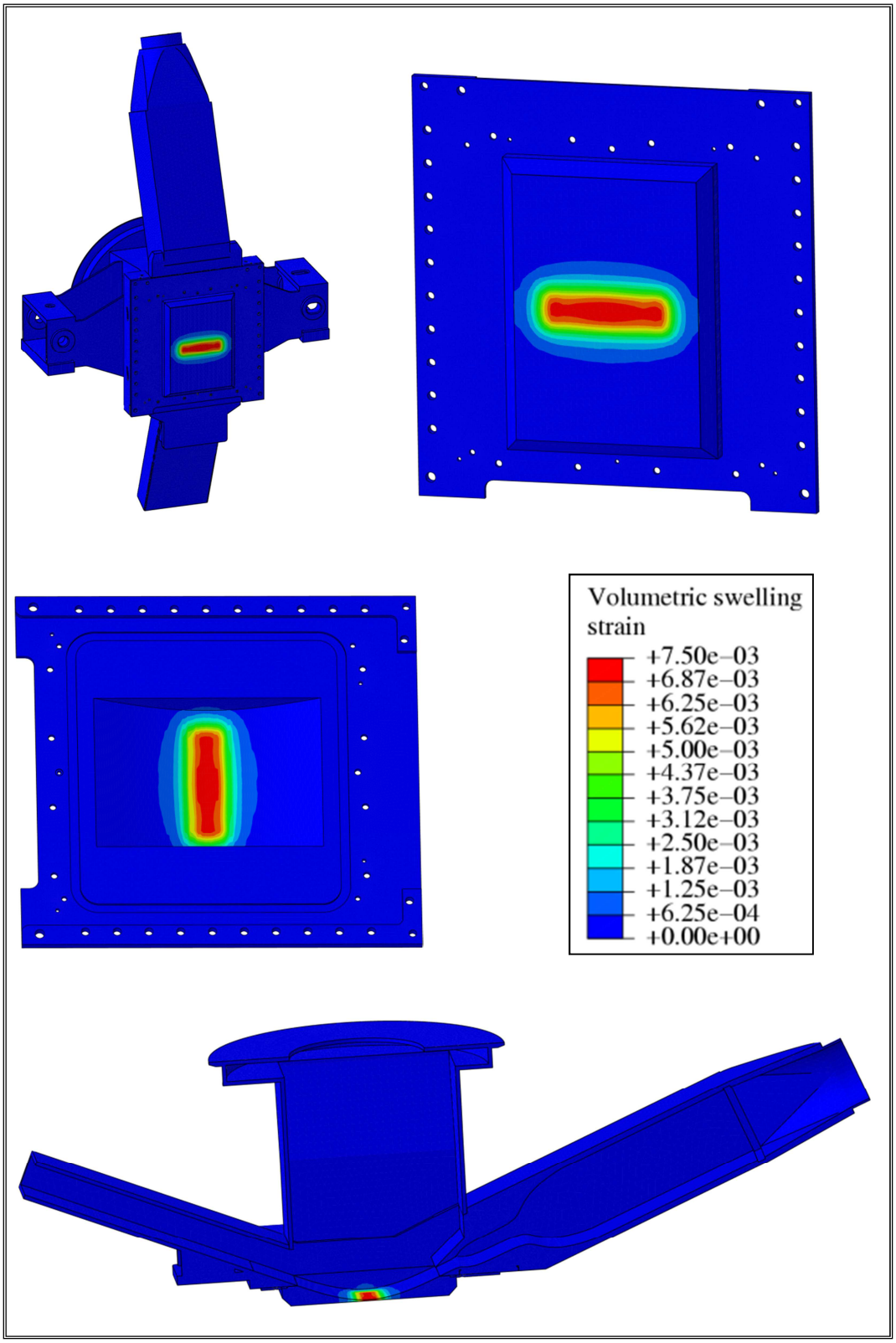

Figure 5-21. Phase 2.Volumetric swelling strain field within TA and BP.

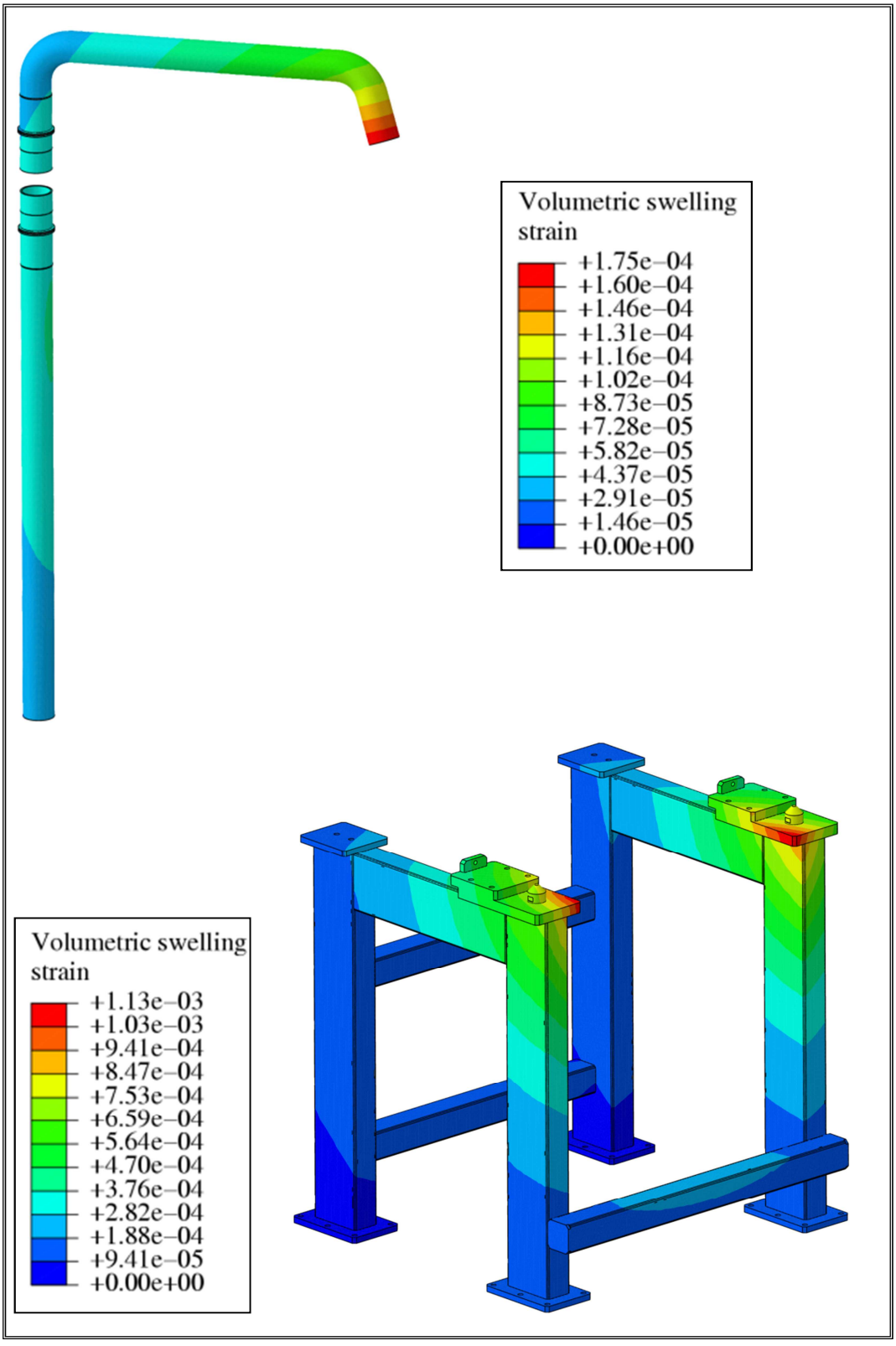

Figure 5-22. Phase 2.Volumetric swelling strain field in framework and Lithium inlet pipe.

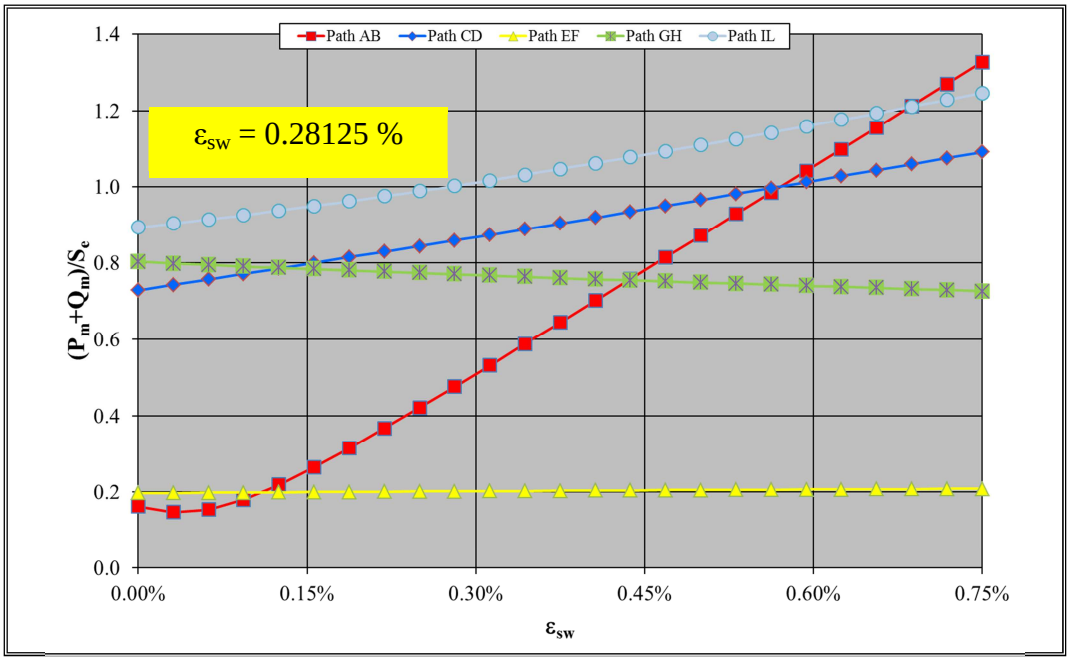

Figure 5-23. Case 18. Immediate plastic flow localisation SDC-IC criterion time evolution.

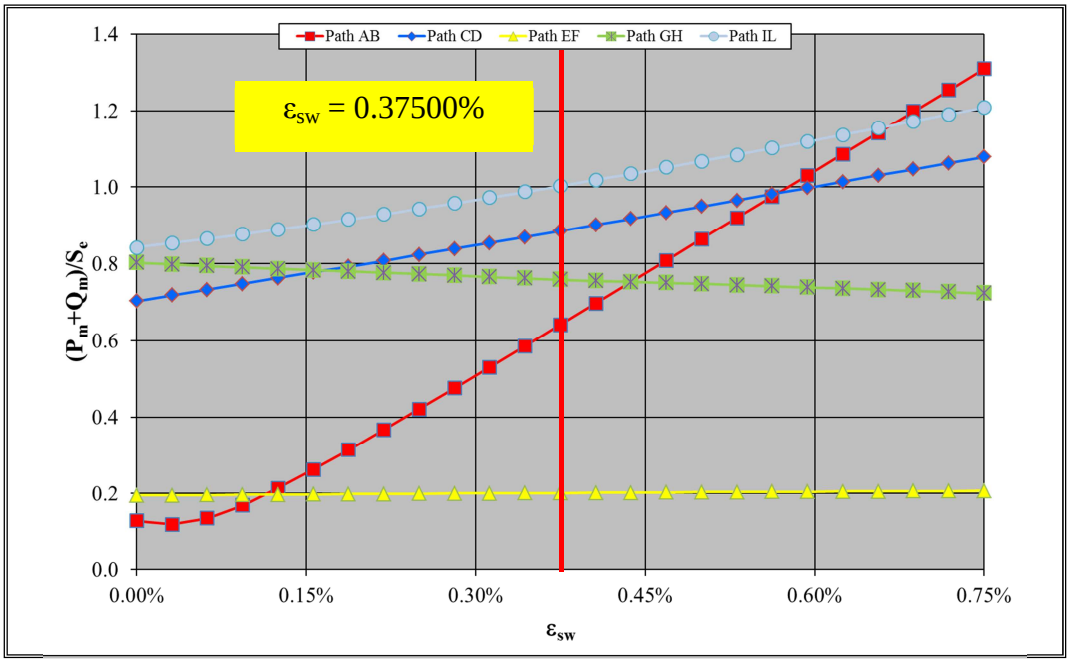

Figure 5-24. Case 48. Immediate plastic flow localisation SDC-IC criterion time evolution.

Concerning Case 18 transient analysis, results in terms of Von Mises equivalent stress spatial distribution at the end of BP lifetime, predicted to be equal to 135 days, is shown in figures 5-25 and 5-26. As to Case 48 transient results, Von Mises equivalent stress field after 180 days of neutronic irradiation, corresponding to the end of the BP lifetime, is shown in

figures 5-27 and 5-28.

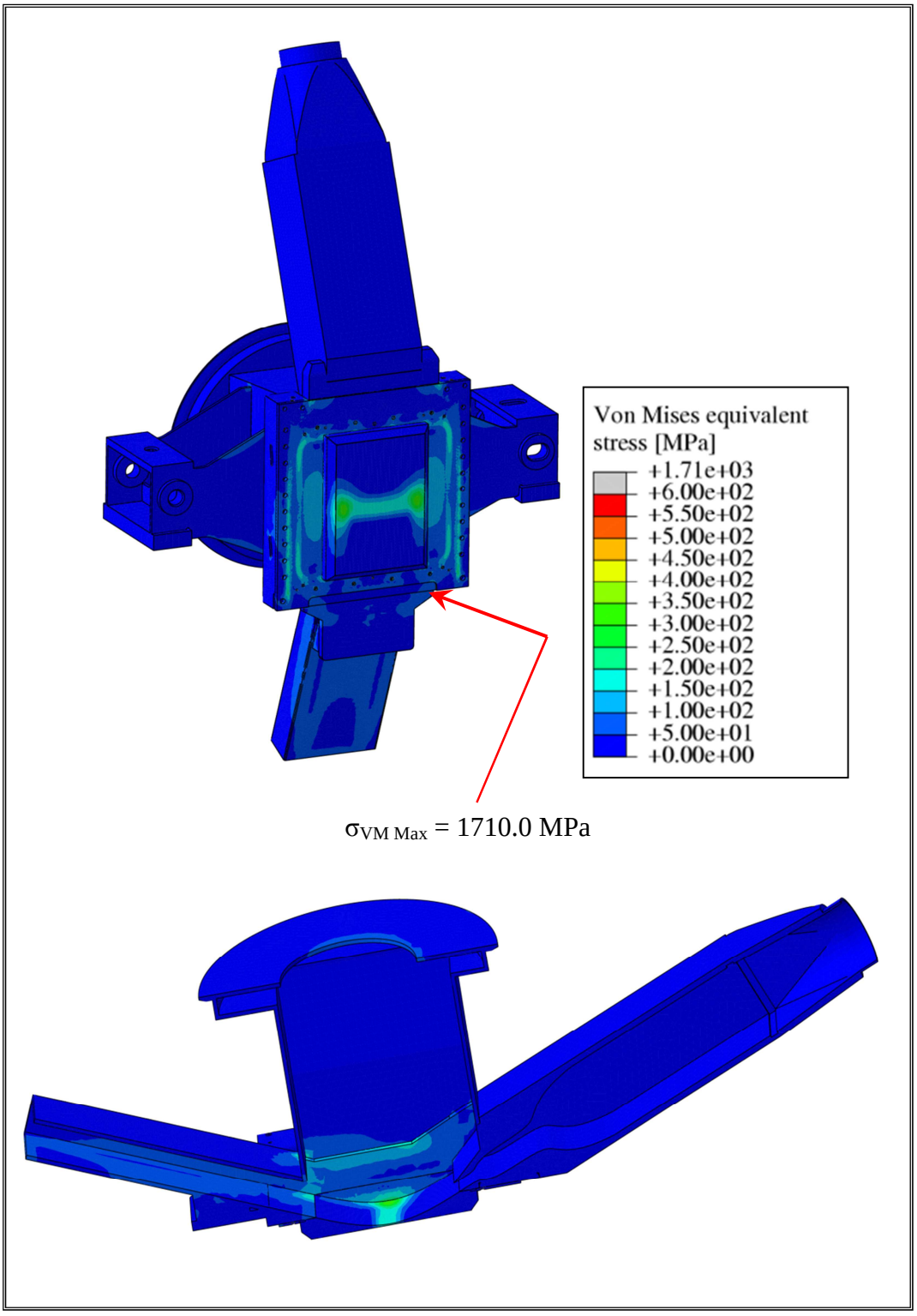

Figure 5-25. Phase 2. Case 18. TA Von Mises stress field at t = 135 days.

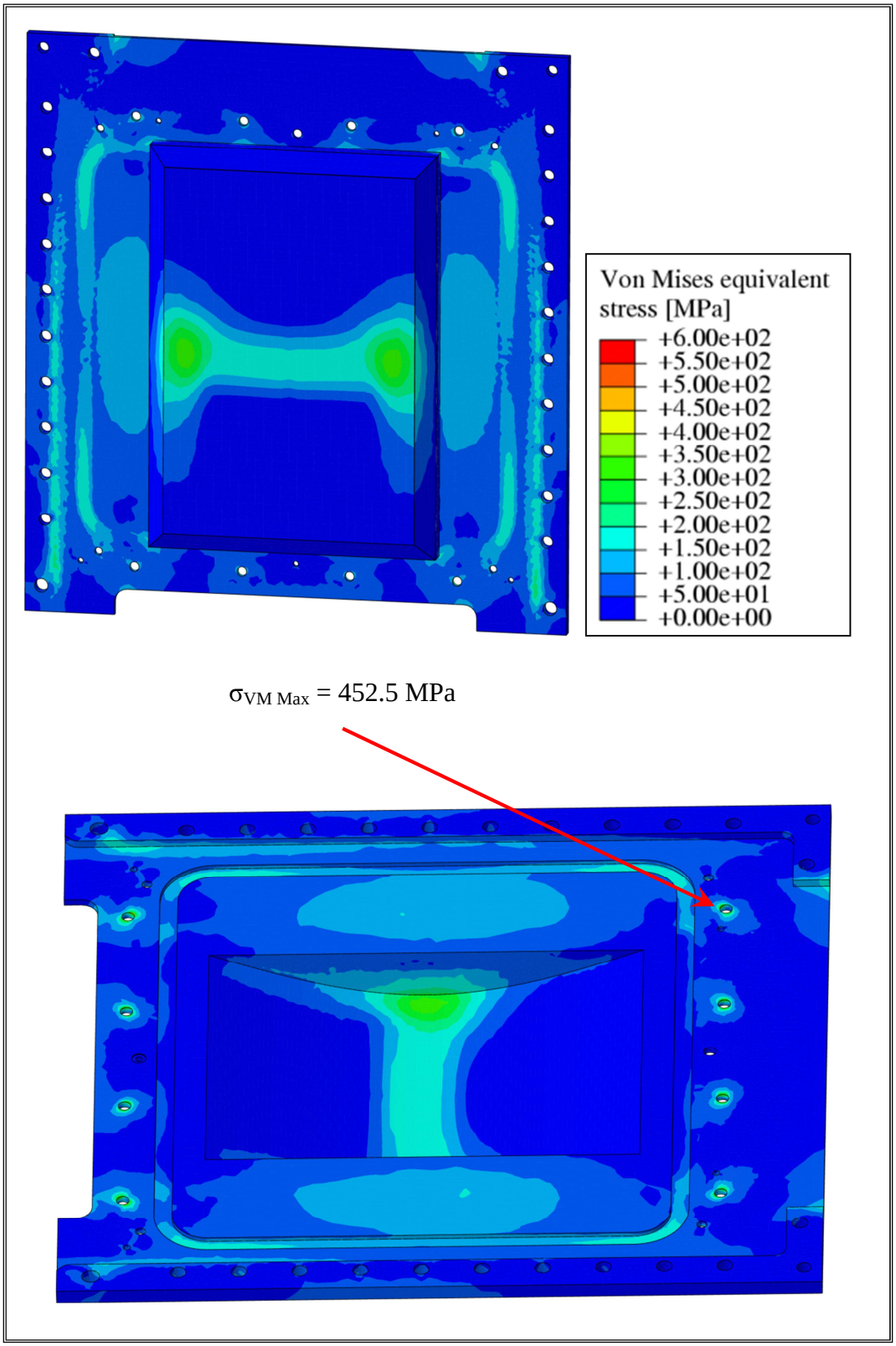

Figure 5-26. Phase 2. Case 18. BP Von Mises stress field at t = 135 days.

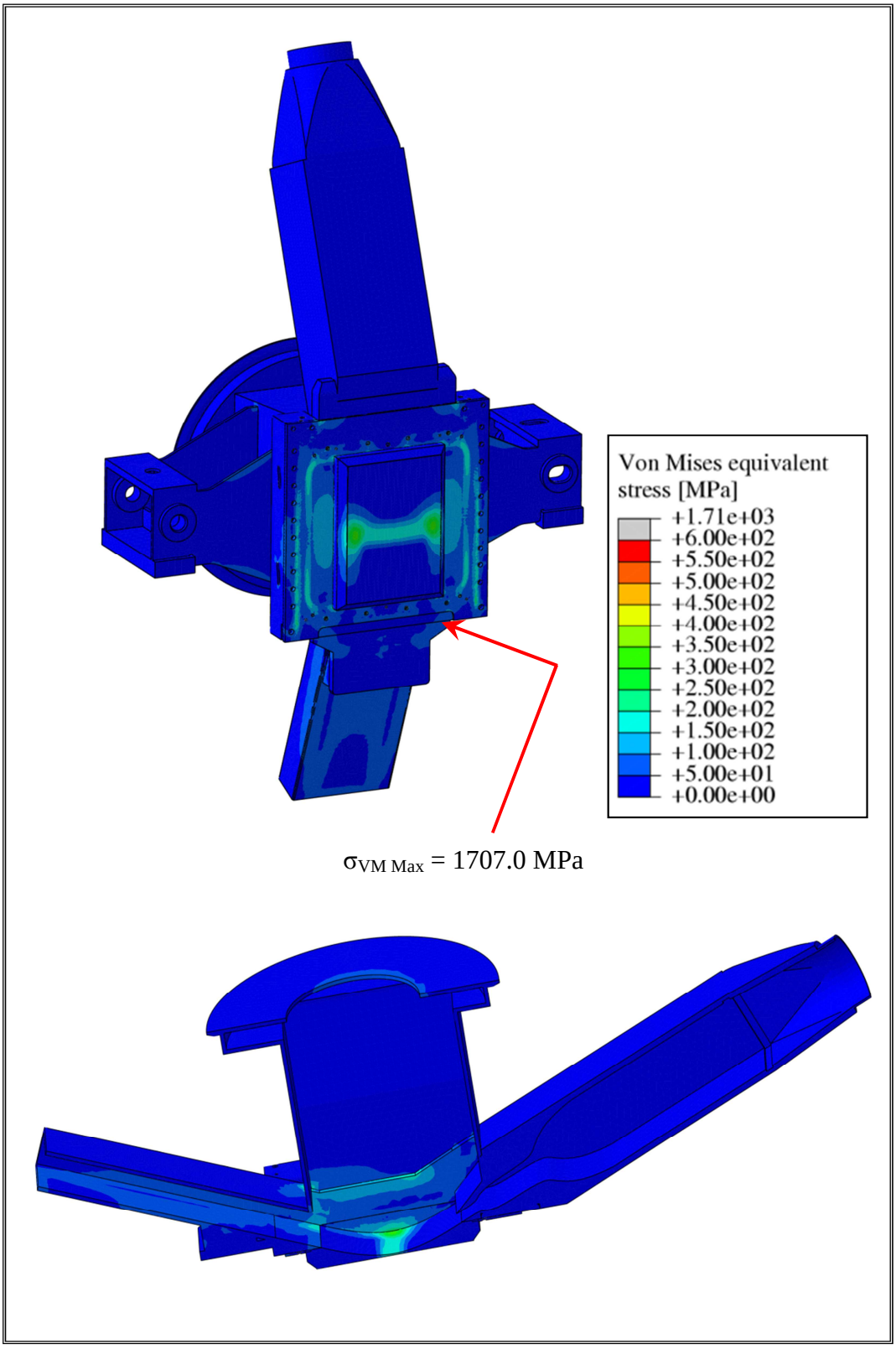

Figure 5-27. Phase 2. Case 48. TA Von Mises stress field at t = 180 days.

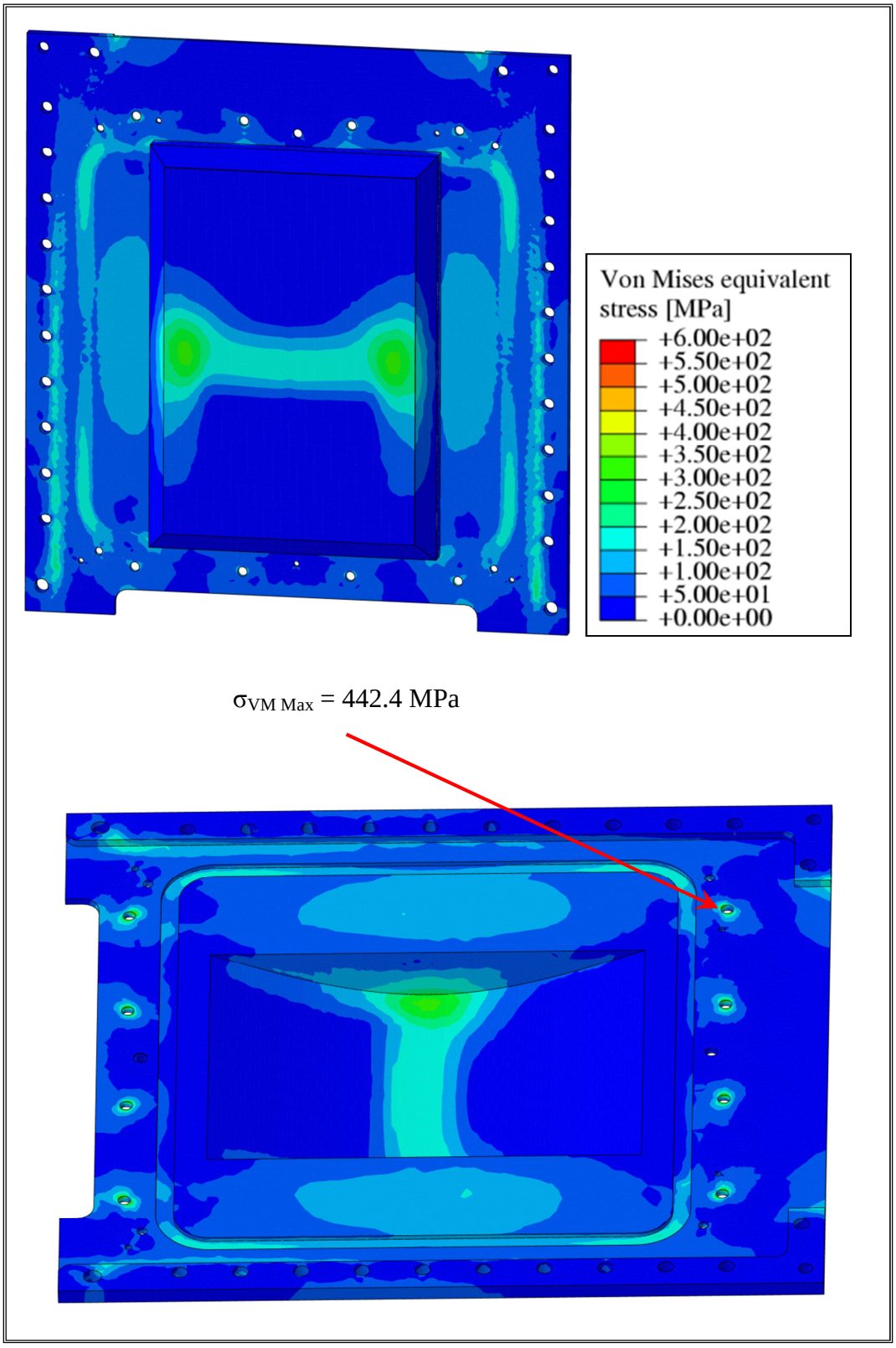

Figure 5-28. Phase 2. Case 48. BP Von Mises stress field at t = 180 days.

As far as the stress linearization procedure is concerned, from the observation of the time evolution of the $(P_m + Q_m) / S_e$ ratio it can be noted that, as to Case 18, a volumetric swelling strain equal to 0.28125 %, achieved after 135 days of neutronic irradiation, causes the failure of the immediate plastic flow localisation criterion along path IL while, concerning Case 48, the corresponding criterion is not met after 180 days (ε_{sw} = 0.375 %) along the same path. Since the two cases differ each other exclusively for the lithium channel thickness, which amounts to 1.7 mm in Case 48 against the 1.2 mm of Case 18, it can be concluded that, for the same BP overall thickness, the BP thermo-mechanical behaviour improves with the increasing of the BP lithium channel thickness, as already partially observed in the previous BP design review procedure phases.

Concerning the Von Mises equivalent stress distribution arising within both models at the end of the BP lifetime, no particular remarks are needed considering that the Von Mises stress maximum values have been calculated within tiny regions located close to geometric discontinuities, while the rest of the structure experiences, in both Case 18 and Case 48, Von Mises stress values well below the 450 MPa. Nevertheless, in both Case 18 and Case 48, the predicted BP lifetime is lower than the nominal operational period envisaged for it so further BP design review strategies are needed to improve the BP thermo-mechanical performances under nominal operational loading conditions in order to maximize its lifetime.

5.3. Phase 3

Results obtained from steady state and transient analyses performed in Phase 2 of the BP design review procedure have allowed two promising BP configuration to be find out, although analyses have put in evidence that further BP design review strategies should be considered in order to select a BP geometric configuration able to safely withstand the thermo-mechanical loads it undergoes during the whole nominal operational period of one year under neutronic irradiation.

In the meanwhile Phase 2 was performed, a more accurate database of the EUROFER steel thermo-physical properties and maximum allowable stress limits has been released [48].

Therefore, in order to check the effect of these new assumptions, the nominal steady state thermo-mechanical analyses of the BP configurations relevant to Case 18 and 48, already carried out during Phase 2, have been re-run and their relevant stress linearization procedures have been properly repeated.

The realistic 3D TA FEM models already used during Phase 2, endowed with the revised BP configurations named Case 18 and 48, have been adopted also in Phase 3.

The updated EUROFER thermo-mechanical properties assumed for the Phase 3 of the BP design review procedure have been summarized in table 5-7 and in figure 5-29.

The material has been considered homogeneous, uniform and isotropic and its thermo-mechanical properties have been assumed to depend uniquely on temperature, as already done

in previous analyses. In particular, EUROFER mechanical behaviour has been simulated adopting a linear elastic model.

As to lithium flow, the same thermo-physical properties assumed for previous analyses have been adopted.

Table 5-7. EUROFER updated thermo-mechanical properties at 20°C [48].

EUROFER	
λ_0	28.30 W/m K
c_{p0}	448.0 J/kg K
α_0	$1.04 \cdot 10^{-5}$ K^{-1}
E_0	$2.17 \cdot 10^{11}$ Pa

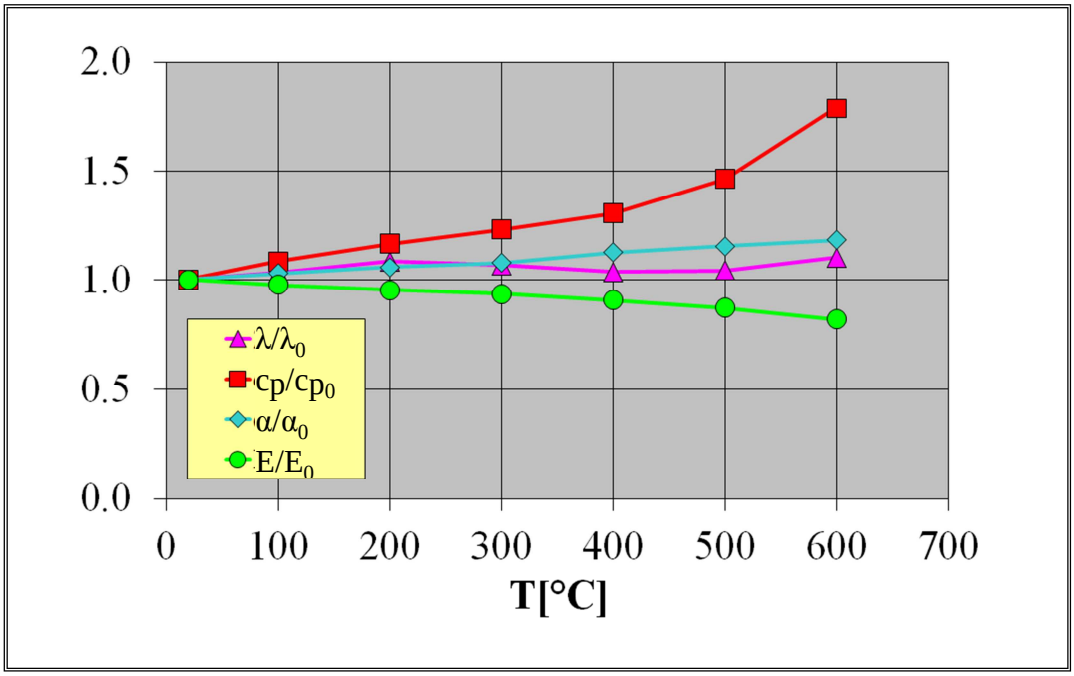

Figure 5-29. EUROFER updated thermo-mechanical properties vs. temperature [48].

5.3.1. Steady state analysis

The so updated 3D FEM model has been used for the re-running of the thermo-mechanical calculations under the steady state nominal operational scenario of IFMIF.

The temperature spatial distributions arising within the two assessed models and the corresponding Von Mises equivalent stress fields have not been herewith reported since they are qualitatively the same of those already shown for Phase 2 steady state thermo-mechanical analyses. On the other hand, the obtained results in terms of SDC-IC safety rule verifications are shown in tables 5-8, 5-9.

Table 5-8. Phase 3. Case 18. SDC-IC safety rule verifications.

	Path AB	Path CD	Path EF	Path GH	Path IL
$T_{Max\text{-}Path}$ [°C]	283.4	251.8	264.2	362.1	252.6
P_m/S_m	0.0018	0.0011	0.0008	0.0007	0.0014
$(P_m+P_b)/(K_{eff}*S_m)$	0.0017	0.0008	0.0006	0.0006	0.0010
$(P_m+Q_m)/S_e$	0.1797	1.0720	0.2675	0.7641	1.3213

Table 5-9. Phase 3. Case 48. SDC-IC safety rule verifications.

	Path AB	Path CD	Path EF	Path GH	Path IL
$T_{Max\text{-}Path}$ [°C]	284.5	252.1	264.2	362.1	253.1
P_m/S_m	0.0017	0.0013	0.0007	0.0022	0.0016
$(P_m+P_b)/(K_{eff}*S_m)$	0.0017	0.0009	0.0005	0.0016	0.0012
$(P_m+Q_m)/S_e$	0.1388	1.0333	0.2650	0.7642	1.2357

The obtained results indicate that, in spite of analyses performed in Phase 2, the new material properties and the revised stress limits lead to the non-fulfilment of the $(P_m + Q_m) / S_e$ criterion within paths CD and IL. This strongly suggests the need for a further revision of the BP design review strategy, possibly involving also the BP adjacent components which act mechanically on it originating a certain stress amounting.

Since the SDC-IC level A design criteria have not been totally fulfilled under the steady state loading conditions, no transient analyses have been performed in Phase 3 of the BP design review procedure because, as already observed in Phase 2, the time increasing volumetric swelling strain generates an increase of the $(P_m + Q_m) / S_e$ value.

5.4. Phase 4

Despite the previous phases of the BP design review procedure have not allowed to select a BP geometric configuration able to safely withstand the thermo-mechanical loads it undergoes during the normal operation period envisaged for it, results obtained in Phases 2 and 3 have suggested that the BP geometric configuration named Case 48 is the most promising among those investigated, showing an encouraging thermo-mechanical performances under both steady state and transient thermo-mechanical loading conditions. Obviously, further investigation is needed to attain a BP geometric configuration which complies with the design rules prescribed by SDC-IC codes when subjected to neutronic irradiation for one year. For these reasons, Case 48 BP configuration, characterized by an added steel layer of 1.7 mm on the lithium channel external surface, for a total lithium channel thickness of 3.5 mm, and by an overall BP thickness reduced down to 12.8 mm, has been selected as the reference one for Phase 4 calculations.

This phase of the BP design review procedure has been specifically intended to optimize the BP steady-state thermo-mechanical performances under nominal loading conditions (described in § 4.2.2 and in § 4.2.3) by the implementation of further design review strategies inferred from the observations drawn from the outcomes of previous analyses.

In particular two main considerations have been followed towards the choice of the BP design review strategies taken into account in Phase 4.

The first is the observation that the lithium channel thickness seems to be stressed by the adjacent BP region mechanical action, so a reduction of the steel volume around it may be useful to reduce the stress amount along paths CD and IL. The second consideration is represented by the necessity to reduce the predicted temperature values within BP geometric domain, achieving the double goal of reducing the secondary stress amount and of dealing with higher stress limits values.

Moreover, the high temperature values achieved within the lithium guides of the Target Chamber (TC), probably due to their considerable thickness, have suggested that a reduction of this steel volume could be taken into account in order to avoid the conductive heat transfer between them and the BP.

On the basis of these considerations, the BP layout has been modified by means of the elimination of the lithium channel lateral thickness (Fig. 5-30) in order to relax the most stressed BP regions.

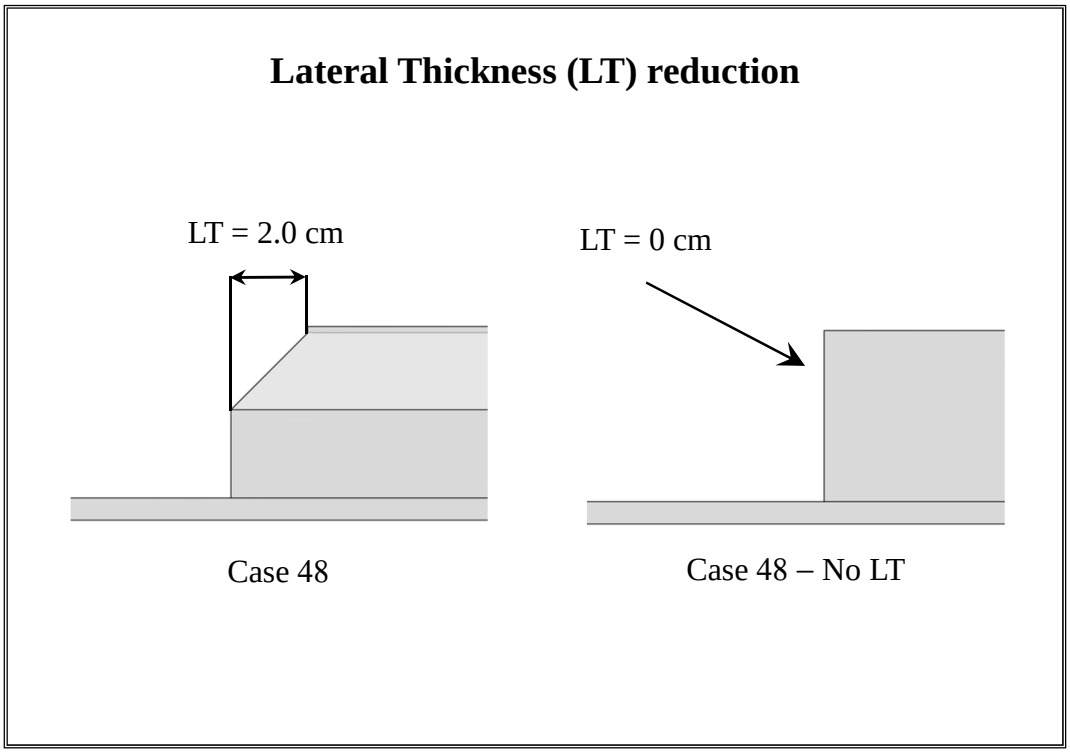

Figure 5-30. Phase 4. Reduction of the BP lithium channel lateral thickness.

With the aim of reducing the intense thermal gradient arising within the BP body, the finning of the BP external surface has been taken into account as a further innovative design review strategy and it has been implemented in the Case 48-No LT BP configuration.

The initial step of the BP external surface finning has been the analysis of the thermal effect of different sets of fins, differing each other in the geometric characteristics. As a consequence of a parametric study, two batches of 115 fins have been assumed on the external surface of the Case 48 - No LT BP geometric configuration, assessed in the previous thermo-mechanical analysis, and a proper revised 3D model of the BP has been set-up (figure 5-31) to investigate the steady state thermo-mechanical performances of the resulting finned BP configuration under nominal loading conditions.

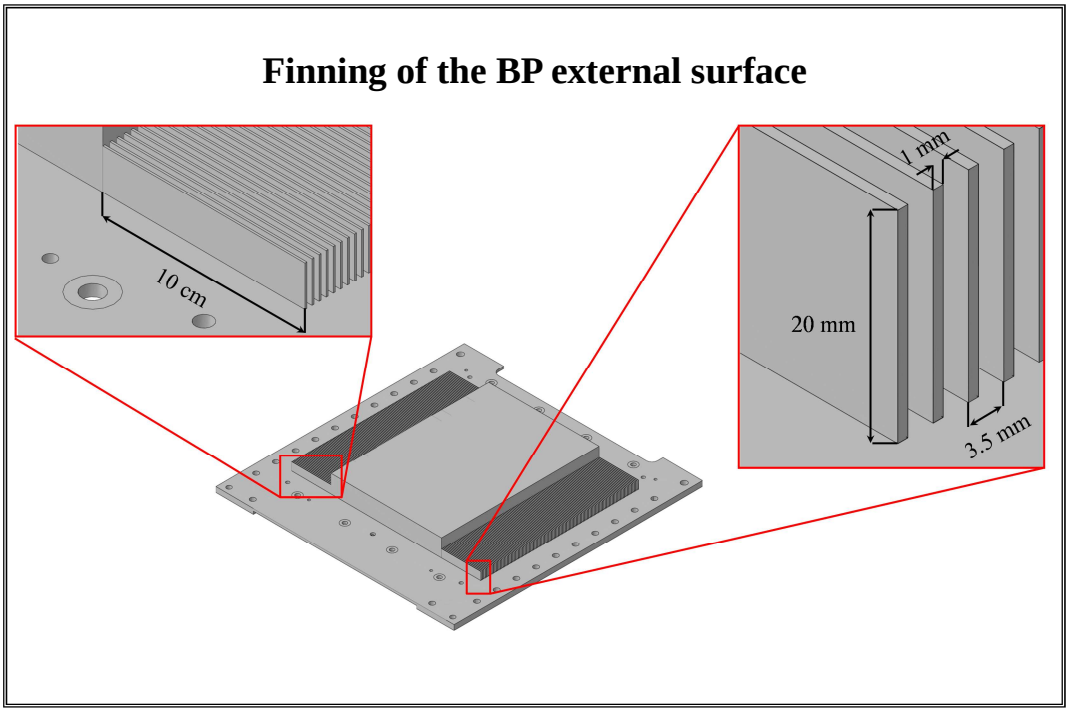

Figure 5-31. Phase 4. Case 48 - No LT finned BP configuration.

Finally, since it has been observed that a large amount of heat power is deposited by neutrons and gammas within the volume of the TC Lithium Guides (LGs), giving a strong contribute to BP heating, a reduction of their volume has been taken into account (figure 5-32) as an additional BP design review strategy, to be implemented together with all those thus far considered.

A proper 3D FEM model of the IFMIF TA, properly endowed with the Case 48-No LT finned BP geometric configuration, in which the LG volume has been reduced, has been set-up. It is characterized by 604093 nodes connected in 2137246 linear tetrahedral and hexahedral elements.

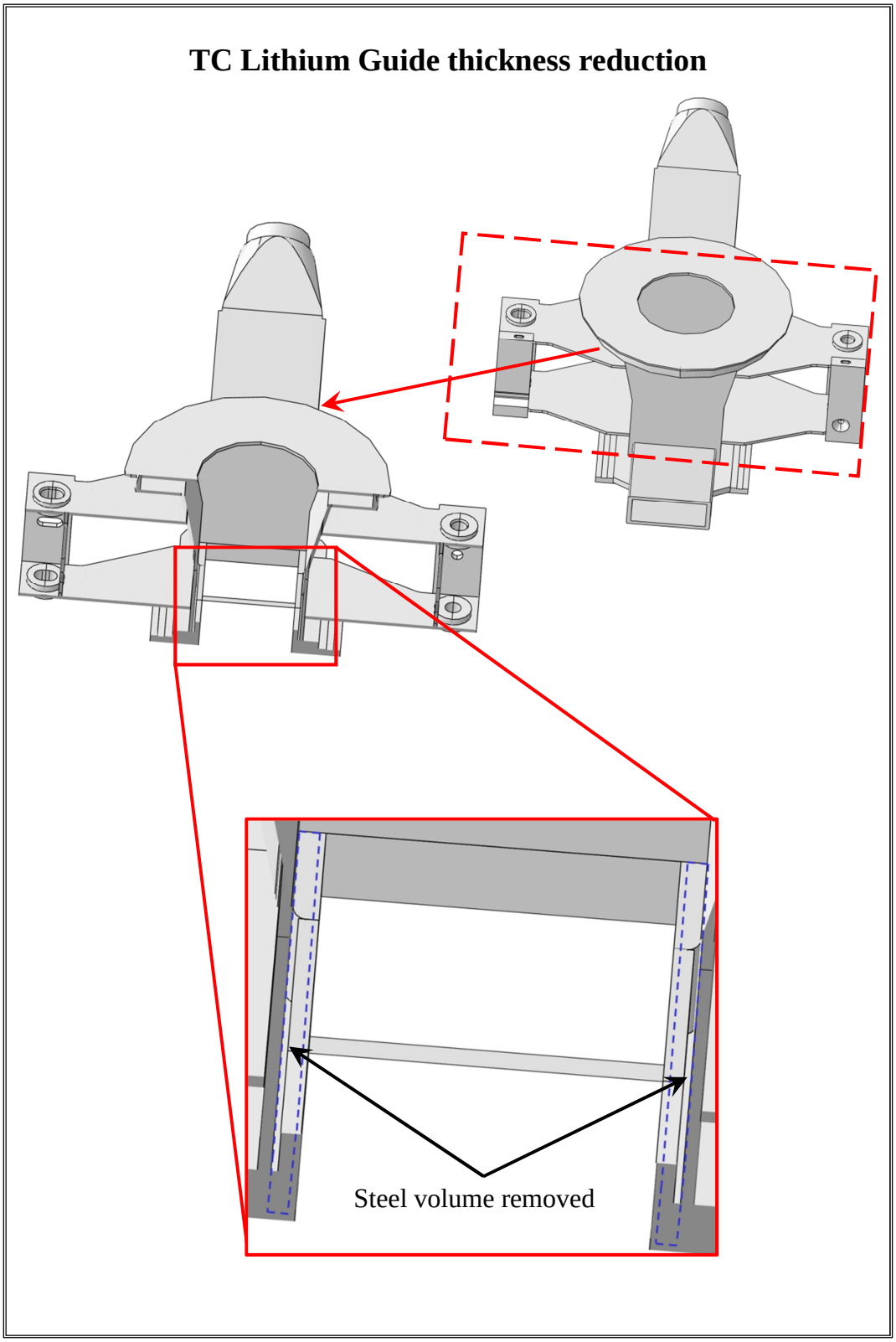

Figure 5-32. Phase 4.Reduction of the TC LG thickness.

5.4.1. Steady state and transient analysis

The thermo-mechanical performances of the reviewed BP configuration have been carried out taking into account the loading conditions foreseen for the IFMIF nominal operational scenario already described. Moreover, the natural convection heat transfer taking place in the gaps between helium and fins has been considered by means of a heat transfer model characterized by a convective heat transfer coefficient h equal to 5 W/(m² °C) and a helium bulk temperature of 50 °C, while the rest of the BP external surface has been supposed to be thermally coupled to the HFTM surface, kept at 50 °C, by means of a thermal conductance depending on the distance between BP and HFTM external surface.

From the thermal point of view, results have shown that the review procedure of both BP and TC LGs leads to a strong reduction of the predicted BP average temperature, with a remarkable drop in the maximum value of ~50 °C. Also the maximum temperature achieved within the TA is predicted to decrease down to a value of ~400°C against the 427.5 °C of the previous model (Figs. 5-33 and 5-34).

As far as mechanical results are concerned, the new predicted thermal field within the IFMIF TA leads to a strong reduction of the thermal stresses, together with an average decrease of the stress limit values due to the aforementioned reduction of the predicted BP average temperature. In fact, from the mechanical point of view, except for extremely localized regions in which, due to numerical singularities, really high Von Mises stress values have been calculated, the stress field achieves values well below the 250 MPa (Figs. 5-35 and 5-36).

Moreover, all SDC-IC safety criteria are largely fulfilled in all paths considered, due the reduction of the thermal field carried out from analyses. In particular, the criterion aimed at the checking of the immediate flow plastic collapse, namely that involving the $(P_m + Q_m) / S_e$ ratio, is still the most critical among those considered, achieving a value equal to 0.7830 along path IL (Table 5-10).

Table 5-10. Phase 4. SDC-IC safety rules verification.

	Path AB	Path CD	Path EF	Path GH	Path IL
$T_{Max\text{-}Path}$ [°C]	288.8	251.6	157.4	225.5	270.0
P_m/S_m	0.0023	0.0010	0.0003	0.0008	0.0015
$(P_m+P_b)/(K_{eff}*S_m)$	0.0017	0.0008	0.0002	0.0006	0.0011
$(P_m+Q_m)/S_e$	0.3232	0.4439	0.1362	0.7117	0.7830

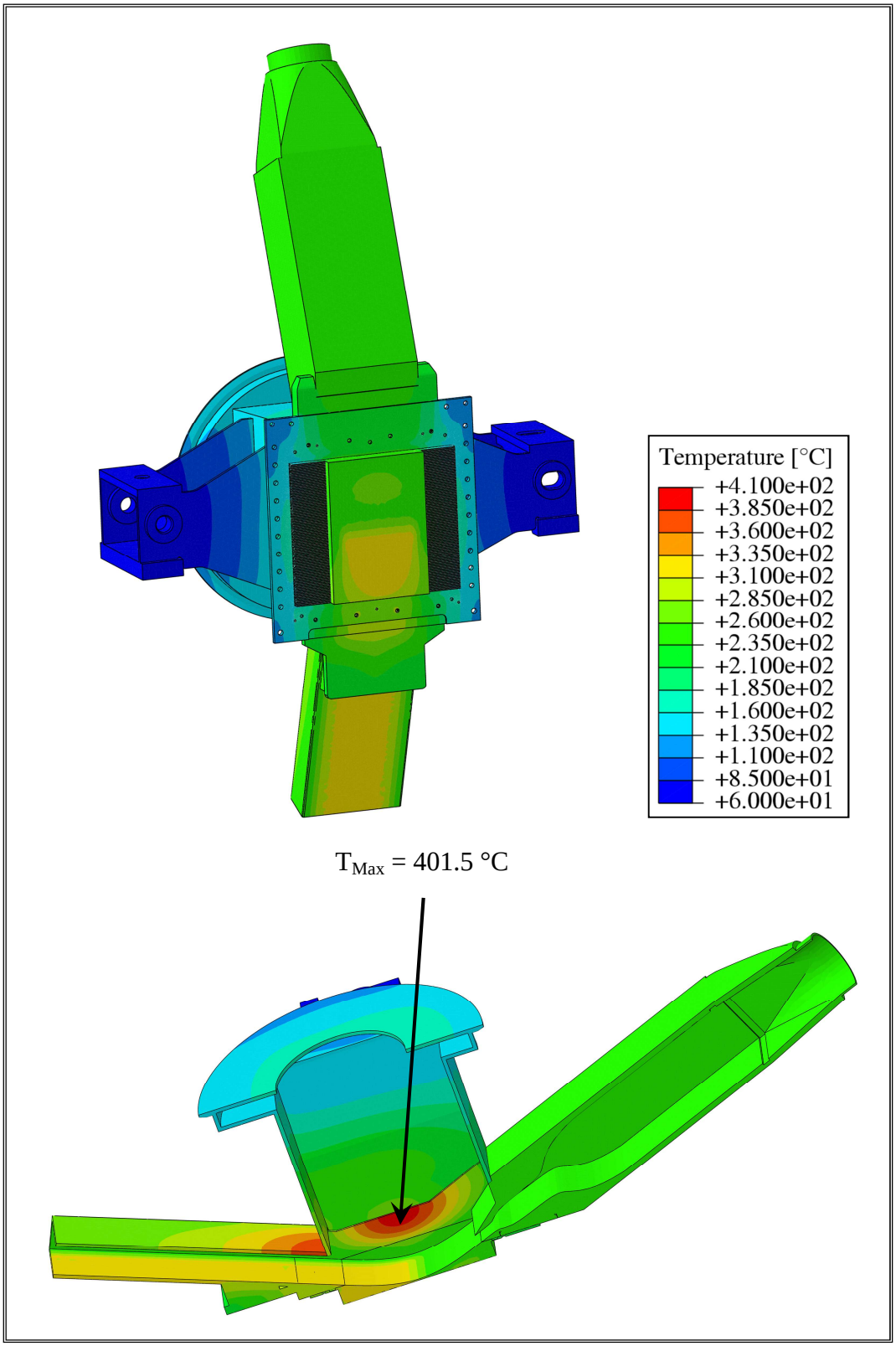

Figure 5-34. Phase 4.TA thermal field.

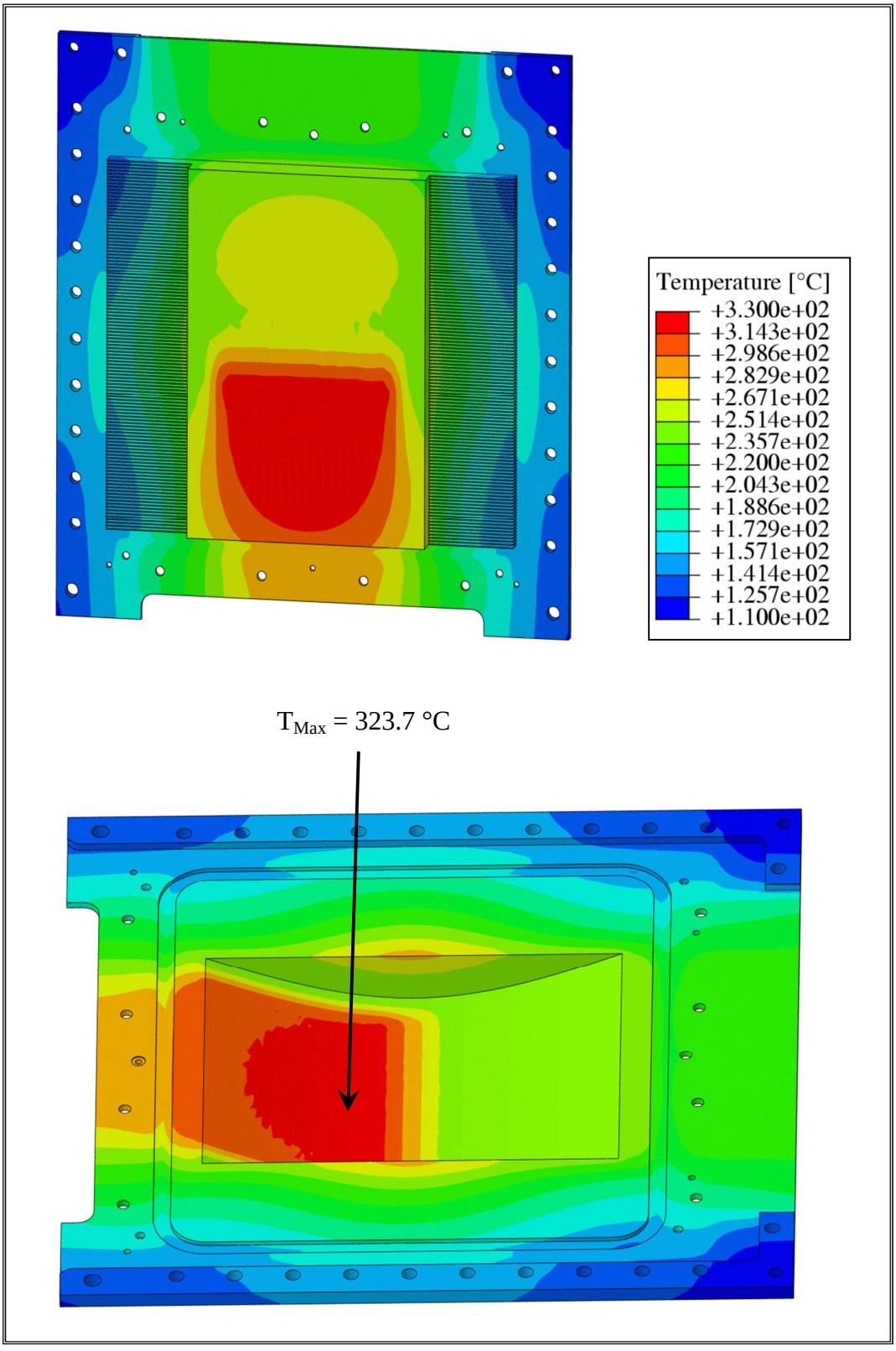

Figure 5-35. Phase 4. BP thermal field.

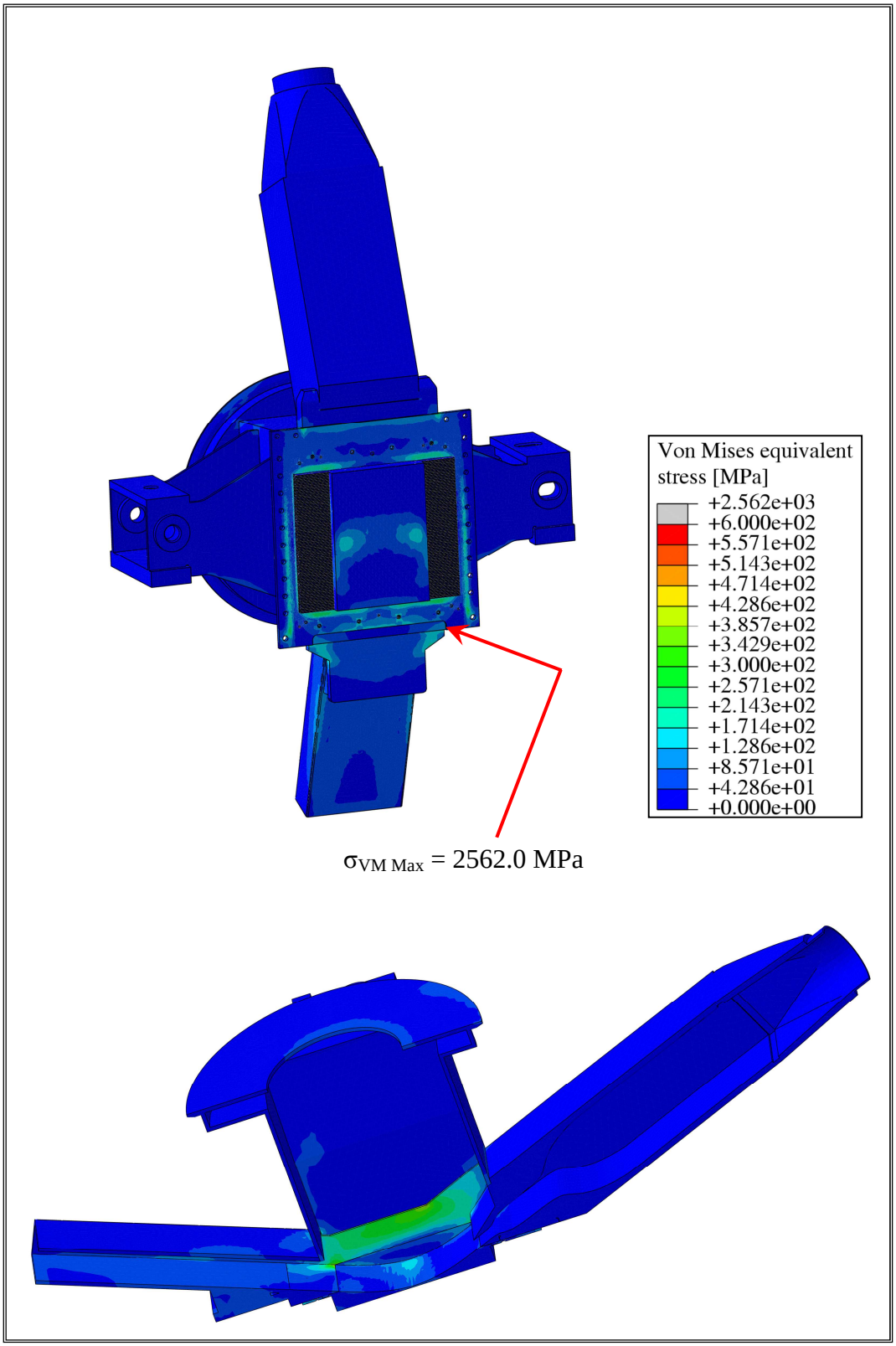

Figure 5-36. Phase 4. TA Von Mises stress field.

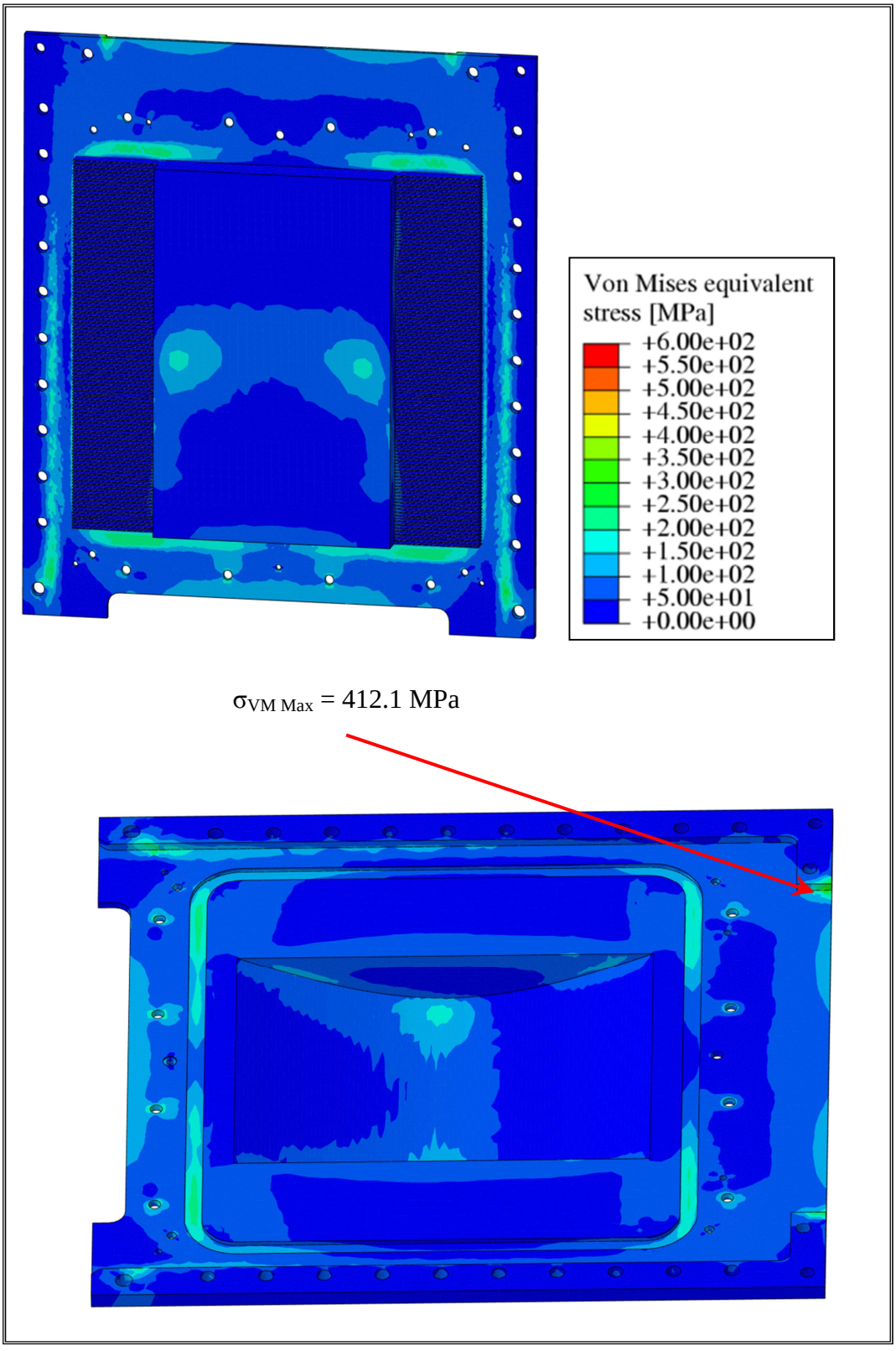

Figure 5-36. Phase 4. BP Von Mises stress field.

Results thus far obtained allow to conclude that the combined effect of all the BP design review strategies taken into account permits to select a BP geometric configuration able to safely withstand the thermo-mechanical loads it undergoes under steady state conditions.

Therefore, in order to investigate the effect of the volumetric swelling strain field on the BP, a transient thermo-mechanical analysis has been performed taking into account the IFMIF TA model in which the original BP has been replaced with the Case 48-No LT finned one. The transient normal operation loading scenario has been adopted and a linear dependence of swelling strain on DPA has been assumed, imposing that after one year of neutronic irradiation the swelling strain value achieved at the beam footprint region centre amounts to 0.75 %.

Results carried out from the analysis indicate that, from the mechanical point of view, the most critical SDC-IC safety criteria is still that involving the $(P_m + Q_m) / S_e$ ratio, while the remaining level A criteria are fulfilled during the entire normal operation period of one year along all BP paths taken into account.

For this reason only the time evolution of the $(P_m + Q_m) / S_e$ ratio has been reported in Figure 5-37. From the observation of the $(P_m + Q_m) / S_e$ ratio time evolution it can be noted that a volumetric swelling strain equal to 0.40625 %, achieved after 195 days of neutronic irradiation at the assumed swelling strain rate, causes the failure of the BP due to the immediate plastic flow localisation along path AB.

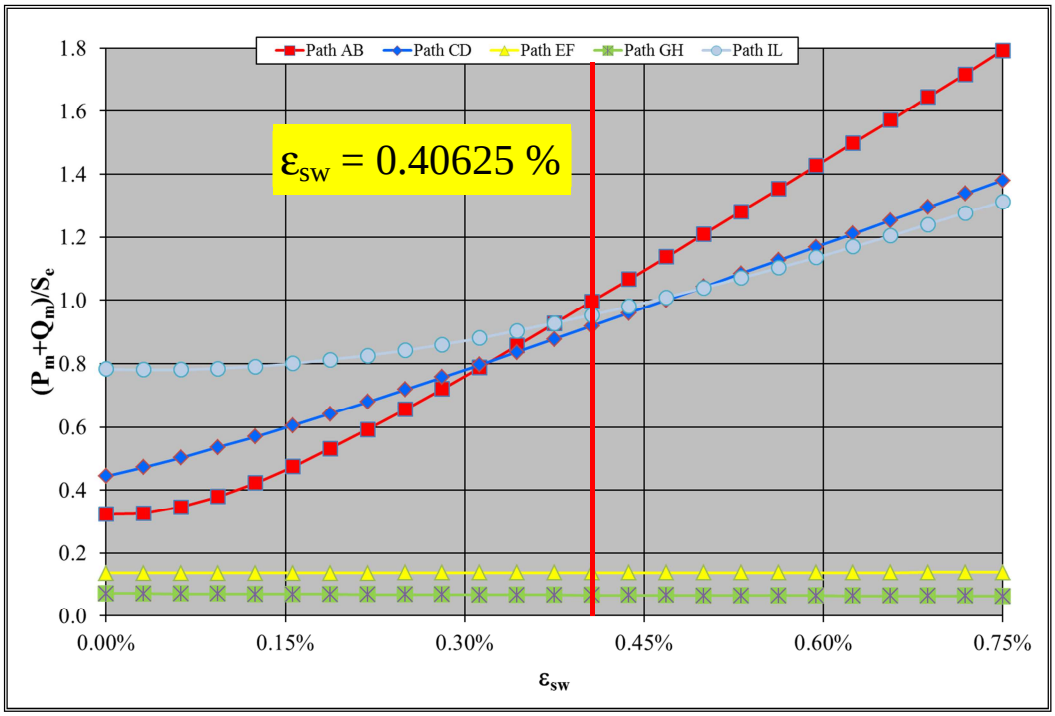

Figure 5-37. Phase 4. $(P_m + Q_m) / S_e$ ratio time evolution.

5.5. Phase 5

The BP design review procedure has allowed a BP geometric configuration to be selected. This configuration is able to safely withstand the steady state thermo-mechanical loads relevant to the IFMIF nominal scenario and assure a BP lifetime of 195 days in case transient nominal operational conditions under neutronic irradiation are taken into account. Nevertheless, results of the BP optimization procedure are affected by the uncertainty of the volumetric density of nuclear heat power and DPA spatial distributions assumed, which are those calculated by ENEA with reference to the original IFMIF TA geometric model, without considering the geometric modifications generated by the optimization procedure of the investigated domain.

For this reason, on the basis of BP and TA geometric configurations selected at the end of the optimization procedure, a new neutronic analysis campaign has been performed at ENEA in 2015, aimed at the determination of an appropriate volumetric density of nuclear heat power and DPA spatial distributions relevant to the optimized BP and TA geometric configurations carried out from the optimization procedure. These new spatial distributions have been adopted for a further campaign of both steady state and transient thermo-mechanical analyses, aimed at the assessment of the performances of the IFMIF TA optimized configuration when subjected to pertinent neutron-induced thermo-mechanical loads.

It has to be noted that, for both volumetric density of heat power and DPA spatial distributions, the new data provided by ENEA have concerned uniquely the BP and TA optimized geometric domains, while as to Lithium inlet pipe and support framework, a $1/r^2$ dependence has been supposed. In particular, Eq (4-1) has been adopted, implementing the new calculated q''' value at the BP centre. The same approach has been adopted for the evaluation of the DPA field arising within Lithium inlet pipe and support framework.

5.5.1. Steady state analysis

Steady-state un-coupled thermo-mechanical analyses have been performed under nominal loading conditions to assess the influence of the new volumetric density of heat power (figures 5-38 and 5-39) spatial distribution on the revised BP and TA thermo-mechanical performances. As it has been assumed in the optimization procedure, the steady state loading conditions relevant to the nominal scenario of IFMIF have been taken into account, modelling the natural convective heat transfer between helium and BP external finned surface as described in § 5.4. The temperature distributions obtained from thermal calculations have been reported in figures 5-40 and 5-41, while Von Mises equivalent stress fields arising within the structure are shown in figures 5-42 and 5-43. Moreover, SDC-IC safety rules have been checked and they are reported in table 5-11.

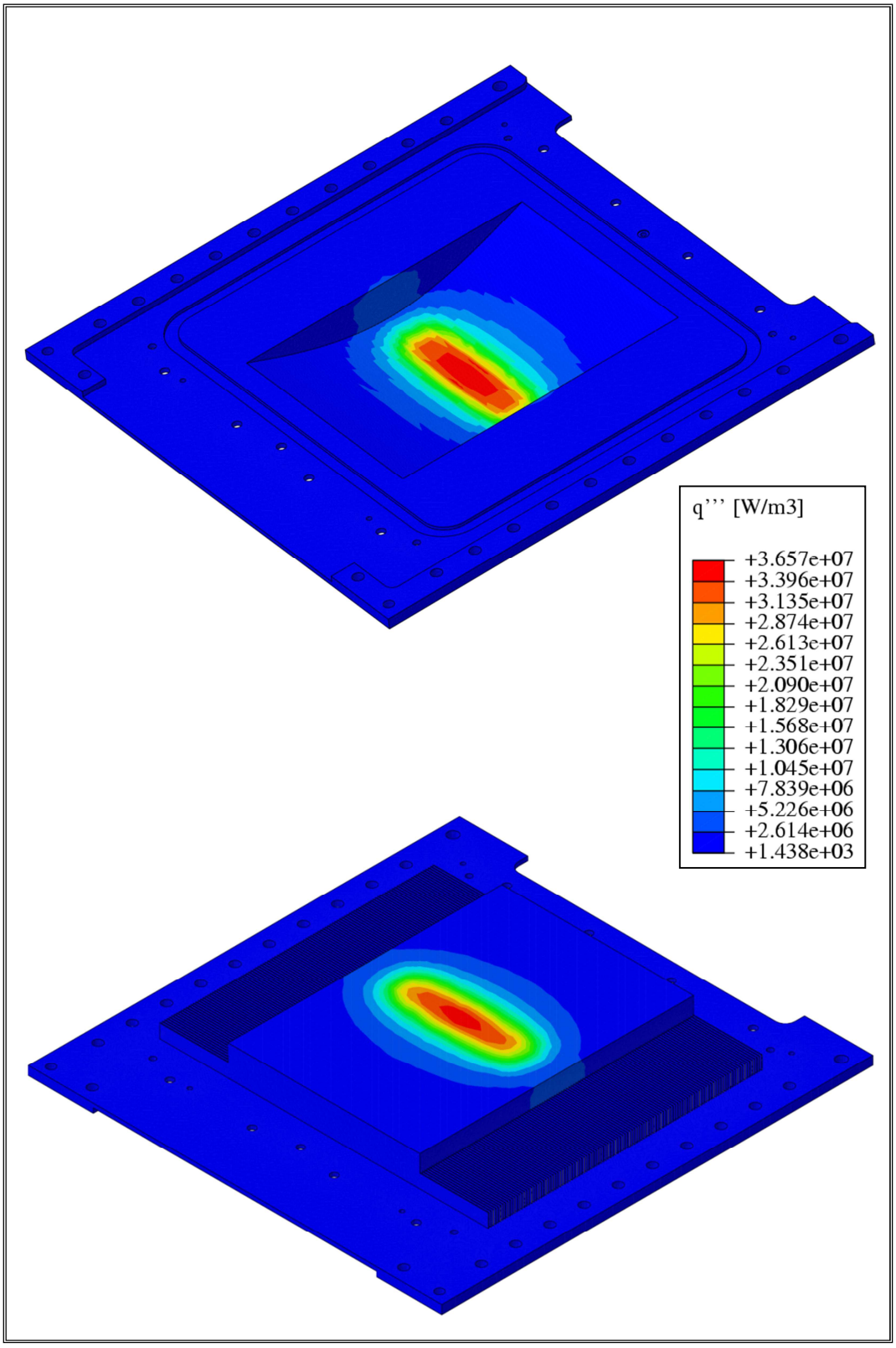

Figure 5-38. New BP volumetric density of nuclear heat power spatial distribution.

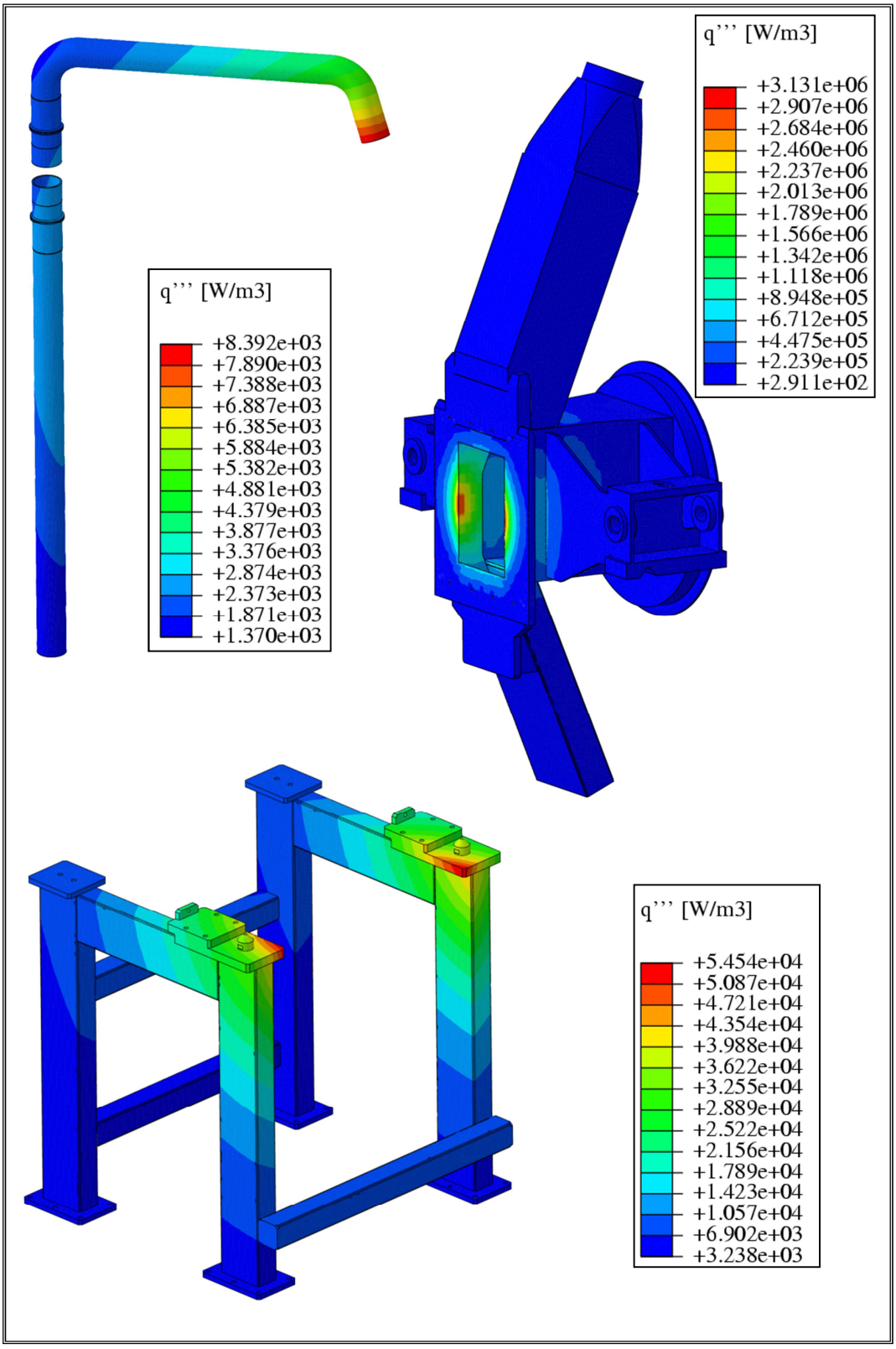

Figure 5-39. New TA volumetric density of nuclear heat power spatial distribution.

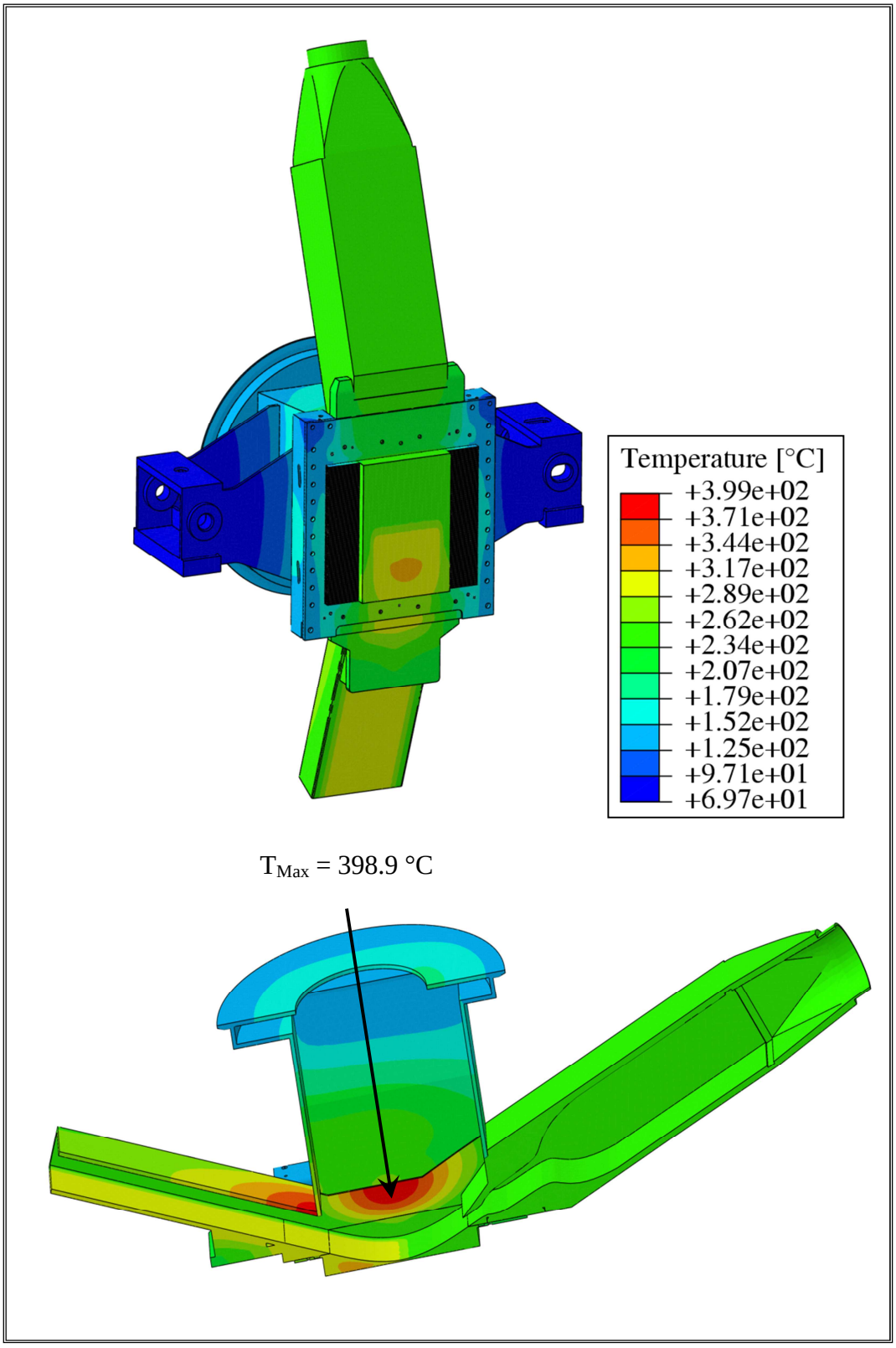

Figure 5-40. Steady state analysis. TA thermal field.

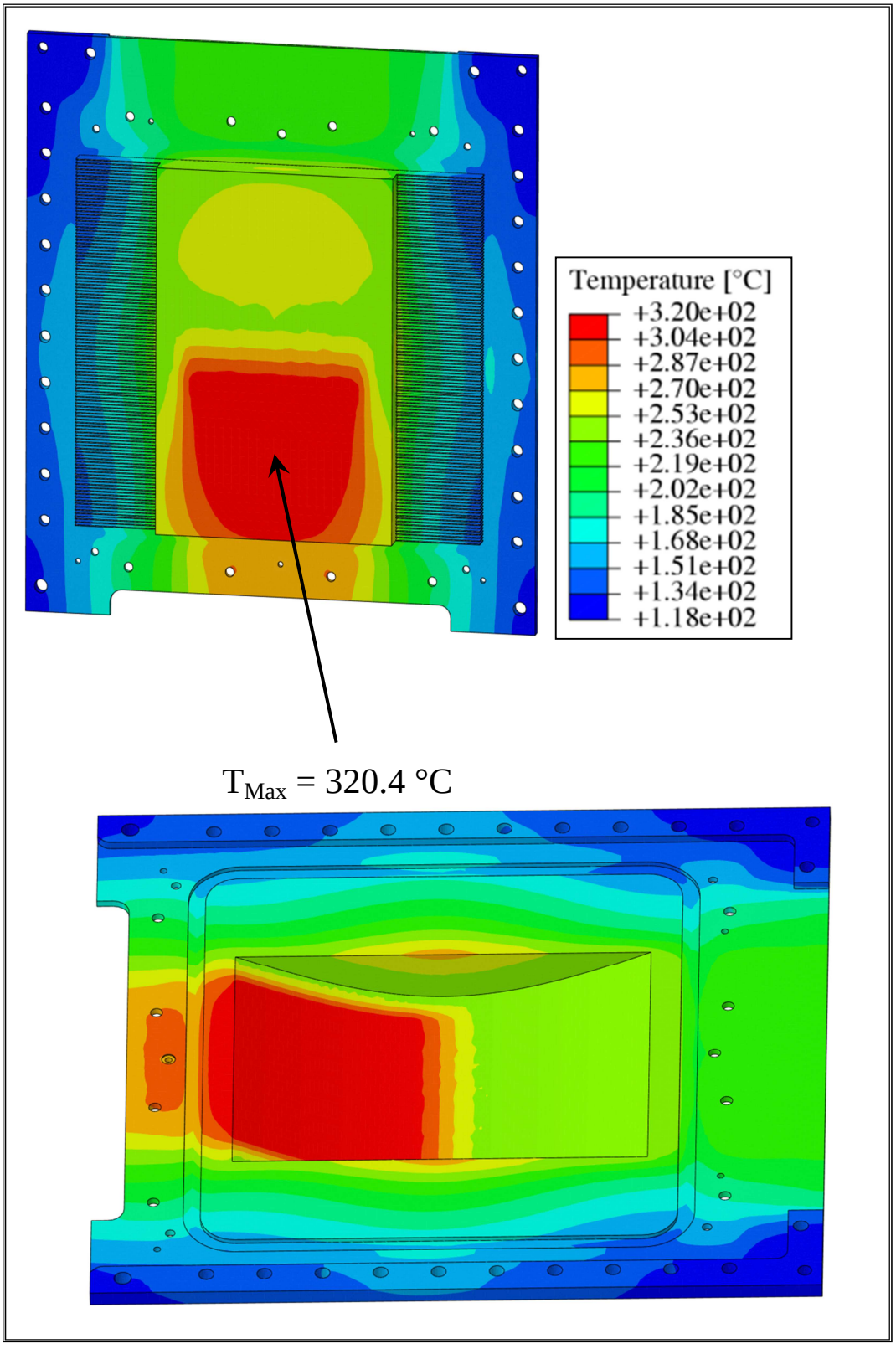

Figure 5-41. Steady state analysis. BP thermal field.

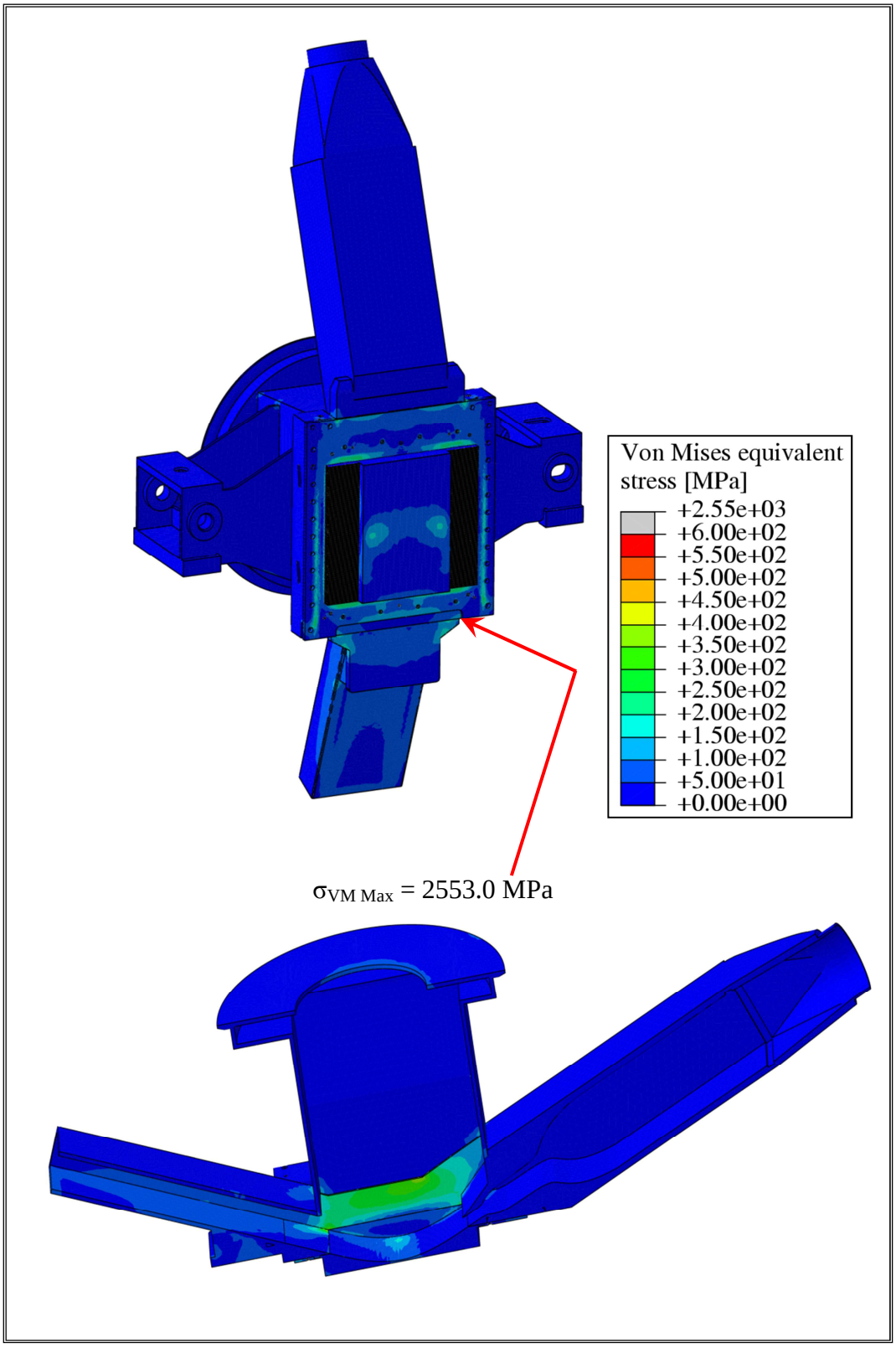

Figure 5-42. Steady state analysis. TA Von Mises stress field.

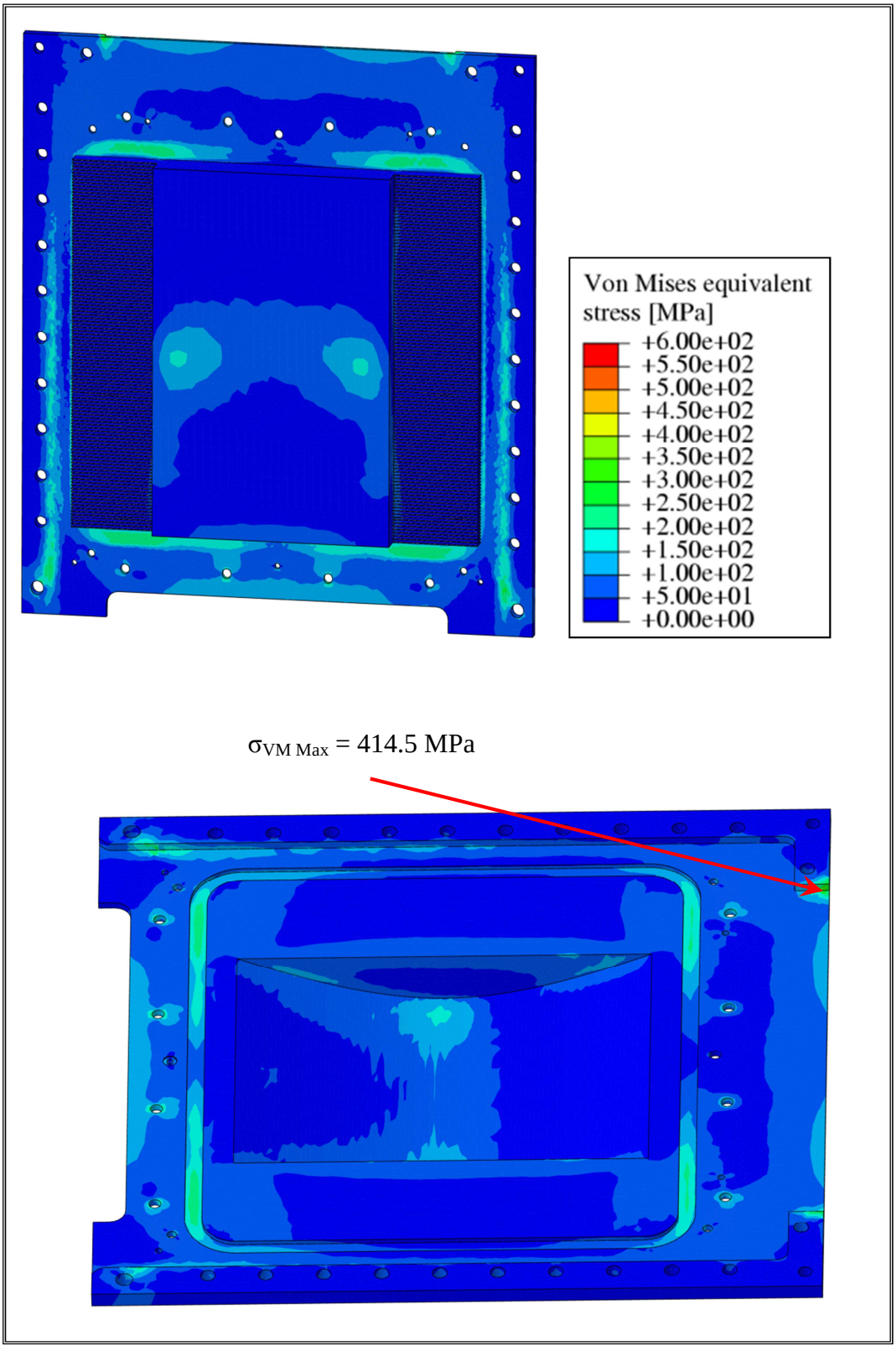

Figure 5-43. Steady state analysis. BP Von Mises stress field.

Table 5-11. Phase 5. SDC-IC safety rule verification.

	Path AB	Path CD	Path EF	Path GH	Path IL
$T_{Max\text{-}Path}$ [°C]	282.4	250.3	153.8	214.7	267.9
P_m/S_m	0.0023	0.0012	0.0003	0.0007	0.0017
$(P_m+P_b)/(K_{eff}*S_m)$	0.0017	0.0009	0.0002	0.0005	0.0011
$(P_m+Q_m)/S_e$	0.3278	0.4170	0.1142	0.4266	0.7705

The obtained steady state results have highlighted that, from the thermal point of view, adopting the new volumetric density of nuclear heat power spatial distribution, the maximum predicted BP temperature is equal to 320.4 °C while, as far as the TA is concerned, the maximum value of 398.9 °C is still calculated within lithium guides volume. These results allow to conclude that the new calculated volumetric density of nuclear heat power field has no significant impact on the BP thermal behaviour.

From the mechanical point of view, Von Mises equivalent stress reaches values below 300 MPa in almost all the BP geometric domain, except for a very localized region in which Von Mises equivalent stress maximum value occurs, probably due to a geometric singularity. The same observation can be done assessing the TA Von Mises stress field.

Furthermore, SDC-IC Level A safety rules are totally satisfied along all paths taken into account. Also in this case the most critical criterion is that involving the $(P_m + Q_m) / S_e$ ratio, which attains its highest value, equal to 0.7705, along path IL.

5.5.2. Transient analysis

In order to take into account the volumetric swelling strain effects on the thermo-mechanical performances of TA and BP, a campaign of transient analyses has been launched adopting the new DPA spatial distribution carried out by ENEA, aimed at the evaluation of the BP lifetime under neutronic irradiation. To this purpose, the normal operation transient loading scenario has been assumed.

In this campaign of transient analyses, two different scenarios, differing each other for the assumptions aimed at the simulation of the swelling strain mechanical effect, have been investigated.

In the first one, named Scenario 1, the volumetric swelling strain field has been considered to be uniquely dependent on the DPA spatial distribution, as already done in the geometric optimization procedure. In figures 5-44 and 5-45 the new volumetric swelling strain field at the end of the nominal operational period of one year is shown, with reference to Scenario 1.

In the second scenario, named Scenario 2, the volumetric swelling strain has been assumed to be a function of both DPA and temperature spatial distributions, as shown by experimental data reported in [49]. Following this approach, a more realistic simulation of the mechanical

effect of the swelling strain may be performed, taking into account the effect of the temperature on Self Interstitial Atom (SIA) and vacancy dynamics.

According to experimental data, the uniquely DPA-dependent swelling strain values, ε(DPA), already adopted for Scenario 1 analysis, have been properly scaled by means of a purposely set up temperature-dependent weight function ω(T).

It has been thereby possible to introduce the volumetric swelling strain dependence on local temperature T, defining the ε(DPA,T) local swelling strain values as follows:

$$\varepsilon(DPA,T) = \omega(T)\cdot\varepsilon(DPA) \qquad (5\text{-}1)$$

According to experimental data [49] and imposing a linear dependence of swelling by temperature, ω(T) function has been assumed to be 0 for temperature values less than 360 °C, while the condition of ω(T) equal to 1 is attained at T = 400 °C. For temperatures above 400 °C, experimental data show a decreasing of the volumetric swelling strain.

Since thermal analysis allows to predict a maximum BP temperature equal to 320.4 °C, it can be observed that no swelling occurs within BP in Scenario 2 analysis (Figure 5-46), where temperature effect on the dislocation and vacancy dynamics has been taken into account. Anyway, non-zero volumetric swelling strain values are predicted within TA lithium guides, being the hottest TA regions (Figure 5-46).

Thermo-mechanical transient analyses under the normal operation loading scenario have been performed, taking into account both the abovementioned swelling scenarios, checking the fulfilment of the SDC-IC level A safety criteria.

Results obtained have indicated that, from the mechanical point of view, the criterion aimed at the verification of the immediate flow plastic localisation is still the most critical in both scenarios investigated, while the others are totally fulfilled.

For this reason, in order to evaluate the BP lifetime, the time evolution of the $(P_m + Q_m) / S_e$ ratio has been reported in figures 5-47 and 5-48, while the Von Mises equivalent stress field arising within BP at the end of its lifetime, estimated to be equal to about 190 days for Scenario 1 and to 360 days for Scenario 2, is shown in figures 5-49 and 5-50.

Results obtained have shown that the total fulfilment of the SDC-IC level A safety criteria is predicted along all paths taken into account when the dependence of the volumetric swelling strain on the local temperature is implemented within the FEM model in order to perform a more realistic simulation of the swelling effect.

On the basis of this observation, it can be concluded that the optimized BP configuration selected at the end of the design review process is able to safely withstand thermo-mechanical loads it undergoes during the one year long normal operation period.

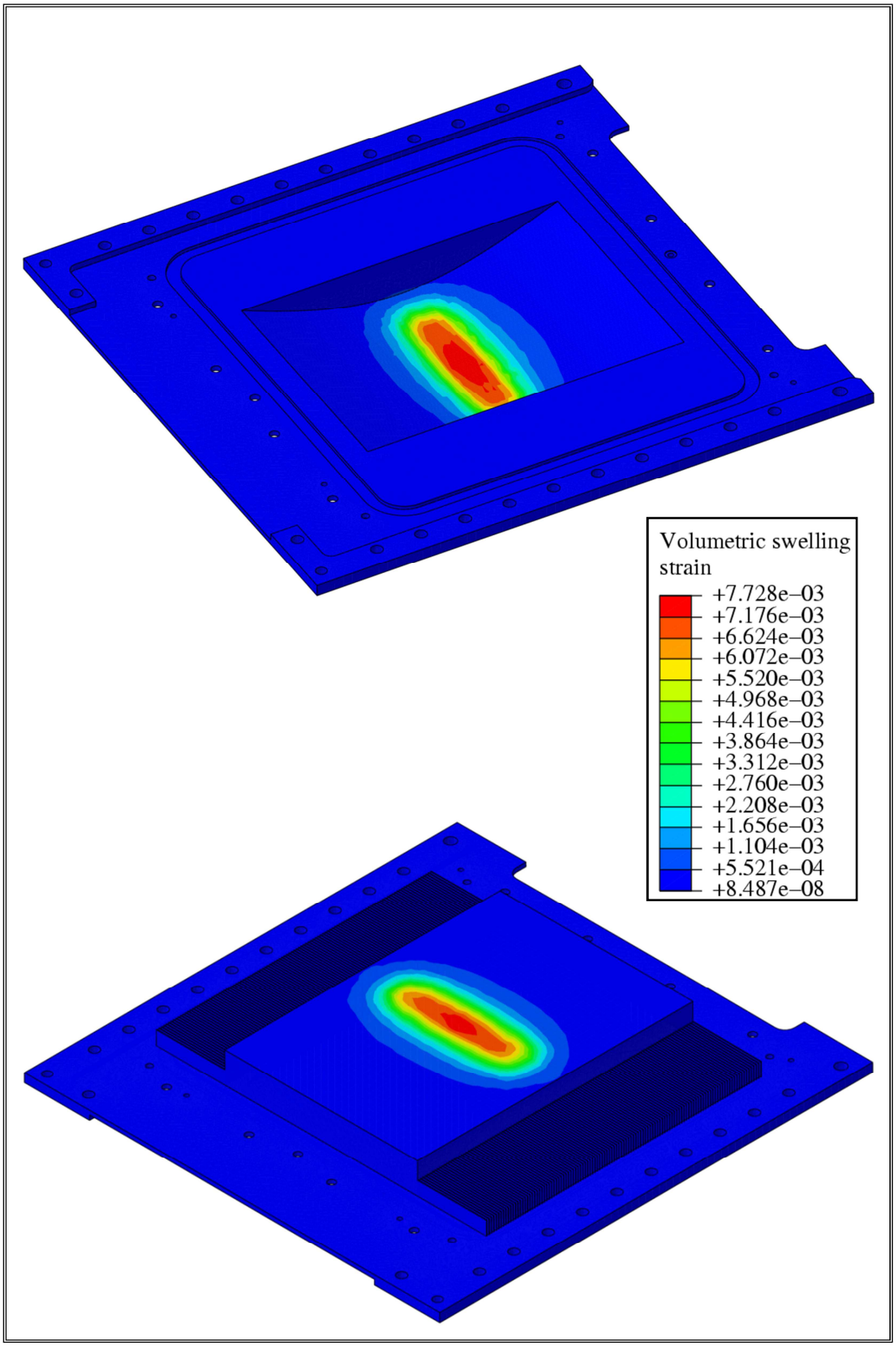

Figure 5-44. Scenario 1. BP volumetric swelling strain spatial distribution at t = 360 days.

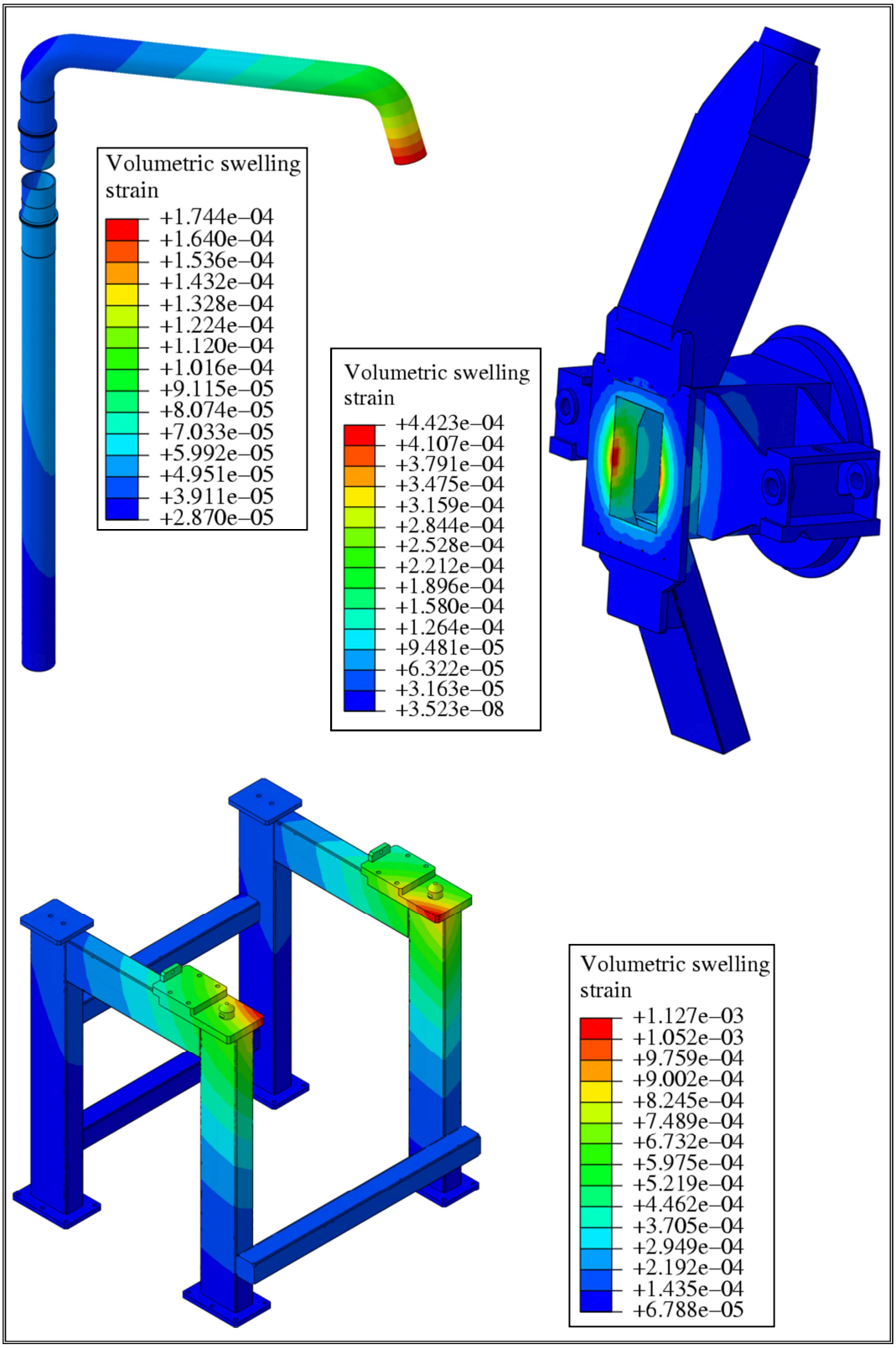

Figure 5-45. Scenario 1. TA volumetric swelling strain spatial distribution at t = 360 days.

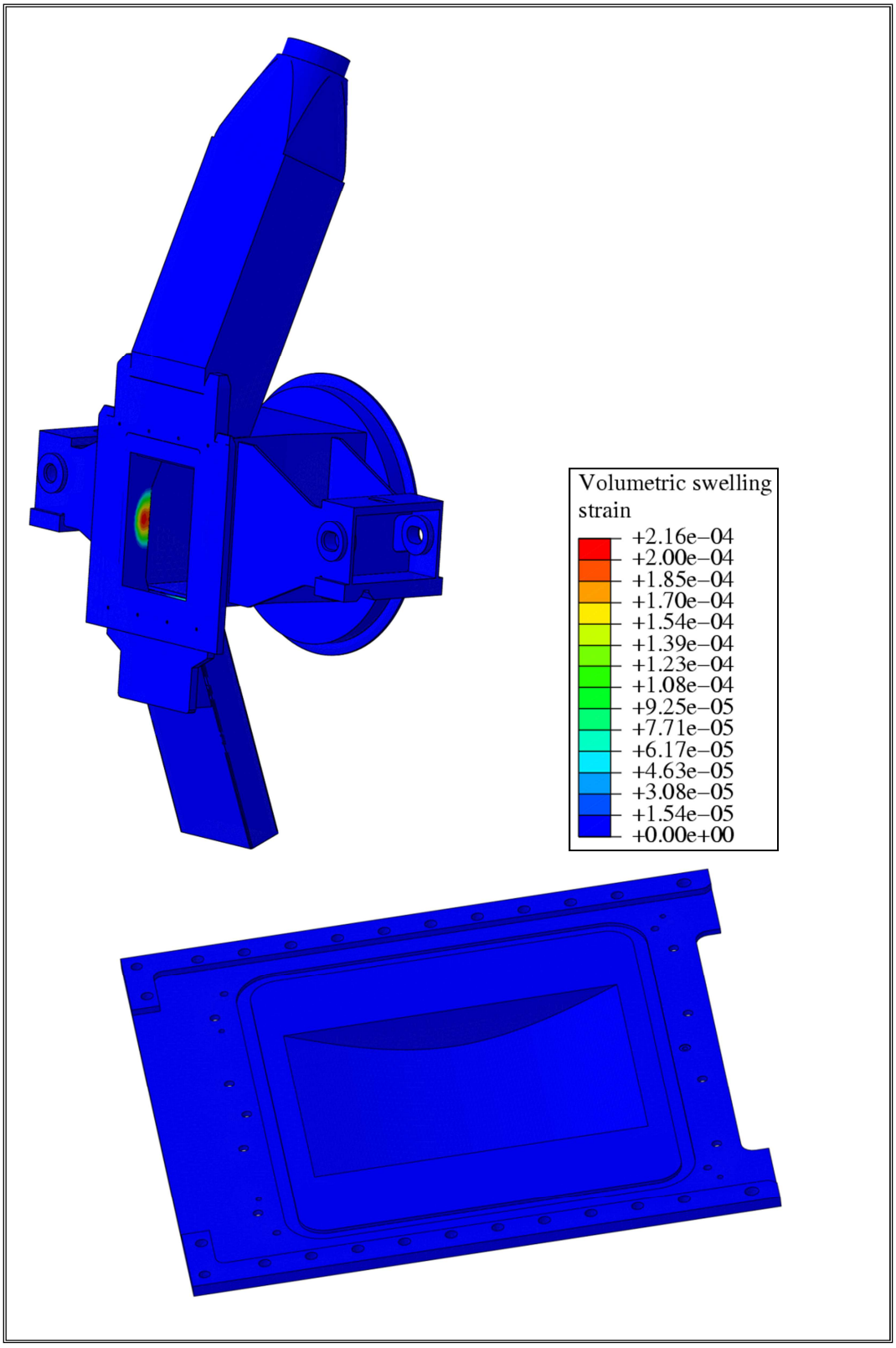

Figure 5-46. Scenario 2. Volumetric swelling strain spatial distribution at t = 360 days.

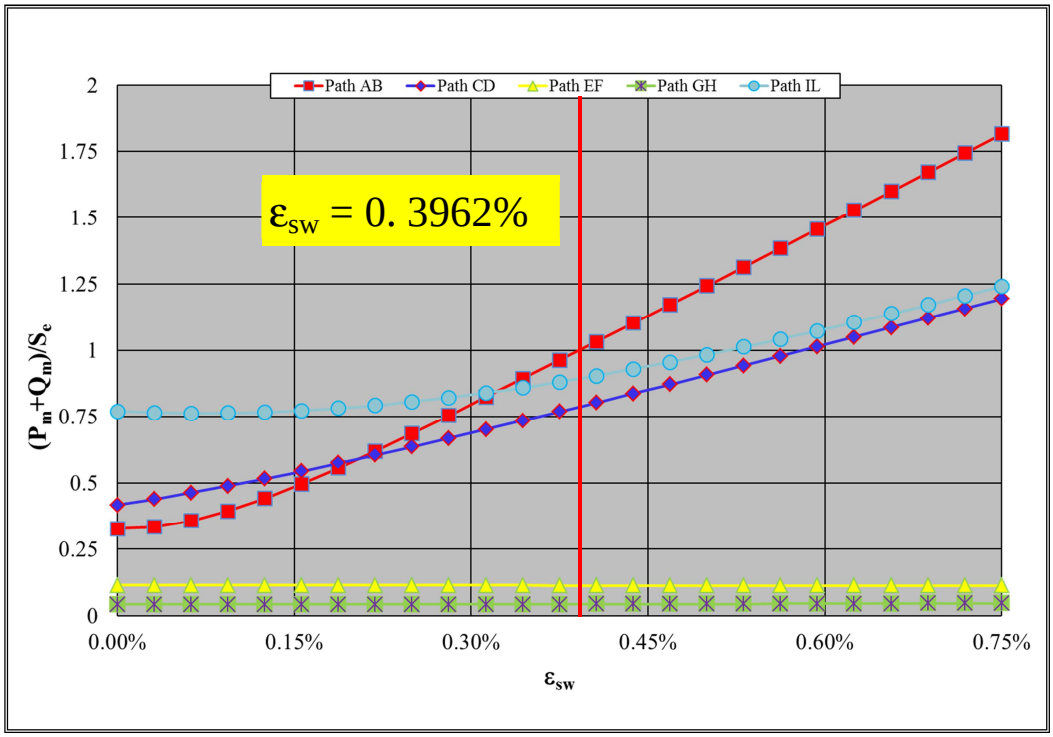

Figure 5-47. (P_m + Q_m) / S_e ratio time evolution. Scenario 1.

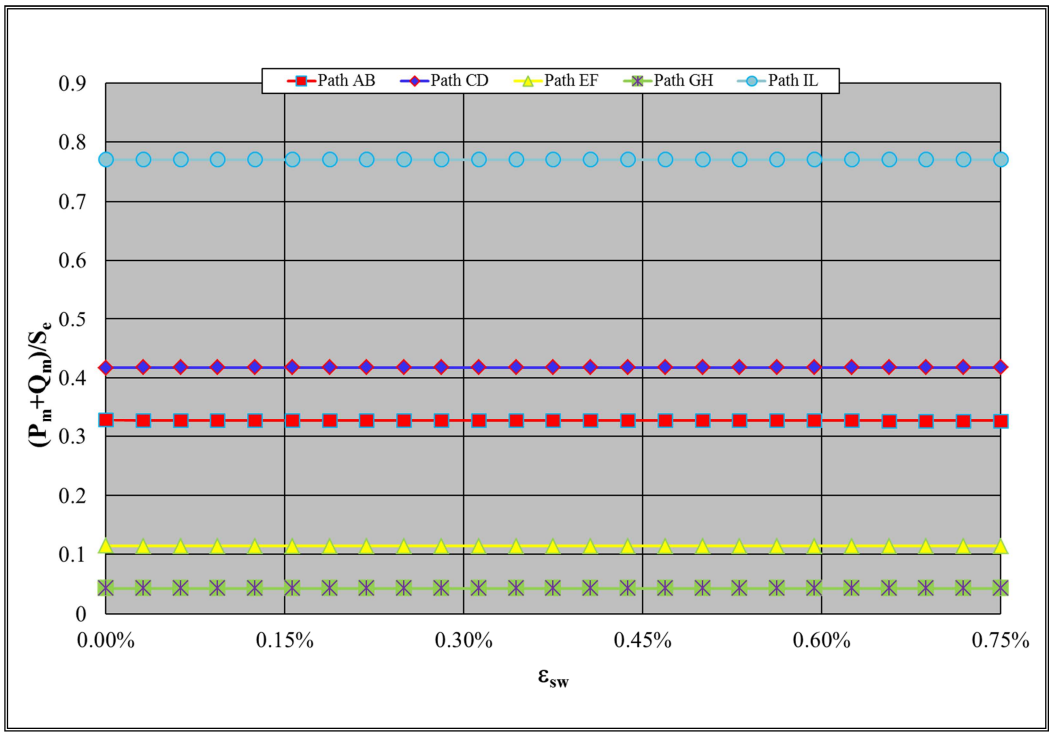

Figure 5-48. (P_m + Q_m) / S_e ratio time evolution. Scenario 2.

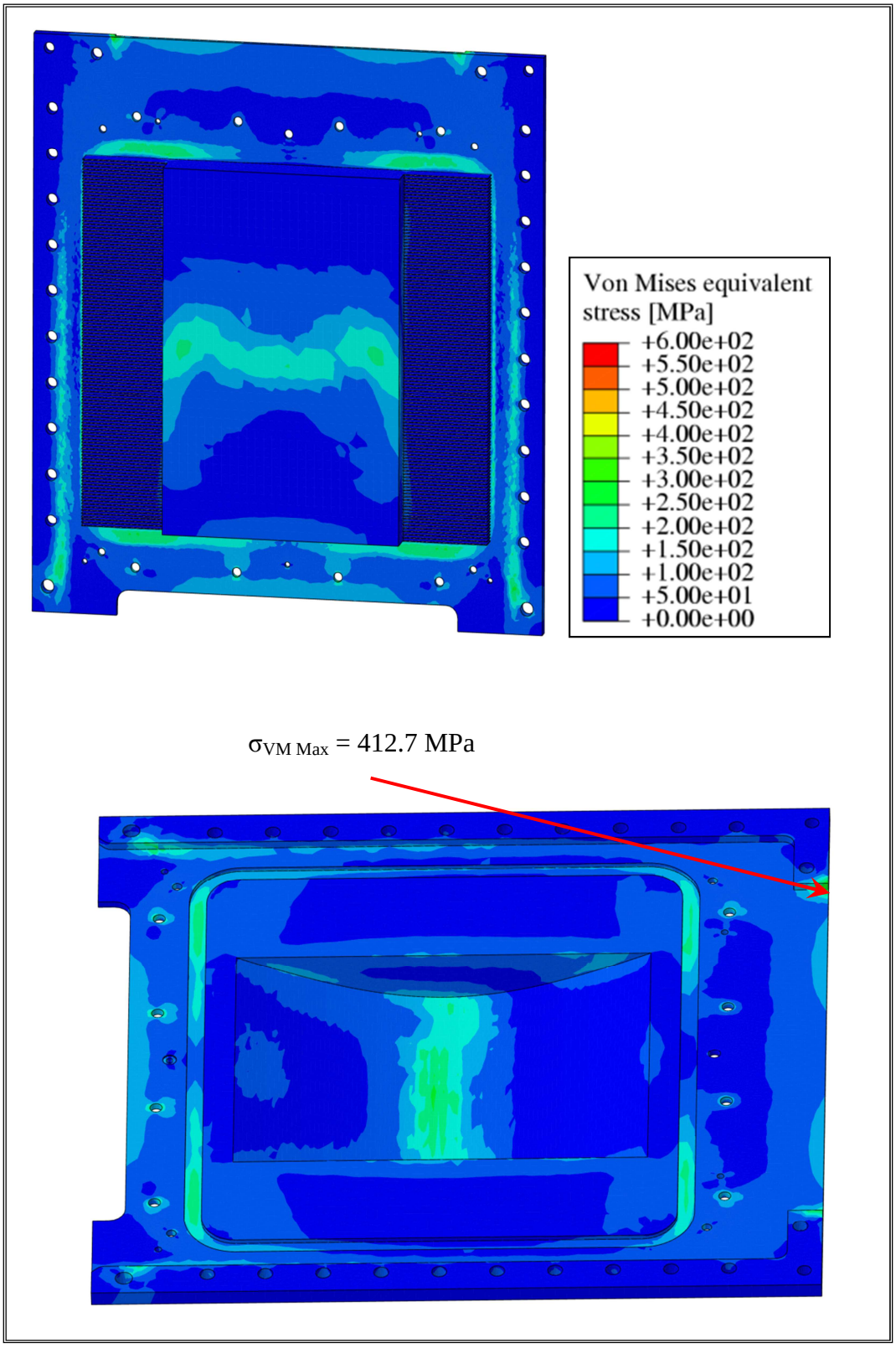

Figure 5-49. Transient analysis. Scenario 1. BP Von Mises stress field at t = 190 days.

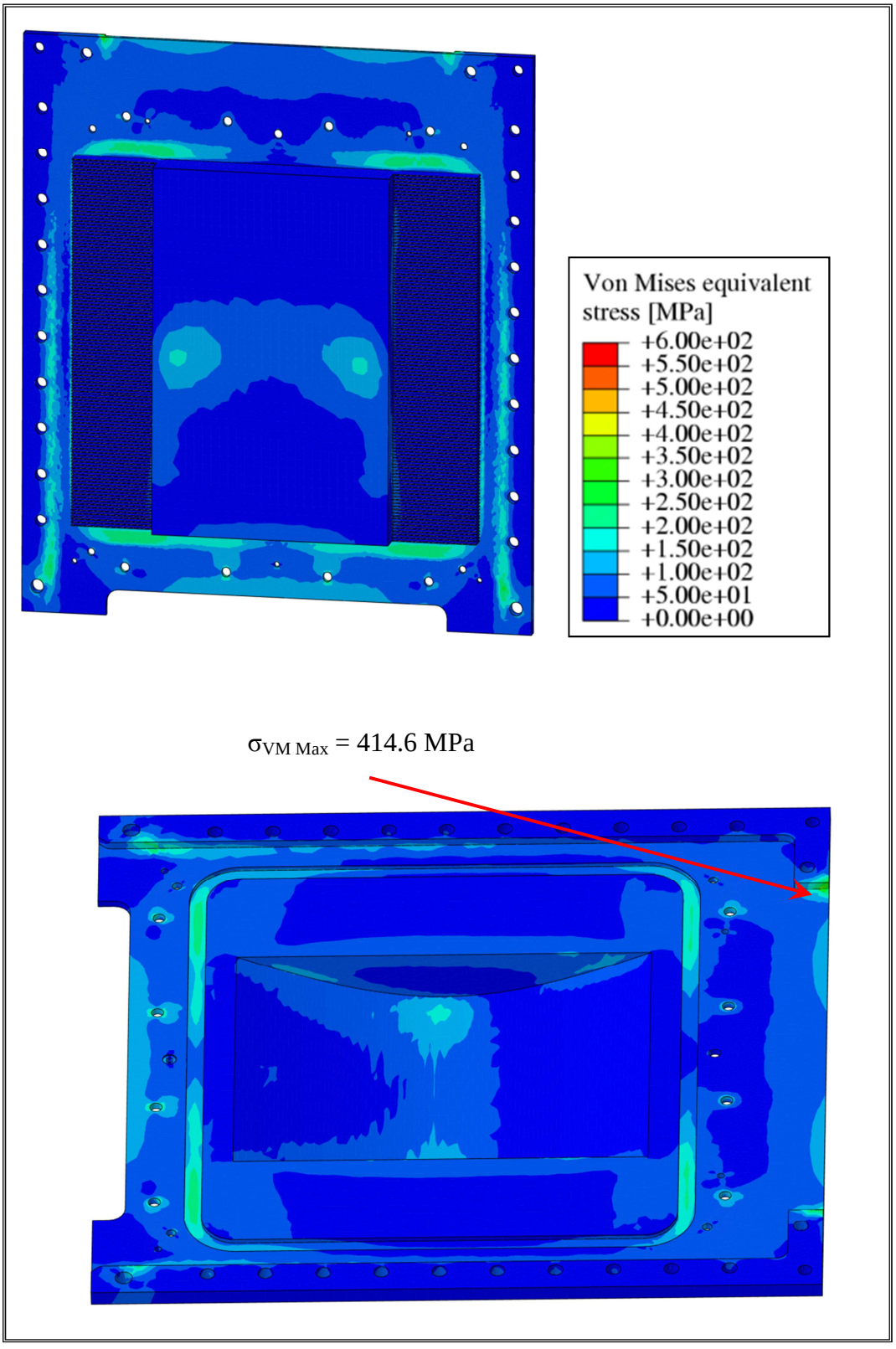

Figure 5-50. Transient analysis. Scenario 2. BP Von Mises stress field at t = 360 days.

6. Conclusions

During the Ph.D. course of the XXIX Ciclo in Energia e Tecnologie dell'Informazione - curriculum Fisica tecnica e Ingegneria Nucleare (*Energy and Information Technologies - curriculum Applied physics and Nuclear Engineering*), held at the University of Palermo, and in the framework of a fruitful collaboration between the Department of Energy, Information Engineering and Mathematic Models (DEIM) of the University of Palermo and the ENEA-Brasimone, the thermo-mechanical behaviour of the IFMIF Target Assembly has been widely investigated under different loading scenarios.

The work has been carried out following a theoretical-numerical approach based on the Finite Element Method (FEM) and using the quoted FEM code ABAQUS v.6.14.

The study has been divided in three main phases, each one aimed at the investigation of a specific issue of the IFMIF Target Assembly.

In particular, the first phase of the study has aimed at the set-up of a FEM model of the IFMIF Target system mock-up present at the ENEA-Brasimone research centre and at the simulation of the pre-heating phase of the IFMIF start-up transient scenario. This phase of the start-up scenario is foreseen in order to raise the target system temperature up to the operational value of 250 °C as much uniformly as possible by means of a set of electric heaters placed on its external surfaces. In order to achieve this goal, a transient thermal campaign of analysis has been carried out and a time-dependent load profile for the electric heaters has been found out.

Results obtained from this first phase have highlighted that the steady state conditions are reached after about 320 minutes. Nevertheless, the thermal field achieved within the structure does not totally fulfil the thermal requirements, since the maximum temperature registered at the centre of the BP is well below the reference value of 250 °C. A revision of both the size and the arrangement of the electric heaters is mandatory in order to achieve higher temperature values within the lithium channel and the BP, in particular.Moreover, results obtained in this phase will be used to *ex-post* validate the FEM model of the target system mock-up adopted in the calculations once the foreseen pre-heating experimental campaign will be performed adopting the TA mock-up.

In the second phase, the thermo-mechanical behaviour of the IFMIF Target Assembly, whether endowed with its framework and the Lithium inlet pipe, has been assessed under the steady state nominal scenario.

A 3D FEM model of the IFMIF TA has been set-up and the loads and boundary conditions pertinent to the IFMIF nominal scenario have been considered. In particular, two different cooling strategies, simulated by means of proper thermal boundary conditions, have been taken into account for the TA framework.

The results carried out have shown that an acceptable thermal field is achieved within the investigated domain, since the maximum temperature is well below the EUROFER critical temperature of 550 °C. From the mechanical point of view very high values of the Von Mises equivalent stress are predicted in a localized region, probably due to a numerical singularity in the FEM model, while the rest of the domain shows stress values lower than 400 MPa.

Moreover, a stress linearization procedure has been performed along five significant paths of the Back-Plate and the SDC-IC safety criteria have been checked. Results have shown that for two paths the safety rules against the immediate plastic flow localization, taking into account both primary and secondary stresses, are not verified.

Therefore, a review in the BP design seems to be necessary in order to assure a complete fulfilment of the SDC-IC design criteria.

On the basis of these results, the third phase of the study has thus regarded the optimization of the BP design. This phase has been organized in different sub-phases, in which the influence of several geometric parameters or loading conditions on the BP thermo-mechanical behaviour have been considered. In particular, the geometric parameters taken into account have been the thickness of the BP lithium channel in both lateral and beam direction, the BP total thickness and the thickness of the lithium guides on the TA. The additional cooling of the BP external surface by means of a set of fins has been moreover considered. Finally, the updated EUROFER material properties have been implemented in the FEM model.

The adoption of all these modifications has led to a TA configuration able to safely withstand the thermo-mechanical loads envisaged for the steady state IFMIF nominal scenario and fulfilling all the design criteria foreseen by the SDC-IC code.

Moreover, the influence of the volumetric swelling strain on the IFMIF thermo-mechanical behaviour has been assessed by means of a transient analysis. In particular, two different approaches have been adopted for the volumetric swelling strain simulation.

Firstly, the volumetric swelling strain field has been carried out imposing a linear dependence of swelling strain on DPA and assuming that after one year of neutronic irradiation the swelling strain value achieved at the beam footprint region centre amounts to 0.75 %.

Secondly, the volumetric swelling strain has been assumed to be a function of both DPA and temperature spatial distributions. Following this approach, a more realistic simulation of the mechanical effect of the swelling strain may be performed, taking into account the effect of the temperature on self-interstitial atom and vacancy dynamics. According to experimental data, the uniquely DPA-dependent swelling strain values, $\varepsilon(DPA)$, have been properly scaled by means of a purposely set up temperature-dependent weight function $\omega(T)$, which has been assumed to be 0 for temperature values less than 360 °C, while the condition of $\omega(T)$ equal to 1 is attained at T = 400 °C. For temperatures above 400 °C, experimental data show a decreasing of the volumetric swelling strain.

Results obtained from transient analysis performed on the TA endowed with the potentially optimized design of the BP have shown that a BP lifetime of about 190 days is predicted in case the volumetric swelling rate dependent on only DPA spatial distribution is taken into account, while a BP lifetime of one year is predicted when temperature effects on dislocations are considered, since the BP temperature is well below the threshold value of 360 °C.

Bibliography

[1] J. Knaster et alii, *"IFMIF, the European–Japanese efforts under the Broader Approach agreement towards a Li(d,xn) neutron source: Current status and future options"*, Nuclear Materials and Energy, 9 (2016) 46-54.

[2] J. Knaster et alii, *"Assessment of the beam–target interaction of IFMIF: A state of the art"*, Fusion Engineering and Design, 89 (2014) 1709-1716.

[3] H. Nakamura et alii, *"Status of engineering design of liquid lithium target in IFMIF-EVEDA"*, Fusion Engineering and Design, 84 (2009) 252-258.

[4] M. Ida et alii, *"Target system of IFMIF/EVEDA in Japanese activities"*, Journal of Nuclear Materials, 417 (2011) 1294-1298.

[5] G. Micciché, B. Riccardi, *"Design, manufacture and testing of the IFMIF lithium target bayonet concept"*, Fusion Engineering and Design, 75-79 (2005) 807-811.

[6] M. Ida, H. Nakamura, K. Shimizu, T. Yamamura, *"Thermal and thermal-stress analyses of IFMIF liquid lithium target assembly"*, Fusion Engineering and Design, 75-79 (2005) 847-851.

[7] M. Ida et alii, *"Thermal-stress analysis of IFMIF target back-wall made of reduced-activation ferritic steel and austenitic stainless steel"*, Journal of Nuclear Materials, 386-388 (2009) 987-990.

[8] K. Watanabe, M. Ida, H. Kondo, M. Miyashita, H. Nakamura, *"Thermo-structural analysis of target assembly and back plate in the IFMIF/EVEDA lithium test loop"*, Journal of Nuclear Materials, 417 (2011) 1299-1302.

[9] K. Watanabe, M. Ida, H. Kondo, K. Nakamura, E. Wakai, *"Thermo-structural analysis of integrated back plate in IFMIF/EVEDA liquid lithium target"*, Fusion Engineering and Design, 86 (2011) 2482-2486.

[10] P.A. Di Maio, R. Giammusso, G. Miccichè, *"On thermo-mechanical issues induced by irradiation swelling inside the back-plate of the IFMIF target assembly"*, Fusion Engineering and Design, 86 (2011) 2597-2601.

[11] P.A. Di Maio, P. Arena, G. Bongiovì, R. Giammusso, G. Miccichè, A. Tincani, "*Study of the thermo-mechanical performances of the IFMIF-EVEDA Lithium Test Loop target assembly*", Fusion Engineering and Design, 87 (2012) Pages 822-827.

[12] P. Arena, D. Bernardi, G. Bongiovì, P.A. Di Maio, G. Micciché, "*On the thermomechanical behavior of the European target assembly design of IFMIF-EVEDA lithium test loop under start-up transient scenarios*", Fusion Engineering and Design, 88 (2013) 774-777.

[13] Abaqus v.6.14, Dassault Systemes Simulia.

[14] D. Bernardi, P. Arena, G. Bongiovì, P.A. Di Maio, M. Frisoni, G. Miccichè, M. Serra, "*Start-up and shutdown thermomechanical transient analyses of the IFMIF European lithium target system"*, Fusion Engineering and Design, 89 (2014) 1913-1922.

[15] P. Garin, M. Sugimoto, "*Main baseline of IFMIF/EVEDA project"*, Fusion Engineering and Design, 84 (2009) 259-264.

[16] H. Nakamura et alii, "*Latest design of liquid Lithium target in IFMIF"*, Fusion Engineering and Design, 83 (2008) 1007–1014.

[17] H. Nakamura et alii, "*Status of engineering design of liquid Lithium target in IFMIF-EVEDA"*, Fusion Engineering and Design, 84 (2009) 252–258.

[18] *IFMIF Comprehensive Design Report*, IFMIF International Team, January 2004.

[19] D. Bernardi, *Target assembly with bayonet backplate - DDD-III_ED03EU*, IFMIF DMS BA_D_22W67Z, 2013.

[20] K. Tian et alii, "*Overview of the IFMIF test facility design in IFMIF/EVEDA phase*", Fusion Engineering and Design, 98-99 (2015) 2085-2088.

[21] A. Möslang, "*IFMIF: the intense neutron source to qualify materials for fusion reactors*", C. R. Physique, Vol 9 (2008) 457-468.

[22] A. Ibarra et alii, "*A stepped approach from IFMIF/EVEDA toward IFMIF*", Fusion Science and Technology, 66 (2014) 252-259.

[23] G. Miccichè, D. Bernardi, "*Rapporto di fabbricazione del prototipo di Target Assembly"*, ENEA Report RdS/2013/127, September 2013.

[24] G. Miccichè, L. Lorenzelli, F. Frascati, "*Rapporto sulla progettazione dei dispositivi per la validazione delle operazioni di manutenzione remotizzata del target di IFMIF"*, ENEA Report RdS/2013/129, September 2013.

[25] G. Miccichè, L. Lorenzelli, "*Rapporto sulla progettazione del sistema di manipolazione remota*", ENEA Report IM-G-R 014, RdS/2011/384, November 2011.

[26] Code Afcen RCC-MRx 2012 – Section III – Tome 1 – Volume Z – Annex A3.2S.

[27] P. D. Desai, C. Y. Ho, "*Thermal linear expansion of nine selected AISI stainless steels"*, CINDAS report for the American iron and steel institute, April 1978.

[28] "*Engineering properties at elevated temperatures"*, International Nickel Company databooks, 1963.

[29] A. Tincani, D. Bernardi, G. Miccichè, *"Engineering design report of the EVEDA bayonet concept Back-Plate"*, ENEA Report IM-M-R-002, 04/02/2010, 2010.

[30] R. Siegel, J. R. Howell, *"Thermal Radiation Heat Transfer"*, McGraw Hill, New York, 1980.

[31] J.P. Holman, "*Heat Transfer*", McGraw-Hill, 1990.

[32] F. P. Incropera, D. P. De Witt, *"Fundamentals of Heat and Mass Transfer"*, John Wiley & Sons, 4th Edition, 1996.

[33] H. Kondo et alii, *"Validation of IFMIF liquid Li target for IFMIF/EVEDA project"*, Fusion Engineering and Design, 96-97 (2015) 117-122.

[34] K. Mergia, N. Boukos, "*Structural, thermal, electrical and magnetic properties of Eurofer 97 steel*", Journal of Nuclear Materials, 373 (2008) 1–8.

[35] T. Chehtov, J. Aktaa, O. Kraft, "*Mechanical characterization and modeling of brazed EUROFER-tungsten-joints*", Journal of Nuclear Materials, 367–370 (2007) 1228–1232.

[36] E.I.Gol'tsova, "*Densities of Lithium, Sodium, and Potassium at Temperatures up to 1500-1600 °C*", High Temperature 4, (1966) 348.

[37] E. E. Shpil'rain, I.F.Krainova, *"Measurement of the thermal conductivity of liquid lithium"*, "High Temperature 8", (1970) 1036-1038.

[38] J.W. Cooke, "*Experimental Determination of the Thermal Conductivity of Molten Lithium from 320° to 830°C*", The Journal of Chemical Physics, 40 (1964) 1902.

[39] M. Frisoni, D. Bernardi, G. Miccichè, M. Serra, "*Nuclear Analysis of the IFMIF European Lithium Target Assembly System*", Fusion Engineering and Design, 89 (2014) 1959-1963.

[40] N. Uda et alii, *"Forced Convection Heat Transfer and Temperature Fluctuations of Lithium under Transverse Magnetic Fields"*, Journal of Nuclear Science and Technology, 38 (2001) 936-943.

[41] M. Rosenberg, R. D. Smirnov, A. Yu. Pigarov, "*On thermal radiation from fusion related metals*", Fusion Engineering and Design, 84 (2009) 38–42.

[42] http://www.dicronite.com/technical-data/

[43] H. Kondo, M. Ida, K. Watanabe, T. Furukawa, Y. Hirakawa, H. Nakamura, et al., IFMIF-DMS Ref 229N6V (2012).

[44] *ITER Structural Design Criteria for In-vessel Components (SDC-IC) code*, ITER IDM G 74 MA 8 R0.1, 2004.

[45] A. Li Puma et alii, "*Potential and limits of water cooled divertor concepts in view of their use for DEMO*", CEA report SERMA/LPEC/RT/12-5272, (2012) 17-20.

[46] A.F. Tavassoli et alii, "*Materials design for reduced activation martensitic steel type EUROFER"*, Journal of Nuclear Materials, 329-333 (2004) 257-262.

[47] G. Aiello et alii, "*Assessment of design limits and criteria requirements for EUROFER structures in TBM components*", Journal of Nuclear Materials, 414 (2011) 53-68.

[48] F. Gillemot, E. Gaganidze, I. Szenthe, "*Final Report on Deliverable Material Property Handbook pilot project on EUROFER97*", IDM No. EFDA D-2MRP77, ID: MAT-1.2.1-T2-D1.

[49] E. Wakai et alii, "*Effect of gas atoms and displacement damage on mechanical properties and microstructures of F82H*", Journal of Nuclear Materials, 356 (2006) 95-104.